THE UNIVERSITY OF HULL

Liquid Crystalline and Polymer Network Organic Semiconductors for Application in Opto-electronic Devices

being a Thesis submitted for the Degree of

Doctor of Philosophy (PhD)

in the University of Hull

by

Guang Hu

December 2015

Acknowledgement

Abstract

A series of novel liquid crystalline and photopolymerisable monomer organic semiconductors for plastic electronics applications, such as organic light-emitting diodes (OLEDs) and/or organic photovoltaics (OPVs) were synthesised and evaluated in this thesis. A number of synthetic reactions were carried out to obtain the desired compounds and intermediates under different reaction conditions. Different aryl-aryl cross-coupling reactions such as Suzuki reactions and direct arylations, palladium-catalysed systems [Pd(OAc)$_2$, Pd(OAc)$_2$+P(Ph)$_3$, and Pd(PPh$_3$)$_4$] for Suzuki aryl-aryl cross-couplings, and the choices of reaction solvents and base aqueous for *N*-alkyl substitutions were compared, optimised and analysed in this thesis.

A variety of electron-withdrawing- or electron-donating moieties, including 2,7-disubstituted carbazole, 2,5-disubstituted thiophene rings, 1,4-disubstituted phenylene, 2,7-disubstituted fluorene, dibenzothiophene, benzothiadiazole and thieno[3,4-*c*]pyrrole-4,6-dione cores, were designed to incorporate in the molecular structure of various aromatic heterocyclic organic semiconductors. The relationship of liquid crystalline mesophases and molecular structures were analysed and established. Linear and co-axial aromatic backbones and short lateral chains contribute to the presence of liquid crystalline mesophases due to a large length-to-breadth ratio. Structural design of different aromatic cores promote the presence of different electroluminescent colours (i.e., organge for compound **53**, green for compound **38**, and blue for compound **41**) and the tuning of device performance. Particularly, the nematic liquid crystalline **42** with a desired glass transition temperature above room temperature (32 $^{\circ}$C) and high clearing point (161 $^{\circ}$C) shows lower switch-on voltages (2.4 V) and higher OLED device brightness, current density and efficiency. Furthermore, There are excellent matches between the values of the ionization potential (IP = -5.53 eV) and the electron affinity (EA = -2.89 eV) of electroluminescent liquid crystalline **42** and the HOMO energy level of the hole-transport layer cross-linked OTPD (IP = -5.48 eV) and the LUMO energy level of electron-transporting layer of SPPO13 (EA = -2.91 eV), respectively. This advantageous combination of energy

levels within the test OLED results in low charge-injection barriers for electrons and holes, respectively, leading to a high current density and a corresponding high density of excitons in the emissive layer where efficient recombination occurs efficiently with emission of light.

In addition, novel photopolymerisable carbazole-functionalised triazatruxenes incorporating three or more cross-linkable endgroups including non-conjugated dienes and oxetanes at the end of aliphatic flexible spacers, were first reported and synthesised using simple one-step N-position substitution reactions. The cross-linking abilities of C=C double bonds, C≡C triple bonds, non-conjugated dienes and oxetanes attached to the triazatruxene core were compared and investigated. The result proved that non-conjugated dienes attached to more chemically and photochemically stable tertiary amides (90% @400 J/cm^2 UV for monomer **96**) showed a greater tendency to photopolymerise than that attached to common ester bonds (72% @800 J/cm^2 UV for monomer **K1**). The photopolymerisable monomers also afford a cheap thin-film fabrication by solution spin-coating in organic optical-electrical devices. Hole test device of photopolymerisable triazatruxene **100** was fabricated by solution spin-coating. The effect of cross-linking and doping on hole-transporting capacity were studied in this work. It was found that cross-linking of photopolymerisable triazatruxenes **100** does not lead to a decrease of current density while photopolymerisable triaryamine monomer with similar star-shape does. Furthermore, the use of highly electronegative p-type dopant results in an increase of current density due to the formation of more free holes in a device by removing electrons from the host material.

1 Introduction

1.1 Organic Semiconductors

1.1.1 Insulators, Conductors and Semiconductors

Materials can be grouped into insulators, conductors and semiconductors according to their conductivity under standard conditions[1]. In classical physics insulators, semiconductors and conductors are regarded as having a valence band (VB) and conduction band (CB). The VB has a low energy level fully filled with electrons and the CB is a high energy level with no electrons[2]. Specifically, for insulators such as rubber, the energy gap between valance band and conduction band is so wide that electrons in valance band cannot overcome the gap to be promoted into conduction band. In such case, valance electrons cannot move freely within the bulk of the insulators. However, freely moving electrons or ions are essential for conducting an electric current. In terms of conductors such as metals, the valance band and the conduction band overlap, which means electrons can move freely throughout both the valance band and the conduction band. Furthermore, metals as good conductors, have a partly filled valance band, so that electrons can flow easily and thus conduct electricity, e.g., sodium has fully filled 1s, 2s, 2p bands, but the 3s band is half filled.

On the other hand, semiconductors have a much smaller energy gap than insulators. In such case, electrons in the valance band can be excited by absorption of electromagnetic radiation or thermal energy or by the application of an applied electric or magnetic field. Consequently, an electric current can be produced in that valance electrons are excited to the conduction band. The schematic representation of VB, CB, and energy gap (Eg) for insulators, conductors, and semiconductors is shown in **Fig. 1.1**.
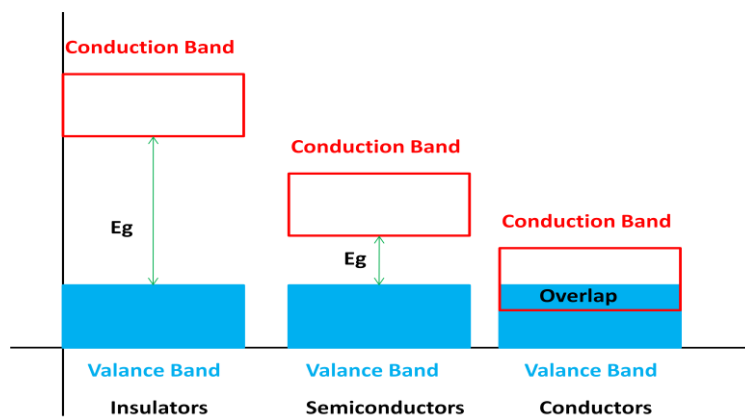
Fig. 1.1 The schematic representation of valence band, conduction band, and energy gap for insulators, conductors, and semiconductors

1.1.2 Organic Semiconductors and Conjugated Structures

Crystalline semiconductors can be generally categorised into inorganic and organic semiconductors. Traditional solid electronic equipment, such as integrated circuit (IC) and light-emitting diodes (LEDs), usually consists of inorganic semiconductors including elemental semiconductors, e.g., Se, Ge, Si, and inorganic compounds, e.g., SiC, ZnS, GaAsP, etc. However, plastic electronics based on organic semiconductors are now replacing classical electronic components and/or devices, such LEDs, Field-Effect Transistors (FETs), Photovoltaics (PVs), based on doped silicon for many consumer electronic applications. Plastic electronic devices, such as Organic Light-Emitting Diodes (OLEDs), Organic Field-Effect Transistors (OFETs) and Organic Photovoltaics (OPVs) are also creating new markets and applications[3-7].

Organic molecules are usually known as insulators, but compounds with a high concentration of highly conjugated aromatic rings, such as 1,4-disubstituted phenylene or 2,5-disubstituted thiophene rings, in the molecular core, can form conjugated electron cloud with a high degree of delocalisation, which renders aromatic organic compounds semiconductive under certain conditions. According to the Hybrid Orbital Theory[8-9], the sp_z-hybridisation of unsaturated carbon-carbon (C=C) double bonds forms a pair of π molecular orbitals - the lower energy molecular orbital is the π-bonding orbitals and the higher energy molecular orbital is the π*-anti-bonding

orbitals. The π bonding and π* anti-bonding orbitals in organic semiconductors, which can be seen as equivalent to valance band and conduction band, respectively, are the highest occupied molecular orbital (HOMO) and lowest unoccupied molecular orbital (LUMO), respectively. A schematic representation of energy levels and orbitals in organic semiconductors is shown in **Fig. 1.2**. Compared with head-to-head highly-overlapped σ and σ* orbitals of saturated carbon-carbon (C-C) single bonds, in which electrons are tightly constrained, the π-molecular orbitals overlap less and the electron cloud is delocalised over the conjugated atoms. Therefore, if a high concentration of highly conjugated aromatic rings is present in the molecular core of organic compounds, then some examples of this class of aromatic materials could well also act as organic semiconductors, which are now used extensively in a variety of optical-electrical devices, such as Organic Light-Emitting Diodes (OLEDs), Organic Photovoltaic (OPVs) and Organic Field-Effect Transistors (OFETs).
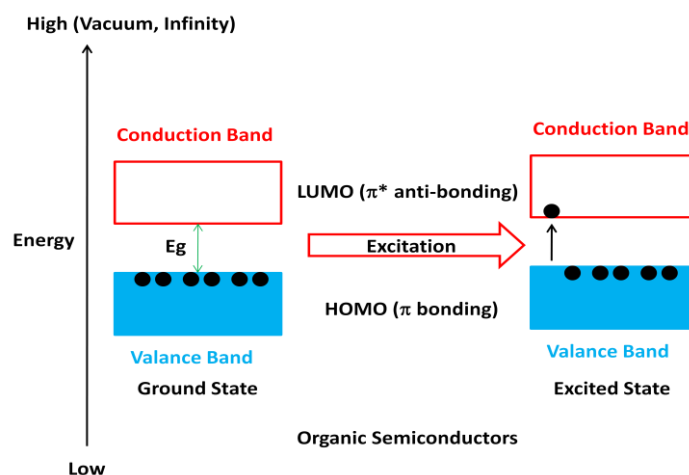
Fig. 1.2 The schematic representation of HOMO, LUMO and excitation in organic semiconductors

1.2 Luminescence

Luminescence, a term first coined by Eilhard Wiedemann in 1888[10], refers to emission of light from the excited state of a substance. Thus, luminescence is not generated by heat, so it is a type of cold body radiation. Luminescence can be divided into several types according to the source of the excitation energy, such as chemiluminescence from a chemical reaction, crystalloluminescence produced during crystallisation, electroluminescence due to an electric current passing through a substance, photoluminescence as a result of absorption and re-emitting of light, etc.

1.2.1 Photoluminescence, fluorescence and phosphorescence

Photoluminescence refers to the process, whereby electromagnetic radiation, i.e., light, is absorbed and subsequently re-emitted at a longer wavelength due to energy loss, which is also known as the Stokes (red) Shift[11]. More specifically, electrons in the valance band (ground state) can be excited to the - higher energy - conduction band following the absorption of photons. These electrons in the excited state in the conduction band can then relax back to the - lower energy - ground state accompanied by the emission of photons of light. The process of absorption and re-emission of light can be well illustrated by the typical Jablonski diagram[12-13], see **Fig. 1.3**.
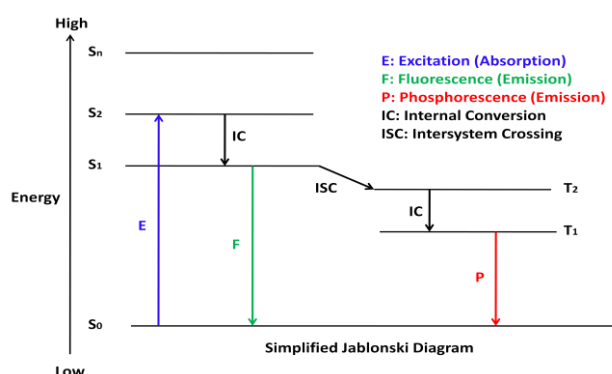
Fig. 1.3 A typical Simplified Jablonski diagram

The ground state is depicted as S_0 and the excited states with different energy levels are shown as S_1, S_2...S_n. The electrons in ground state (S_0) can be excited into different

vibrational energy levels (S_1, S_2...) instantaneously after absorbing a photon with an energy greater than that of the band gap. The electrons in higher vibrational energy levels (S_2, S_3...) first relax quickly by a thermal process to the lowest vibrational energy level (S_1). This internal conversion process is very fast, e.g., typically less than 10^{-12} s. Then, when these excitons in the lowest vibrational energy level (S_1) relax directly back to the ground state (S_0), fluorescence is observed with the emission of a photon with an energy equal to the band gap. This process is also very fast, e.g., ca 10^{-8} s. However, if the excitons in lowest excited singlet state (S_1) undergo a spin conversion to the triplet state (T_1), phosphorescence would be generated from the relaxation of the first triple state T_1 with the lifetime of approximately 10^{-4}-10^2 s, which is much longer than that (about 10^{-8} s) of fluorescence due to the nearly irreversible transition between triple states and ground state. Even for certain phosphorescent materials, absorbed radiation can be re-emitted, even though at a very low intensity, for up to several hours after the original excitation.

1.2.2 Electroluminescence

Electroluminescence (EL) refers to the direct conversion of electrical energy into light under as a result of an electric current passing through an appropriate semiconductor, which can be inorganic or organic materials. The first commercial electroluminescent LEDs were based on the inorganic semiconductor, GaAsP, in the early 1960s[14]. However, inorganic LEDs are monochromatic and devices containing them are usually low-information-content. The high cost and complex fabrication technology for manufacturing inorganic LEDs with full-colour and high-information-content drives the research and development of OLEDs as a promising full-colour and large-screen flat panel displays.

Electroluminescence from organic semiconductors was first observed by Pope and co-workers[15] in 1963 from a single crystal of anthracene (**Fig. 1.4**) using liquid electrodes. However, the device required high voltages 400 V-2000 V due to the

thickness of the single crystals used, i.e., 5 mm. Improved OLEDs were then fabricated incorporating thin wafers of cleaved anthracene crystals using solid electrodes[16]. Unfortunately, it was found that these devices still exhibited a very low working efficiency probably due to the mismatch of electrodes and emissive layers, although a much lower threshold voltage was achieved.
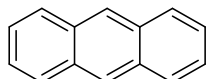
Fig. 1.4 The chemical structure of anthracene

A significant advance in the development of OLEDs was the introduction of uniform vapour-deposited thin films[17], which gave rise to prototype OLEDs with a high efficiency and low switch-on voltages. A big breakthrough for OLED technology, reported by Tang et al in 1987, was the efficient electroluminescence obtained from OLEDs using *tris*(8-hydroxyquinolinate)aluminium (III) (Alq$_3$) as the emissive layer[18-19]. Later Friend et al[20] reported electroluminescence from Polymer Light-Emitting Diodes (PLEDs) using the highly conjugated polymer, poly(*para*-phenylenevinylene) (PPV). The chemical structures of Alq$_3$ and PPV are shown in **Fig. 1.5 (a)** and **(b)**, respectively.

(a)   (b)
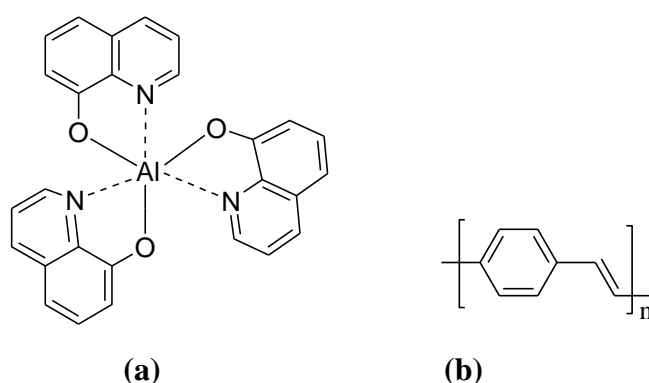
Fig. 1.5 The chemical structures of Alq$_3$ **(a)** and PPV **(b)**

A variety of organic materials, including low-molar-mass molecules (LMMMs), oligomers or polymers, can be applied in electroluminescent devices. The advantage of using these organic semiconductors is that the chemical structures of these classes of

materials can be easily designed and modified according to the requirement of OLEDs and PLEDs. The emission colour, for instance, is determined by the band gap (Eg), i.e., the difference (eV) between HOMO and LUMO energy levels, which can be controlled by modifying the nature of molecular structures, particularly of the highly conjugated aromatic core, of organic materials. Therefore, the entire range of visible spectrum can be achieved by designing appropriate chemical structures of organic semiconductors.

1.3 Organic & Polymer Light-Emitting Diodes (OLEDs & PLEDs)

Organic light emitting diodes (OLEDs) and Polymer Light-Emitting Diodes (OLEDs & PLEDs) with high information content, active matrix addressing and full colour are a type of novel flat-panel display. OLEDs & PLEDs are based on organic electroluminescence, i.e., they emit light on the passage of a small electric current between the device electrodes. Therefore, OLEDs & PLEDs do not require backlighting and other - mostly light-absorbing - components, such as the diffusers, colour filters and polarisers, used in LCDs. Consequently, OLEDs & PLEDs are more efficient in terms of light emission due to the absence of so many light-absorbing or scattering layers and due to the absence of a backlight. At the same time, OLEDs & PLEDs have very wide viewing angles due to the nature of luminescence. They are very thin, light-weight, planar devices with high brightness, low switch-on and operating voltages and low power consumption[21].

1.3.1 Single Layer OLEDs & PLEDs

A single-layer OLED or PLED is the simplest configuration of this type of electroluminescent device. They consist of a single thin film sandwiched between a cathode and an anode, see **Fig. 1.6**. The electroluminescent thin film with a thickness of about 30 nm to 50 nm is comprised of either a fluorescent or phosphorescent organic or organo-metallic semiconductor. A transparent glass substrate, usually coated with transparent indium tin oxide (ITO), is generally used as the anode in commercial OLEDs. A very thin layer of an electropositive metal, such as magnesium, aluminium or calcium, are employed as the cathode in order to promote efficient electron injection. The difference in the work-functions of the cathode and anode ($\phi_{cathode}$ and ϕ_{anode}, respectively) means that the charge-carriers, i.e., the electrons and holes, flow in only one, but opposite, directions, i.e., electrons from the cathode to the anode and holes from the anode to the cathode. Hence, OLEDs & PLEDs are diodes.
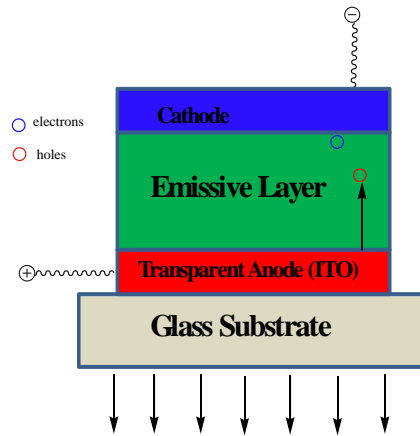
Fig. 1.6 A typical single-layer OLED & PLED device structure

If an external voltage bias beyond a specific threshold voltage, which is determined by the organic materials serving as the luminescent layer, and the nature of the electrodes, is applied between the two electrodes, charge carriers, i.e., holes from the anode and electrons from the cathode, are injected into the organic emissive layer. Due to the external electric field, these charge carriers will move to the opposite electrode through the organic layer. If holes and electrons reach the opposite electrode respectively without encountering each other and recombining through the organic layer, they would be discharged non-radiatively. However, if a hole and an electron encounter each other and combine, while moving through the organic layer, excitons are formed, as an excited state, which can then relax to the ground state from the excited state by the emission of a photon. The magnitude of the currents of electrons and holes is often not identical and depends on a combination of factors, such as the nature of emissive material and the electrodes, but also on the nature of the interfaces between the electrodes and the semiconductor.

On the other hand, many holes reach the cathode and discharge without recombining with any electrons during passing through the emissive organic layer, which only generates heat. Therefore, the work functions of the cathode material and the anode material ($\phi_{cathode}$ and ϕ_{anode} respectively) should ideally match the electron affinity (EA) and the ionisation potential (IP) of organic electroluminescent materials, respectively, especially in multi-layer OLEDs & PLEDs, see below, in order to inject charge carriers

into organic layer efficiently and in a balanced way in order to maximise the recombination – and therefore light emission – of the currents of holes and electrons. The energy barrier for charge injection depends in a significant way on the work functions of electrodes and the relative positions of the energy levels (EA and IP) of the organic layer[22]. The work function, EA and IP are determined by the nature of materials and are directly related to the LUMO and HOMO of materials, respectively.

In terms of single-layer OLEDs & PLEDs, the majority of organic materials conduct holes and electrons at different rates. For instance, polyphenylene vinylene (PPV) transports holes faster than electrons, which results in an unbalanced charge injection and charge mobility. Charge recombination then occurs predominantly near the cathode[23] (**Fig. 1.7**), which results in quenching of the excitons – without light emission – and, therefore, it usually results in a very low device efficiency. Therefore, OLEDs & PLEDs with two or more organic layers for specific functions were invented and fabricated, as described below, to address these issues.
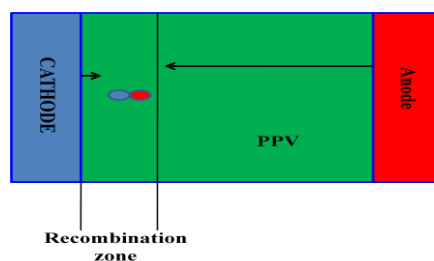
Fig. 1.7 Formation of excitons near the cathode of a single layer OLEDs

1.3.2 Bi-layer OLEDs & PLEDS

It has been demonstrated that multilayer OLEDs and PLEDs can exhibit higher luminous efficiency, longer lifetime, lower threshold and operating voltages as well as lower current than those of the single-layer equivalents using the same emissive layer, for example. This combination of advantages features can thus reduce power consumption considerably. Specifically, an electron-transporting/hole-blocking (ETHB) layer is added and sandwiched between the emissive layer and the cathode compared

with the structure of single-layer OLEDs. A typical structure of a bi-layer OLED – in this case a PLED, but the device configuration is the same - is shown schematically in **Fig. 1.8**.
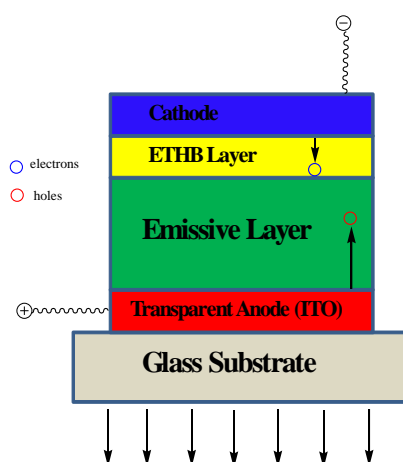
Fig. 1.8 A typical device of bi-layer OLEDs & PLEDs

A typical example of a bi-layer PLED is the device reported by Friend et al [35] in 1992. The electron-transporting/hole-blocking layer (ET-HB) was formed by using 2-(biphenyl-4-yl)-5-(tert-butylphenyl)-1,3,4-oxadiazole (PBD) (see **Fig. 1.9**), and PPV was used as a combined hole-transporting and emissive layer. This bi-layer PLED enables the holes and electrons to recombine at, or close, to the PPV/PBD interface away from the electrodes. The high density of holes and electrons at the interface results in a high rate of charge recombination, exciton formation and light emission. Therefore, bi-layer PLEDs & OLEDs exhibit higher a light-emission efficiency than that of single-layer analogue devices. A simple comparison experiment has proved that the bi-layer device of Friend et al[24] is eight times more efficient than a similar single layer PPV OLED with the same electrodes.
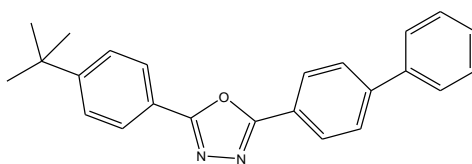
Fig. 1.9 The chemical structure of PBD

1.3.3 Tri-layer OLEDs and Multi-stack Pin OLEDs

The typical configuration of a tri-layer OLED or PLED, shown schematically in **Fig. 1.10**, involves the presence of an additional hole-transporting layer sandwiched between the emission layer and the anode compared to the structure of a similar bi-layer OLED or PLED. Three distinct layers involve electron-transporting layer (ETL), emission layer and hole-transporting layer (HTL). The tri-layer OLED was first developed by Adachi et al[25]. Some reports[26-28] have proved that tri-layer OLED devices exhibit a higher external quantum efficiency and lower operating voltages than single layer and bi-layer devices. Furthermore, lots of other advantages have been shown for tri-layer OLEDs & PLEDs. For instance, holes and electrons can recombine in the central emission layer. The low work function of the metal cathode and the LUMO of the ETL can be well matched so that efficient electron injection occurs, the high work function of the anode can match the HOMO of HTL well, and the ETL and the HTL can prevent the holes and electrons from travelling through the emission layer to the opposite electrode respectively without recombination occurring.
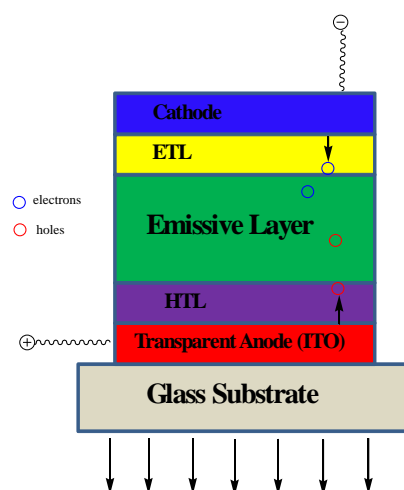
Fig. 1.10 A typical tri-layer OLEDs device structure

On the other hand, one of the drawbacks of such multi-layer devices is that interlayer mixing may occur during the deposition of each layer. Typical layer deposition methods involve vapour deposition of small molecules (LMMMs) under high vacuum and at high temperature or wet-chemistry deposition techniques, such as drop casting,

spin-coating, inkjet printing, doctor blade techniques, from solutions of oligomers, polymers, reactive mesogens, etc., from common organic solvents.

Unfortunately, these conventional single, bi- or tri-layer OLED devices have some disadvantages, such as a high barrier for charge injection from the anode into the hole-transporting layer and the requirement for high values of charge-transport mobility. In order to address these issues, so-called multi-stack OLEDs and *p*-doped, intrinsic, *n*-type doped PIN-OLEDs have been studied and developed[29-31]. In multi-stack OLEDs additional hole/electron injection layers are introduced between the hole-/electron-transporting layer and the anode of tri-layer OLEDs, for example, to produce a lower barrier for hole injection into the other layers of the device. Many variants of multi-stack OLEDs have been developed with improved overall performance, e.g., in terms of brightness, power conversion efficiency, threshold voltage and operating voltage, etc.[32-33].

In so-called and *p*-doped, intrinsic, *n*-type doped PIN-OLEDs a variety of *p*-type or *n*-type dopants are used to dope either the hole-transporting- or electron-transporting-layers or both, respectively, to improve the charge transporting properties of these materials. The anode and the cathode can also be doped with *p*-type or *n*-type dopants, respectively, in order to improve their charge injection properties and thereby, either increase the current density through the device to increase the device efficiency, brightness, etc., or lower its operating voltage[34]. Additionally the use of doped layers allows a much broader range of material choice for charge-transporting layers and the device electrodes in PIN-OLEDs. Multi-stack OLEDs and PIN-OLEDs usually exhibit enhanced device performance, e.g., higher power efficiency, longer lifetimes, enhanced stability and greater reliability, than that of conventional multi-layer OLEDs and PLEDs[29-33]. However, the higher degree of complexity of multi-stack OLEDs and PIN-OLEDs generally leads to higher costs of manufacture and a diverse spectrum of challenges in terms of manufacturing processes, overall production yield and reproducibility of performance of such optoelectronic devices.

1.3.4 Stability and Reliability of OLEDs & PLEDs

A crucial parameter in the success of commercial display devices is their lifetime. However, the lifetime of current OLEDs & PLEDs remain inferior to those of comparable inorganic LEDs. This is because the organic materials used in OLED & PLEDs are, of course, semiconductors and thus extremely thin films are necessary in order to facilitate low switch-on and operating voltages and power consumption at high device brightness and intensity. However, such thin films are prone to defects due to the presence of trace amounts of chemical impurities of materials, crystallisation and a variety of degradation pathways, etc., which all can impair the stability and reliability of OLEDs.

First and foremost, the purity of organic materials is one of the most important issues. Organic impurities can be removed via column chromatography (CC) and high performance liquid chromatography (HPLC) so that the organic purity can reach values above 99.9%. However, ionic impurities, which can act as traps for excitons during the recombination and thus have a significantly adverse impact on the efficiency and lifetime of display devices, cannot be removed by CC and HPLC, but can be eliminated using ion-exchange resins and metal trapping agents.

Another problem that can impair the stability of OLEDs & PLEDs is the crystallisation of the organic materials used as thin layers in OLEDs during the lifetime of devices, especially for some low-molecular-mass materials (LMMMs). Polymer materials can often have a high glass transition temperature (Tg), which can inhibit crystallisation during the lifetime of OLED & PLEDs. However, some LMMMs often exhibit a low Tg or even have no Tg. Crystallisation can result in the formation of crystal grain boundaries and non-uniformity in the organic films, thereby reducing the quantum efficiency and lifetime of devices. A variety of degradation mechanisms can also affect the stability and reliability of devices, including photochemical, electrochemical, environmental, electrode, colour degradation, etc.

1.4 Materials for OLEDs

OLEDs & PLEDs require organic charge-transporting and electroluminescent materials. One of the advantages of using organic materials for OLEDs & PLEDs is that they can be designed specifically with the desired functions, such as high hole mobility, high electron-transportability and efficient electroluminescence. Furthermore, the electron affinity (EA, LUMO energy level) and ionisation potentials (IP, HOMO energy level) of charge-transport materials can be tuned to match the work functions of electrodes. These requirements for the material properties can be achieved by the design and synthesis of a variety of organic and organometallic molecules. Currently, the materials for OLEDs are usually low-molecular-mass materials (LMMMs), oligomers or polymers, see below for more details.

1.4.1 Polymers and Highly Cross-linked Polymer Networks

The main advantage of polymers for PLEDs is that they can form stable glasses with a high glass transition temperature compared with LMMMs, which tend to form polycrystalline films. Small molecules with stable glasses are relatively rare. However, high-molecular-weight polymers with highly conjugated aromatic components are often difficult to dissolve in common organic solvents and, consequently, deposition from solution of polymers onto the substrate surface of PLEDs can be hard to achieve. However, some soluble and highly efficient semiconducting oligomers and polymers, such as polyfluorenes – see below, have been prepared and are used in commercially successful PLEDs fabricated by wet-chemistry deposition techniques, such as drop casting, inkjet printing, spin-coating from solutions of the polymers from common organic solvents.

Poly(*para*-phenylenevinylene) (PPV), was the first polymer reported for the fabrication of PLEDs devices[20]. However, like most polymers, a big obstacle for device application is from the insolubility of PPV due to the numerous extended conjugated structures. In order to overcome the insolubility, soluble polymer precursors were synthesised, spin-coated as thin, homogeneous films, and then converted into PPV *via* a vacuum thermal treatment[35]. Poly(dioxyethylenethienylene) (PEDOT) doped with polystyrenesulphonic acid (PSS), see **Fig. 1.11**, are often used as hole-injection and hole-transporting layers[36].

(a)   **(b)**
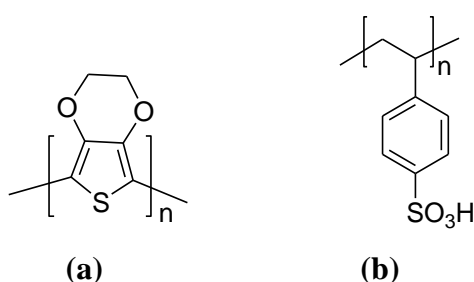
Fig. 1.11 The chemical structures of PEDOT **(a)** and PSS **(b)**

Polyfluorenes have been researched and reported as good optoelectronic semiconducting and light-emitting materials for many years[37-42] since Ohmori et al first reported poly(9,9-dihexylfluorene) emitting blue light in 1991[43]. The facile substitution in the 9-position of a 2,7-disubstituted fluorene moiety contributes to the achievement of good solubility and desired transition temperatures.

The presence of the hetero-atoms in aromatic heterocyclic moieties in some highly conjugated organic semiconductors contributes to the improved optoelectronic properties of such materials[44-45]. For example, the use of 2,6- and 2,7-disubstituted carbazole units for preparing organic semiconductors has attracted much attention in recent years[46-49]. Compared with the corresponding 2,7-disubstituted fluorene moiety, the electron-donating nature of the nitrogen hetero-atoms present in the carbazole moieties can increase the electron density of the delocalised π-electronic cloud and thereby affect the magnitude of the physical properties of interest for OLEDs and PLEDS. The carbazole moiety has long been recognised as an excellent construction of photoconductive organic semiconductors due to strong fluorescence, good

hole-transporting ability, low redox potential and chemical/environmental stability.

In addition, carbazole moieties can also be easily functionalised at C-2, C-3, or *N*-positions to achieve good solubility and the desired magnitude of the thermal, optical, and electro-chemical properties, for example[50-51]. In particular, star-shaped, carbazole-functionalised triazatruxene materials with a central aromatic core and flexible aliphatic chains have been studied as potential organic semiconductors, especially for use in OLEDs & PLEDs due to the presence of intense luminescence and suitable hole-transporting ability[52]. The disc-like, C_3-symmetric triazatruxene can be considered as an extended π-system in which three carbazole units are sharing an aromatic ring. The chemical structure, resembling the classic hole-transporting carbazole and its planar disc-like nature, renders triazatruxene a potentially attractive hole-transporting materials[53]. Moreover, the starburst structure of triazatruxene can be characterised by superior structural uniformity and are capable of preventing close packing and spatial reorientation, thus suppressing self-aggregation and forming high-quality thin films[54]. Triazatruxenes synthesised from triindole have been rarely researched and reported[55] and the majority of research papers describe functionalised triazatruxene derivatives described alkyl-substituted intermediates and some oligomers[56-62].

The use of highly cross-linked polymer networks in stable and reliable OLEDs with good device performance has been extensively reported[63-72]. The main advantages of this approach to the fabrication of multilayer OLEDs are lower cost, scalability, i.e., the possibility to manufacture very large display devices, and the use of standard fabrication equipment and processes used to manufacture LCDs in a continuous, rather than a batch, production, process, e.g., the potential for continuous roll-to-roll manufacturing on plastic substrates.

The semiconducting and/or emissive photopolymerisable monomers and oligomers can usually be deposited from solution in common organic solvents using wet chemistry methods, such as ink-jet printing, doctor blade techniques, drop casting, spin coating,

etc., to form uniform thin films of the desired homogeneity and thickness on a device substrate. These organic semiconducting and/or emissive layers then become insoluble and intractable after photochemical cross-linking so that multi-layer OLEDs can be easily fabricated, layer-by-layer, without inter-layer mixing or dissolving existing layers, using standard photolithographic techniques used in the LCD industry. Furthermore, photopolymerisation facilitates pixellation, especially for full-colour OLEDs, by using standard photolithography processes, i.e., exposed areas are left as insoluble and intractable pixels with the desired shape and size whereas unexposed and non-crosslinked regions can be easily removed by washing with the original spin-casting solvent. Such processes can be carried out in a step-wise fashion to build up multilayer OLEDs with a minimum of photochemical damage to the organic semiconductors being converted into insoluble polymer networks.

In order to attain different optical/electro-chemical properties, a variety of conjugated aromatic structures, especially those based on photopolymerisable liquid crystalline monomers and oligomers, so-called reactive mesogens (RMs), have also been reported to combine with fluorene moieties to construct photoreactive, cross-linkable monomers in recent years[73-79], shown in **Fig. 1.12**.
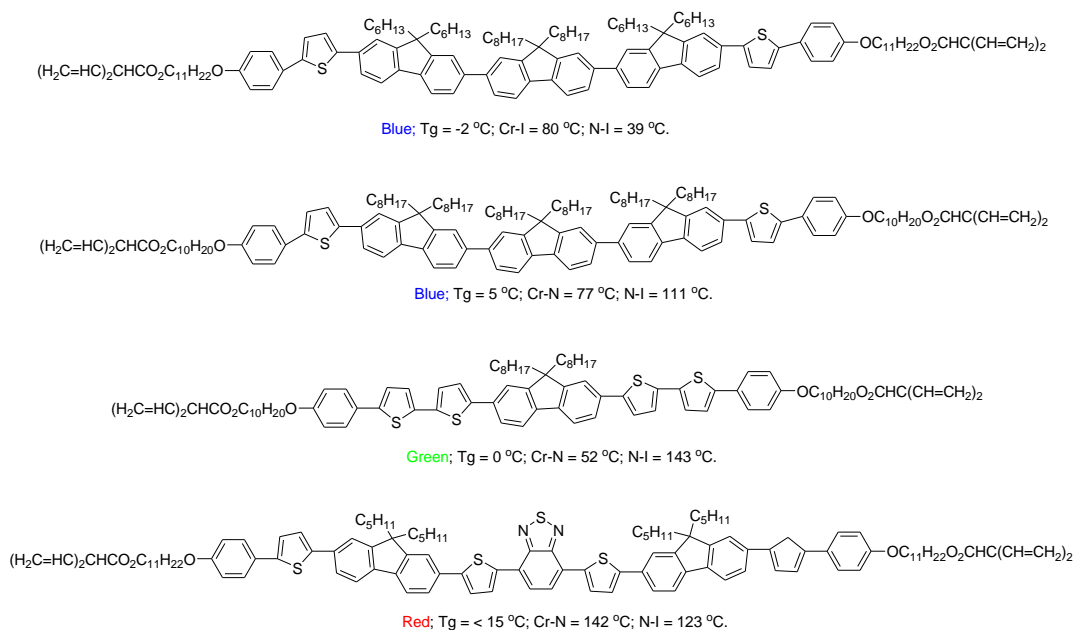
Fig. 1.12 The chemical structures of photoreactive, cross-linkable monomers

Photopolymerisation or cross-linking can be achieved either by thermal mechanism or photo-initiation to form free radicals normally using ultraviolet light in the absence of a photoinitiator or sometimes, e.g., for oxetanes, using a combination of UV-irradiation and ionic photo-initiators doped into the photopolymerisable monomers or oligomers [80, 73]. **Fig. 1.13** gives the general structures of polymer backbones formed from common methacrylate, acrylate, non-conjugated dienes and oxetane photo-reactive groups. Overall, methacrylate and acrylate reactive groups require less energy, i.e., a lower fluence of UV irradiation, to form highly cross-linked polymer networks than that required to photochemically crosslink dienes and oxetanes. Although non-conjugated dienes require relatively high exposure in order to be photochemically cross-linked to form stable polymer networks as stable, thin films, they are much less likely to spontaneously polymerise, e.g., during purification, than analogous acrylates or methacrylates. Oxetane reactive groups generally require the presence of a photo-initiator for polymerisation and cross-linking to occur.
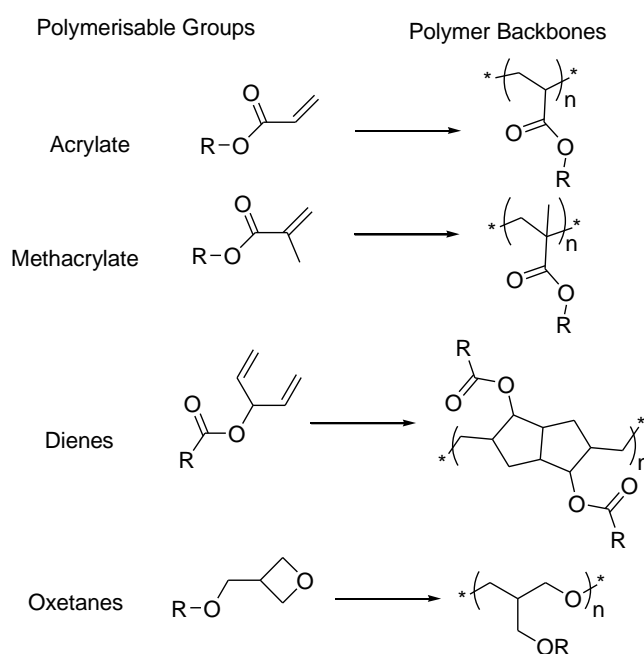
Fig. 1.13 Polymerisable groups and corresponding polymer backbones formed on polymerisation

Sometimes the photochemical cross-linking process can cause a reduction in the charge-carrier mobility, perhaps to the formation of deep traps, or due to the fact that the ordered layer structure might be disrupted when the polymerisable end-groups form a covalently bonded polymer backbone[73]. Sometimes the high fluence required to cross-link nematic reactive mesogens with non-conjugated diene photoreactive end-groups results in a reduction of the charge-carrier mobility determined using time-of-flight measurements[73]. In such case, doping some of the organic semiconductors layers in such OLEDs with a variety of p-type or n-type dopants could possibly be an approach to improve the charge carrier mobility.

1.4.2 LMMMs, Oligomers and Liquid Crystalline Semiconductors

LMMMs and oligomers can usually be purified to a higher degree, or at least with less effort, compared with highly conjugated main chain polymers. This is important as ionic impurities in low concentration can be impair the performance and shorten the lifetime of OLEDs & PLEDs. Moreover, small molecules can be readily dissolved at relatively high concentration in most common organic solvents, which facilitates deposition of homogeneous thin layers of the desired thickness from solution, e.g., by spin coating, drop casting, inkjet printing or doctor blade techniques. Vapour deposition under vacuum and at high temperature in order to fabricate thin films can be much more expensive compared with wet-chemistry deposition of uniform thin films from solution. The latter techniques can be used in continuous manufacturing processes, such as roll-to-roll printing.

As shown above, anthracene was the first low-molecular-mass organic electroluminescent material reported in 1963[15]. A big breakthrough for OLED materials came from the research of Tang et al who reported *tris*(8-hydroxyquinolinate)aluminium (III) (Alq_3) as an efficient combined emissive and electron-transporting material for bi-layer OLEDs in 1987[18-19]. Later Friend reported 2-(biphenyl-4-yl)-5-(tert-butylphenyl)-1,3,4-oxadiazole (PBD) as an efficient

electron-transporting material for bi-layer OLEDs & hybrid PLEDs[20]. In order to achieve glass transition above room temperatures and higher device efficiency, more efficient star-shaped PBD derivatives such as oxadiazole dendrimers (see **Fig. 1.14**) as electron-transporting materials, also have been developed[81].
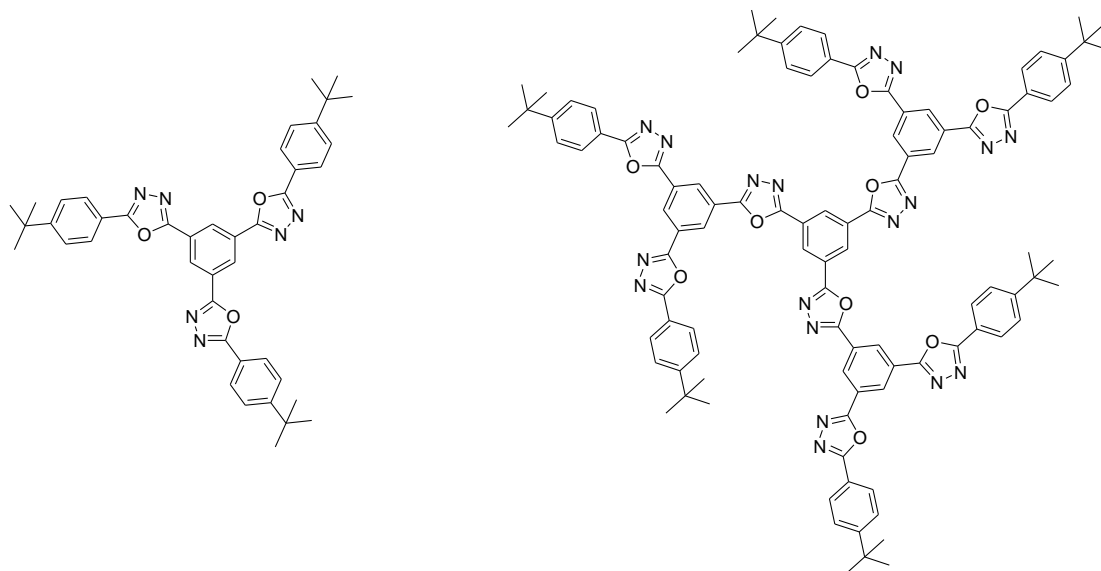
Fig. 1.14 The chemical structures of oxadiazole dendrimers

Pentacene was among the first conjugated organic oligomer semiconductors reported by Gundlach and co-workers[82]. Oligothiophenes are one of the most common organic semiconductors due to the presence of high conjugation and low energy gaps. Moreover, thiophenes allow the possibility of fuctionalisation so that desired chemical modifications can be achieved[83-84, 49]. Furthermore, nitrogen-containing oligomers such as triarylamine, carbazole and triazatruxene, have also been studied as good hole-transporting materials for optical-electrical devices in recent years[85-89, 82, 53, 49]. The chemical structures of various oligomers incorporating thiophene moieties or nitrogen-atoms were shown in **Fig. 1.15**.
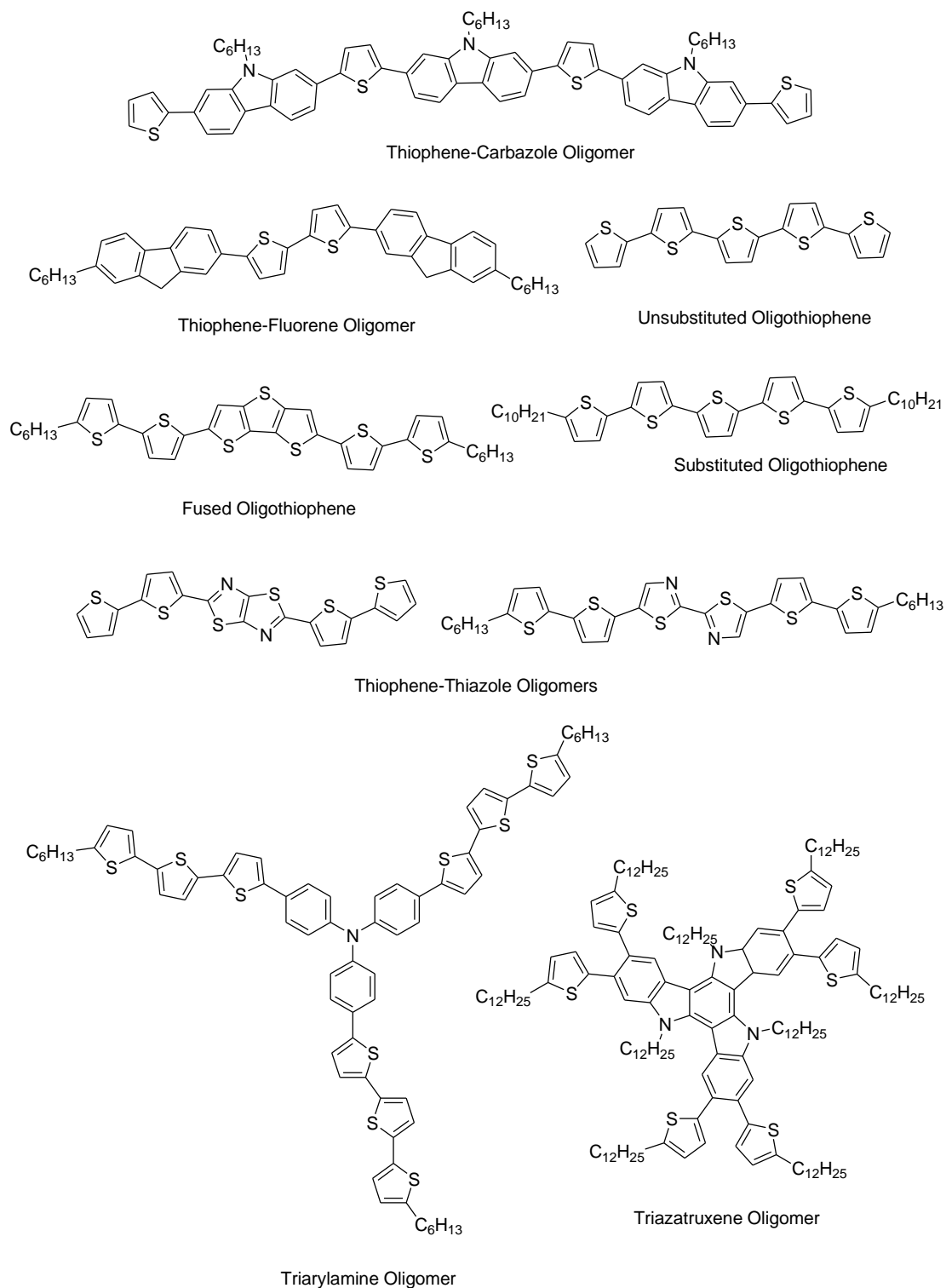
Fig. 1.15 The chemical structures of various oligomers

Many LMMMs and oliogmers are often used as hole-transporting materials for OLEDs & PLEDs due to the presence of a high degree of delocalised electrons in conjugated aromatic cores, e.g., a very wide range of triarylamine derivatives have received much

attention due to a combination of advantageous properties, such as intrinsically high values for hole mobility and efficient vacuum deposition of uniform thin films of the desired thickness[90-93]. Some typical derivatives such as TPD and NPD, were reported and their chemical structures are shown in **Fig. 1.16**[94-97]. However, these triarylamine with relatively simple structures are more likely to crystallise during the lifetime of devices due to low glass transition temperatures. Vacuum deposited TPD, for instance, was found to crystallise at room temperature after a few hours of device operation[97]. Therefore, the TBD with a spiral molecular structure, see **Fig. 1.16**, was synthesised and found to exhibit a significantly higher glass transition temperature and device stability[98].
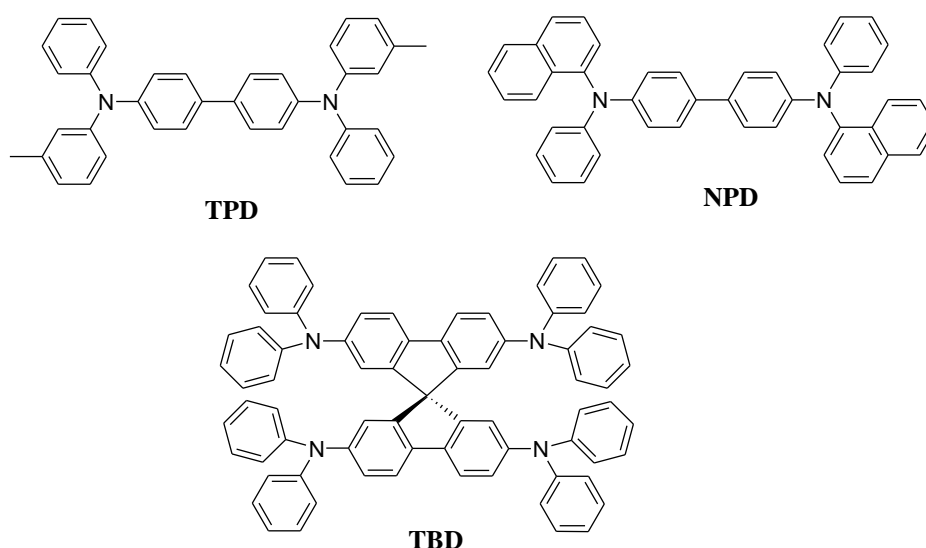
Fig. 1.16 The chemical structures of triarylamine derivatives TPD, NPD and TBD

However, many LMMMs or oligomers can form crystal boundary defects as traps for quenching of electrons or holes injections due to the absence of glass transition significantly above room temperature. As an attempt to address this issue, liquid crystalline LMMMs or liquid crystalline oligomers were prepared for use in plastic electronic devices, such as OLEDs, OPVs and OFETs, due to the presence of liquid crystalline mesophases, with the desired transition temperatures, and a glass transition above room temperature. A combination of these attributes leads to the absence of crystalline grain boundary defects in thin films of this new class of organic

semiconductor[80]. Extensive research has been carried out to establish the relationship between liquid crystalline mesophases and optoelectronic performance of liquid crystalline displays (LCDs)[99]. However, in recent years, researchers have realized that liquid crystalline mesophases and appropriate transition temperatures contributes to an achievement of high charge-transport mobility in OLEDs, OFETs, OPVs, etc.[80, 99].

Common liquid crystalline mesophases include nematic, smectic and columnar (discotic). Columnar liquid crystalline first attracted interest as components of OLEDs due to the nature of their columnar phases. More precisely, the aromatic cores of the discotic molecule are arranged above each other in fluid columns, so that the overlapping π-electron orbitals in neighbouring conjugated aromatic cores facilitate high values of the charge carrier mobility[100]. Typical columnar liquid crystalline semiconductors of interest for application in plastic electronics are hexa-substituted triphenylene derivatives, which exhibit large values for the charge carrier mobility, such as the hexagonal columnar phase *hexakis*(*n*-alkoxy)triphenylenes (see **Fig. 1.17 a**)[101-102].

Cr 193 °C **D** 197 °C **I**

(a)

Cr 90 °C **SmA** 100 °C **I**

(b)
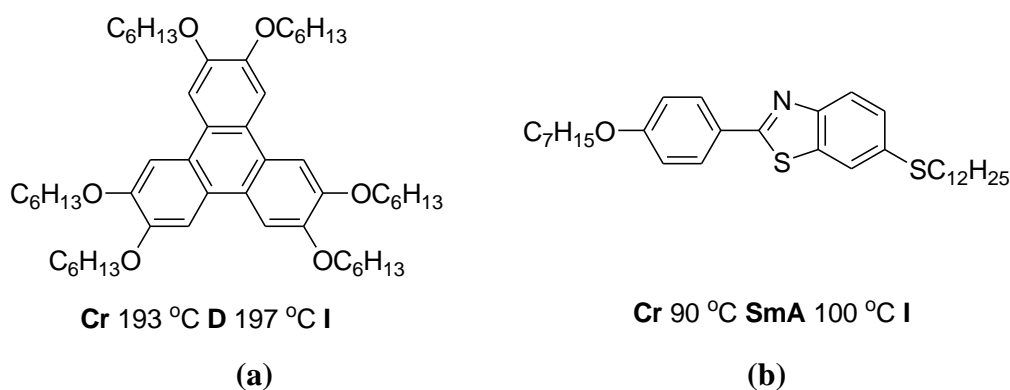
Fig. 1.17 Liquid crystal structures of the *hexakis*(*n*-alkoxy)triphenylenes **(a)** and heterocyclic thiobenzazole **(b)**

Smectic liquid crystals also have a relatively highly ordered structure comprised of layers of molecules with a rod-like, calamitic structure. Therefore, smectic liquid crystals were also investigated as potential organic semiconductors for use in plastic electronic applications. Some smectic materials, such as the highly conjugated heterocyclic thiobenzazole, see **Fig. 1.17 b**, were indeed found to exhibit high values

for the hole mobility primarily due to their low ionization potential attributable to the highly electron-rich aromatic core[103-104].

Nematic mesophases with the least ordered structure of the many different types of liquid crystals have low viscosity, so they can be easily ordered or macroscopically aligned in thin films at low temperatures[80]. Nematic liquid crystals possess orientational order and no positional order. In terms of optical-electrical applications, the presence of orientational order can lead to a favourable Forster energy transfer in guest-host system, which involves a dipole-dipole interaction between an excited donor and ground-state acceptor so that excitation is spatially transferred to the latter and the efficient energy transfer leads to an extremely low threshold fluence for optically pumped lasing[80]. The anisotropic liquid crystalline properties as visible light-emitters can also reduce the laser threshold in thin film lasers. The oriented film shows lower loss due to the higher optical quality of a monodomain sample. Furthermore, Many nematic or smectic liquid crystals spontaneously adopt homogeneous (in-plane) alignment in mesophase state and thus can enhance outcoupling[80]. In terms of thermal properties, liquid crystalline mesophases exhibit preferred transition temperatures, i.e., glassy state above room temperature and high clearing point, which results in the favourable absence of crystal boundary defects as traps for quenching of electrons or holes injections. Many nematic liquid crystalline semiconductors as charge-transporting materials have now been reported[73]. Therefore, the design and synthesis of novel liquid crystalline materials are becoming increasingly important for efficient optoelectronic applications, such as OLEDs, OFETs and OPVs.

The oligomers with liquid crystalline mesomorphic behaviour combine the advantages of ordered mesophases, designed transition temperatures and high chemical purity. In contrast to polymers, liquid crystalline oligomers can avoid the decrease of charge carrier mobility after polymerisation or cross-linking. Furthermore, oligomers are capable of preventing condense packing and spatial re-orientation, thereby restricting self-aggregation and fabricating high-quality thin films, compared with small

molecules. Some typical chemical structures of liquid crystalline oligomers are collected in **Fig. 1.18**[73].

Cr-SmC = 92 °C; SmC-SmA = 111 °C; SmA-N = 115 °C; N-I = 180 °C.

Cr-SmX = 316 °C; SmX-I = 351 °C.

Tg = 46 °C; Cr-N = 55 °C; N-I = 235 °C.

Tg = 102 °C; N-I = 240 °C.
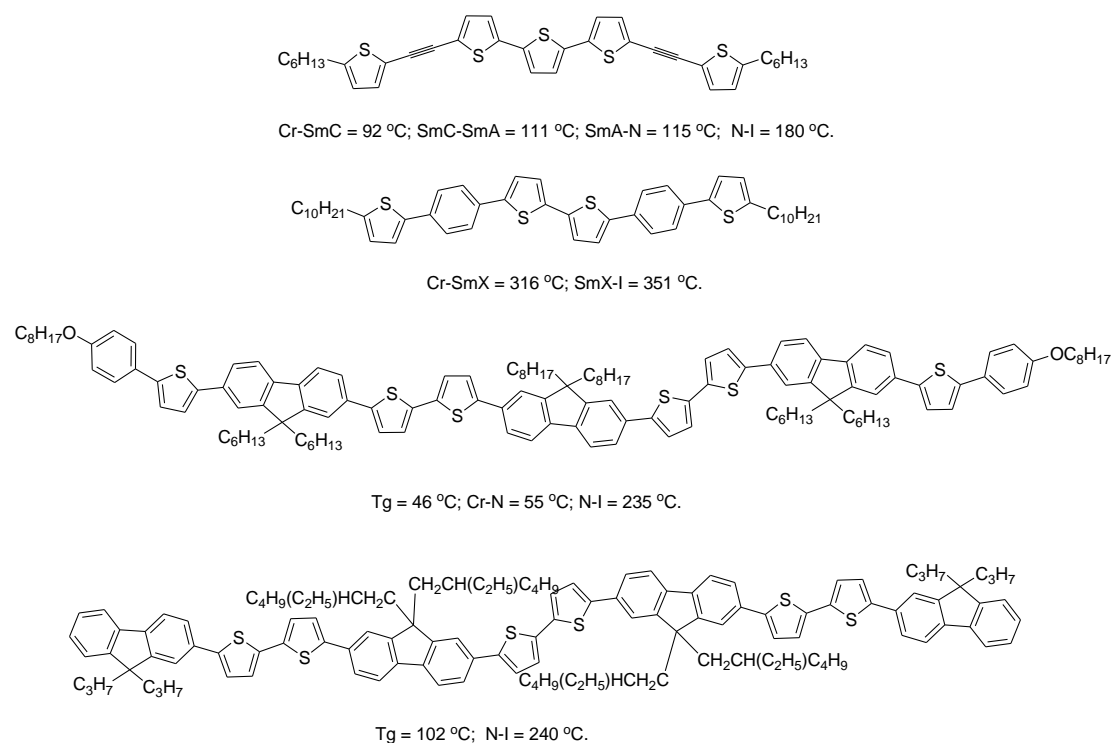
Fig. 1.18 Some typical chemical structures of liquid crystalline oligomers

The structural design of liquid crystalline materials depends on the desired role, such as transporting holes or electrons or/and emitting visible light, for plastic electronic applications. The charge-transporting materials, for instance, should be designed to possess appropriate HOMO and LUMO energy levels to match the work function of the anode and the cathode, respectively. The different colour and brightness of emissive materials can also be achieved by the modification of molecular structures, especially by the design of aromatic cores and functional groups, as required. Some typical aromatic cores are shown in **Fig. 1.19**.
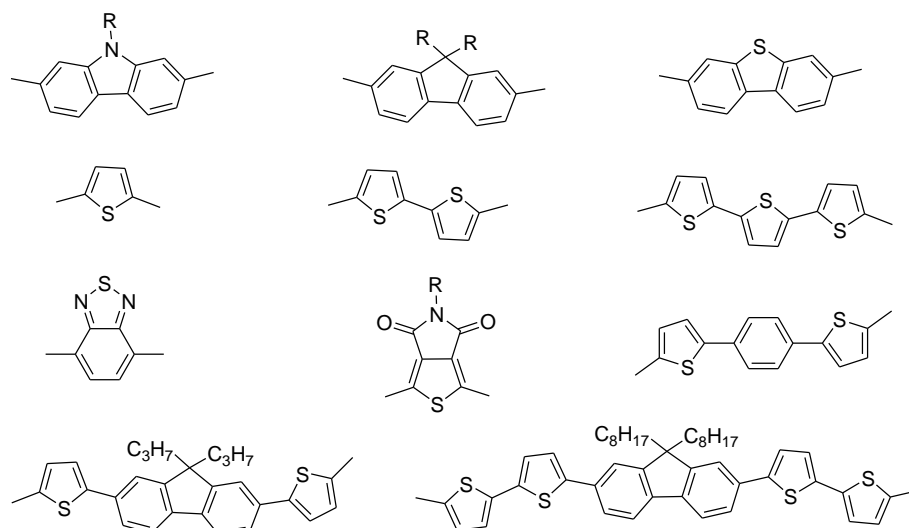
Fig. 1.19 Some typical aromatic cores for constructing optical-electrical materials

A systematic study of liquid crystalline LMMM or oliogmers organic semiconductors is of particular importance, because it can precisely identify the relevance of molecular structures, liquid crystalline mesophases, and optical/electro-chemical properties. Liquid crystalline LMMMs or oliogmers with sophisticated functionality are now key components in molecular electronics[105-106]. In addition, the flexible nature of the alkyl- and alkoxy-chains in lateral and/or terminal positions of liquid crystalline organic semiconductors results in good solubility in common organic solvents used in the wet-chemistry deposition of thin films from solution.

In particular, such aliphatic chains are readily functionalised with polymerisable end-groups. The substitution is usually carried out as the last step for synthesising polymerisable precursor due to the weak tolerance of polymerisable groups, e.g., non-conjugated dienes, in organic reactions. Therefore, the transformation of liquid crystalline LMMMs or oligomers into polymerisable liquid crystalline precursors is feasible and facile where required. In brief, the synthesis of liquid crystalline LMMMs or oligomers is one of the most essential and indispensable areas of research into organic semiconductors.

1.5 Liquid Crystals

The term "liquid crystals" refers to a state of matter in between that of liquids and solids. Of course, the difference between crystals and liquids, the two most common condensed matter phases, is that the molecules in a crystal are ordered in a regular pattern and there is still a high degree of order in amorphous, non-crystalline solids, whereas in a liquid there is no order at all. Liquids are fluid and flow to fill a void, whilst solids are immobile. Interestingly enough, many phases with more order than that present in liquids, but less order than that typical of crystals, also exist in nature, as seen in **Fig. 1.20**. These phases are grouped together and called liquid crystals, since they share properties normally associated with both liquids and crystals.
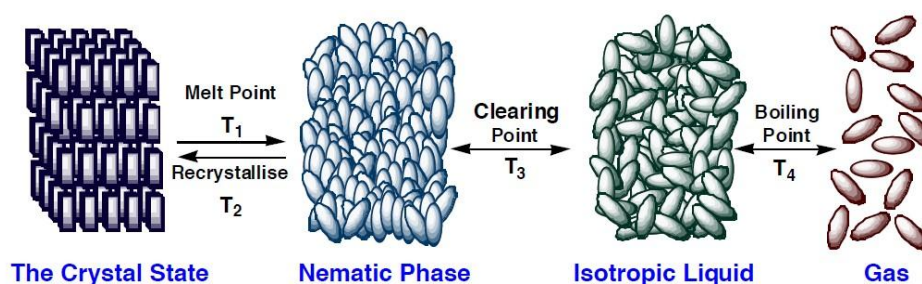
Fig. 1.20 Schematic arrangement of molecules in various phases - taking a nematic phase as an example

Liquid crystals are currently an important phase of matter both scientifically and technologically. They are recognised as a stable phase exhibited by many compounds, thus putting them on equal footing to the solid, liquid, and gas phases. It has been postulated that one of every ten new compounds synthesised is a liquid crystal. This situation is not a recent development and liquid crystals have been used in Liquid Crystalline Displays (LCDs) for over 40 years. It is both interesting and informative to review briefly how the present understanding of this phase of matter developed.

1.5.1 Historical Development

The discovery of liquid crystals is usually attributed to an Austrian botanist by the name of Friedrich Reinitzer[107]. In 1888, he experimented with a substance, he had synthesised called 'cholesteryl benzoate' and noted that it had two melting points. At 145.5℃ it melted from a solid to form a cloudy liquid, and at 178.5℃ it turned into a clear liquid. He also observed some unusual optical behaviour upon heating and cooling the sample. First a pale blue colour appeared as the clear liquid turned cloudy and second a bright blue-violet colour was present as the cloudy liquid then crystallised. These colours were temperature-dependent and varied with the viewing angle.

Reinitzer sent samples of this unusual substance to Otto Lehmann, a professor of natural philosophy (physics) in Germany. Lehmann was one of the few people studying the crystallisation properties of various substances using an optical, polarising microscope that he had developed and Reinitzer wondered whether what he had observed was related to what Lehmann was reporting. Lehmann had constructed an optical polarising microscope with a heating stage on which he could precisely control the temperature of his samples. This instrument allowed him to observe the melting and recrystallisation of the sample under controlled conditions. Lehmann observed Reinitzer's substance with his microscope and noted its similarity to some of his own samples. He first referred to them as soft crystals. As he became more convinced that the opaque phase was a uniform phase of matter sharing properties of both liquids and solids, he began to call them 'Krystalline Flussigkeiten' translated as crystalline liquids or now more commonly liquid crystals[108].

Gatterman and Ritschke prepared the first totally synthetic liquid crystal with the synthesis of *p*-azoxyanisole in 1890[109]. One of the most important aspects in liquid crystals development was the mesophase classification introduced by a French chemist Georges Friedel in 1922[110]. The terminology of different types of liquid crystals, 'the nematic, smectic, and cholesteric phases', were coined and published in his research

paper 'Les Etats Mesomorphes de la Matière'. Furthermore, several scientists, such as Fréedericksz[111], Born[112], Kast[113], and Lichtenecker[114], investigated the influences of electric and magnetic fields on the physical properties of liquid crystalline phases. In 1950s, Onsager[115] and Flory[116] theoretically predicted the relationships between the critical conditions and molecular structural parameters when liquid crystal line phases were formed from rigid molecular solutions of rigid rod polymers. This prediction offered a research guide of polymer liquid crystals and promoted its further development.

Interest in liquid crystals and research related to them lapsed to a large degree in the inter-war years partly due to the lack of any obvious application for them, in spite of the fact that the basic underlying physics behind the operation of LCDs, e.g., the electrooptic response of the nematic phase to applied magnetic and electric fields, the ability to homogeneously align the nematic phase of flat device substrates and the generation of homogenous and homeotropic alignment and a twisted structure for the nematic phase, wave-guiding and the birefringent nature of the nematic phase, etc., see below, having been studied and reported.

Shortly before 1960, interest in liquid crystals reawakened in the United States, Great Britain and the Soviet Union in particular. This renaissance was probably due to the attraction of electro-optical applications, but it was also recognised that these phases were also scientifically significant. During the 1970s and 1980s, research activity on liquid crystals exploded. A series of LCDs were invented in the late 1960s and early 1970s. These early reports of flat-panel displays encouraged and stimulated more sustained research effort into liquid crystals in general and the synthesis of new liquid crystalline materials for use in LCDs in particular. Glenn Brown, an American chemist, established the Liquid Crystal Institute at Kent State University in 1965 and for during that period a special working group for liquid crystal research was also founded in Moscow by I. G. Chrystyakov[117].

George Gray[118], a British chemist, published a full-length book entitled 'Molecular

Structure and Properties of Liquid Crystals' in 1962, which played a vitally important role in the future research and development of liquid crystals. Furthermore, the nematic liquid crystals 4'-alkyl-1,1'-biphenyl-4-carbonitriles, especially 4-pentyl-4'-cyanobiphenyl (see **Fig. 1.21**), synthesised by Professor Gray's colleagues[119-122] at the University of Hull in the early 1970s, is of landmark significance in the development history of liquid crystals. They can be presented as liquid crystalline phase with the advantages of being photochemically, chemically, thermally and electrochemically stable over a significant temperature range above room temperature. The cyanobiphenyls started a new era in flat panel displays using liquid crystal materials and especially room-temperature mixtures of chosen homologues of 4-alkyl-4'-cyanobiphenyls, 4-alkoxy-4'-cyanobiphenyls and 4-alkyl-4'-cyano-terphenyls in industrial and commercial LCDs.

C_5H_{11}——⬡——⬡——CN

4-Pentyl-4'-cyanobiphenyl (**5CB**)
Cr 24 °C **N** 35 °C **I**
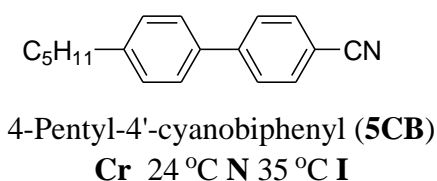
Fig. 1.21 Nematic liquid crystalline of 4-pentyl-4'-cyanobiphenyl

There are many kinds of other liquid crystals that can be used in electro-optic devices. For example, in 1975, Mayer, et al[123] synthesised the liquid crystal '4-decyloxybenzylidene-4'-amino-2-methylbutylcinnamate' and discovered its ferroelectric properties for the first time. In 1980, N. A. Clark and S. T. Largerwall[124] described an improved model of the electro-optical response of a new kind of ferroelectric liquid crystal display.

In 1977, Chandrasekhar S[125] initially published research papers about the synthesis and characterisation of discotic liquid crystals, which are now used in a modified form as optical compensation layers in LCDs.

Currently, liquid crystals have become a part of our daily life, from wristwatches and pocket calculators to displays in all kinds of instruments, including portable computers, iPads, iPods, mobile telephones and flat-panel televisions. The advantages of liquid crystal devices can be summarised as low power consumption, low-voltage operation, thinness and low weight. Furthermore, liquid crystals compete with other flat-panel display technologies for attractiveness, ease of viewing, cost, and durability.

Moreover, the research and development of liquid crystals have taken them way beyond just the field of displays. Scientifically, liquid crystals play an essential role in interdisciplinary research, which are involved with chemistry, physics, mathematics, engineering, biology, etc, for a wide range of applications, such as photochromics, pressure sensitive paints, optical retarders and optical compensation films, organic semiconductors for use in plastic electronics, etc.

1.5.2 Mesomorphic Behaviour of Liquid Crystals

The general classifications of liquid crystalline can be summarised according to its derivation, mesogenic structures and molecule weight. The definitions of thermotropic and lyotropic liquid crystals are proposed on the basis of temperatures and solvents, respectively, i.e., the presence of a solvent is required for the formation of a wide range of lyotropic mesophases, whereas thermotropic mesophases are observed for single compounds on heating and cooling in the complete absence of solvents.

The research of liquid crystalline for optoelectronic applications is mainly focused on thermotropic liquid crystals due to the requirements of individual types of devices. Thus, there is no detailed discussion for lyotropic liquid crystals in this thesis, although they are used widely for a broad range of other applications.

Thermotropic liquid crystals mainly involve lathe-like, rod-like or calamitic molecular structures and disc-like, planar molecular structures. The rod-like liquid crystals, also known as 'calamitics', can be subdivided into nematic, smectic A, smectic C, etc,

according to the degree and type of the order and structure of their mesogenic phases. The columnar liquid crystalline phases are one of the most common and are usually formed by compounds with a discotic, flat, planar, rigid disk-shaped molecular structure. In addition, liquid crystalline molecules can be classified in a general way into low-molar-mass molecules (LMMMs), oligomers, (mainchain or sidechain) polymers and polymer networks according to size and molecular weight. The schematic representation of general classifications for liquid crystals is shown in **Fig. 1.22** as below.
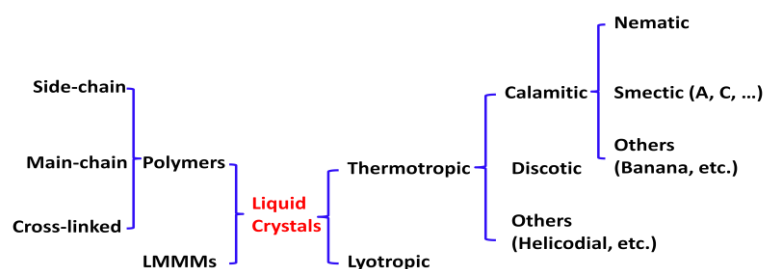
Fig. 1.22 The schematic representation of general classification of liquid crystals

1.5.2.1 Calamitic Liquid Crystals

Calamitic, rod-like liquid crystals are one of the most useful materials for opto-electrical and electrooptic applications such as LCDs and OLEDs. A general molecular structure of rod-like liquid crystals is shown in **Fig. 1.23**.

Fig. 1.23 A general structure of rod-like liquid crystalline

The rigid backbone is typically constructed by aromatic/cycloaliphatic A and B which are linked by bridged-bond groups (Y) such as carboxy ($-CO_2-$), ethenyl (-CH=CH-) or ethyl ($-CH_2CH_2-$). A and B can also be directly linked without the bridged-bond. Such rigidity contributes to the anisotropy of calamitic molecules, but the presence of liquid crystalline phases still requires relatively molecular flexibility resulted from aliphatic chains (R and R') such as straight alkyl or alkoxy groups. The linking groups (X and Z) usually consist of hetero-atoms such as the oxygen atom. The introduction of lateral

chains (M and N) can be used to modify the physical properties and mesomorphic behaviour of the materials, although lateral chains is adverse to the formation of liquid crystalline mesophases due to a broadening of the molecular rotation volume, *i.e.,* the reduction of the length-to-breadth ratio.

Smectic and nematic phases are the most common and important liquid crystalline mesophases. A common rule is that compounds with two shorter terminal alkoxy or alkyl chains tend to exhibit a nematic phase because the longer terminal chains may induce a layer structure, which contributes to the presence of smectic mesophases. An empirical order of terminal groups for the tendency of inducing nematic phase formation is established below, although the order does vary with different molecular structures in some cases[126].

$$RO > R > CN > OCH_3 > NO_2 > Cl > Br > CH_3 > I > F > H$$
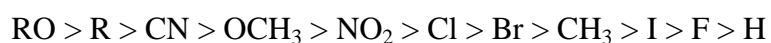
1.5.2.2 Nematic Liquid Crystals

The nematic liquid crystalline mesophase maintains a preferred one-dimensional orientational order, but no long-range positional ordering is present in the nematic phase. Specifically, the rod-like molecules tend to align with the molecular long axis pointing more-or-less in the same direction, which is called the nematic director (n). The molecular alignment of the nematic mesophase is shown in **Fig. 1.24**.
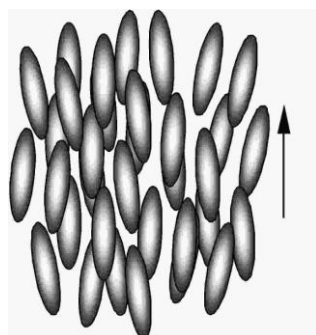
Fig. 1.24 The molecular alignment of the nematic mesophase

The term 'nematic' is derived from the Greek word '*nematos*' meaning thread-like and

was probably coined to describe this state of matter due to the appearance of nematic Schlieren texture observed using polarised optical microscopy (POM). A typical Schlieren texture with two- and four-point brushes or point defects, characteristic of a nematic is seen in **Fig. 1.25**.

Fig. 1.25 A typical nematic Schlieren texture (Compound **46** on cooling at $130\,^{o}$C)

The rod-like molecules in the nematic phases can rotate freely along their short molecular axes and, to some degree, along their long molecular axes. The macroscopic order parameter, *S*, is employed to represent the degree of molecular average orientation relative to the director. The parameter equation is shown below:

$$S = \frac{1}{2} < 3\cos^2 \theta - 1 >$$

Where θ is the angle between the long axis of each molecule and the director (n), and *S* can vary from 0 to 1. For completely disordered liquid molecules with rod-like structures, *S* is zero. However, a value of *S* = 1 indicates that all the rod-like molecules are ideally aligned parallel with the director and the phase is completely ordered, such as in a perfect crystalline solid. In terms of nematic mesophases, the value of *S* generally lies from 0.4 to 0.7.

1.5.2.3 Smectic Liquid Crystals

Smectic phases, which appear at lower temperatures than those observed for a nematic phase, if present, are more ordered than the nematic phase because smectic molecules are aligned within relatively fluid layers, which may also be described as density waves. Compared with one-dimensional orientational ordering of nematic phases, smectic phases exist both orientational and positional ordering due to the presence of layer structures.

Smectic phases can be divided into several types including five liquid crystalline smectic phases (SmA, SmB, SmC, SmI, SmF) and six crystal smectic phases (B, J, O, E, K, H) according to the mobility of the layers and the different orientations of the molecules within the layers. The molecular long axis in respect to the layer plane, for instance, can be orthogonal or titled for smectic A or C phases, respectively. The two typical molecular structures of smectic A and C phases are shown in **Fig. 1.26 (a) and (b)**, respectively.

(a)   (b)
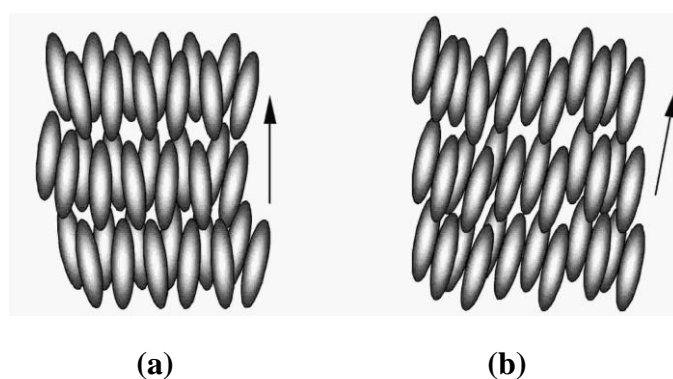
Fig. 1.26 The molecular alignments of Smectic A **(a)** and Smectic C **(b)** mesophase, respectively

1.5.2.4 Columnar Liquid Crystals

Columnar mesophases are exhibited by molecules consisting of disc-shaped aromatic cores, such as triphenylene, porphyrin, truxene moieties, stacked above each other in fluid columns. The intercolumnar distance (about 150-400 nm) is much bigger than the

intracolumnar distance (less than 45 nm), depending, to some degree, on the conformational mobility and length of flexible aliphatic chains, such as alkyl- and/or alkoxy-chains attached to the highly conjugated aromatic cores. The columnar arrangement of the rigid, planar and disk-shaped aromatic cores allows the overlap of π-electron orbitals of neighbouring conjugated molecules, which facilitates the charge carrier migration and transport along the length of the column[100].

However, columnar molecules within the stacked discs can be titled or even disordered, with respect to the columnar axis, thus giving rise to different types of columnar phases, such as hexagonal, orthorhombic columnar phases. The nematic columnar phase possesses no columnar order and exhibits the lowest degree of order of all the columnar mesophases. The molecular alignment of typical nematic discotic **(a)** and columnar **(b)** liquid crystals is shown in **Fig. 1.27.**

(a) (b)
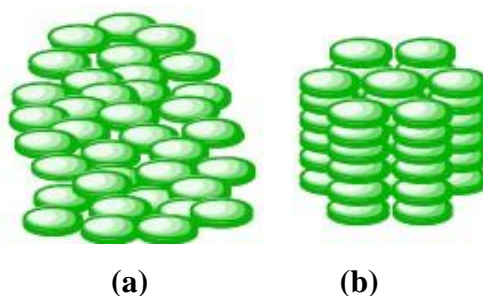
Fig. 1.27 The molecular alignment of typical nematic discotic **(a)** and columnar **(b)** liquid crystals

1.5.3 Characterisation of Liquid Crystalline Mesophases

The characterisation and identification of liquid crystal phases or mesophases are of great importance taking into account the fact that liquid crystal phases are the fourth state of matter. However, this is often not a simple matter as there are many different types of liquid crystal phases, which can be characterised, identified and classified according to the molecular ordering present in each of the particular mesophase types.

Liquid crystals appear opaque to the naked eye due to director fluctuations in the bulk

of non-aligned samples. However, the observed difference between many different liquid crystal phases or mesophases is generally minimal to the naked eye. Several additional instrumental equipment and analytical techniques are indispensable in the identification of the kind of mesophases to be determined and the temperatures at which liquid crystalline transition occur. Some of most widely used techniques used for liquid crystal phase identification include optical polarising microscopy (OPM), differential scanning calorimetry (DSC), and X-Ray analysis (XRD). However, the XRD is not always required because the combined technique of OPM and DSC usually proves sufficient to identify common liquid crystalline mesophases such as nematic, smectic A or smectic C phases. X-ray is more useful in the identification of highly ordered phase structures such as smectic or crystalline phases.

1.5.3.1 Optical polarising microscopy

The most widely used and basic methodology to identify liquid crystalline phases is polarised optical microscopy (POM), which depends on the identification of unique optical textures for characteristic of the different liquid crystal mesophases. If a liquid crystalline material is situated on a temperature-controlled hot-stage between two crossed polarisers, the characteristic Schlieren texture with two- and four-point brushes can be observed under the microscope over a certain temperature range. The textures observed are often influenced by the presence of defects in other mesophases (paramorphasis) present for a given material. This technique allows a preliminary identification of liquid crystal mesophases. The common and simple liquid crystal phases, such as nematic, smectic A and smectic C, can be identified in a relatively straightforward manner. However, the more ordered phases can be difficult to identify based on optical microscopy alone and it can require other analytical techniques used in combination, such as DSC and XRD, to identify same phases.

1.5.3.2 Differential Scanning Calorimetry

After optical microscopy, differential scanning calorimetry (DSC) is the most widely

used and useful technique for the identification of a liquid crystalline mesophase. Microscopy is a complimentary technique, but not all optical transitions correspond to a phase transition, or alternatively not all phase transitions are accompanied by an obvious change in optical texture. However, DSC reveals the presence of phase transitions in a material by detecting the enthalpy change associated with each phase transition. The DSC instrument measures the energy absorbed or released by a sample as it is heated or cooled.

For liquid crystals, transitions between phases are usually thought of as being weakly first order, although second order transition transitions are not uncommon. The melting transition is, however, always first order. Typical enthalpy changes between successive liquid crystal phases or between an liquid crystal phase and an isotropic liquid are usually small at around 1 kJ/mol, while transitions between a crystal and a liquid crystalline phase are strongly first order and often in the range 30-50 kJ/mol.

In terms of polymer liquid crystals, it can be difficult to observe the expected transitions between mesophases and their characteristic textures due to the extremely high viscosity of the mesophases of polymeric liquid crystals that hinders the flow required for the formation of these typical optical textures. However, there is an added feature of the DSC traces of most polymer liquid crystals - the glass transition (Tg). This is a fundamental property of polymers and is accompanied in the DSC by a change in baseline. Therefore, the glass transition is a second order event.

1.5.4 Liquid Crystal Displays

When it comes to liquid crystal research, it is almost impossible not to refer to liquid crystal displays (LCDs). In the past half-century, countless facts demonstrate that liquid crystals as a class of functional materials and liquid crystal displays (LCDs) are inextricably linked together. Liquid crystal displays have become the domain flat panel display (FDP) whose turnover is expanding continually, although other FDP technologies, such as OLEDs and PLEDs are taking market share from LCDs.

As described in more detail above, it has been noted that liquid crystals were discovered more than 100 years ago by Reinitzer[107] and Lehmann[108] and the opto-electrical properties of liquid crystals were also described in early works[127]. However, it was not until late 1960s, that the first operational liquid crystal displays were fabricated by Heilmeier et al[128] working at the RCA laboratories based on what he called the 'dynamic scattering mode'. The dynamic scattering (DS) effect, using liquid crystals with a negative dielectric anisotropy, is characterised by a strong scattering of light when the electric field exceeds a certain threshold value. The first room temperature liquid crystal compound, MBBA (4-methoxybenzylidene-4'-n-butylaniline), synthesised by German researchers[129], is suitable for DS-LCD applications reported in 1969. However, these kinds of nematic compounds have relatively low clearing point and practical LCDs require a higher clear point and a lower melting point. Furthermore, the disadvantages of DS-LCD are considerable, including high operating voltages, considerable current and low working lifetime due to the doping of electrolytes. The combination of these disadvantageous features inhibited the widespread application, market uptake and general commercialisation of DS-LCDs. However, as the first liquid crystal display, the DS-LCD is of great historical significance.

The first commercial twisted nematic (TN) LCDs, which were reported by M Schadt and W Helfrich, appeared in the early of 1970s[130]. As a field effect mode, the TN-LCD had a number of advantages over the previously known electro-optic modes. TN-LCDs provide black-and-white switching under low applied voltages with relatively fast response time and low power consumption. The TN-LCD exhibits a sufficiently long lifetime of TN-LCDs due to the absence of electrochemical degradation of the liquid crystal material. However, TN-LCDs with high information exhibit poor contrast and very narrow viewing angles. Thus, only small and medium-size TN-LCDs, such as digital calculators, watches, clocks, etc., were produced initially.

Although the TN mode represented a big step forward in comparison with the DS mode, the direct addressing technology used in the first TN-LCDs only allowed up to dozens

of rows of information to be displayed. This performance is not sufficient for the fabrication of personal computers or TV screens due to a low steepness of the transmission-voltage characteristics (TVC). In an attempt to address these problems, Super Twisted Nematic (STN-) LCDs with high information content were discovered by Scheffer and Nehring in 1984[131]. STN-LCDs provide passive addressing of up to 512 rows, for example, due to the increased steepness of the Transmission Voltage Curve (TVC) and also allowed for much wider viewing angles. Later, new ways of simultaneously and actively addressing rows, combined with multiline selection, considerably improved the response times and the contrast ratio of STN-LCDs, opening up the possibilities of their application in video monitors and desktop computers, PDAs and mobile telephones, for example.

The appearance of Thin Film Transistor (TFT) LCDs transformed the LCD market for very fast, very high-information-content displays and started a new era of large-area LCD manufacture. TFT-LCDs make use of active matrix addressing which is different from traditional multiplexed addressing (passive). In active matrix-addressed displays, each pixel is connected to a nonlinear element, so that the required level of voltage is maintained during the whole frame period, thus providing the necessary level of contrast. Active matrix-addressed TFT-LCDs with high information content became the dominant LCD types in 1995 when their price unexpectedly and dramatically fell[132]. TFT-LCDs are mainly used in lap-top computers, LCD TVs, computer game consoles, video monitors, mobile telephones, iPads, iPods, etc.

However, the nature of LCDs, i.e., it is a light valve with a transmission factor of ca 10%, means that most LCDs, except for the simplest applications, require a powerful back-light[99]. This leads to a much higher power consumption and lower device efficiency compared with OLEDs & PLEDs that emit their own light and thereby do not require a back-light. Therefore, OLEDs & PLEDs will definitely play an increasingly important role in the flat panel display industry in the future.

1.6 Organic Photovoltaics (OPVs) Devices

Organic Photovoltaics Devices (OPVs) are solar cells, which use organic semiconductors to convert the energy of light, usually visible light, but sometimes infrared or ultraviolet radiation, into direct electric current. Compared with inorganic solar cells, most commonly silicon-based photovoltaic devices, OPVs, using organic materials, should be cheaper and much easier to manufacture particularly for large-area devices. Unfortunately, the power conversion efficiency of OPVs, under standard sunlight irradiation conditions, still remains lower than that of inorganic solar cells. The cost of inorganic solar cells has been steadily reduced, as the efficiency has been continuously improved, over the last fifty years, so that such solar cells are now competitive in many parts of the world with most other standard sources of electricity generation. Therefore, significantly more efficient organic semiconductors need to be designed and synthesised for future OPVs with a power conversion efficiency high enough for OPVs to be competitive even in niche markets.

The greater ruggedness and flexibility of OPVs compared to standard PVs are additional advantages for some niche markets, especially in the developing world. The main potential advantages of OPVs, although still to be realised, are lower cost and scalability, i.e., the possibility to manufacture very large solar cells, and the use of standard fabrication equipment and processes used to manufacture LCDs in a continuous, rather than a batch, production, process, e.g., the potential for continuous roll-to-roll manufacturing, especially on plastic substrates.

1.6.1 Working Principles of OPVs

A typical device configuration of a typical bi-layer OPV is shown in **Fig. 1.28**. It contains an electron-accepting (EA) layer and an electron-donating (ED) layer, sandwiched between two electrodes with different work functions in order to form a diode configuration. One of the electrodes is transparent in order to facilitate the

transmission of incident light. The electron-donating materials should have a low ionisation potential (IP), while the electron-accepting materials should have a high electron affinity (EA). On illumination with incident light, the photo-generated excitons diffuse to the EA/ED interface, where they may be ionised to generate free electrons and holes, if the difference between the IP and EA energy levels of the organic EA and ED materials at this interface is greater than the exciton binding energy. The electrons and holes generated migrate towards, and are then collected, at the positive and the negative electrodes, respectively, as long as they do not recombine or become trapped before reaching the eelctrodes.
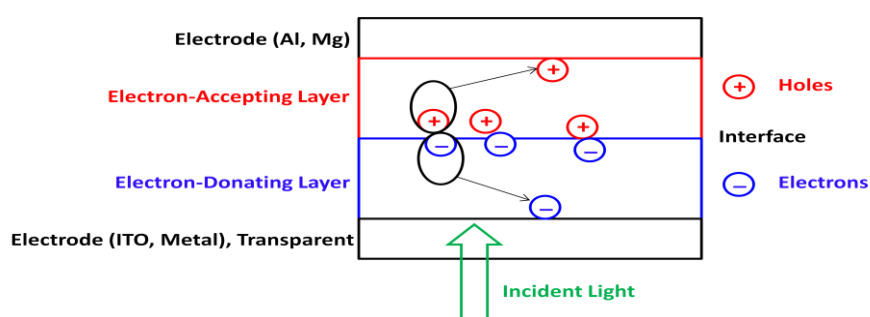
Fig. 1.28 A typical device construction of bi-layer OPVs

An important factor that influences the quantum efficiency of OPV devices is the efficiency of charge photo-generation at the interface between electron-accepting and electron-donating layers. Therefore, distributed, rather than single, hetero-interfaces have been frequently used in order to maximise charge separation by creating a much larger interfacial area. For example, the large-area interfaces formed in interpenetrating, phase-separated blends of electron-accepting and electron-donating semiconducting main chain polymers, which have a nanoscale morphology, also have been proved successful in producing efficient OPVs[80]. A simple schematic device configuration of OPV cells for such interpenetrating polymeric blends is shown in **Fig. 1.29**.

Fig. 1.29 A simplified device of OPV cells for polymeric blends

1.6.2 Materials for OPVs

The organic semiconductors used in OPVs also include low-molecular-mass materials, oligomers and polymers in a similar fashion to those materials of used in OLEDs and PLEDs. The first reported organic solar cell was based on phthalocyanine and perylene derivatives. Phthalocyanine derivatives, with large, planar, and conjugated structures exhibit intense absorption in the UV-Visible spectrum and are capable of donating electrons from excited states to the LUMO of the perylene derivative acceptor material.

The discovery of the buckminsterfullerene organic molecule (C_{60}), which might be regarded as a spherical analogue of graphene, was also reported at about the same time and investigations of its optical and electrical properties followed shortly afterwards. The high conductivity of C_{60} was quickly established and its potential for use as a highly efficient electron-acceptor in OPVs was soon recognised, especially in combination with highly conjugated polythiophene and polyfluorene derivatives as electron donors[133], see **Fig. 1.30** for the structures of some typical organic semiconductors used in prototype OPVs.
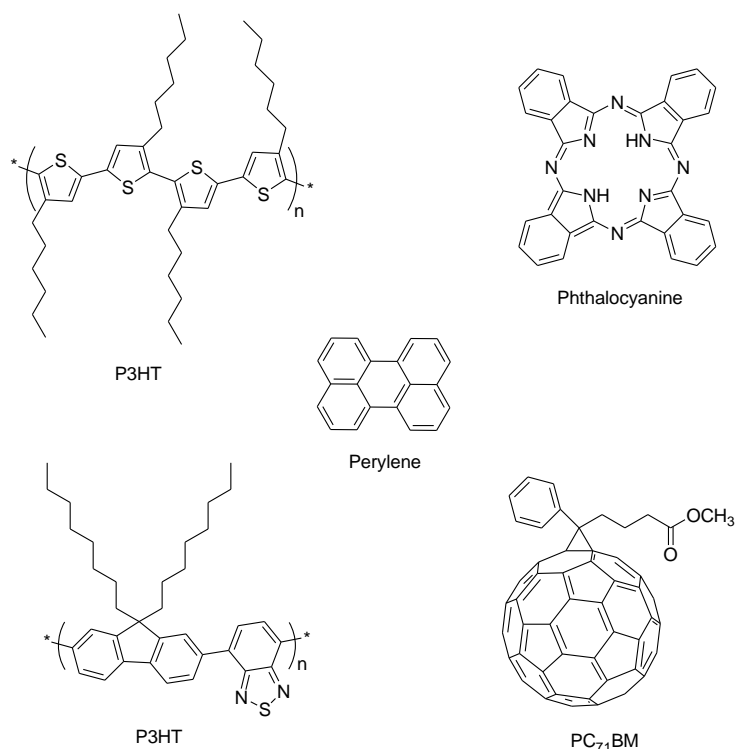
Fig. 1.30 Some typical LMMMs and polymer structures for OPVs.

Liquid crystalline organic semiconductors were also considered much later as potential OPV materials, as well as OLED materials as demonstrated above, due to their high charge carrier mobility attributable, at least in part, to the relatively high degree of order for organic materials in their liquid crystalline mesophases. In particular, a novel approach based on nematic reactive mesogens was used to create electron-acceptor and electron-donors layers with a distributed interface with a very large surface area. Reactive mesogens are polymerisable liquid crystals with two or more polymerisable groups at the end of flexible aliphatic chains (spacers) attached to the aromatic molecular core, see section 1.4. Photopolymerisation of these monomers or oligomers to form highly cross-linked polymer networks can be achieved using irradiation with ultraviolet light of the appropriate wavelength either in the absence of photoinitiators or in combination with radical or ionic photo-initiators, depending on the nature of the photoreactive endgroups, see sections 1.4.1 and 1.4.2. A key advantage for cross-linked thin films is their insolubility so that complex OPV structures, e.g., interpenetrating polymer networks with a high interfacial area, can be readily fabricated. Furthermore, photopolymerisation of reactive mesogens for the fabrication of OPVs also offers the potential of manufacturing flexible a, rugged and shock-stable OPVs on very large plastic substrates, for example, by roll-to-roll techniques[80, 73]. Typical examples of the molecular structure for columnar and nematic liquid crystals or reactive mesogens designed for use in OPVs are shown in **Fig. 1.31**.

HBC12, Cr-Col$_1$ < -100 °C; Col$_1$-Col1$_2$ = 18 °C; Col$_2$-Col$_3$ = 83 °C; Col$_3$-I > 400 °C.

Tg = -4 °C; Cr-N = 72 °C; N-I = 61 °C.

Tg = 39 °C; Cr-N = 92 °C; N-I = 108 °C.

Tg = 25 °C; N-I = 187 °C.

Fig. 1.31 Typical columnar, nematic liquid crystals or reactive mesogens for OPVs

1.7 Synthetic Reactions for Organic Semiconductors

The synthesis of organic semiconductors, particularly for liquid crystal materials, is vitally important for the whole flat panel display field because obviously materials must be prepared before their physical properties are evaluated and they are further exploited in practical devices, such as LCDs or OLEDs. In the field of organic chemistry, there are a very many different synthetic methodologies, which can be employed to prepare intermediates and final organic semiconducting materials.

There are relatively few basic reaction types that generate a new carbon-carbon bond. Some of most typically and commonly used reactions for carbon-carbon bond formation are the Suzuki, Stille, Kumada, Negishi, Heck and Sonogashira aryl-aryl cross-coupling reactions. In terms of the tolerance of a wide variety of substituents on reagents and extreme versatility, the Suzuki and Stille aryl-aryl cross-coupling reactions using a palladium-based catalytic system are particularly useful for the synthesis of liquid crystals incorporating aromatic rings. The catalytic mechanism of palladium-based aryl-aryl, cross-coupling reactions generally involves the oxidative addition of palladium (0), transmetalation and reductive elimination[134-135]. In addition, Direct Arylations are also useful for the synthesis of the intermediates and final compounds of organic semiconductors. Palladium-catalysed Direct Arylations are preferred in some cases due to shorter synthetic steps without the presence of intermediates with organometallic functional groups[136-138].

1.7.1 Suzuki Cross-coupling Reactions

Overall, Suzuki reactions are the best synthetic methodology in terms of unsymmetrical aryl-aryl cross-coupling systems due to a greater tolerance to sensitive functional groups of the coupling partners and a high selectivity of C-C bond formation. Liquid crystalline materials incorporating hetero-aromatic cores insensitive to the Suzuki reaction system, for instance, can be feasibly designed and synthesised.

The Suzuki reaction is an cross-coupling reaction between an aryl- or vinyl-boronic acid and an aryl- or vinyl-halide catalysed by a palladium (0) complex [generally by Pd(PPh$_3$)$_4$][139-140]. This reaction was discovered and reported first in 1979 by Akira Suzuki, who was awarded the 2010 Nobel Prize in Chemistry for this discovery and the development of this reaction. It is widely employed to synthesise poly-olefins, styrenes and substituted bi-aryls or multi-aryls and has also been extended to incorporate alkyl bromides[141].

A typical reaction procedure of the Suzuki aryl-aryl cross-coupling between aryl$_1$-boronic acid and aryl$_2$-halide (generally aryl bromide or aryl iodide) is shown in **Fig. 1.32**. The aryl-boronic acid can be readily synthesised in good yield from the lithiation with *n*-butyllithium in THF at -78 ℃ under an anhydrous inert atmosphere (such as nitrogen atmosphere), further treatment with commercially available 2-triisopropyl borate, and final acidification with hydrochloric acid at room temperature. The aryl-bromide can be obtained by brominated substitutions, such as the commonly-used NBS bromination in high yield.

$$\textbf{R}_1\textbf{-B(OH)}_2 \quad + \quad \textbf{R}_2\textbf{-X} \quad \xrightarrow[\text{Base}]{\text{Pd-based Catalyst}} \quad \textbf{R}_1\textbf{-R}_2$$
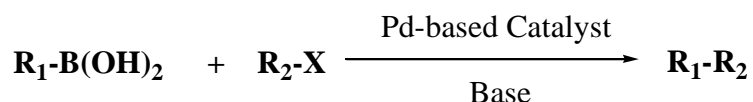
Fig. 1.32 The Suzuki aryl-aryl cross-coupling reaction

Palladium-based catalysts generally with phosphine-based ligands are used in the Suzuki reactions under the conditions of aqueous base (typically K$_2$CO$_3$ or Na$_2$CO$_3$) in polar solvents such as DMF, THF or DME. Therefore, an important merit of the Suzuki cross-coupling reaction is that it allows the presence of water, so that the reaction can be carried out under general conditions in air. The use of phosphine-based ligands can help stabilise the zero valence of palladium under prolonged heating for inducing the initial oxidative addition, which is the rate-determining step. The role of the base is widely considered as activating organoboron compounds, so that further transmetalation can be achieved successfully. In addition, a homogenous system for most organic reactions is favoured and thus organic solvents are selected, that have good solubility for the

starting materials and catalytic systems, as well as good inter-miscibility with the aqueous phase. The solvent dimethoxyethane (DME), for instance, works satisfactorily as a water-miscible solvent with aqueous sodium carbonate as a basic solution. A typical catalytic cycle of the Suzuki reaction is shown in **Fig. 1.33**.
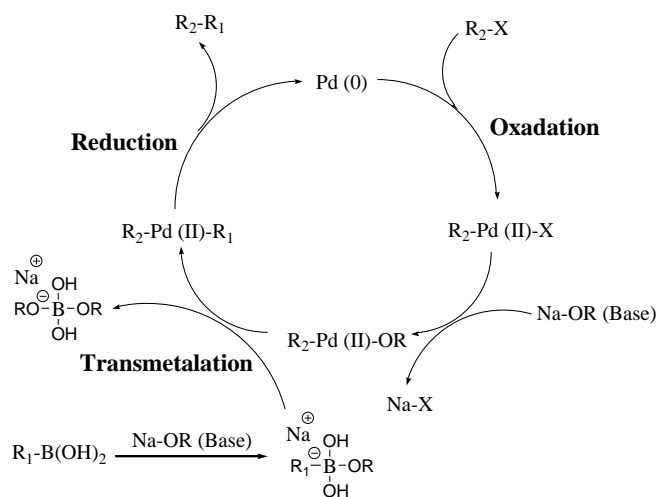
Fig. 1.33 A typical catalytic cycle of the Suzuki reaction

1.7.2 Stille Cross-coupling Reactions

The Stille cross-coupling refers to a chemical reaction coupling an organotin (organostannyl) compound to an organic halide catalysed by a palladium complex. It was discovered by Stille and Milstein in 1977[142]. A typical reaction procedure of the Stille cross-coupling between $aryl_1$-tin ($Aryl_1$-SnR_3, R = butyl or methyl) and $aryl_2$-halide ($Aryl_2$-X, generally X = Br or I) is shown in **Fig. 1.34**. In a similar fashion to the synthesis of organic boronic acids, the desired organo tin compounds can also be easily obtained in good yield from the lithiation with *n*-butyllithium in THF at -78 ℃ under an anhydrous inert atmosphere, and then treatment with commercially available 2-tributylstannyl chloride. In terms of the organic tin compounds, a tributylstannyl or trimethylstannyl derivative is usually used. However, in the laboratory, tributylstannyl compounds are usually used in most cases, as the toxicity of trimethylstannyl compounds is about 1000 times larger than that of the correspondent tributylstannyl compounds, although trimethylstannyl compounds usually exhibit higher reactivity compared with tributylstannyl compounds. Furthermore, compared with solid organic

boronic acid, typical oily or liquid organic stannyl compounds are usually more difficult to purify.

$$R_1\text{-Sn(Bu)}_3 \quad + \quad R_2\text{-X} \quad \xrightarrow{\text{Pd-based Catalyst}} \quad R_1\text{-}R_2$$

Fig. 1.34 The reaction scheme of Stille cross coupling

Palladium-catalysed Stille cross-coupling reactions are carried out under an inert atmosphere using an anhydrous and degassed solvent, as oxygen can lead to the oxidation of the palladium catalyst and promote homo-coupling of organic stannyl compounds. These side reactions will result in a reduced yield of the desired product from the cross-coupling reaction. Given the drawback of the low reactivity of alkyl stannanes, strongly polar solvents, e.g., DMF, THF, are generally employed in these reactions. However, a difference between the Suzuki and Stille cross-coupling reactions lies in the presence and absence of aqueous base solution, respectively. The organoboron intermediate cannot undergo the transmetalation in the absence of aqueous base, but the more reactive organostannane can perform transmetalation directly without requiring aqueous base. The reaction mechanism of the Stille cross-coupling can also be illustrated from the perspective of palladium catalyst. A typical catalytic cycle of the Stille reaction is shown in **Fig. 1.35**.

Fig. 1.35 A typical catalytic cycle of the Stille reaction
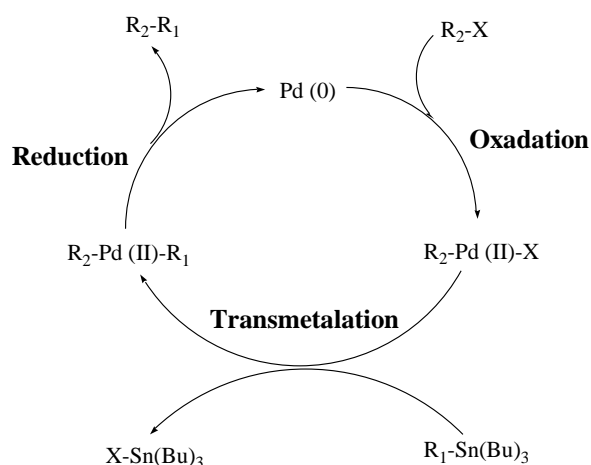
1.7.3 Direct Arylation of Hetero-aromatic C-H Bond

Aryl C-C bond formation is of great importance for organic chemistry and material science. As described above, it can be achieved by some aryl-aryl, cross-coupling reactions where one aryl halide is substituted by the other aryl incorporating organometallic moieties such as $-B(OH)_3$ (Suzuki), $-SnR_3$ (Stille), $-MgX$ (Kumada), $-ZnR$ (Negishi). However, the C-H bond of hetero-aromatic compounds, in some cases, can be directly activated and substituted by an aryl halide without requiring the absence of an organometallic intermediate, thus reducing the extra synthetic steps and achieving green chemistry conditions. Specifically, direct arylation refers to a specific hetero-aromatic C-H functionalisation where C-H bond is activated and then the H is replaced by an aryl group generally provided by an aryl halide.

Semiconducting materials incorporating hetero-aromatic groups, such as thiophene moieties, are favoured because desired optical/electro-chemical properties can be achieved by the presence of different hetero-atoms. Therefore, the direct arylation is particularly useful for the synthesis of organic electronics.

A typical reaction procedure for the direct arylation between the $aryl_1$ with hetero-cycles (Hetero-$Aryl_1$-H) and the $aryl_2$-halide ($Aryl_2$-X, generally X = Br or I) is shown in **Fig. 1.36**.

$$\textbf{Hetero-Aryl}_1\textbf{-H + Aryl}_2\textbf{-X} \xrightarrow{\text{Pd-based Catalyst}} \textbf{Hetero-Aryl}_1\textbf{-Aryl}_2$$

Fig. 1.36 The reaction scheme of direct arylation
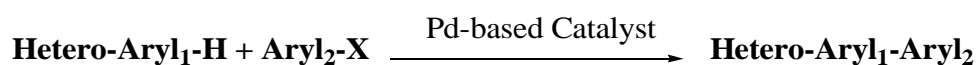
The palladium acetate catalyst coordinated with alicyclic phosphine ligands, such as typically tricyclopentylphosphine tetrafluoroborate $PCy_3 \cdot HBF_4$, are used in the direct arylation reactions under the conditions of both stoichiometric pivalic acid (usually approximate 0.3 mol equivalent) and potassium carbonate base in strong polar solvents such as DMF, NMP.

A challenging aspect for the C-H activation in direct arylation reactions is the regioselectivity. Aromatic molecules involves many C-H bonds and it is determining which C-H bond can be highly active and selective. A common choice of active C-H bonds is from aromatic compounds incorporating hetero-atoms including thiophenes, thiazoles, indoles, pyrroles, etc.

In terms of palladium-catalysed direct arylation, the reaction mechanism of C-H activation has been studied and reported for several possible pathways, such as electrophilic aromatic substitution, Heck-type coupling, concerted metallisation deprotonation (CMD)[143-144]. However, most hetero-aromatic rings, such as thiophenes and indoles, widely involve a CMD reaction pathway[144]. Specifically, the general reaction procedures include the oxidation addition of palladium to the C-Br bond of aryl bromide, the exchange of the halogen ligand, deprotonation of the thiophene substrate while simultaneous formation of a metal-carbon bond, then the formation of an important transition state, which determines whether the direct arylation can be achieved or not, and final reductive elimination of the transition state. Furthermore, density functional theory (DFT) calculations for the CMD process are usually used to reveal the required energy for the distortion, cleavage and interaction of hetero-aromatic C-H bonds[144-145]. A typical CMD catalytic cycle of the direct arylation is shown in **Fig. 1.37**.
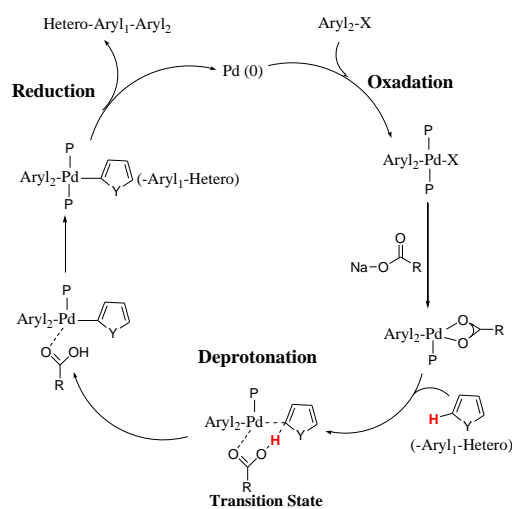
Fig. 1.37 A typical CMD catalytic cycle of the direct arylation

1.8 References

[1]   Book, "*Semiconductor materials*", by L. I. Berger, CRC Press, US, 1996.

[2]   Book, "*Introduction to Solid State Physics*", by C. Kittel, 8th Edition, John Wiley & Sons, US, 2005.

[3]   J. de Mello, J. Anthony and S. Lee, *ChemPhysChem,* 2015, **16**, 1099

[4]   P. J. Skabara, *Chem. Commun.,* 2013, **49**, 9242.

[5]   C. Sekine, Y. Tsubata, T. Yamada, M. Kitano and S. Doi, *Sci. Technol. Adv. Mater.,* 2014, **15**, 034203.

[6]   A. Moliton and R. C. Hiorns, Polym. Int., 2012, 61, 337.

[7]   D. D. C. Bradley, Faraday Discuss., 2014, 174, 429.

[8]   Book, *"An Introduction to Molecular Orbitals",* by Y. Jeans and F. Volatron, Oxford University Press, New York, 1993.

[9]   Book, *"Physical Chemistry for the Bioscience"*, by R. Chang, Sansalito, CA: University Science, 2005.

[10]   E. Wiedemann, *Ann. Phys.,* 1888, **34**, 446.

[11]   G. G. Stokes, *Phil. Trans. Roy. Soc.,* 1852, **142**, 463.

[12]   A. Jablonski, *Nature,* 1933, **131**, 839.

[13]   A. Jablonski, *Z. Physik,* 1935, **94**, 38.

[14]   N. Holonyak Jr and S. F. Bevacqua, *Appl. Phys. Lett.,* 1962, **1**, 82.

[15]   M. Pope, H. P. Kallman and P. Magnate, *J. Chem. Phys.,* 1963, **38**, 2042.

[16]   P. S. Vincent, W. A. Barlow, R. A. Hann and G. G. Roberts, *Thin Solid Films,* 1982, **94**, 171.

[17]   F. J. Campas and M. Goutermann, *Chem. Phys. Lett.,* 1977, **48**, 233.

[18]   C. W. Tang and S. A. Van Slyke, *Appl. Phys. Lett.,* 1987, **51**, 913.

[19]   C. W. Tang, S. A. Van Slyke and C. H. Chen, *Appl. Phys. Lett.,* 1989, **65**, 3610.

[20]   J. H. Burroughes, D. D. C. Bradley, A. R. Brown, R. N. Marks, R. H. Friend, P. L. Burn and A. B. Holmes, *Nature,* 1990, **347**, 539

[21]   U. Mitschke and P. Bauerle, *J. Mater. Chem.,* 2000, **10**, 1471.

[22]   J. Salbeck and B. Bunsenges, *Phys. Chem.,* 1996, **100**, 1667.

[23]   G. Vaubel, H. Baessler and D. Meobius, *Chem. Phys. Lett.,* 1971, **10**, 334.

[24]   A. R. Brown, D. D. C. Bradley, P. L. Burn, J. H. Burroughes, R. H. Friend, N. Greenham, A. B. Holmes and A. Kraft, *Appl. Phys. Lett.,* 1992, **61**, 2793.

[25]   C. Adachi, T. Tsutsui and S. Saito, *Appl. Phys. Lett.,* 1990, **57**, 531.

[26]   B. W. D'Andrade and S. R. Forrest, *Adv. Mater.,* 2004, **16**, 1585.

[27]   W. C. Su, D. Poplavskyy, F. So, H. Clearfield, D. Welsh and W. Wu, *SID Symp. Dig. Tech. Pap.,* 2005, **36**, 1871.

[28]   T. A. Beierlein, H. P. Ott, H. Hofmann, H. Riel, B. Ruhstaller, B. Crone, S. Karg and W. Riess, *Proc. SPIE,* 2002, **4464**, 178.

[29]   D. Gebeyehu, *Ethiopian J. Sci. Technol.,* 2014, **7**, 1.

[30]   S. Hofmann, M. Thomschke, B. Lussem and K. Leo, *Opt. Express,* 2011, **19**,

A1250.

[31]   Y. J. Choi, S. C. Gong, K. M. Kang and H. H. Park, *J. Mater. Chem. C,* 2014, **2**, 8344.

[32]   Y. Chen and D. Ma, *J. Mater. Chem.,* 2012, **22**, 18718.

[33]   D. Qin, *Proc. SPIE 9137, Org. Photonics VI, 91370K,* 2014.

[34]   J. H. Chang, W. H. Lin, P. C. Wang, J. I. Taur, T. A. Ku, W. T. Chen, S. J. Yan & C. I. Wu, *Sci. Rep. 5*, 2015, **9693**, 1.

[35]   P. L. Burn, D. D. C. Bradley, R. H. Friend, D. A. Haliday, A. B. Holmes, R. W. Jackson and A. Kraft, *J. Chem. Soc., Perkin Trans.,* 1992, **1**, 3225.

[36]   Y. Cao, G. Yu, C. Zhang, R. Menon and A. J. Heeger, *Synth. Met.,* 1997, **87**, 171.

[37]   U. Scherf and E. J. W. List, *Adv. Mater.,* 2002, **14**, 477.

[38]   M. P. Aldred, R. Hudson, S. P. Kitney, P. Vlachos, A. Liedtke, K. L. Woon, M. O'Neill and S. M. Kelly, *Liq. Cryst.,* 2008, **35**, 413.

[39]   U. Giovanella, M. Pasini, C. Freund, C. Botta, W. Porzio and S. Destri, *J. Phys. Chem. C.,* 2009, **113**, 2290.

[40]   Y. Honmou, S. Hirata, H. Komiyama, J. Hiyoshi, S. Kawauchi, T. Iyoda and M. Vacha, *Nature Communication,* 2014, **5**, 4666.

[41]   C. S. Fischer, M. C. Baier and S. Mecking, *J. Am. Chem. Soc.,* 2013, **135**, 1148.

[42]   A. R. Davis and K. R. Carter, *Macromolecules,* 2015, **48**, 1711.

[43]   Y. Ohmori, M. Uchida, K. Muro and K. Yoshino, *Jpn. J. Appl. Phys.,* 1991, **30**, 1941.

[44]   W. Jiang, Y. Li and Z. Wang, *Chem. Soc. Rev.,* 2013, **42**, 6113.

[45]   US Patent, *"Heterocyclic Compound"*, by H. Osaka, S. Shitagaki and Y. Kitano, US20120197020A1, 2012.

[46]   P. I. Shih, C. L. Chiang, A. K. Dixit, C. K. Chen, M. C. Yuan, R. Y. Lee, C. T. Chen, E. W. G. Diau and C. F. Shu, *Org. Lett.,* 2006, **8**, 2799.

[47]   K. Brunner, A. Van Dijken, H. Borner, J. J. A. M. Bastiaansen, N. M. M. Kiggen and B. M. W. Langeveld, *J. Am. Chem. Soc.,* 2004, **126**, 6035.

[48]   Z. M. Hudson, Z. Wang, M. G. Helander, Z. H. Lu and S. Wang, *Adv. Mater.,* 2012, **24**, 2922.

[49]   S. Kato, S. Shimizu, A. Kobayashi, T Yoshihara, S Tobita and Y. Nakamura, *J. Org. Chem.,* 2014, **79**, 618.

[50]   P. Data, P. Pander, M. Lapkowski, A. Swist, J. Soloducho, R. R. Reghu and J. V. Grazulevicius, *Electrochim. Acta*, 2014, **128**, 430.

[51]   K. H. Park, H. Yun, W. Lu, D. S. Chung, S. Kwon and Y. Kim, *Dyes Pigments,* 2014, **103**, 214.

[52]   G. L. Feng, W. Y. Lai, S. J. Ji and W. Huang, *Tetrahedrom Lett*., 2006, **47**, 7089

[53]   J. Luo, B. Zhao, J. Shao, K. A. Lim, H. S. O. Chan and C. Chi, *J. Mater. Chem.,* 2009, **19**, 8327.

[54]   W. Y. Lai, Q. Q. Chen, Q. Y. He, Q. L. Fan and W. Huang, *Chem. Commun.,* 2006, 1959.

[55]   B. Gomez-Lor, B. Alonso, A. Omenat and J. L. Serrano, *Chem. Commun.,* 2006, 5012.

[56]   M. S. Yuan, T. B. Li, W. J. Wang, Z. T. Du, J. R. Wang and Q. Fang, *Spectrochim. Acta Part A: Mol. Biomol. Spectrosc.,* 2012, **96**, 1020.

[57]   L. Rong, Q. Liu, Y. Shi and J. Tang, *Chem. Commun.,* 2011, **47**, 2155.

[58]   F. Gallego-Gomez, E. M. Garcia-Frutos, J. M. Villalvilla, J. A. Quintana, E. Gutierrez-Puebla, A. Monge, M. A. Diaz-Garcia and B. Gomez-Lor, *Adv. Funct. Mater.,* 2011, **21**, 738.

[59]   E. M. Garcia-Frutos and B. Gomez-Lor, *J. Am. Chem. Soc.,* 2008, **130**, 9173.

[60]   J. Shao, Z. Guan, Y. Yan, C. Jiao, Q. Xu and C. Chi, *J. Org. Chem.,* 2011, **76**, 780.

[61]   B. Zhao, B. Liu, R. Q. Png, K. Zhang, K. A. Lim, J. Luo, J. Shao, P. K. H. C. Chi and J. Wu, *Chem. Mater.,* 2010, **22**, 435.

[62]   L. Ji, Q. Fang, M. Yuan, Z. Liu, Y. Shen and H. Chen, *Org. Lett.,* 2010, **12**, 22.

[63]   M. P. Aldred, P. Vlacho, A. E. A. Contoret, S. R. Farrar, W. Chung-Tsoi, B. Mansoor, K. L. Woon, R. H.udson, S. M. Kelly and M. O'Neill, *J. Mater. Chem.,* 2005, **15**, 3208.

[64]   C. Xiang, N. Chopra, J. Wang, C. Brown, S. Ho, M. Mathai and F. So, *Organic Electronics,* 2014, **15**, 1702.

[65]   J. Lee, H. Han, J. Lee, S. C. Yoon and C. Lee, *J. Mater. Chem. C,* 2014, **2**, 1474.

[66]   H. K. Shih, Y. L. Chu, F. C. Chang, C. Y. Zhu and S. W. Kuo, *Polym. Chem.,* 2015, **6**, 6227.

[67]   N. Aizawa, Y. J. Pu, H. Sasabe and J. Kido, *Organic Electronics,* 2013, **14**, 1614.

[68]   A. Liedtke, M. O'Neill, S. M. Kelly, S. P. Kitney, B. Van Averbeke, P. Boudard, D. Beljonne and J. Cornil, *J. Phys. Chem. B,* 2010, **114**, 11975.

[69]   A. Liedtke, M. O'Neill, A. Wertmöller, S. P. Kitney and S. M. Kelly, *Chem. Mater.* 2008, **20**, 3579.

[70]   W. C. Tsoi, M. O'Neill, M. P. Aldred, S. P. Kitney, P. Vlachos and S. M. Kelly, *Chem. Mater.,* 2007, **19**, 5475.

[71]   K. L. Woon, M. P. Aldred, P. Vlachos, G. H. Mehl, T. Stirner, S. M. Kelly and M. O'Neill, *Chem. Mater.,* 2006, **18**, 2311.

[72]   Y. D. Zhang, R. D. Hreha, G. E. Jabbour, B. Kippelen, N. Peyghambarian and S. R. Marder, *J. Mater. Chem.,* 2002, **12**, 1703.

[73]   M. O'Neill and S. M. Kelly, *Adv. Mater.,* 2011, **23**, 566.

[74]   Y. Xu, H. Wang, X. Liu, Y. Wu, Z. Gao, S. Wang, Y. Miao, M. Chen and B. Xu, *J. Lumin.,* 2013, **134**, 858.

[75]   H. Wang, Y. Xu, T. Tsuboi, H. Xu, Y. Wu, Z. Zhang, Y. Miao, Y. Hao, X. Liu, B. Xu and W. Huang, *Organic Electronics,* 2013, **14**, 827.

[76]   I. Osken, A. S. Gundogan, E. Tekin, M. S. Eroglu and T. Ozturk, *Macromolecules,* 2013, **46**, 9202.

[77]   M . P. Aldred, A. J. Eastwood, S. M. Kelly and Panos Vlachos, *Chem. Mater.,* 2004, **16**, 4928.

[78]   M. R. Billa, K. Kassireddy, M. Haro, M. S. Al-Kalifah, S. M. Kelly, S. P.

Kitney, and M. O'Neill, *Liq. Cryst.,* 2011, **38**, 813.

[79]   M. J. Eslamibidgoli and J. B. Lagowski, *J. Phys. Chem. A,* 2012, **116**, 10597.

[80]   Book, *"Liquid Crystalline Semiconductors: Materials, Properties and Applications"*, by R. J. Bushby, S. M. Kelly and M. O'Neill, Springer, The Netherlands, 2013.

[81]   A. Kraft, A. C. Grimsdale and A. B. Holmes, *Angew. Chem. Int. Ed.,* 1998, **37**, 402.

[82]   A. R. Murphy and J. M. J. Frechet, *Chem. Rev.,* 2007, 107, 1066.

[83]   O. Usluer, S. Demic, M. Kus, F. Ozel and N. S. Sariciftci, *J. Lumin.,* 2014, **51**, 79.

[84]   H. Usta, W. C. Sheets, M. Denti, G. Generali, R. Capelli, S. Lu, X. Yu, M. Muccini and A. Facchetti, *Chem. Mater.,* 2014, **26**, 6542.

[85]   Y. N. Luponosov, A. N. Solodukhin and S. A. Ponomarenko, *Polym. Sci., Ser. C.,* 2014, **56,** 104.

[86]   S. Zhang, L. Xue, Y. Jing, X. Liu, G. Lu, X. Liang, H. Li, Y. Zheng and J. Zuo, *Dyes Pigments,* 2015, **118**, 1.

[87]   T. Zhang, J. Wang, M. Zhou, L. Ma, G. Yin, G. Chen and Q. Li, *Tetrahedron,* 2014, **70**, 2478.

[88]   G. Krucaite, D. Tavgeniene, D. Sipaviciute, G. Buika, J. V. Grazulevicius, L. Liu, B. Zhang, Z. Xie and S. Grigalevicius, *Optical Mater.,* 2014, **37**, 788.

[89]   K. Chen, H. Zhao, Z. Fan, G. Yin, Q. Chen, Y. Quan, S. Li and S. Ye, *Org. Lett.,* 2015, **17**, 1413.

[90]   Z. Ning and H. Tian, *Chem. Commun.,* 2009, 5483.

[91]   Z. Fang, V. Chellappan, R. D. Webster, L. Ke, T. Zhang, B. Liu and Y. H. Lai, *J. Mater. Chem.,* 2012, **22**, 15397.

[92]   N. Satoh, I. S. Cho, M. Higuchi and K. Yamamoto, *J. Am. Chem. Soc.,* 2003, **125**, 8104.

[93]   H. Y. Cho, L. S. Park, Y. S. Han, Y. Kwon and J. Y. Ham, *Mol. Cryst. Liq. Cryst.,* 2009, **499**, 323.

[94]   U. Mitschke and P. Bauerle, *J. Mater. Chem.,* 2000, **10**, 1471.

[95]   A. M. Krause-Heuer, N. R. Yepuri, T. A. Darwish and P. J. Holden, *Molecules,* 2014, **19**, 18604.

[96]   Y. Tao, C. Yang and J. Qin, *Chem. Soc. Rev.,* 2011, **40**, 2943.

[97]   C. H. Chen, J. Shi and C. W. Tang, *Macrocol. Symp.,* 1997, **125**, 1.

[98]   J. Salbeck, N. Yu, J. Bauer, F. Weissortel and H. Bestgen, *Synth. Met.,* 1997, **91**, 209.

[99]   Book, *"Flat Panel Display: Advanced Organic Materials",* by S. M. Kelly, The Royal Society of Chemistry, Cambridge, 2000.

[100]   C. Mertesdorf, H. Ringsdorf and J. Stumpe, *Liq. Cryst.,* 1991, **9**, 337.

[101]   D. Adam, D. Haarer, F. Closs, T. Frey, D. Funhoff, K. Siemensmeier, P. Schumacher and H. Ringsdorf, *Ber. Buns. Phys. Chem.,* 1993, **97**, 1366.

[102]   D. Adam, F. Closs, T. Frey, D. Funhoff, D. Haarer, P. Schumacher, H. Ringsdorf and K. Siemensmeier, *Phys. Rev. Lett.,* 1993, **70**, 457.

[103]   M. Funahashi and J. I. Hanna, *Jpn. J. Appl. Phys.,* 1996, **35**, L703.

[104] M. Funahashi and J. I. Hanna, *Phys. Rev. Lett.,* 1997, **78**, 2184.

[105] N. J. Tao, *Nat. Nanotechnol.,* 2006, **1**, 173.

[106] S. Kato, S. Shimizu, A. Kobayashi, T Yoshihara, S Tobita and Y. Nakamura, *J. Org. Chem.,* 2014, **79**, 618.

[107] F. Reinitzer, *Monatsh. Chem.,* 1888, **9**, 421.

[108] O. Lehmann, *Z. Physik. Chem.,* 1889, **4**, 462

[109] L. Gattermann and A. Rischke, *Ber. Dtsch. Chem. Ges.,* 1890, **23**, 1738.

[110] G. Friedel, *Ann. Phys.,* 1922, **18**, 273

[111] V. Fréedericksz, V. Zolina, *Trans. Faraday Soc.,* 1933, **29**, 919

[112] M. Born, *Chem. Zentr.,* 1916, **11**, 366

[113] W. Kast, *Z. Physik.,* 1932, **76**, 115

[114] K. Lichtenecker, *Z. Physik.,* 1926, **27**, 116

[115] L. Onsager, *ANN. N. Y. Acad. Sci.,* 1949, **51**, 627.

[116] P. J. Flory, *Proc. Roy. Soc., Ser. A. (London),* 1956, **234**, 73.

[117] Book, *"Introduction to Liquid Crystals (Chemistry and Physi*cs)", by P. J. Collings and M. Hird, Taylor & Francis, London, UK, 1997.

[118] Book, *"Molecular Structure and Properties of Liquid Crystals",* by G. W. Gray, Academic Press, New York, US, 1962

[119] G. W. Gray, K. J. Harrison and J. A. Nash, *Electron. Lett.,* 1973, **130**, 9

[120] G. W. Gray, K. J. Harrison and J. A. Nash, *J. Chem. Soc. Commun.,* 1974, 431.

[121] G. W. Gray, *J. Phys. (Paris),* 1975, **36**, 337

[122] G. W. Gray and A. Mosley, *J. Chem. Soc. Perkin,* 1976, **11**, 97

[123] R. B. Mayer, L. Liebert, L. Strzelecki and P. Keller, *J Phys. Lett.,* 1975, **36**, L69.

[124] N. A. Clark and S. T. Largerwall, *Appl. Phys. Lett.,* 1980, **88**, 899.

[125] S. Chandrasekhar, B. K. Sadashiva and K. A. Suresh, *Pramana,* 1977, **9**, 471

[126] Book, *"Liquid Crystals and Plastic Crystals Volume 1: Preparation, Constitution and Applications"*, by G. W. Gray and P. A. Winsor, Chichester, England: Ellis Horwood, 1974.

[127] Book, *"Electro-optical and Magneto-optical Properties of Liquid Crystals",* by L. M. Blinov, NY: John Wiley & Sons, New York, US, 1983

[128] G. H. Heilmelier, L. A. Zanoni and L. Barton, *Proc. IEEE,* 1968, **56**, 1162.

[129] M. Schadt, *Liq. Cryst.,* 1989, **5**, 57.

[130] M. Schadt and W. Helfrich, *Appl. Phys. Lett.,* 1971, **18**, 127

[131] T. J. Scheffer, J. Nehring, M. Kaufmann, H. Amstutz, D. Heimgarmer and P. Eglin, *SID'85 Digest,* 1985, L20

[132] T. Geelhaar, K. Tarumi and H.Hirschmann, *Trends in LC Materials, SID'96 Digest,* 1996, 167.

[133] J. M. Szarko, J. Guo, B. S. Rolczynski and L. X. Chen, *Citation: Nano Rev.,* 2011, **2**, 7249.

[134] K. C. Nicolaou, P. G. Bulger and D. Sarlah, *Angew. Chem. Int. Ed.,* 2005, **44**,

4442.

[135] R. F. Heck, E. Negishi and A. Suzuki, *The Nobel Prize in Chemistry,* 2010.

[136] B. Liegault, D. Lapointe, L. Caron, A. Vlassova and K. Fagnou, *J. Org. Chem.,* 2009, **74**, 1826.

[137] D. Alberico, M. E. Scott and M. Lautens, *Chem. Rev.,* 2007, **107**, 174.

[138] D. J. Schipper and K. Fagnou, *Chem. Mater.,* 2011, **23**, 1594.

[139] N. Miyaura, K. Yamada and A. Suzuki, *Tetrahedron Lett.,* 1979, **20**, 3437.

[140] N. Miyaura and A. Suzuki, *Chem. Rev.,* 1995, **95**, 2457.

[141] J. H. Kirchhoff, M. R. Netherton, I. D. Hills and G. C. Fu, *J. Am. Chem. Soc.,* 2002, **124**, 13662.

[142] D. Milstein and J. K. Stille, *J. Am. Chem. Soc.,* 1978, **100**, 3636.

[143] S. I. Gorelsky, *Coord. Chem. Rev.,* 2013, **257**, 153.

[144] S. I. Gorelsky, D. Lapointe and K. Fagnous, *J. Org. Chem.,* 2011, **77**, 658.

[145] L. G. Mercier and M. Leclerc, *Acc. Chem. Res.,* 2013, **46**, 1597.

2 Aims

The overall purpose of the research carried out for this thesis is to synthesise novel organic semiconductor materials as charge-transporting and/or emissive layers in optical-electrical devices such as organic light emitting diodes (OLEDs) and organic photovoltaics (OPVs). Liquid crystalline semiconductors and photo-polymerisable precursors are extensively studied and used as promising plastic electronics in particular. Therefore, another general aim is to study the relationships between molecular structures of these synthesised materials and liquid crystalline properties, optical/electro-chemical properties (energy gap, HOMO level and LUMO level) and photo-polymerisable ability.

A number of Liquid crystalline materials for opto-electronic devices focus on fluorene-based compounds. However, organic semiconductors incorporating carbazole moieties often exhibit useful optical properties, fine delocalisation, low redox potential and high chemical stability. Nematic mesophases, as the least ordered liquid crystalline, have low bulk viscosity so that they can be easily ordered and macroscopically alignment in fabricating an oriented high-quality film. Therefore, it was intended to incorporate both nematic liquid crystalline mesophases and symmetrical hetero-aromatic carbazole moieties designed in molecular structures.

A nematic liquid crystalline molecular structure requires a large length-to-breadth ratio which can be achieved by combining a rigid, linear and co-axial aromatic backbone and flexbile aliphatic chains. Furthermore, the presence of different hetero-aromatic cores, i.e., thiophene moiety, contributes to fine tuning of band gap and HOMO & LUMO energy levels, so that an appropriate match of energy levels and a low charge-injection barriers in multi-layer OLED devices can be achieved. Therefore, a main aim of this research was to design a series of novel liquid crystalline organic semiconductors with linear and co-axial hetero-aromatic backbones, including 2,5-disubstituted thiophene, 1,4-disubstituted phenylene, 2,7-disubstituted fluorene, dibenzothiophene, benzothiadiazole and

thieno[3,4-c]pyrrole-4,6-dione constructed with symmetrical carbazole moieties. The different combinations of these aromatic units are expected to exhibit desired liquid crystalline properties and optical-electrical properties. Furthermore, a further aim of this work was to investigate the effect of different flexible alkyl chains (long straight octyl, short methyl, and long branched dioctyl) in terminal and lateral positions on liquid crystalline mesophases and the thermal transition temperatures. These highly conjugated compounds with a lath-like molecular shape with a high length-to-breadth (aspect) ratio were designed to yield a range of novel liquid crystalline organic semiconductors possessing a low melting point (Cr-N), a high clearing point (N-I) and a glass transition temperature (Tg) above room temperature (RT), so as to the absence of crystal boundary defects as traps for quenching of electrons or holes mobility. **Fig. 2.1** shows the molecular structural units of these aromatic cores used as constituent parts of synthesised organic semiconductors.
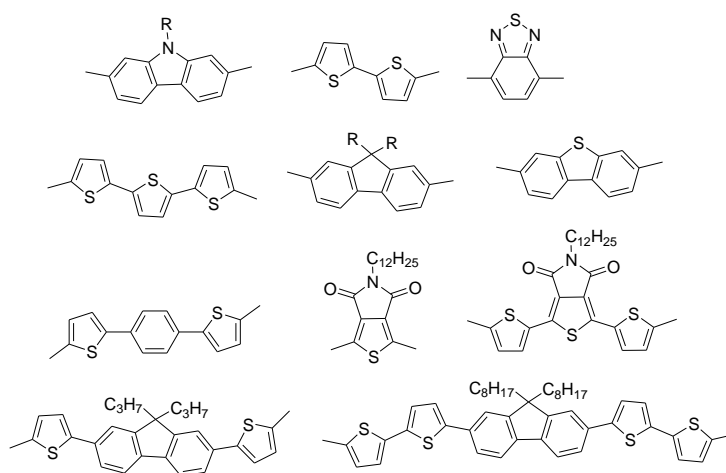

Fig. 2.1 The molecular structural units used as constituent parts of synthesised organic semiconductors

The disc-like, C_3-symmetric triazatruxene with an extended π-system in which three carbazole units are sharing an aromatic ring was studied in this work as potential organic semiconductors, especially for organic light-emitting diodes (OLEDs)[1-8]. The chemical structure resembling the classic hole-transporting carbazole and its planar disc-like nature renders triazatruxene a potentially attractive hole-transporting

materials[9]. Moreover, the starburst structure of triazatruxene can be characterised by superior structural uniformity and are capable of preventing close packing and spatial reorientation, thus suppressing self-aggregation and forming high-quality thin films[10]. However, these researchers mainly focus on different aryl-aryl couplings at *C*-positions of the triazatruxene core to synthesise some discotic liquid crystal oligomers with the most general alkyl-substitution at three *N*-positions of carbazole units. the advantageous study of cross-linkable triazatruxenes at hetero-aromatic *N*-position functionalisation with photopolymerisable end-groups has not been reported. Therefore, another important aim of the research for this thesis is to design and synthesise some photo-polymerisable precursor materials incorporating cross-linkable end-groups at the flexible aliphatic chains. The molecular structural unit of triazatruxenes was shown in **Fig. 2.2**. Some of these materials were designed to incorporate three or more polymerisable endgroups, including double bonds, non-conjugated dienes, triple bonds and cyclic ether units, at the end of aliphatic flexible spacers, so that they can be deposited from solution, by spin casting or coating, for example, as uniform thin layers with the desired thickness and then turned into the corresponding insoluble and intractable polymer networks as thin films for use in multilayer devices. Therefore, a further aim was to investigate and compare the cross-linking ability of these different photo-polymerisable end-groups when these precursors were spun coated to fabricate a thin film. Furthermore, some non photo-polymerisable side-chains including straight and cyclic alkyl, ester, ether and nitrile, were also designed to attach to the triazatruxene core, in order to compare their optical/electro-chemical properties.
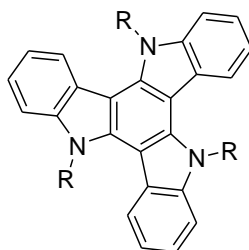

Fig 2.2 The molecular structural unit of triazatruxenes

An essential aim of our research for this thesis, in terms of material synthesis, is to obtain desired compounds with high yields and efficiency. A large number of organic reactions have been carried out to synthesise desired organic semiconductors. These reaction were studied in detail in order to identify and optimise efficient and tolerant reaction conditions and catalytic systems with high yields and facile purification.

2.1 References

[1]   F. Goubard and F. Dumur, *RSC Adv.,* 2015, **5,** 3521.

[2]   C. Ruiz, E. M. Garcia-Frutos, D. A. S. Filho, J. T. L. Navarrete, M. C. R. Delgado and B. Gomez-Lor, *J. Phys. Chem. C,* 2014, **118**, 5470.

[3]   L. Wang, Q. Fang, Q. Lu, S. Zhang, Y. Jin and Z. Liu, *Org. Lett.,* 2015, **17**, 4164.

[4]   G. L. Feng, W. Y. Lai, S. J. Ji and W. Huang, *Tetrahedrom Lett*., 2006, **47**, 7089.

[5]   M. S. Yuan, T. B. Li, W. J. Wang, Z. T. Du, J. R. Wang and Q. Fang, *Spectrochim. Acta Part A: Mol. Biomol. Spectrosc.,* 2012, **96**, 1020.

[6]   L. Rong, Q. Liu, Y. Shi and J. Tang, *Chem. Commun.,* 2011, **47**, 2155.

[7]   F. Gallego-Gomez, E. M. Garcia-Frutos, J. M. Villalvilla, J. A. Quintana, E. Gutierrez-Puebla, A. Monge, M. A. Diaz-Garcia and B. Gomez-Lor, *Adv. Funct. Mater.,* 2011, **21**, 738.

[8]   J. Shao, Z. Guan, Y. Yan, C. Jiao, Q. Xu and C. Chi, *J. Org. Chem.,* 2011, **76**, 780.

[9]   J. Luo, B. Zhao, J. Shao, K. A. Lim, H. S. O. Chan and C. Chi, *J. Mater. Chem.,* 2009, **19**, 8327.

[10]   W. Y. Lai, Q. Q. Chen, Q. Y. He, Q. L. Fan and W. Huang, *Chem. Commun.,* 2006, 1959.

3 Experimental

3.1 Evaluation of the Materials

^{1}H Nuclear Magnetic Resonance (^{1}H NMR) Spectroscopy

The structures of intermediates and final products synthesised in the thesis were confirmed by ^{1}H NMR spectroscopy using a JEOL Lambda 400 MHz spectrometer. Tetramethylsilane (TMS) was used as an internal standard. A series of abbreviations for describing ^{1}H NMR splitting patterns are included in **Table 3.1**.

Table 3.1 Abbreviations for describing ^{1}H NMR splitting patterns

Abbreviation	Meaning
s	Singlet
d	Doublet
dd	Double doublet
t	Triplet
dt	Double triplet
tt	Triple triplet
quart	Quartet
quint	Quintet
sext	Sextet
m	Multiplet

^{13}C Nuclear Magnetic Resonance (^{13}C NMR) Spectroscopy

^{13}C NMR spectroscopy was used to confirm the chemical identity of compounds synthesised in this thesis using a JEOL Lambda 400 spectrometer. Tetramethylsilane (TMS) was used as an internal standard.

Mass Spectrometry (MS)

Mass spectra were used to determine the chemical structures and masses of molecules by measuring the mass-to-charge ration and relative-abundance of gas-phase ions. For compounds with a RMM > 800 g/mol, mass spectra were recorded using a Bruker, reflex IV, Matrix Assisted Laser Desorption/Ionisation (MALDI), Time of Flight (TOF) mass spectrometer. Compounds with a RMM < 800 g/mol were analysed using a Shimadzu Gas Chromatography/Mass Spectrometer (GC-MS)-QP5050A with Electron Impact (EI) detector at a source temperature of 200 ^{o}C. A 384 well microlitre plate format was used with a scout target. From the mass spectrum of a compound, its mass ion is identified as M^+, and the most stable fragment is marked as M100.

Infrared Spectroscopy (IR)

Infrared spectroscopy was used to identify function groups of compounds. IR spectra were recorded using a Nicolet iS5 Fourier Transform-Infrared (FT-IR) spectroscope/spectrometer from Thermo Fisher Scientific.

Elemental Analysis (EA)

Elemental analyses (EA) of all final compounds were performed using a Fisons EA 1108 CHN apparatus in order to confirm the purity of these compounds.

Melting Points and Transition Temperatures

An Olympus BH2 optically polarising microscope equipped with a Mettler FP-5 hot stage or an Olympus BX51 optically polarising microscope fitted with Linkam LTS 350 temperature-controlled stage was performed to determine melting points and other transition temperatures for all compounds synthesised in the thesis. A Perkin-Elmer Differential Scanning Calorimeter (DSC) 7 or a Mettler Toledo DSC 1 equipped with a TAC 7/3 instrument controller, was used to measure the phase transition temperatures and calculate enthalpies of transition of final products. An indium standard sample

reference was used to calibrate of the calorimeter (onset of melting point = 156.6 °C, $\Delta H = 28.45$ J/g).

Chromatography and Re-Crystallisation

The progress of reactions was typically followed by thin layer chromatography (TLC). The TLC plates used consisted of a thin rectangular aluminium back-plates, which were coated with a thin layer of silica gel type 60 F_{254} from Merck. Most of the reaction intermediates and final compounds were purified by column chromatography using silica gel (pore size 60 Å, 200-300 mesh, 40-63 μm particle size, Sigma-Aldrich). However, for some reactions with good yield and few-to-no side-products, purification was performed by dry flash column vacuum chromatography with silica gel (pore size 22 Å, 28-200 mesh, Sigma-Aldrich). The reaction intermediates and final compounds were dried under vacuum and then stored in glass sample tubes. Re-crystallisation was used to further purify target compounds whose side-products could not be easily removed by column chromatography alone.

Reagents and Reaction Solvents

All reactions were carried out under a dry nitrogen atmosphere, unless otherwise stated. Reagents were purchased from commercial sources, such as Fluorochem, Sigma-Aldrich, Alfa Aesar Acros organics, Apollo or TCI, and were used without further purification unless otherwise stated. For reaction solvents, tetrahydrofuran (THF) was distilled over sodium wire under a nitrogen atmosphere and then stored over molecular sieves (3Å). Dimethylformamide (DMF) was distilled over P_2O_5 and stored over molecular sieves (3Å). Triethylamine was distilled over potassium hydroxide (KOH) pellets and stored over molecular sieves (3Å). All other solvents were purchased from Fisher and used without further purification. Some abbreviations of common solvents and reagents are collated in **Table 3.2** as below:

Table 3.2 Abbreviations for solvents and reagents used in this thesis

Abbreviations	Full name
DCM	Dichloromethane
DME	1,2-Dimethoxyethane
DMF	*N*,*N*-Dimethyl formamide
THF	Tetrahydrofuran
EtOH	Ethanol
DMSO	Dimethyl sulfoxide
MeOH	Methanol
Et_2O	Diethyl ether
EtOAc	Ethyl acetate
n-BuLi	*n*-Butyllithium
NBS	*N*-Bromosuccinimide
$Pd(PPh_3)_4$	*Tetrakis*(triphenylphosphine)palladium(0)
$Pd(OAc)_2$	Palladium (II) acetate
PPh_3	Triphenylphosphine
$PdCl_2$	Palladium (II) chloride
TBAB	*Tetra-n*-butylammonium bromide
18-crown-6	1,4,7,10,13,16-Hexaoxacyclooctadecane
DMAP	4-(Dimethylamino)pyridine
PCy_3HBF_4	Tricyclohexylphosphine
PiOH	Pivalic acid
NaH	Sodium hydride
K_2CO_3	Potassium carbonate
$NaCO_3$	Sodium carbonate
KOH	Potassium hydroxide
Cu	Copper
Mg	Magnesium

3.2 Discussion of the Syntheses

The synthetic pathways to the intermediates and final products are shown below. A brief discussion of the syntheses and some of the synthetic problems encountered are included below. Further synthetic analysis and comparison for important reaction styles used in this thesis will be shown in Results and Discussion Chapter.

3.2.1 Scheme 1

The synthesis and application of carbazole-functional derivatives have been of great interest in materials chemistry, especially in organic electronics, due to their intrinsic photo-physical and redox properties, e.g. relatively intense luminescence and reversible oxidation processes, π-stacking capability and ease of further derivation[1-4]. Therefore, a series of carbazole-functionalised derivatives containing different cores were synthesised and are discussed below. An Ullmann aryl-aryl, cross-coupling coupling was carried out between 2,5-dibromonitrobenzene (**1**) and 4-iodoanisole (**2**) using copper powder as catalyst at 175 $^{\circ}$C to give 4-bromo-4'-methoxy-2-nitrobiphenyl (**3**) in moderate yield (55%). A ring closing reaction of compound **3** with triphenyl phosphine as reagent at high temperature gave 2-bromo-7-methoxycarbazole (**4**) in good yield (76%). In the majority of published papers[5-6] triethyl phosphite was used as a reagent in ring-closing reactions and their yields average 70%, which is approximately same obtained when using triphenyl phosphine as an alternative. However, solid triphenyl phosphine is safer and less harmful than liquid triethyl phosphine. Compound **4** was alkylated using commercially available 1-bromooctane using a sodium hydride (NaH) dispersion in hexanes as a base and dimethyl formamide (DMF) as the solvent to give 2-bromo-7-methoxy-9-octylcarbazole (**5**) in good yield (71%). Purification of compound **5** does not require column chromatography, as isolation of the material from impurities could be achieved through exploiting their relative solubilities. Compound **5** was lithiated with *n*-butyllithium at -78 °C and then reacted with commercially available 2-triisopropyl borate. Hydrolysis with aqueous hydrochloric acid gave

(7-methoxy-9-octyl-carbzole-2-yl)boronic acid (**6**) in moderate yield (63%). Compound 2,2'-bithiophene (**7**) was brominated using *N*-bromosuccinimide (NBS) in DCM in darkness to give 5,5'-dibromo-2.2'-bithiophene (**8**) in good yield (73%). Generally, NBS is the preferred as a brominating agent over molecular bromine, due to the post-reaction removal of brominating agent. Silica gel was added in order to free bromine from NBS. Its function is similar to acetic acid, offering hydrogen free radical. However, as silica gel is insoluble, it is easy to remove from the product at the end of reaction. Furthermore, the reaction was carried out in the dark in an attempt to dibrominate the thiophene rings of compound **8** selectively and specifically. TLC monitoring of the reaction was performed in order to stop the reaction before over-bromination of the thiophene groups. 5,5'-*bis*-(7-Methoxy-9-octyl-carbazol-2-yl)-2,2'-bithiophene (**9**) (83%) was synthesised in excellent yield using a Suzuki aryl-aryl, cross-coupling reaction between compounds **6** and **8** using Pd(OAc)$_2$ as the catalyst, K$_2$CO$_3$ as the base, DMF as the solvent.

In terms of the mechanism of the Suzuki aryl-aryl, cross-coupling reaction, the valence of palladium for catalysing should be zero, and so a ligand should be present to stabilise the zero valence. However, the palladium (II) acetate catalyst was added without the ligand and a very good yield was still observed. A possible reason for this observation is that the combination between palladium and acetate is weak, and the valence of palladium is easy to be transferred from two into zero during the reaction in the presence of a polar solvent, such as DMF, and an aqueous potassium carbonate solution. Furthermore, it should be pointed out that direct arylation between compounds **5** and **7** using a mixture of pivalic acid, K$_2$CO$_3$, Pd(OAc)$_2$, PCy$_3$HBF$_4$ and NMP was tried, but failed. A possible reason is that the bromo-functional group of compound **5** with big steric hindrance is not active enough to satisfy the energy requirement of a direct arylation reaction.

3.2.2 Scheme 2

A Suzuki aryl-aryl, cross-coupling reaction was carried out to give 1,4-*bis*-(thien-2-yl)benzene (**12**) in excellent yield (97%). A possible reason for high yield is that work-up of the reaction system is relatively simple, involving just washing away the impurities with methanol due to the relative insolubility of compound **12**. Compound **12** was then brominated by using NBS in DMF in darkness to give 1,4-*bis*-(5-bromothiophen-2-yl)benzene (**13**) in excellent yield (94%). 1,4-*bis*-[5-(7-Methoxy-9-octyl-carbazol-2-yl)thiophen-2-yl]benzene **14** was synthesised in moderate yield (60%) using a Suzuki aryl-aryl cross-coupling reaction between compounds **6** and **13** catalysed by Pd(OAc)$_2$ using PPh$_3$ and K$_2$CO$_3$, with DME as solvent. Polar DME is a commonly employed solvent for Suzuki couplings, and it has good inter-solubility with boronic acid and aqueous base, so that a more homogeneous reaction system was obtained. The solubility of starting materials was also a consideration when solvent was chosen for Suzuki reactions. Additionally, in terms of traditional mechanisms, the presence of the triphenyl phosphine ligand is usually considered beneficial in palladium-catalysed Suzuki aryl-aryl cross-coupling reaction, helping stabilise the nominally zero valence of palladium for catalysing, so that higher yield should be attained. However, it was found that the reaction mixture was more difficult to purify, due to the formation of more by-products in the presence of triphenyl phosphine, which led to the lower yield for the Suzuki reactions carried out in the presence of triphenyl phosphine. This is likely due to the formation of homo-coupled products due to the increased catalyst activation in the presence of triphenyl phosphine.

3.2.3 Schemes 3 & 4

2,7-Dibromo-9,9-dipropyl-fluorene (**16**) was synthesised in a one-step procedure from commercially available 2,7-dibromofluorene (**15**) using 1-bromopropane, a 50% aqueous solution of sodium hydroxide, a phase transfer catalyst (TBAB) and toluene as

solvent in good yield (80%). A Stille aryl-aryl, cross-coupling reaction was carried out using 2,7-dibromo-9,9-dipropyl-fluorene (**16**), 2-(tributylstannyl)thiophene, *tetrakis*(triphenylphosphine)palladium(0) as catalyst, and DMF as solvent to afford symmetrical *bis*-thiophene intermediate **20** in good yield (79%). The position 5 of two thiophene rings of compound **20** was then brominated by using NBS as brominating agent in acetic acid and chloroform as solvent in the dark to give 2,7-*bis*-(5-bromothiophen-2-yl)-9,9-dipropyl-fluorene (**21**) in good yield (77%). The Suzuki aryl-aryl, cross-coupling reactions between the fluorene-derivative cores **16**, **17** and **21** with the boronic acid **6** under the same reaction conditions, with a mixture of Pd(OAc)$_2$, K$_2$CO$_3$ and DMF, to give 7,7'-(9,9-dipropyl-fluorene-2,7-diyl)-*bis*-(2-methoxy-9-octyl-carbazole) (**18**) in excellent yield (93%), 7,7'-(9,9-dioctyl-fluorene-2,7-diyl)-*bis*-(2-methoxy-9-octyl-carbazole) (**19**) in very good yield (82%) and 2,7-[*bis*(thien-2-yl)-9,9-dipropyl-fluorene-5,5-diyl]-*bis*-(2-methoxy-9-octylcarbazole) (**22**) in good yield (74%).

3.2.4 Schemes 5 & 6

3-Ethyl-4-methyl-3,4-dicarboxylate-2-iodothiophene (**24**) was obtained in moderate yield (43%) *via* nitration of 3-ethy-4-methyl-3,4-dicarboxylate-2-aminothiophene (**23**) with nitrous acid generated *in situ* from sodium nitrite and hydrochloric acid at 0 $^{\text{o}}$C, leading to the diazonium salt, which was then reacted *in situ* with potassium iodide. A possible reason for obtaining only a moderate yield is that the aromatic diazonium salt intermediate could degrade before reacting. The dicarboxylate **24** was then acidified using hydrochloric acid to afford 2-iodothiophene-3,4-dicarboxylic acid (**25**) in excellent yield (96%). The dicarboxylic acid **25** was dehydrated using acetic anhydride to give the five-numbered cyclic anhydride, which was then amidated by dodecylamine using 4-(dimethylamino)pyridine (DMAP) as a strong nucleophilic reagent to consume the acid generated from the process of amidation reaction, so that the chemical

equilibrium shifts to yield more of the desired product 5-dodecyl-1-iodo-5*H*-thieno-[3,4-*c*]pyrrole-4.6-dione (**26**) in excellent yield (90%). Compound **26** was brominated by using NBS in trifluoroacetic acid and sulphuric acid to afford 1-bromo-5-dodecyl-3-iodo-5*H*-thieno-[3,4-*c*]pyrrole-4,6-dione (**27**) in good yield (77%). Attempts at bromination using NBS and silica gel in DCM failed. A possible reason for this failure is that compound **26** has large steric bulk, which results in the difficulty of the substitution of the position 5 of the thiophene ring. A Suzuki reaction between compound **27** and thiophen-2ylboronic acid (**11**) was carried out using Pd(PPh$_3$)$_4$ and aqueous sodium carbonate in DME to afford 5-dodecyl-1,3-di(thiophen-2-yl)-5*H*-thieno[3,4-*c*]pyrrole-4,6-dione (**29**) in moderate yield (61%). Compound **29** was then brominated with bromine in acetic acid and chloroform to give 1,3-*bis*-(5-bromothiophen-2-yl)-5-dodecyl-5*H*-thieno-[3,4-*c*]pyrrole-4,6-dione (**30**) in excellent yield (96%). Attempts at synthesising **30** with NBS in acetic and chloroform failed. The Suzuki aryl-aryl, cross-coupling reactions between compounds **27** and **30** and the boronic acid **6** under the same reaction conditions using Pd(OAc)$_2$ as catalyst, K$_2$CO$_3$ aqueous as base and DMF as solvent to give compounds 5-dodecyl-1,3-*bis*-(7-methoxy-9-octyl-9*H*-carbazol-2-yl)-5*H*-thieno[3,4-*c*]pyrrole-4,6 -dione (**28**) and 5-dodecyl-1,3-*bis*-[5-(7-methoxy-9-octyl-9*H*-carbazol-2-yl)thiophen-2-yl]-5*H*-thieno-[3,4-c]pyrrole-4,6-dione (**31**) in good yield (72% and 76%, respectively).

3.2.5 Schemes 7-10

1-(Octyloxy)-4-iodobenzene (**33**) was synthesised in excellent yield (95%) by reacting 4-iodophenol (**32**) with 1-bromooctane, using K$_2$CO$_3$, with DMF as the solvent at 120 ^{o}C. An Ullmann cross-coupling reaction was carried out between 2,5-dibromonitrobenzene (**1**) and compound **33** using copper powder as catalyst at 175 ^{o}C to give 4-bromo-4'-octyloxy-2-nitrobiphenyl (**34**) in good yield (69%). The 2-bromo-7-octyloxycarbazole (**35**) was obtained from the ring closure reaction of

compound **34** with triethyl phosphite in good yield (78%). Compared with the synthesis of compound **4** shown in scheme 1, we tried triethyl phosphate to substitute triphenyl phosphine, proving approximate yield with 78%, and 76%, respectively. However, it should be pointed out that the purification of compound **4** was less efficient as column chromatography had to be carried out with more solvent consumption, with similar yields obtained. Additionally, triphenyl phosphine is safer. Therefore, we tried to use a 25% excess of triphenyl phosphine for the ring closing reaction of compound **34** in order to decrease by-products and facilitate purification, but resulted in a very poor yield. Therefore, liquid triethyl phosphate was tried and the result showed easier purification and good yield. Although triethyl phosphate is more harmful than triphenyl phosphine, all reaction procedures and purification were performed in a fume cupboard. Compound **35** was alkylated using commercially available 1-bromooctane, using NaH, with DMF as the solvent to give 2-bromo-9-dodecyl-7-octyloxy-carbazo (**36**) in excellent yield (99%). Commercially available 2-triisopropyl borate was used to treat the lithiated compound **36** with *n*-butylithium at -78 °C. Hydrolysis of the reaction mixture with aqueous hydrochloric acid gave [*N*-octyl-7-(octyloxy)-carbazol-2-yl]boronic acid (**37**) in excellent yield (92%). Compared with the structures of **scheme 1**, the alkyl chain was extended from methoxy to octyloxy. The synthesis of dibrominated aromatic cores **8**, **13**, **17**, and **21** were described above, which were reacted with the same boronic acid **37** in a Suzuki aryl-aryl cross-coupling reaction using Pd(PPh$_3$)$_4$ as catalyst, K$_2$CO$_3$ aqueous as base and DMF as solvent to give 5,5'-*bis*-[9-octyl-7-(octyloxy)-carbazol-2-yl]-2,2'-bithiophene (**38**) in excellent yield (82%), 1,4-*bis*-{5-[9-octyl-7-(octyloxy)-carbazol-2-yl]thiophen-2-yl}benzene (**39**) (73%), 7,7'-(9,9-dioctyl-fluorene-2,7-diyl)-*bis*-[9-octyl-7-(octyloxy)-carbazole] (**41**) (73%),

2,7-[*bis*(thien-2-yl)-9,9-dipropyl-fluorene-5,5-diyl]-*bis*-[9-octyl-7-(octyloxy)-carbazole] (**42**) (75%). The reaction required the use of freshly generated catalyst *tetrakis*(triphenylphosphine)palladium(0) (Pd(PPh$_3$)$_4$), since all attempts to use commercially sourced, but pre-opened Pd(PPh$_3$)$_4$ resulted in low yields. The

tetrakis(triphenylphosphine)palladium(0) was synthesised from palladium dichloride using triphenyl phosphine, dimethyl sulphoxide, and hydrazine hydrate to afford the catalyst in very good yield (87%) according to a modified literature method[7].

3.2.6 Schemes 11-14

The compound 2,2'-bithiophene (**7**) was reacted with *n*-BuLi in hexanes and then the 2-tributyltin chloride was added to give the mono-substituted tin compound **43** in excellent yield (95%). Only 1% excess of 2-tributyltin chloride was added in order to minimise the bi-substitutions of 2,2'-bithiophene. A Stille aryl-aryl cross-coupling between 2,7-dibromo-9,9-dioctyl-fluorene (**17**) and 2,2'-(5-tributylstannanyl)bithiophene (**43**) was carried out using Pd(PPh$_3$)$_4$ in DMF to afford

2-{9,9-dioctyl-7-[5-(thiophen-2-yl)thiophen-2-yl]-9-fluoren-2-yl}-5-(thiophen-2-yl)thiophene (**44**) in moderate yield (63%). It was then brominated using NBS and silica gel in DCM to give 2-(5-bromothiophen-2-yl)-5-{7-[5-(5-bromothiophen-2-yl)thiophen-2-yl]-9.9-dioctyl-fluoren-2-yl}thiophene (**45**) in excellent yield (95%). 4,7-Dibromo-2,1,3-benzothiadiazole **51** was synthesised in moderate yield (62%) by the bromination of commercially available 2,1,3-benzothiadiazole **50** using molecular bromine in hydrogen bromide solution. After the reaction was deemed to be complete, a saturated aqueous solution of sodium bisulphite (NaHSO$_3$) was added to completely consume any excess of bromine. The cores **45**, **47**, **51** and **27** were reacted with the boronic acid **37** in a Suzuki aryl-aryl cross-coupling reactions using Pd(PPh$_3$)$_4$, aqueous K$_2$CO$_3$ and DMF to give 3,3'-{5',5'''-(9,9-dioctyl-fluorene-2,7-diyl)*bis*[(2,2'-bithiophene)-5',5-diyl]}*bis*-[9-octyl-7-(octyloxy)-carbazole] (**46**) in good yield (72%), 3,7-*bis*-[9-Octyl-7-(octyloxy)-carbazol-2-yl]dibenzo[*b,d*]thiophene (**49**) in very good yield (86%), 4,7-*bis*-[9-Octyl-7-(octyloxy)-carbazol-2-yl]benzo[*c*][1,2,5]thiadiazole (**53**) in excellent yield (93%),

5-Dodecyl-1,3-*bis*-[9-Octyl-7-(octyloxy)-carbazol-2-yl]-5-thieno[3,4-*c*]pyrrole-4,6-di one (**54**) in very good yield (83%), respectively. In addition, the intermediates **47** and **51** were also reacted with the boronic acid **6** to give both 3,7-*bis*-(7-methoxy-9-octyl-carbazol-2-yl)dibenzo[*b,d*]thiophene (**48**) and 4,7-*bis*-(7-methoxy-9-octyl-carbazol-2-yl)benzo[*c*][1,2,5]thiadiazole (**52**) in very good yield (88% and 82%, respectively).

3.2.7 Schemes 15 & 16

Compound **35** was alkylated using commercially available 1-bromododecane, using NaH and DMF, to give 2-bromo-*N*-dodecyl-7-(octyloxy)-carbazole (**55**) in a very good yield (86%). Commercially available 2-triisopropyl borate was used to treat the lithiated compound **55** with *n*-butyllithium at -78 °C. Hydrolysis of the reaction mixture with hydrochloric acid gave [*N*-dodecyl-7-(octyloxy)-carbazol-2-yl]boronic acid (**56**) in very good yield (86%). The intermediates **8** and **13** were reacted with the boronic acid **56** in a Suzuki aryl-aryl cross-coupling reaction, using $Pd(OAc)_2$, $P(Ph)_3$, aqueous K_2CO_3 and DME, to give 5,5'-*bis*-[9-dodecyl-7-(octyloxy)-carbazol-2-yl]-2,2'-bithiophene (**57**) and 1,4-*bis*-{5-[9-dodecyl-7-(octyloxy)-carbazol-2-yl]thiophen-2-yl}benzene (**58**) in moderate yield (64% and 62%, respectively). As discussed above, a possible reason for obtaining only moderate yields is that reaction mixture is more difficult to purify due to the formation of more by-products in the presence of $P(Ph)_3$ used as a ligand *in situ*. In addition, the solubility of reaction mixture in DME is also possibly lower than in DMF.

3.2.8 Schemes 17 & 18

A Grignard reaction was carried out between ethyl formate (**59**) and freshly prepared octyl magnesium bromide, prepared from 1-bromooctane and magnesium in THF, to give heptadecan-9-ol (**60**) in excellent yield (82%). *p*-Toluene-sulfonyl chloride was used to convert the alcohol **60** into corresponding toluene-sulfonate **61** in pyridine in excellent yield (95%). Compounds **4** and **35** were reacted with compound **61,** using

KOH, 18-crown-6 and DMSO, to give 2-bromo-9-(heptadecan-9-yl)-7-methoxy-carbazole (**62**) and 2-bromo-9-(heptadecan-9-yl)-7-octyloxy-carbazole (**65**) in good yield (72% and 78%, respectively). 2-Triisopropyl borate was used to treat the reaction mixture after lithiation of compounds **62** & **65** with *n*-butylithium at -78 ℃. Acidification with hydrochloric acid gave [*N*-(heptadecan-9-yl)-7-methoxy-carbazol-2-yl]boronic acid (**63**) and [9-(Heptadecan-9-yl)-7-octyloxy-carbazol-2-yl]boronic acid (**66**) in excellent yield (98% and 97%, respectively). 2-Bromothiophene (**68**) was brominated with NBS to give 2,5-dibromothiophene (**69**) in good yield (75%). A Stille aryl-aryl cross-coupling reaction between compound **69** and 2-(tributylstannyl)thiophene was carried out to afford 2,2':5',2"-terthiophene (**70**) in good yield (81%). Compound **70** was then brominated with NBS to give 5,5"-dibromo-2,2':5',2"-terthiophene (**71**) in good yield (82%). The intermediates **13** and **71** were reacted with the boronic acids **63** and **66** in Suzuki aryl-aryl cross-coupling reactions using Pd(OAc)$_2$, P(Ph)$_3$ as ligand, aqueous K$_2$CO$_3$ as base and DME as solvent to give 1,4-*bis*-{5-[*N*-(heptadecan-9-yl)-7-methoxy-carbazol-2-yl]thiophen-2-yl}benzene (**64**) in good yield (76%), 1,4-*bis*-{5-9-(heptadecan-9-yl)-7-(octyloxy)-carbazol-2-yl]thiophen-2-yl}benzene (**67**) in moderate yield (46%), 5,5"-*bis*-[9-(heptadecan-9-yl)-7-methoxy-carbazol-2-yl]-2,2':5',2"-terthiophene (**72**) in good yield (67%), and 5,5"-*bis*-[9-(heptadecan-9-yl)-7-(octyloxy)-carbazol-2-yl]-2,2':5',2"-terthiophene (**73**) in poor yield (36%), respectively.

3.2.9 Scheme 19

Commercially available 2-triisopropyl borate was used to treat the reaction mixture after lithiation of 1-bromo-4-methoxybenzene (**74**) with *n*-butylithium at -78 ℃. Then the mixture was warmed to room temperature, stirred overnight and acidified with hydrochloric acid to give 4-methoxyphenylboronic acid (**75**) with excellent yield 90%.

A Suzuki cross-coupling between compound **75** and 2-bromothiophene (**68**) was carried out using Pd(PPh$_3$)$_4$ as catalyst to afford 2-(4-methoxyphenyl)thiophene (**76**) in excellent yield (91%). Compound **76** was lithiated with *n*-butylithium at -78 ℃ and then reacted with commercially available 2-triisopropyl borate. Acidification with hydrochloric acid gave 5-(4-methoxyphenyl)thiophen-2-ylboronic acid (**77**) in excellent yield (93%). 2-Bromofluorene (**78**) was iodinated in position 7 with pulverised iodine and periodic acid in acetic acid, concentrated sulphuric acid, and water to afford 2-bromo-7-iodofluorene (**79**) in moderate yield (68%). 2-Bromo-7-iodo-9,9-dihexylfluorene (**80**) was synthesised in a one-step procedure from compound **79** using 1-bromohexane, powered potassium hydroxide, potassium iodide, and DMSO as solvent in good yield (75%). A Suzuki aryl-aryl, cross-coupling reaction between compounds **80** and **77** was carried out using Pd(PPh$_3$)$_4$, aqueous K$_2$CO$_3$ and DMF to give 2-(7-bromo-9,9-dihexyl-9-fluoren-2-yl)-5-(4-methoxyphenyl)thiophene (**81**) in moderate yield (65%). Commercially available 2-triisopropyl borate was used to treat the reaction mixture after lithiation of compound **81** with *n*-butylithium at -78 ℃. Acidification with hydrochloric acid gave 9,9-dihexyl-7-[5-(4-methoxyphenyl)thiophen-2-yl]-9-fluoren-2-ylboronic acid (**82**) in good yield (71%). A Suzuki aryl-aryl cross-coupling reaction between compounds **82** and **45** was carried out using Pd(PPh$_3$)$_4$, aqueous K$_2$CO$_3$ and DMF to give 3,3'-{5',5'''-(9,9-dioctyl-9-fluorene-2,7-diyl)*bis*[(2,2'-bithiophene)-5',5-diyl]}*bis*-{9,9-dihexyl-7-[5-(4-methoxyphenyl)thiophen-2-yl]-9-fluorene} (**83**) in good yield (92%). A similar compound to compound **83** but with two oxyoctyl end groups instead of methoxyl has been studied in our group[8-9], but the synthetic procedures of some intermediates have been slightly modified and improved with higher yields in this scheme. For example, compound **76** was obtained in this scheme using 2-bromothiophene (**68**) and 4-methoxyphenylboronic acid (**75**) with an excellent yield of 91%, instead of using 1-bromo-4-methoxybenzene and 2-thienylboronic acid or 2-(tributylstannyl)thiophene. Furthermore, 2-Triisopropyl borate, instead of 2-tributyltin chloride, was used to treat the reaction mixture after lithiation of

compound **76**, so that solid boronic acid **77** was obtained with easier purification and storage.

3.2.10 Scheme 20

Star-shaped, carbazole-functionalised triazatruxenes with a central aromatic core and flexible aliphatic chains were studied in this work as potential organic semiconductors, especially for organic light-emitting diodes (OLEDs). The triazatruxene **85** can be obtained by several different synthetic routes. However, the synthetic approach with the highest yield and simplest procedures is that using the starting materials **84** and phosphorus (V) oxychloride (POCl$_3$), which were commercially available and used without further purification. The triatruxene **85** was obtained with better yield (45%) compared with the low yields (13% and 6%) shown in some published papers[10-13]. The triazatruxene core consists of a symmetric cycle-trimer of indoles, which presents a wide aromatic surface with three facile points for the attachment of side chains. The presence of three amino-groups (-NH) facilitates the synthesis of a wide range of materials. The insertion of the desired side chains could be performed by *N*-alkylation under basic conditions to give the corresponding tris-*N*-substituted derivatives. In order to identify appropriate base and solvent for higher yield of N-alkylation reaction, we compared different reaction conditions. Compounds **88** and **87** with excellent yields, 81% and 88% respectively, were synthesised by using NaH and DMF. Compound **86**, however, was obtained in good yield 73% by using KOH in THF. It shows they all have a good yield for *N*-alkylation reactions, although the yield of compound **86** showed a slight decrease. However, we noticed that the purifications of compounds **88** and **87** are easier than that of compound **86**, because the *N*-alkylation reaction for synthesising compound **86** produced more side-products. This is probably due to higher reaction temperature used when THF was used as a solvent, as compared with that used when DMF was used as a solvent. Although the syntheses of tri-*N*-alkyl triazatruxenes as intermediates have been reported, the synthetic procedures, starting materials and reaction solvents are various in different journal papers, some of which showed more

reaction steps with low yield and similar side-products with different purification[14-16].

3.2.11 Scheme 21

The triatruxene **85** was *N*-substituted by allyl bromide and 6-bromo-1-hexene using DMF as solvent and NaH as base to give compounds **89** and **90** with good yield (both 75%). Compound **91,** containing triple bonds, was obtained by alkylation of the triatruxene **85** using 1-bromo-2-butyne in moderate yield (62%) using DMF as the solvent and NaH as the base. Unfortunately, the analogous reaction between 4-bromo-1-butyne and triatruxene **85** in order to obtain the triple bonds at the end of group failed, although a range of different reaction conditions, including NaH and DMF, K_2CO_3 and DMF, as well as K_2CO_3 and butanone, were tried. It was thought that the triple bond at the end of group might not be stable to purification through silica gel. In fact, ^{1}H NMR analysis carried out on the reaction mixture before purification by column chromatography showed that the triatruxene **85** was unaffected, but that 4-bromo-1-butyne had been consumed by the reaction. Therefore, it is possible that the triple bond at the end of group reacts with the alkyl bromide rather than with than amino-groups (-NH) on the carbazole or triazatruxene core under basic condition.

3.2.12 Scheme 22

Non-conjugated dienes can be photo-chemically cross-linked to form stable polymer networks as stable, thin films, but are much less likely to spontaneously polymerise, e.g., during purification, than analogous acrylates or methacrylates. Therefore, we synthesised the non-conjugated diene **92** as a monomer. Penta-1,4-dien-3-yl-11-bromoundecanoate was be obtained from esterification of 11-bromoundecanoic acid with 1,4-pentadien-3-ol and, fortunately, penta-1,4-dien-3-yl-11-bromoundecanoate was available from a previous research programme. The reaction conditions for synthesising compound **92** were different from those used in the *N*-substitution of triazatruxene core using the alkyl bromide shown above. The combinations KOH & THF, K_2CO_3 & DMF, and NaH & DMF, respectively,

were tried. Two of these three reactions failed and the unreacted core was isolated using KOH & THF and K_2CO_3 & DMF. The compound **92** was obtained by using NaH as base and DMF as solvent in low yield (36%). The possible reasons are that ester bonds are unstable under strong basic conditions and triazatruxene core requires strong basic conditions to activate NH positions.

3.2.13 Schemes 23 &24

Compound **95** was obtained in good yield (61%) by amidation of diallyl amine with 5-bromovaleryl chloride, both of which were purchased directly from Aldrich and were used without further purification. A tertiary amide is more stable to hydrolysis than an ester bond, thereby the intermediate compound **95** was synthesised to prepare compound **96,** using NaH and DMF, to give the desired product in very good yield (86%), which is much better than the yield (36%) than that obtained for compound **92**. Compound **99** was synthesised in moderate yield (51%) by amidation of bromoacetyl bromide and diallyl amine with triethylamine and ethyl acetate as solvent. A reaction between 3-bromopropionyl chloride and diallyl amine did not work, even though different solvents, including triethylamine, pyridine and DCM, were tried. The possible reason is that if the distance between the two end groups (bromo-substitution and acyl chloride) is too short, it could affect the activity of acyl chloride. Therefore, bromoacetyl bromide, with a higher activity, was used to complete the amidation in moderate yield (51%). Compound **99** was reacted with the triatruxene **85,** using NaH as a base and DMF as the solvent, to give compound **100** as a white solid in moderate yield (46%), which is lower than that achieved in the synthesis of compound **96** (86%). Probably as described above, if the distance between the two end groups (bromo-substitution and acyl chloride) is too short, it might reduce the activity of not only the acyl chloride, but also that of the bromo-group in compound **99**.

3.2.14 Scheme 25

The triatruxene **85** was alkylated using 3-[(5-bromopentyloxy)methyl]-3-methyloxetane and 3-bromomethyl-3-methyloxetane to give compounds **101** and **102** in moderate yield (42% and 58%, respectively). Most of following substitution reactions of the intermediate **85** were carried out using NaH and DMF.

3.2.15 Scheme 26 & 27

One of the merits of triazatruxene is that three amino-groups (-NH) facilitate the attachment of side chains to synthesise a wide range of materials. Therefore, we also synthesised and investigated a series of trizatruxene-core materials with different function groups. Compound **104** was obtained in excellent yield (87%) from the triatruxene **85** substituted by (bromomethyl)cyclopropane. One of merits of this reaction is purification is easy, without the need for column chromatography. The reasons are probably that cyclic alkyl group is stable, there is no side reaction, and the side chains are not too long. In addition, carbazole-functionalised materials with ether and ester bonds were obtained and compared. Compounds **103** and **105** with cyclic ether and aliphatic ether functional groups were synthesised in good yields (43% and 70%, respectively). Compounds **106** and **107** with ester functional groups, but in different positions, were synthesised in good yields (58% and 71%, respectively). Generally, their yields are good, but the positions of functional groups can affect the reaction efficiency as well. The triatruxene **85** was alkylated using 2-bromoethyl isocyanate to produce compound **108** with the low yield (38%). This is probably because isocyanates can react with themselves. Furthermore, isocyanates are electrophiles, and as such they are reactive toward a variety of nucleophiles including alcohol, amines, and even water. In addition, it should be mentioned that isothiocyanate functional group was also tried, but this reaction failed, even though different bases and solvents, including NaH & DMF, and K_2CO_3 & butanone, were tried. The triatruxene

85 was recuperated from the reaction mixture, but the 3-bromopropyl isothiocyanate had been consumed. This is probably because isothiocyanates are susceptible to hydrolysis and triazatruxene **85** requires strong base to activate NH positions. Compound **109** was obtained from the triazatruxene **85** using 5-bromovaleronitrile in good yield (70%).

3.3 Synthetic Schemes

Scheme 1
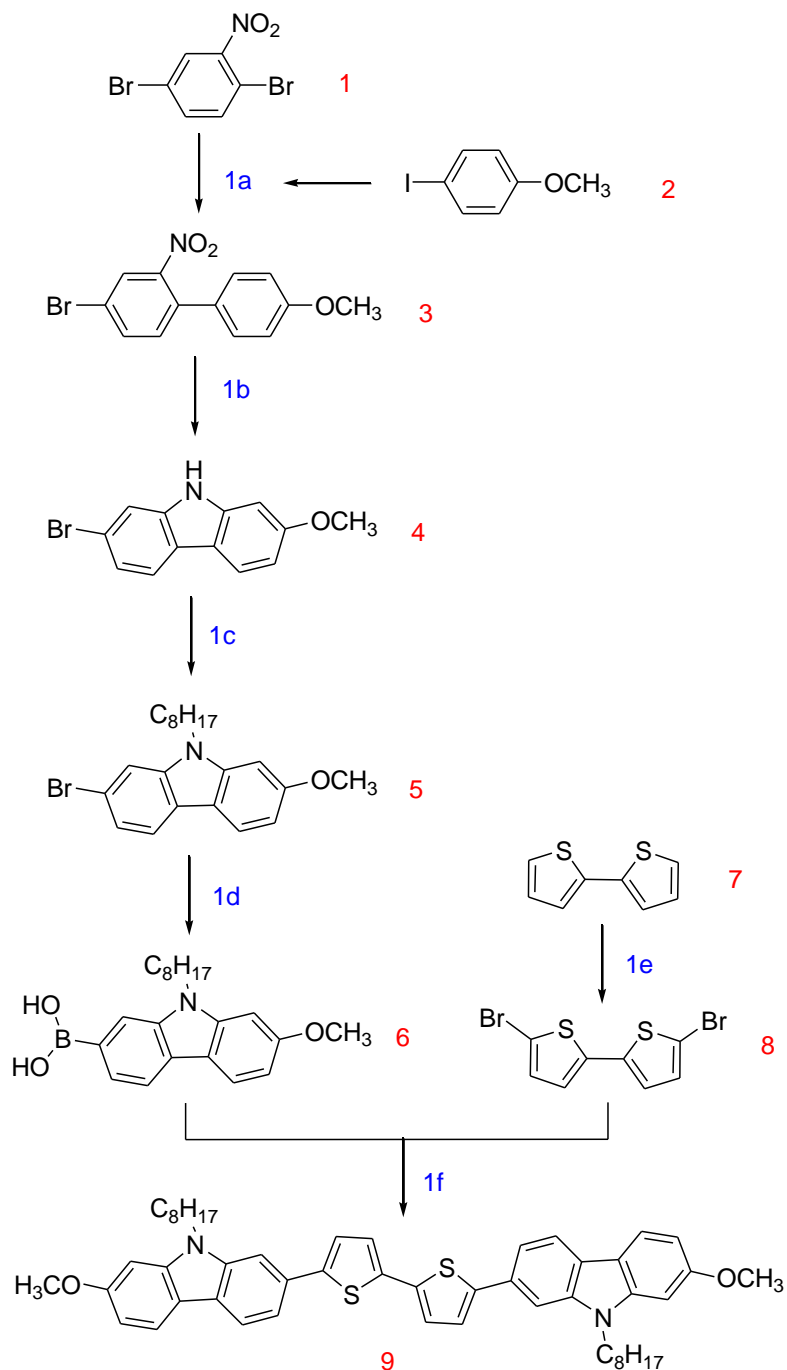
1a: Copper powder, 175 °C;
1b: Triphenyl phosphine (P(Ph)$_3$), reflux;
1c: 1-Bromooctane, NaH (60% dispersion in mineral oil), DMF;
1d: (i): n-BuLi, 2-triisopropyl borate, THF, -78 °C; (ii): Hydrochloric acid, RT;
1e: N-bromosuccinimide (NBS), silica gel, DCM
1f: Pd(OAc)$_2$, K$_2$CO$_3$, water, DMF, 80 °C.
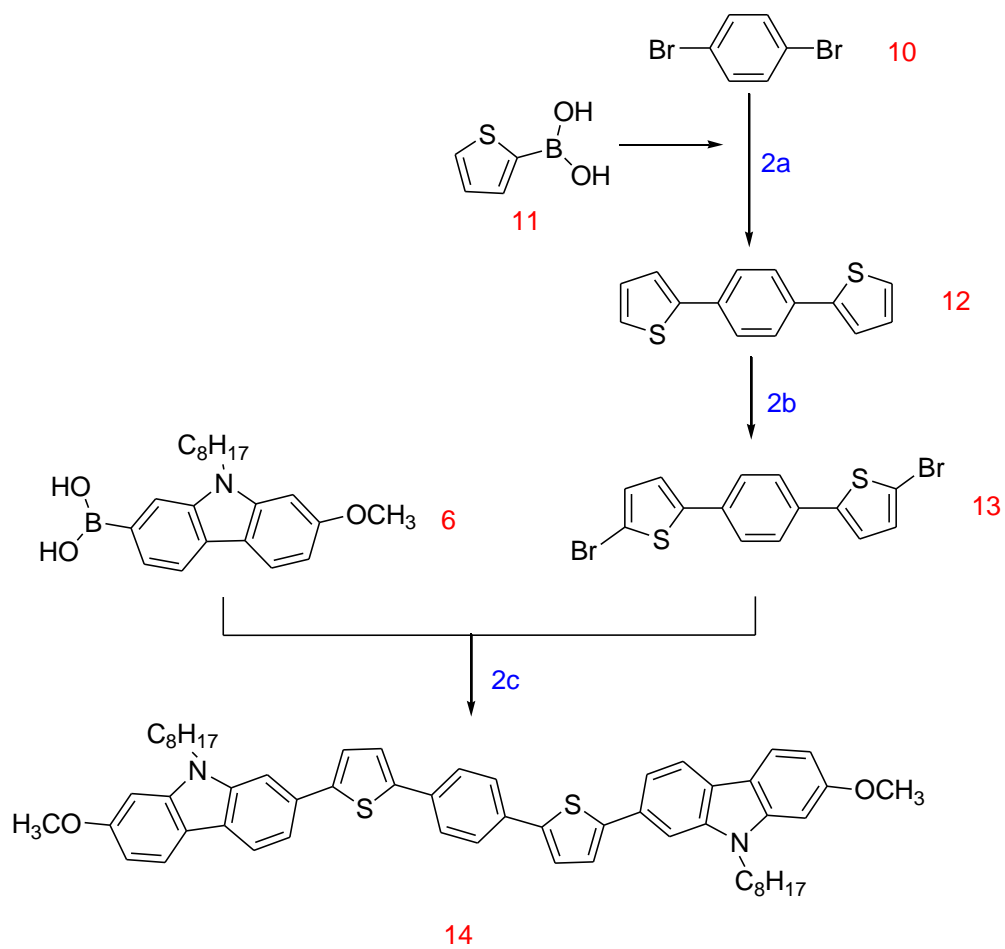
Scheme 2

2a: Pd(PPh$_3$)$_4$, K$_2$CO$_3$, water, DME, reflux;
2b: NBS, DMF;
2c: Pd(OAc)$_2$, PPh$_3$, K$_2$CO$_3$, water, DME, reflux.

Scheme 3

R= -C$_3$H$_7$ 16

-C$_8$H$_{17}$ 17

R= -C$_3$H$_7$ 18

-C$_8$H$_{17}$ 19
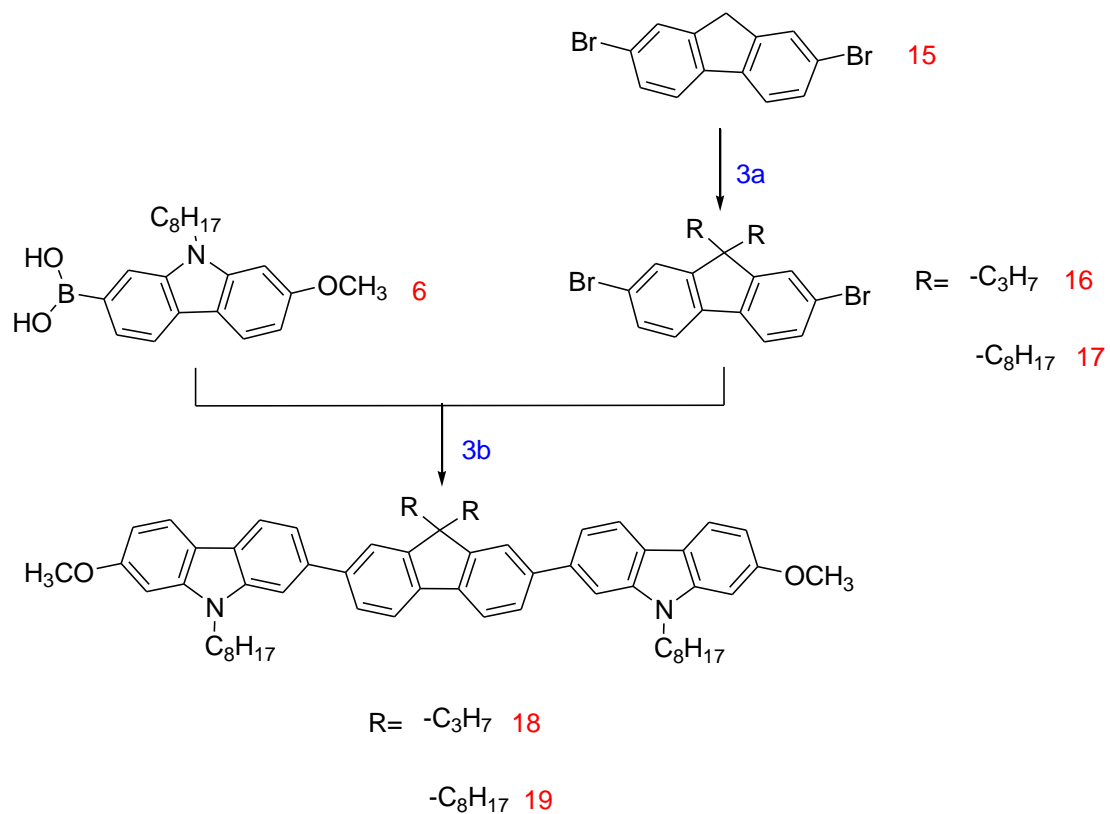
3a: 1-Bromopropane, *tetra-n*-butylammonium bromide (TBAB), NaOH aqueous, toluene;
3b: Pd(OAc)$_2$, K$_2$CO$_3$, water, DMF, 80 ^{o}C.
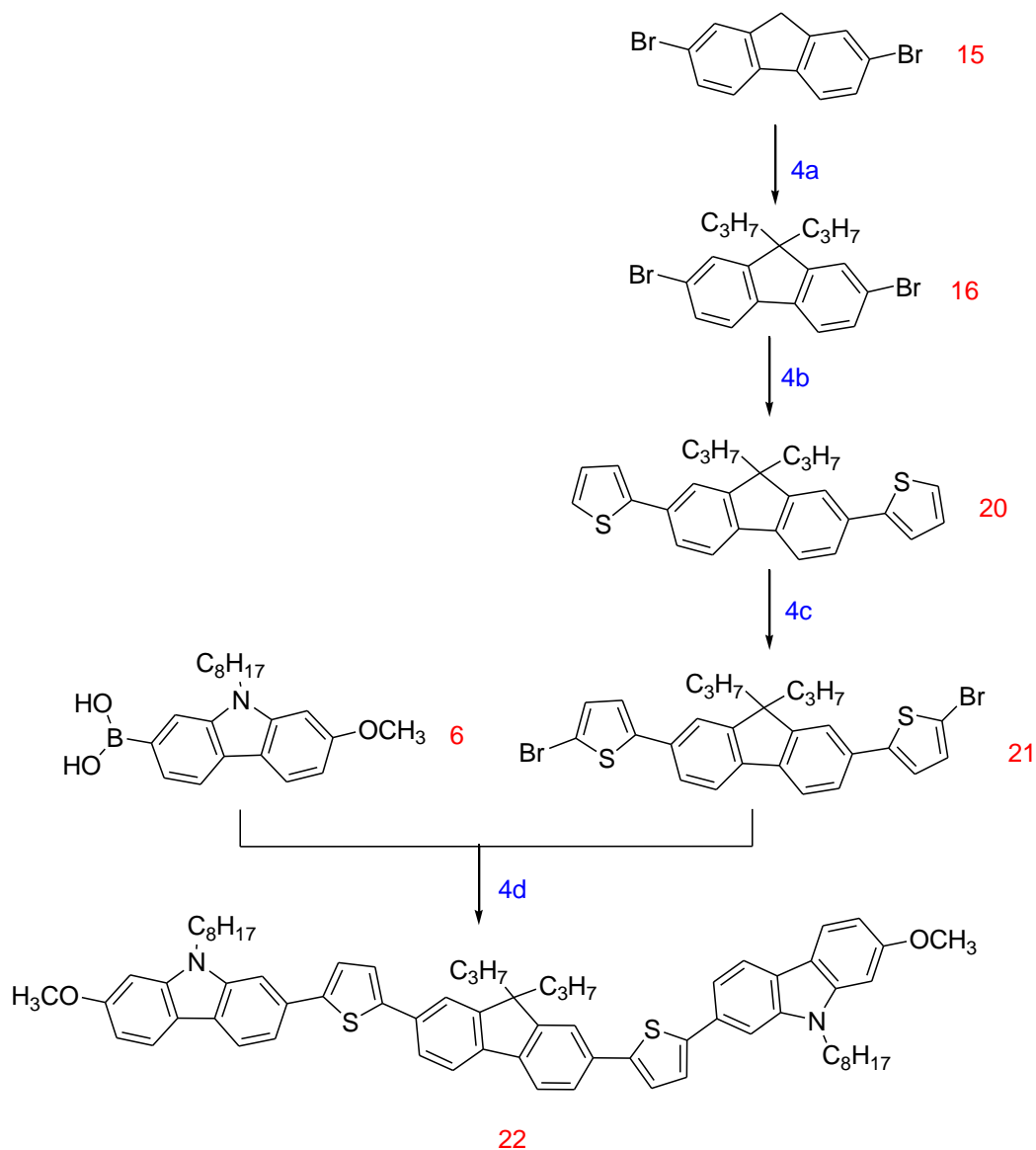
Scheme 4

4a: 1-Bromopropane, *tetra-n*-butylammonium bromide (TBAB), NaOH aqueous, toluene;
4b: 2-(Tributylstannyl)thiophene, $Pd(PPh_3)_4$, DMF, 90 ^{o}C;
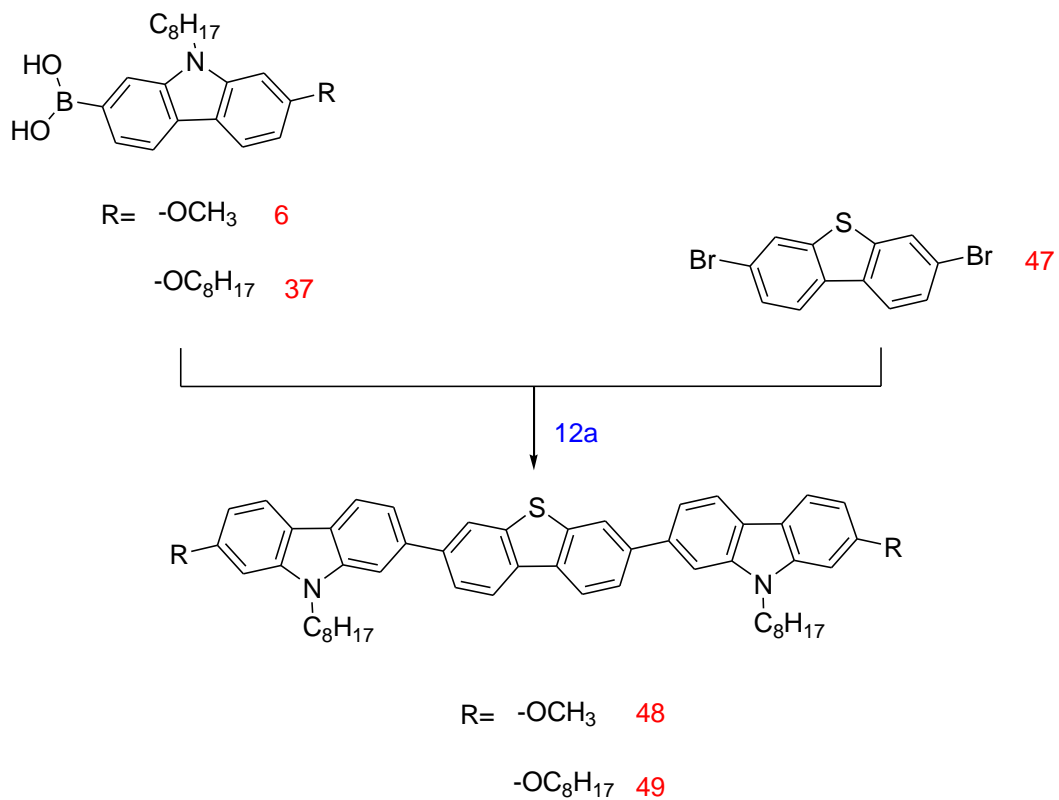4c: NBS, acetic acid, chloroform;
4d: $Pd(OAc)_2$, K_2CO_3, water, DMF, 80 ^{o}C;

Scheme 5
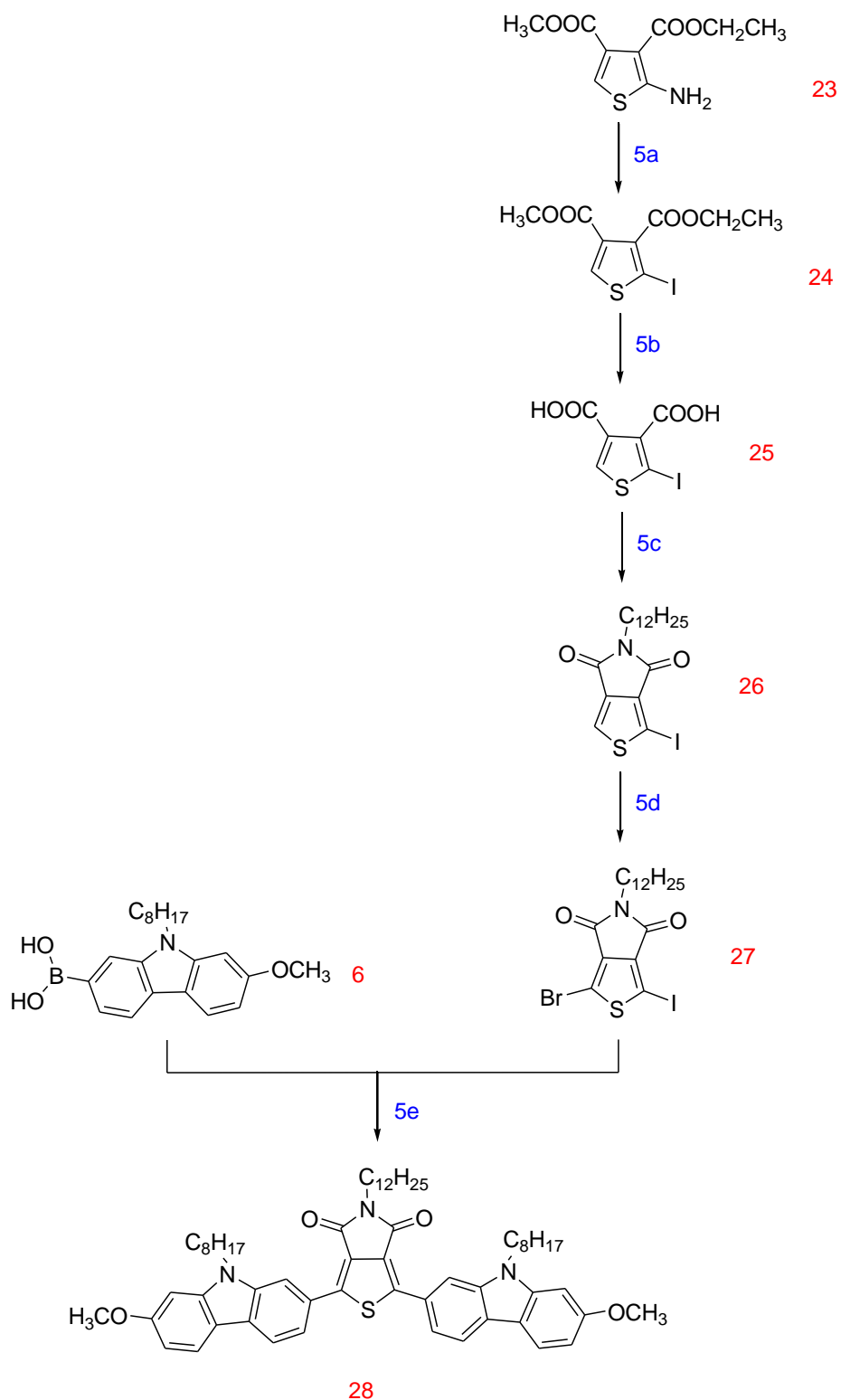
5a: Sodium nitrite (NaNO₂), hydrochloric acid, potassium iodide, water;

5b: Hydrochloric acid, reflux;

5c: Dodecylamine (C₁₂H₂₅NH₂), acetic anhydride, 1,4-dioxane, 4-(dimethylamino)pyridine;

5d: Trifluoroacetic acid, sulfuric acid, NBS;

5e: Pd(OAc)₂, K₂CO₃, water, DMF, 80 ᵒC.
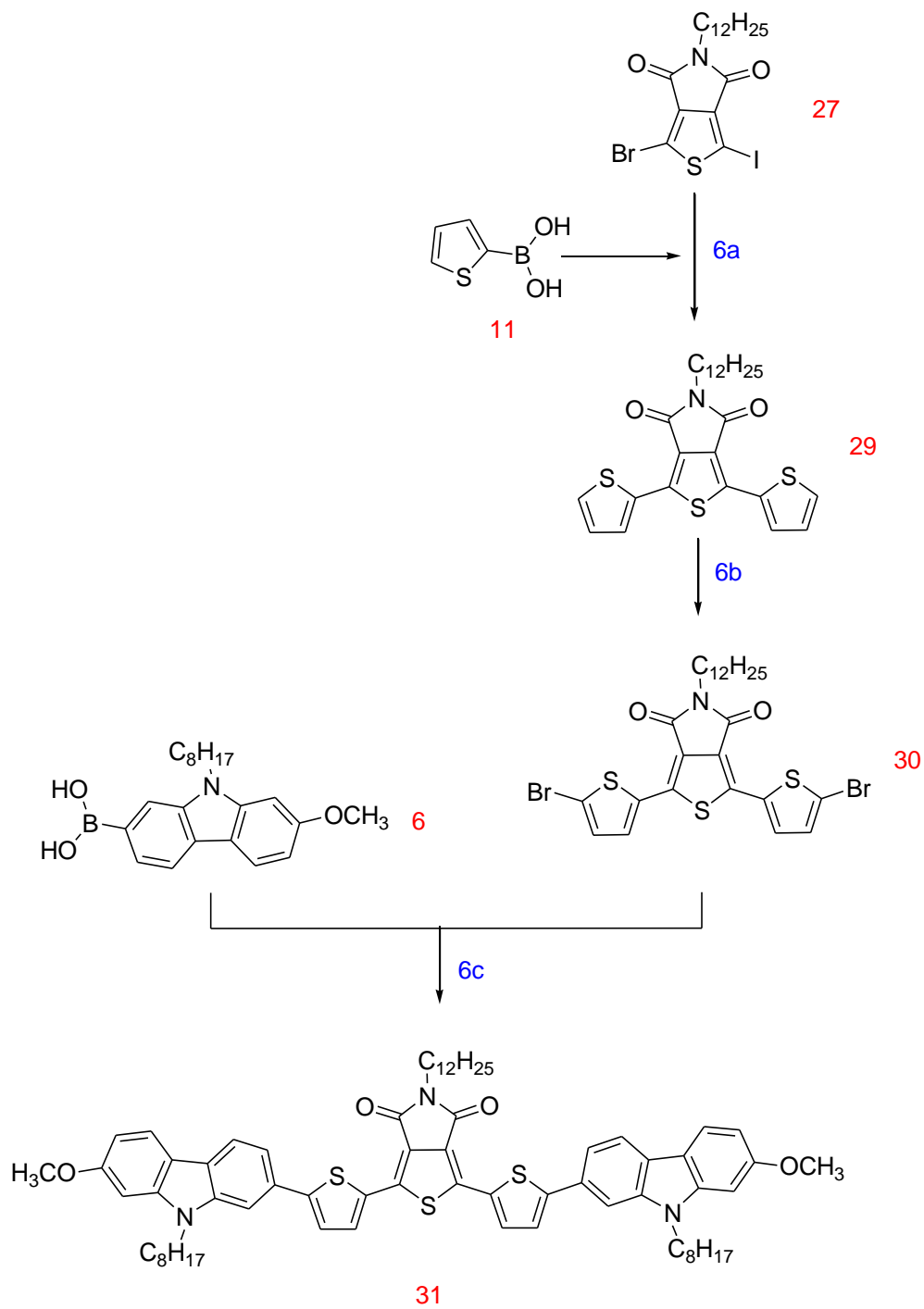
Scheme 6

6a: Pd(PPh$_3$)$_4$, Na$_2$CO$_3$, water, DME, reflux;
6b: Bromine, acetic acid, chloroform;
6c: Pd(OAc)$_2$, K$_2$CO$_3$, water, DMF, 80 °C.

Scheme 7

7a: 1-Bromooctane, K_2CO_3, DMF, 120 $^{\circ}$C;

7b: Copper powder, 175 $^{\circ}$C;

7c: Triethyl phosphite (P(OCH$_2$CH$_3$)$_3$), reflux;

7d: 1-Bromooctane, NaH (60% dispersion in mineral oil), DMF;

7e: (i): n-BuLi, 2-triisopropyl borate, THF, -78 $^{\circ}$C; (ii): Hydrochloric acid, RT;

7f: NBS, silica gel, DCM

7g: Pd(PPh$_3$)$_4$, K_2CO_3, water, DMF, 80 $^{\circ}$C.
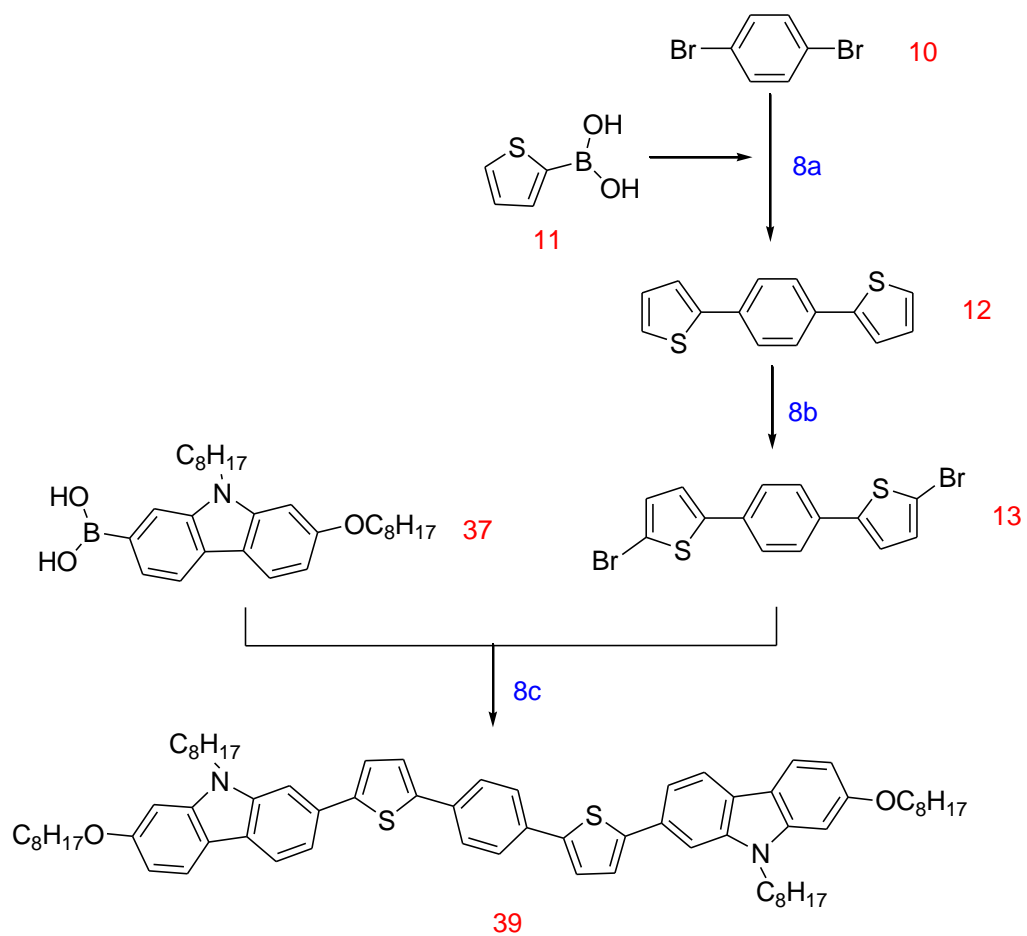
Scheme 8

8a: Pd(PPh$_3$)$_4$, K$_2$CO$_3$, water, DME, reflux;
8b: NBS, DMF;
8c: Pd(PPh$_3$)$_4$, K$_2$CO$_3$, water, DMF, 80 ^{o}C .
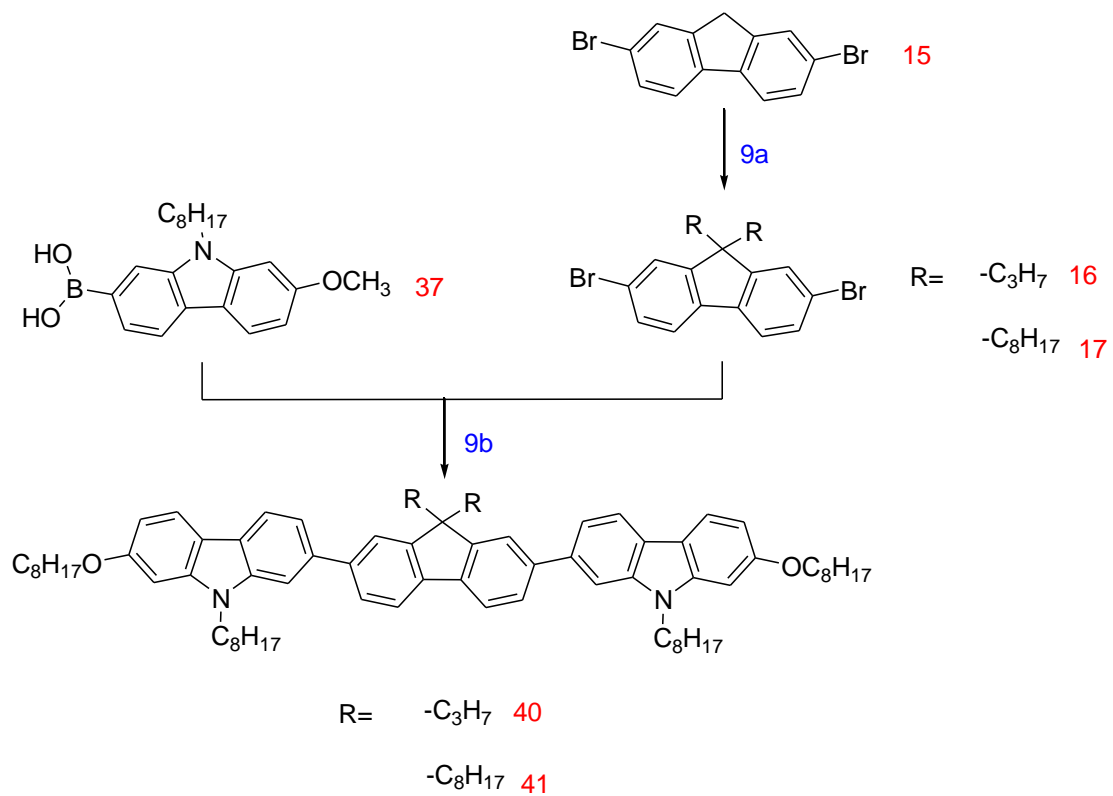
Scheme 9

9a: 1-Bromopropane, *tetra-n*-butylammonium bromide (TBAB), NaOH aqueous, toluene;
9b: Pd(PPh$_3$)$_4$, K$_2$CO$_3$, water, DMF, 80 ^{o}C.
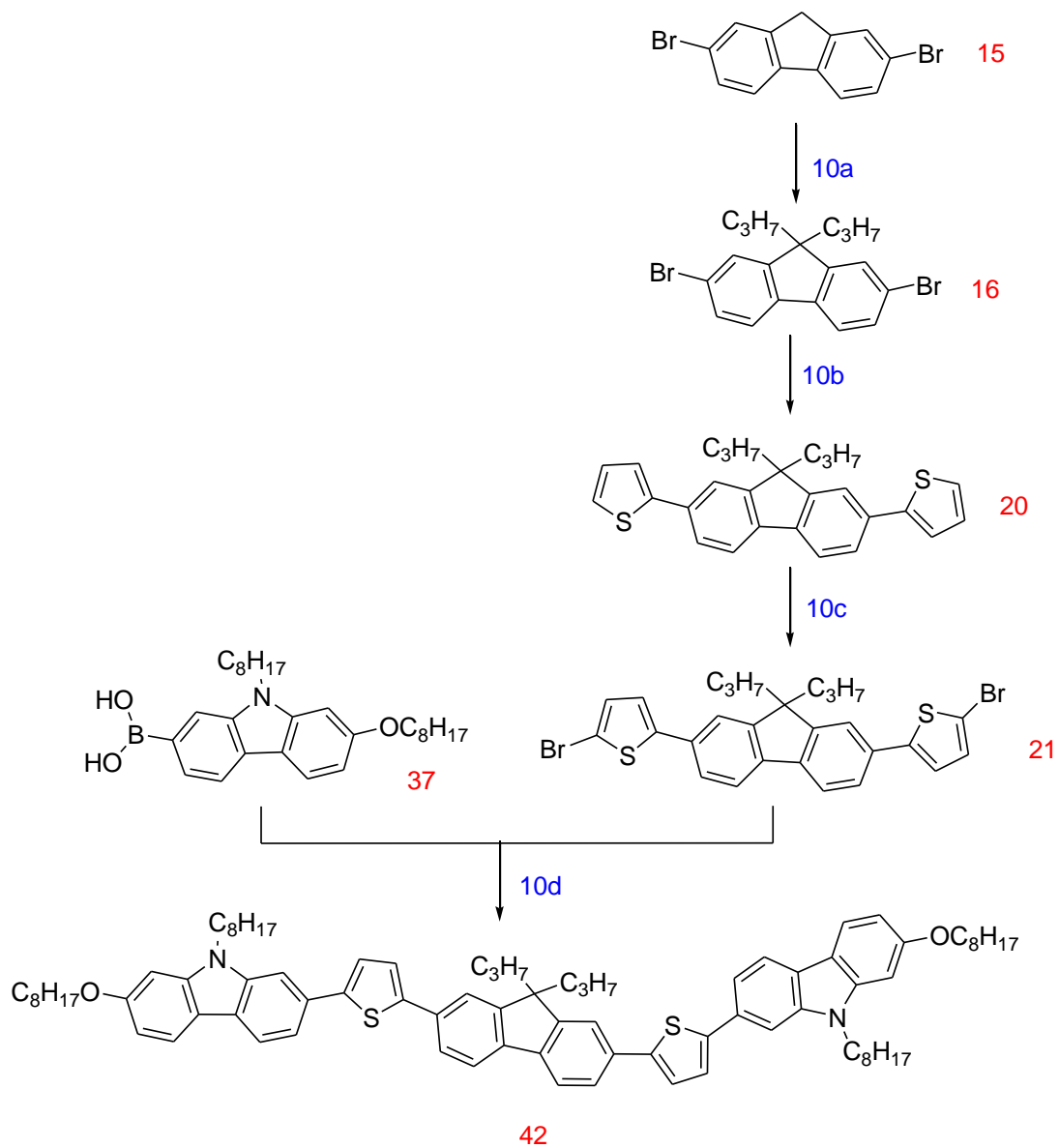
Scheme 10

10a: 1-Bromopropane, *tetra-n*-butylammonium bromide (TBAB), NaOH aqueous, toluene;
10b: 2-(Tributylstannyl)thiophene, Pd(PPh$_3$)$_4$, DMF, 90 ^{o}C;
10c: NBS, acetic acid, chloroform;
10d: Pd(PPh$_3$)$_4$, K$_2$CO$_3$, water, DMF, 80 ^{o}C;
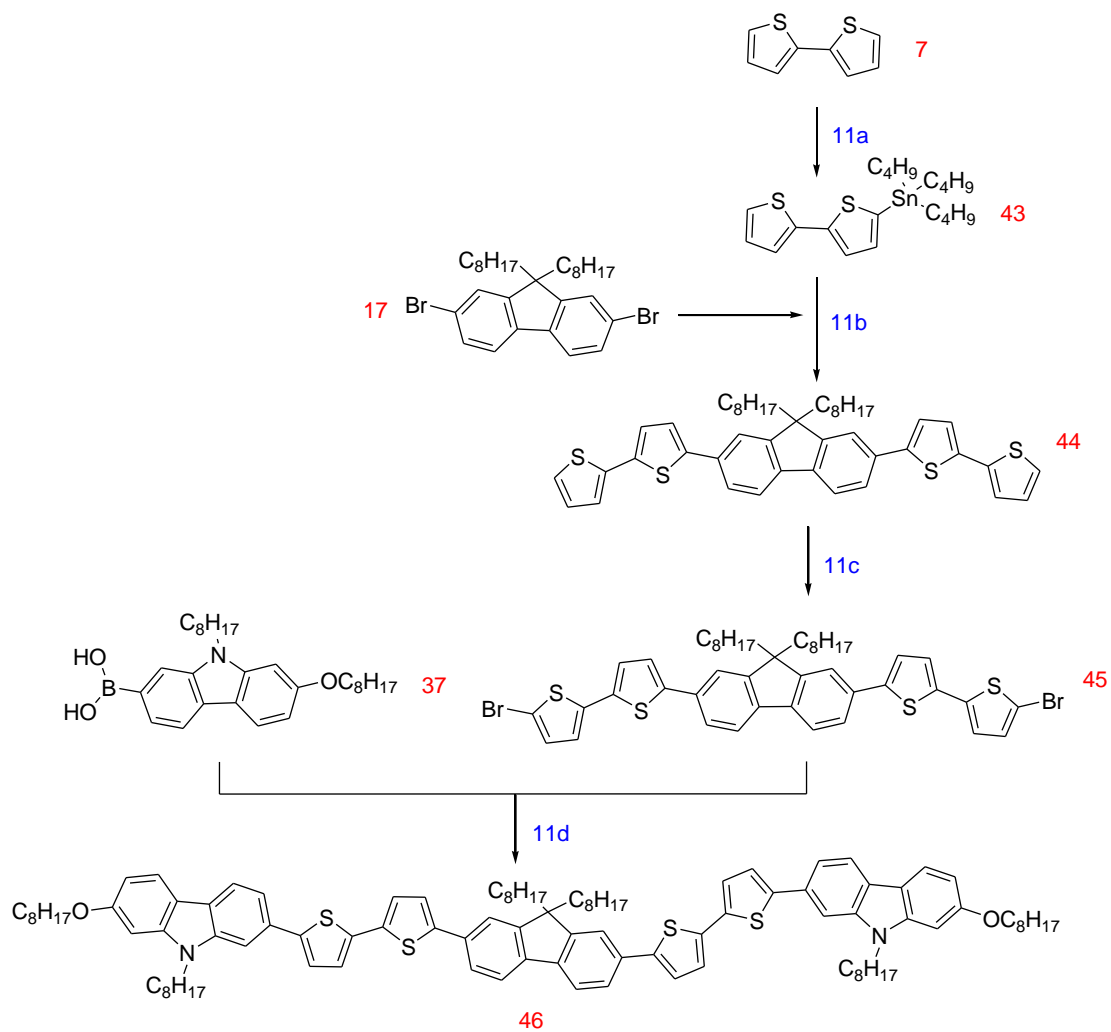
Scheme 11

11a: *n*-BuLi, tributyltin chloride, THF;
11b: Pd(PPh$_3$)$_4$, DMF, 100 °C;
11c: NBS, silica gel, DCM;
11d: Pd(PPh$_3$)$_4$, K$_2$CO$_3$, water, DMF, 80 °C.

105

Scheme 12

R= -OCH$_3$ 6

-OC$_8$H$_{17}$ 37

47

12a

R= -OCH$_3$ 48

-OC$_8$H$_{17}$ 49

12a: (48) Pd(OAc)$_2$, K$_2$CO$_3$, water, DMF, 80 ^{o}C;
(49) Pd(PPh$_3$)$_4$, K$_2$CO$_3$, water, DMF, 80 ^{o}C.

Scheme 13

R= -OCH₃ 6

-OC₈H₁₇ 37

R= -OCH₃ 52

-OC₈H₁₇ 53
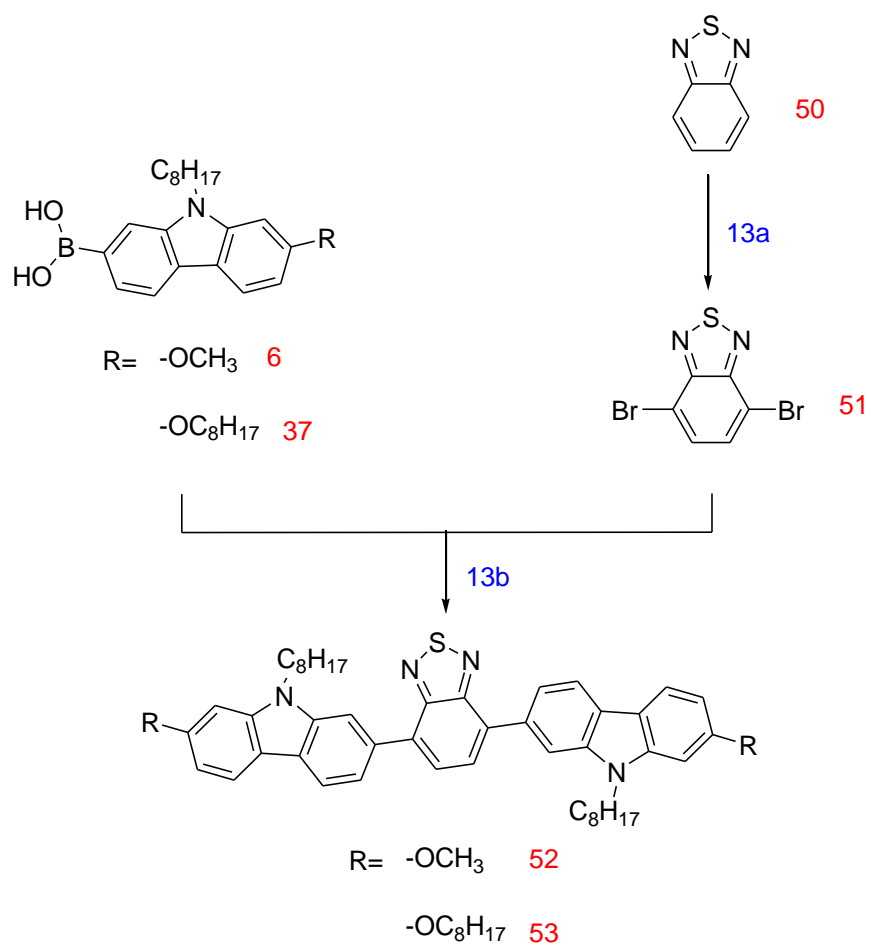
13a: Bromine, hydrobromic acid, reflux;
13b: (52) Pd(OAc)₂, K₂CO₃, water, DMF, 80 °C;
       (53) Pd(PPh₃)₄, K₂CO₃, water, DMF, 80 °C.

Scheme 14
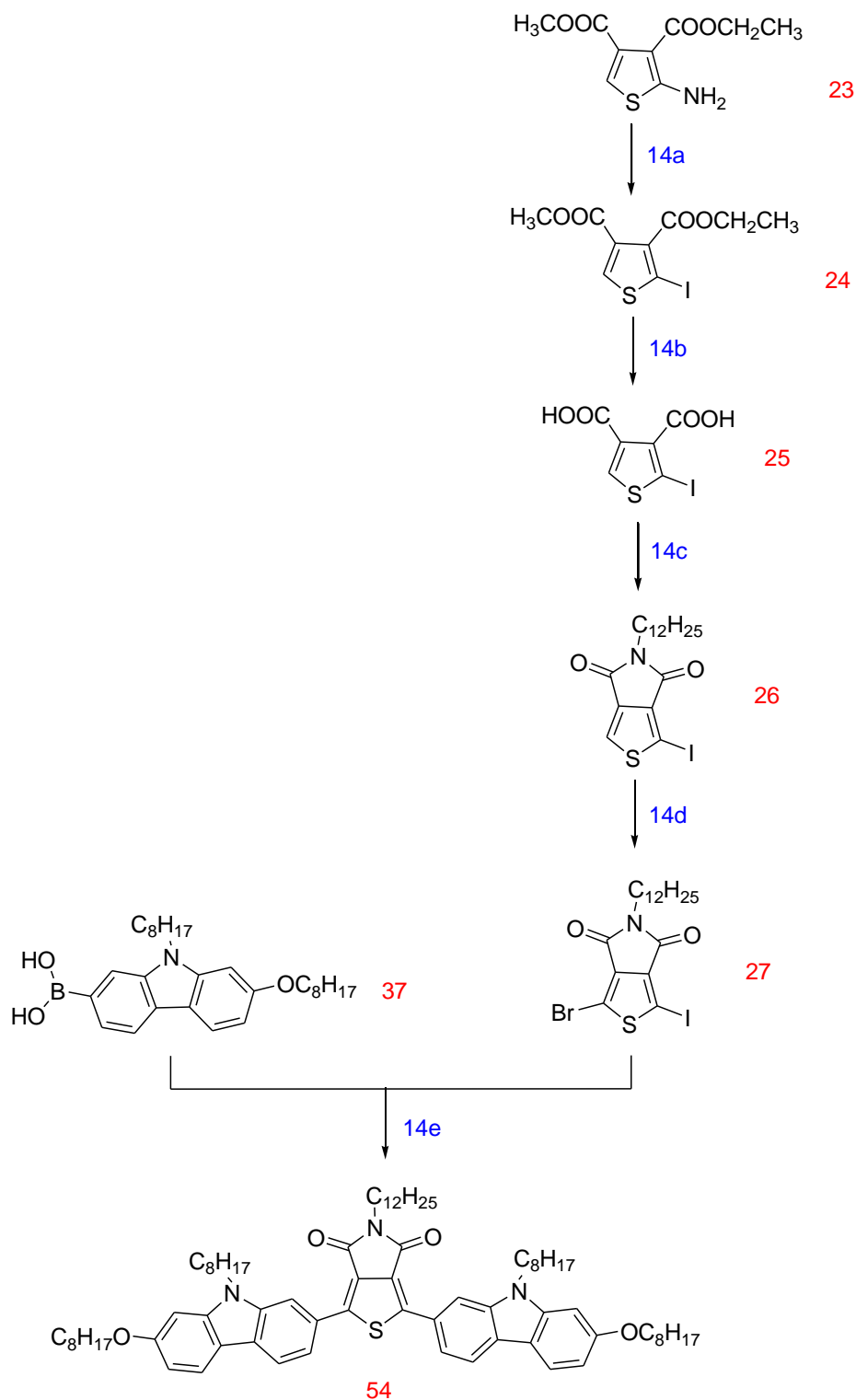
14a: Sodium nitrite (NaNO$_2$), hydrochloric acid, potassium iodide, ice water;

14b: Hydrochloric acid, reflux;

14c: Dodecylamine (C$_{12}$H$_{25}$NH$_2$), acetic anhydride, 1,4-dioxane, 4-(dimethylamino)pyridine;

14d: Trifluoroacetic acid, sulfuric acid, NBS;

14e: Pd(PPh$_3$)$_4$, K$_2$CO$_3$, water, DMF, 80 ^{o}C.
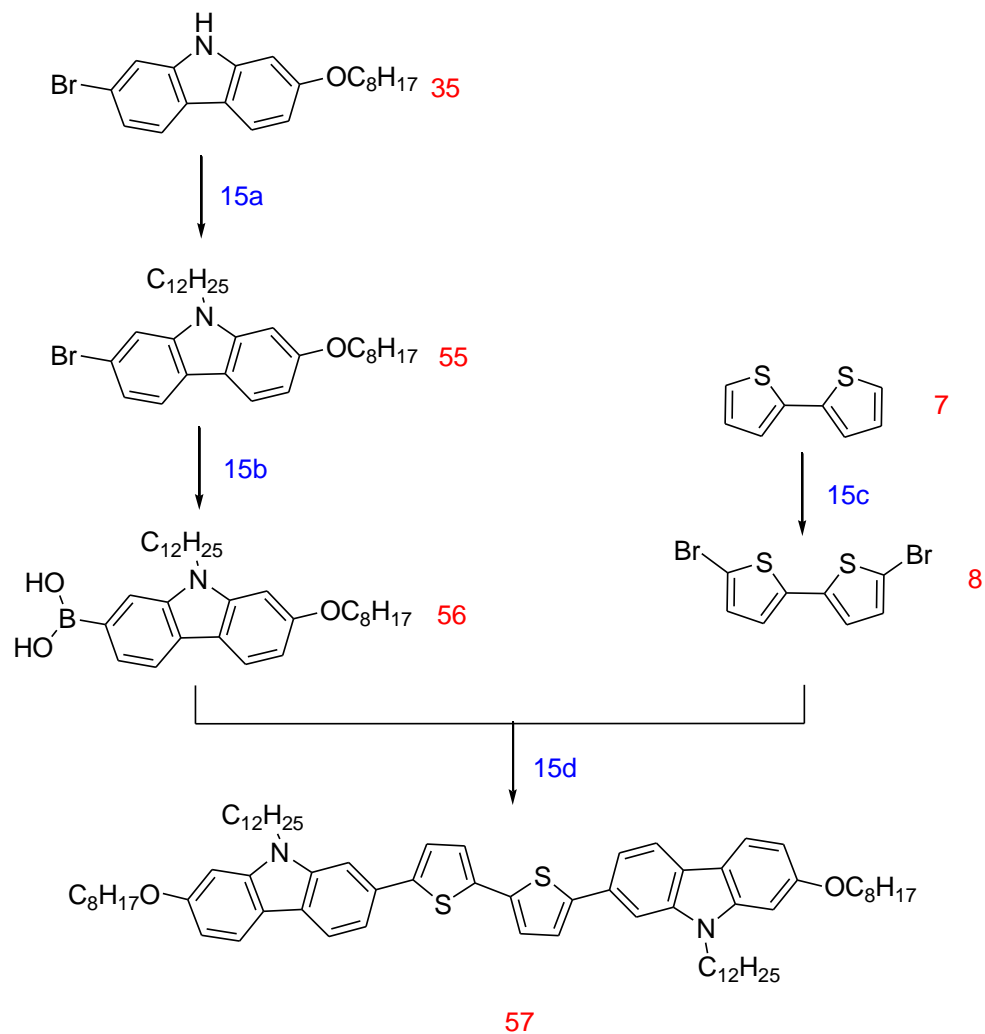
Scheme 15

15a: 1-Bromododecane, NaH (60% dispersion in mineral oil), DMF;
15b: (i): n-BuLi, 2-triisopropyl borate, THF, -78 °C; (ii): Hydrochloric acid, RT;
15c: NBS, silica gel, DCM
15d: Pd(OAc)$_2$, PPh$_3$, K$_2$CO$_3$, water, DME, reflux.

Scheme 16
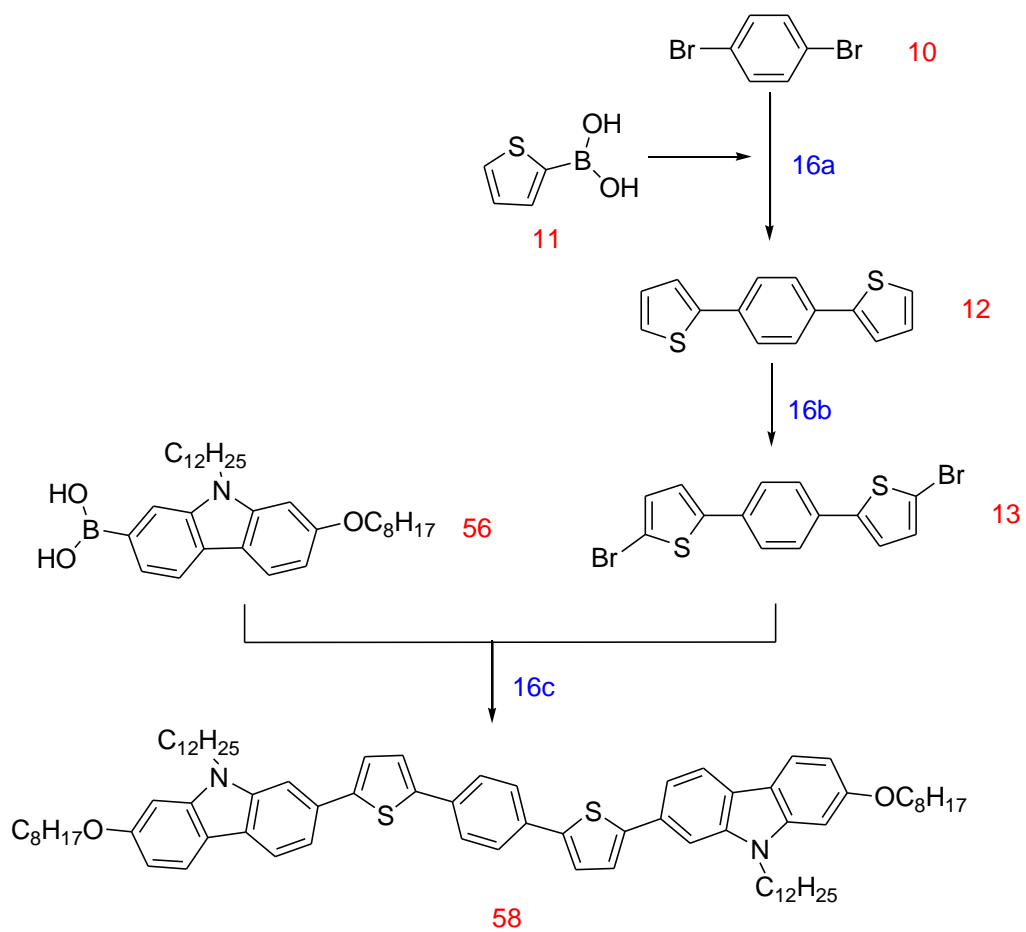
16a: Pd(PPh$_3$)$_4$, K$_2$CO$_3$, water, DME, reflux;
16b: NBS, DMF;
16c: Pd(OAc)$_2$, PPh$_3$, K$_2$CO$_3$, water, DME, reflux.

Scheme 17
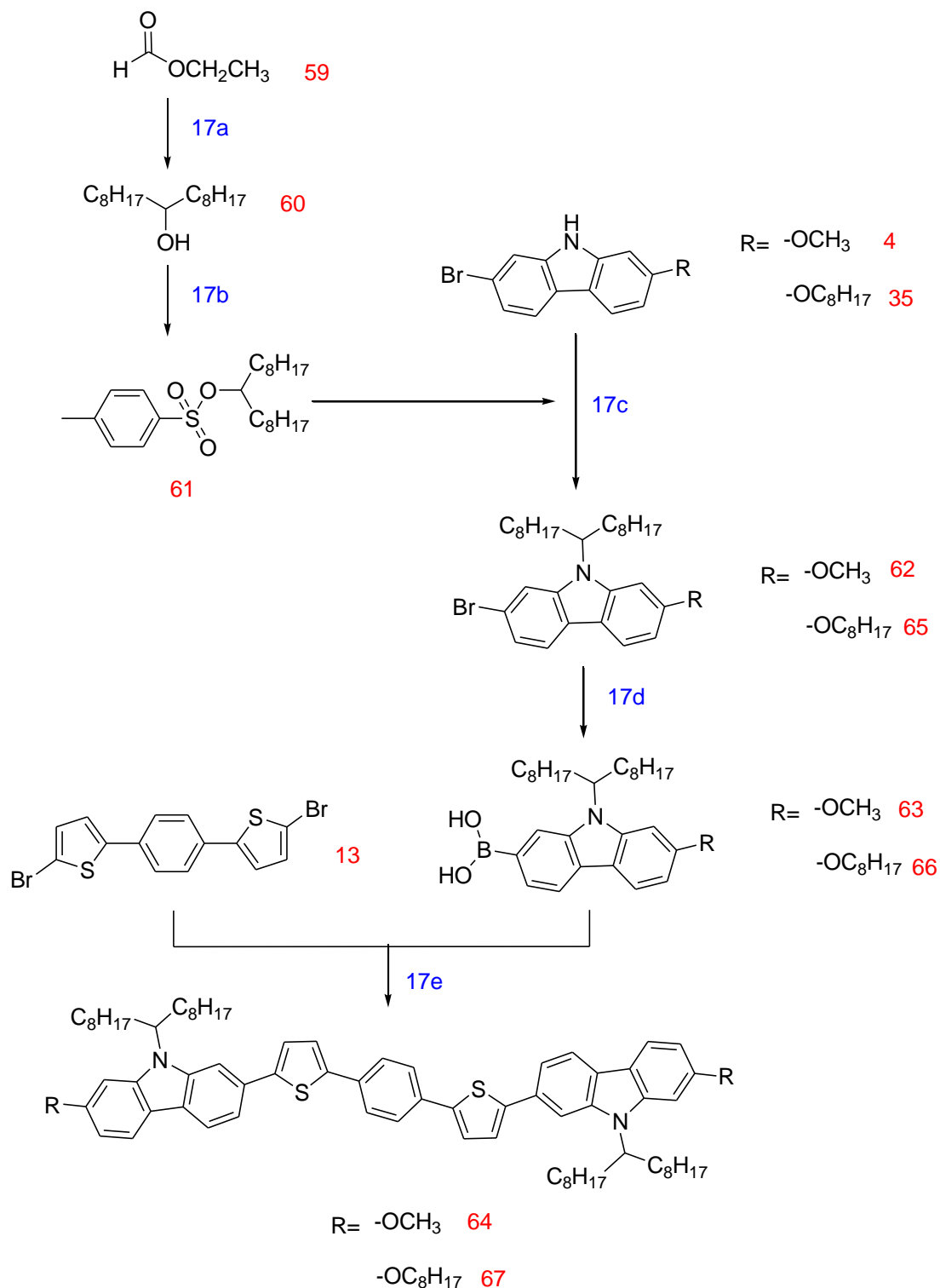
17a: 1-Bromooctane, magnesium, dry THF;
17b: *p*-Toluene-sulfonylchloride, pyridine;
17c: KOH, 18-crown-6, dry DMSO;
17d: (i): *n*-BuLi, 2-triisopropyl borate, THF, -78 °C; (ii): Hydrochloric acid, RT;
17e: Pd(OAc)$_2$, PPh$_3$, K$_2$CO$_3$, water, DME, reflux.

Scheme 18

R= -OCH$_3$ 63

-OC$_8$H$_{17}$ 66

R= -OCH$_3$ 72

-OC$_8$H$_{17}$ 73
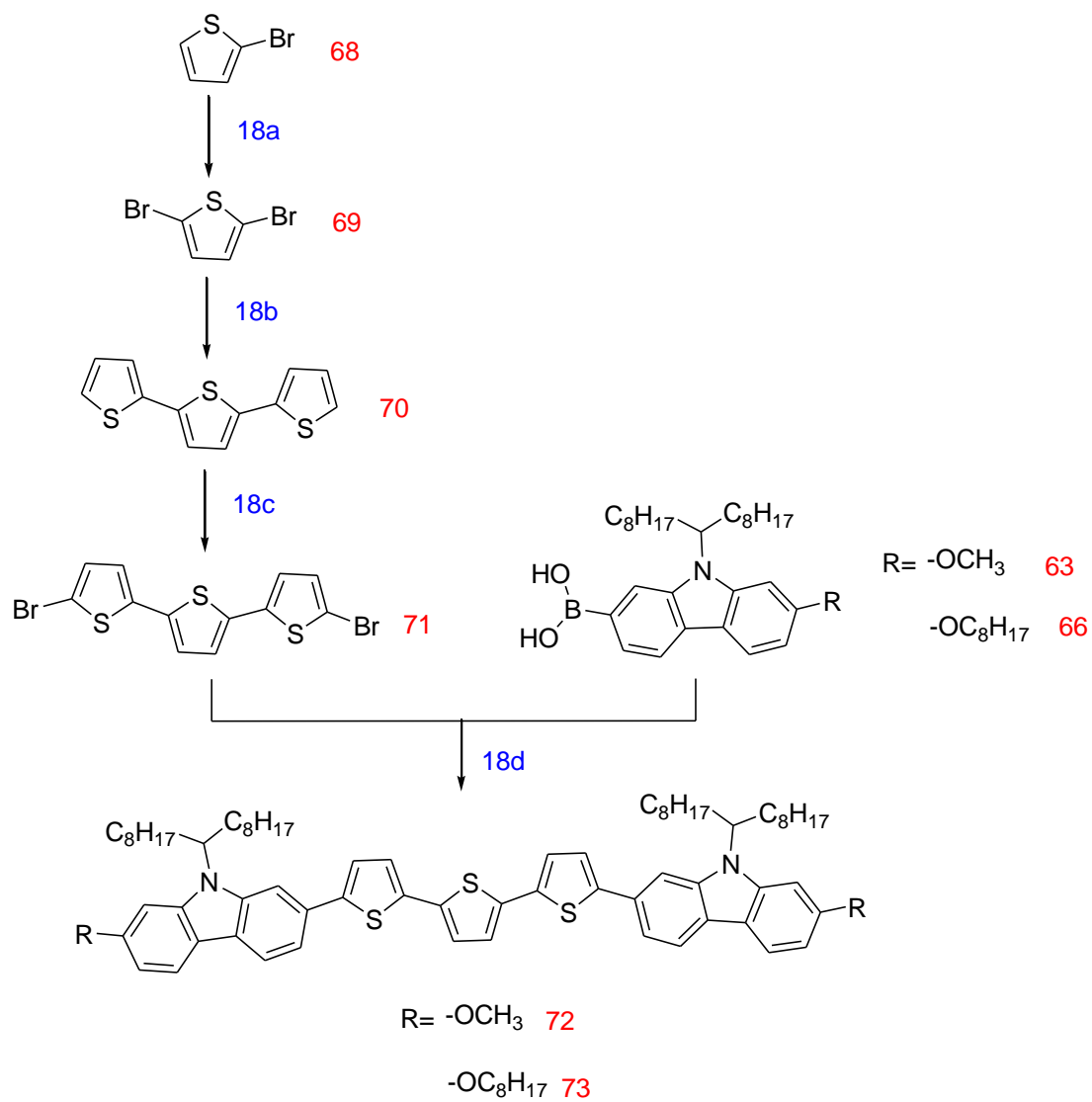
18a: NBS, silica gel, chloroform;
18b: 2-(Tributylstannyl)thiophene, Pd(PPh$_3$)$_4$, DMF, 90 ^{o}C;
18c: NBS, silica gel, chloroform;
18d: Pd(OAc)$_2$, PPh$_3$, K$_2$CO$_3$, water, DME, reflux.

Scheme 19
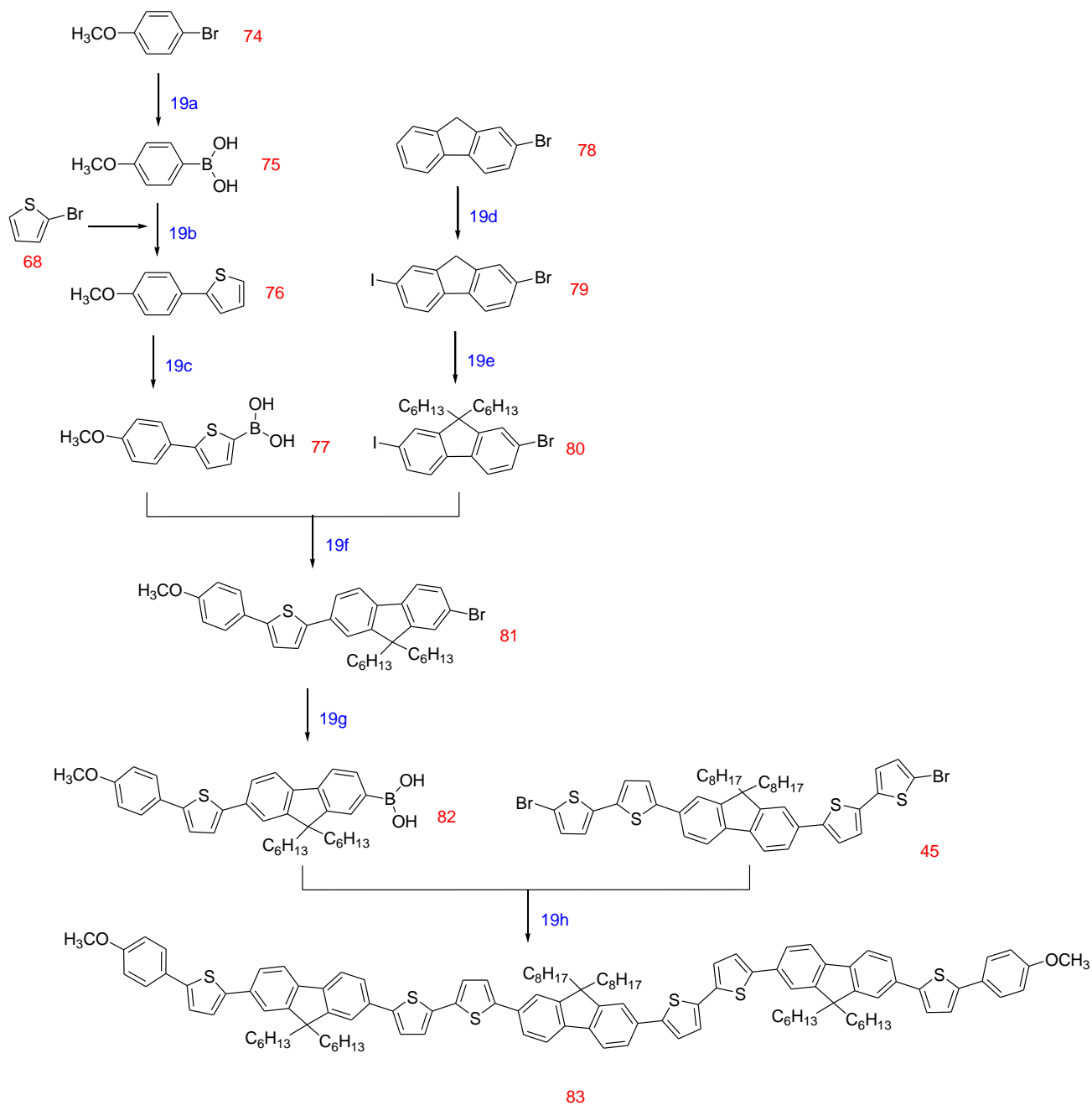
19a: (i): *n*-BuLi, 2-triisopropyl borate, THF, -78 °C; (ii): Hydrochloric acid, RT;
19b: Pd(PPh$_3$)$_4$, K$_2$CO$_3$, water, DME, reflux;
19c: (i): *n*-BuLi, 2-triisopropyl borate, THF, -78 °C; (ii): Hydrochloric acid, RT;
19d: Acetic acid, concentrated sulphuric acid, water, periodic acid, pulverised iodine, 75 °C;
19e: Powered potassium hydroxide, 1-bromohexane, potassium iodide, DMSO, RT;
19f: Pd(PPh$_3$)$_4$, K$_2$CO$_3$, water, DME, reflux;
19g: (i): *n*-BuLi, 2-triisopropyl borate, THF, -78 °C; (ii): Hydrochloric acid, RT;
19h: Pd(PPh$_3$)$_4$, K$_2$CO$_3$, water, DMF, 80 °C.

Scheme 20

R= -C$_8$H$_{17}$ 86

-C$_6$H$_{13}$ 87

-C$_4$H$_9$ 88
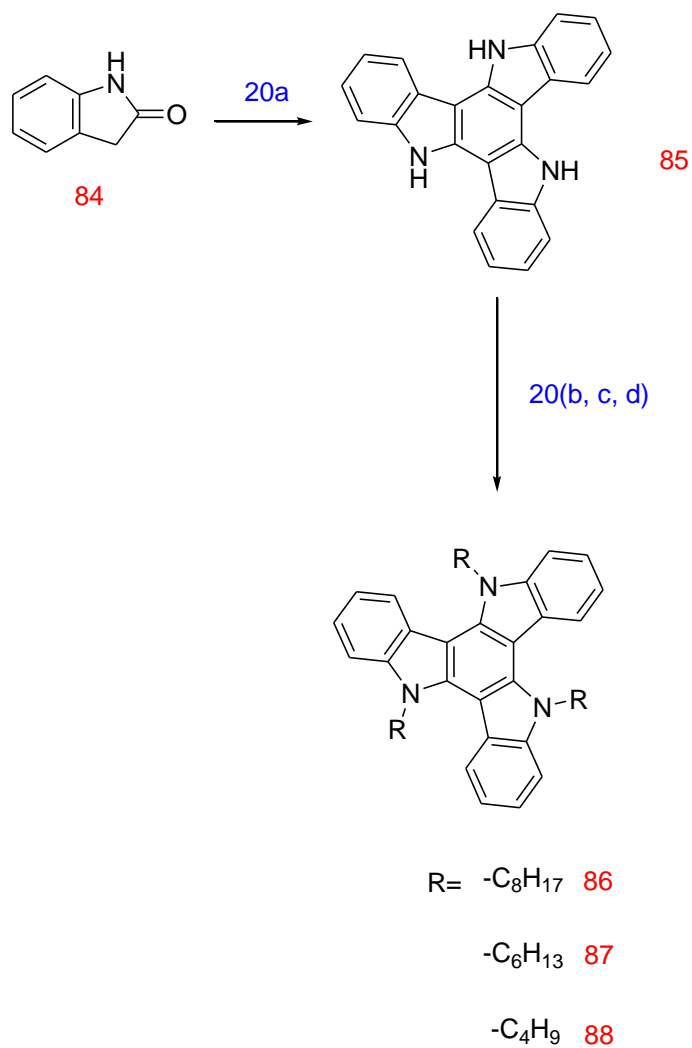
20a: Phosphorus (V) oxychloride, 100 $^{\circ}$C;
20b: 1-Bromooctane, KOH, THF, reflux;
20c: 1-Bromohexane, NaH (60% dispersion in mineral oil), DMF;
20d: 1-Bromobutane, NaH (60% dispersion in mineral oil), DMF.

Scheme 21

84

85
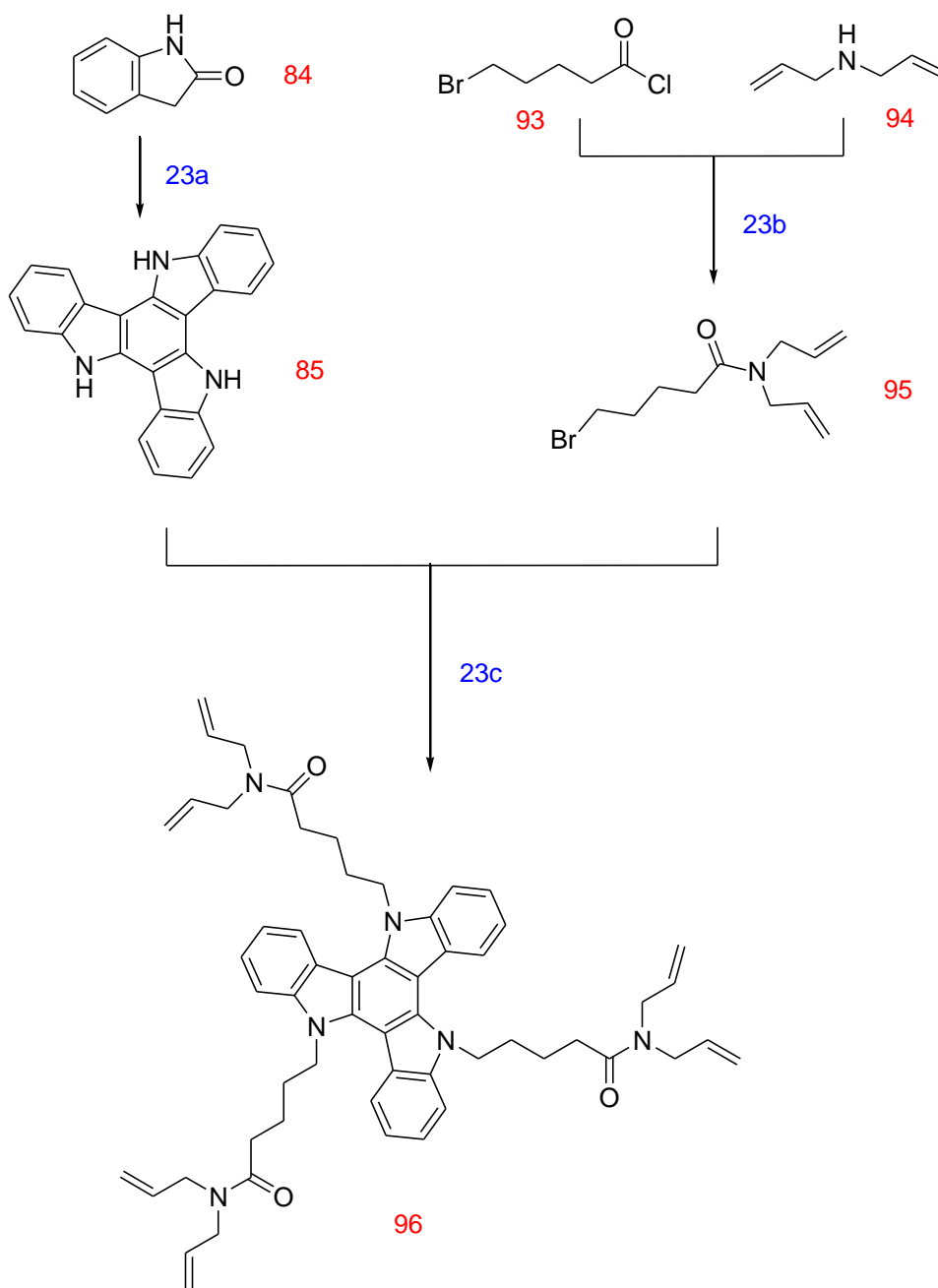
89

90

91
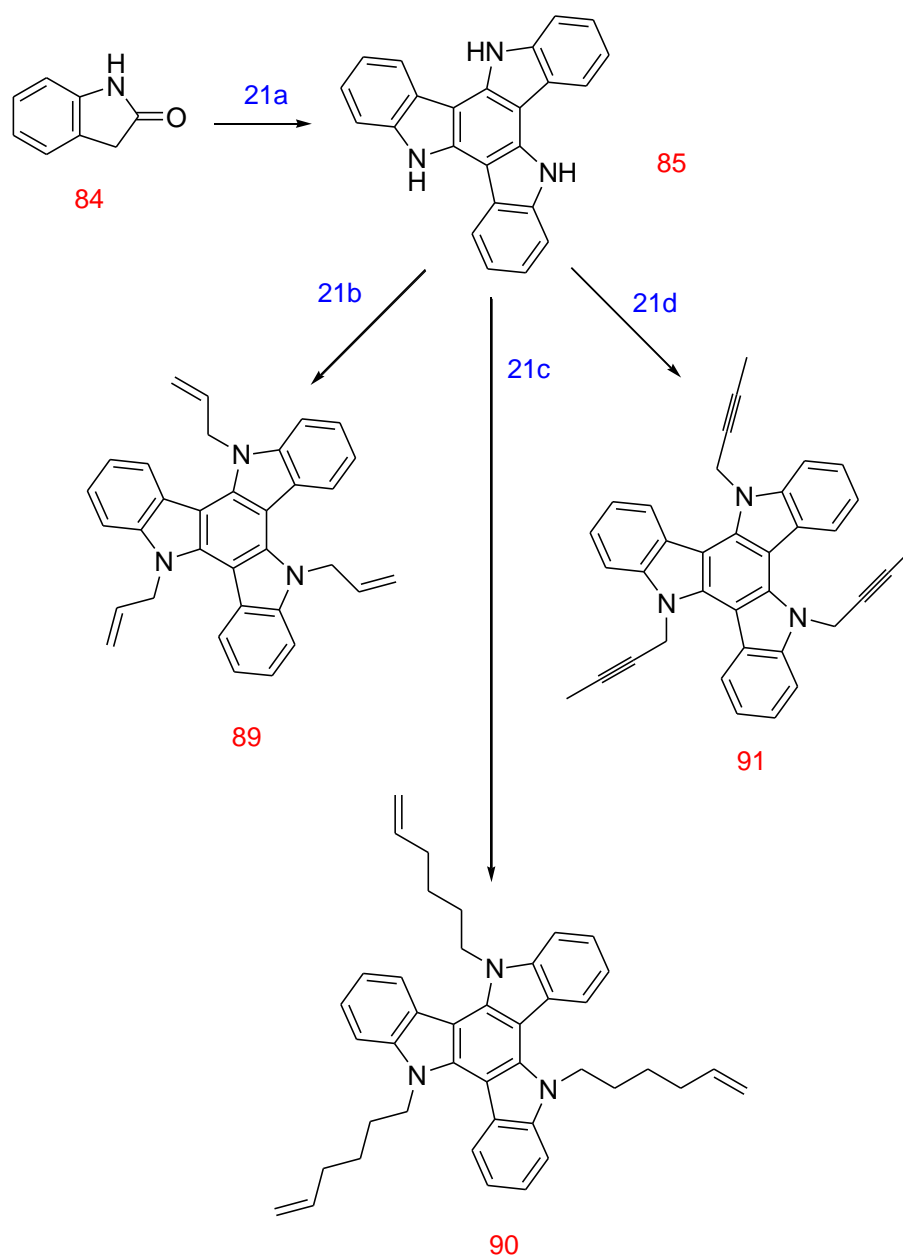
21a: Phosphorus (V) oxychloride, 100 $^{\circ}$C;
21b: Allyl bromide, NaH (60% dispersion in mineral oil), DMF;
21c: 6-Bromo-1-hexene, NaH (60% dispersion in mineral oil), DMF;
21d: 1-bromo-2-butyne, NaH (60% dispersion in mineral oil), DMF.

Scheme 22

84

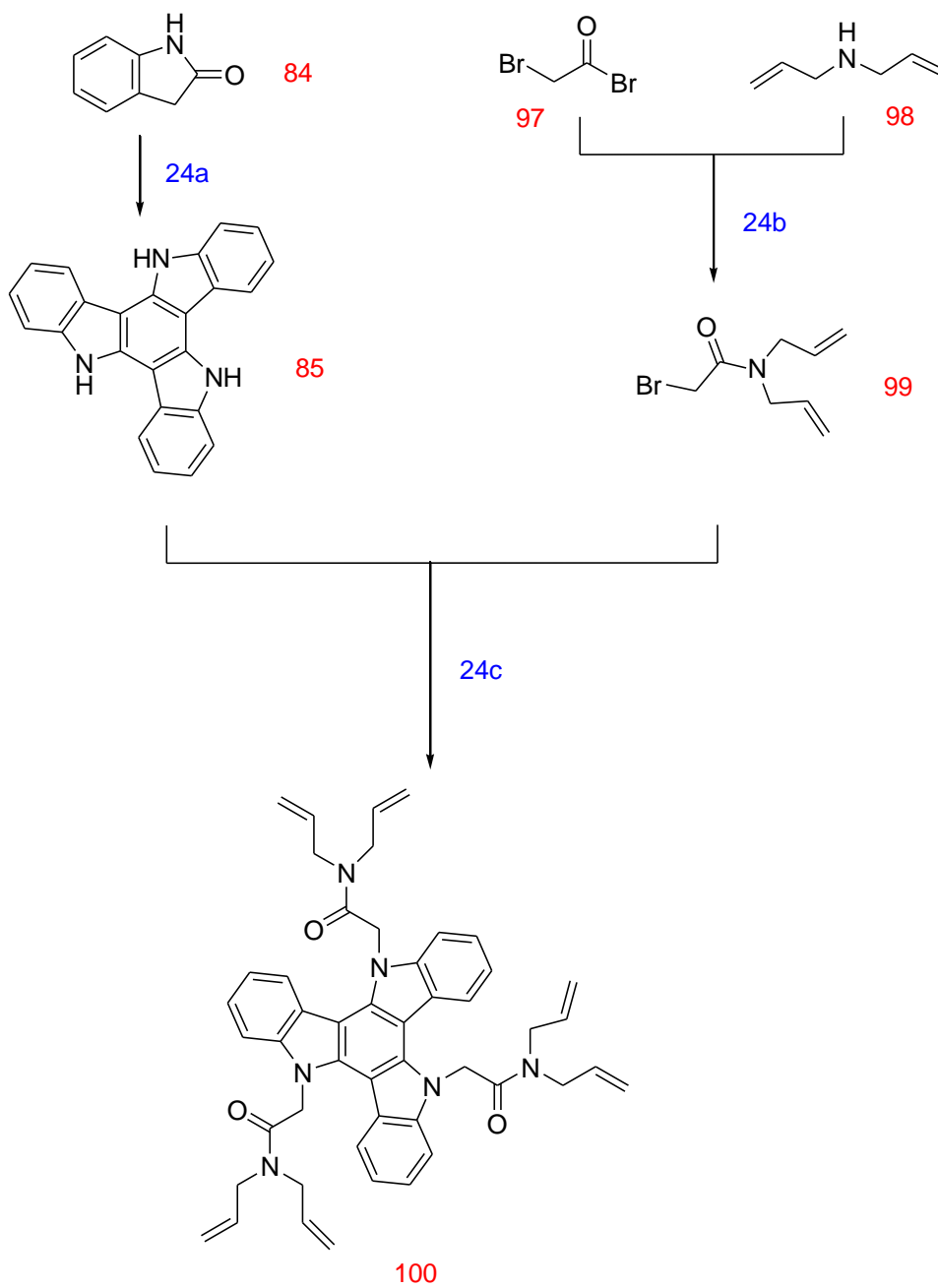85

92
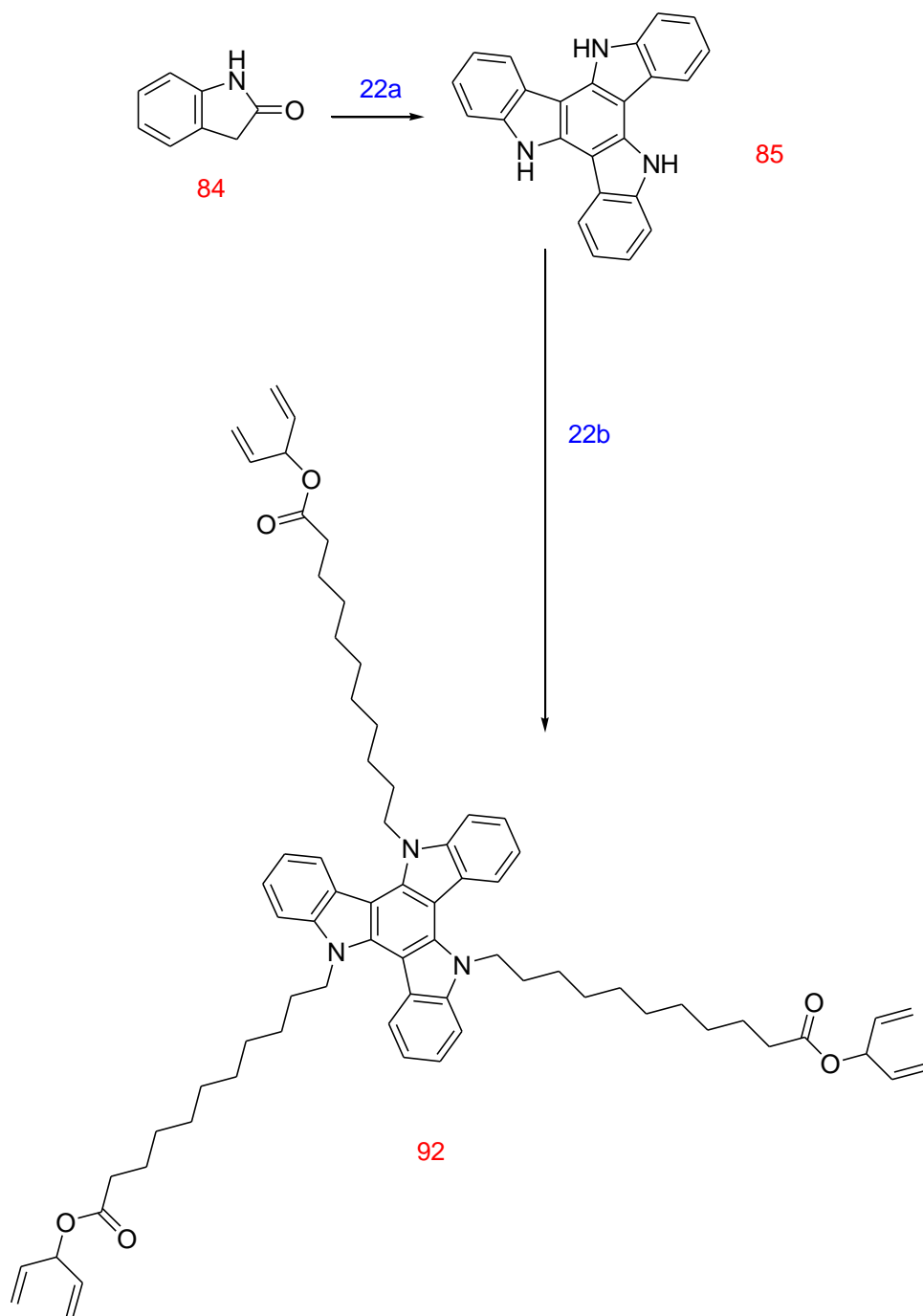
22a: Phosphorus (V) oxychloride, 100 °C;
22b: Penta-1,4-dien-3-yl-11-bromoundecanoate, NaH (60% dispersion in mineral oil), DMF.

Scheme 23

23a: Phosphorus (V) oxychloride, 100 °C;
23b: Pyridine, triethylamine;
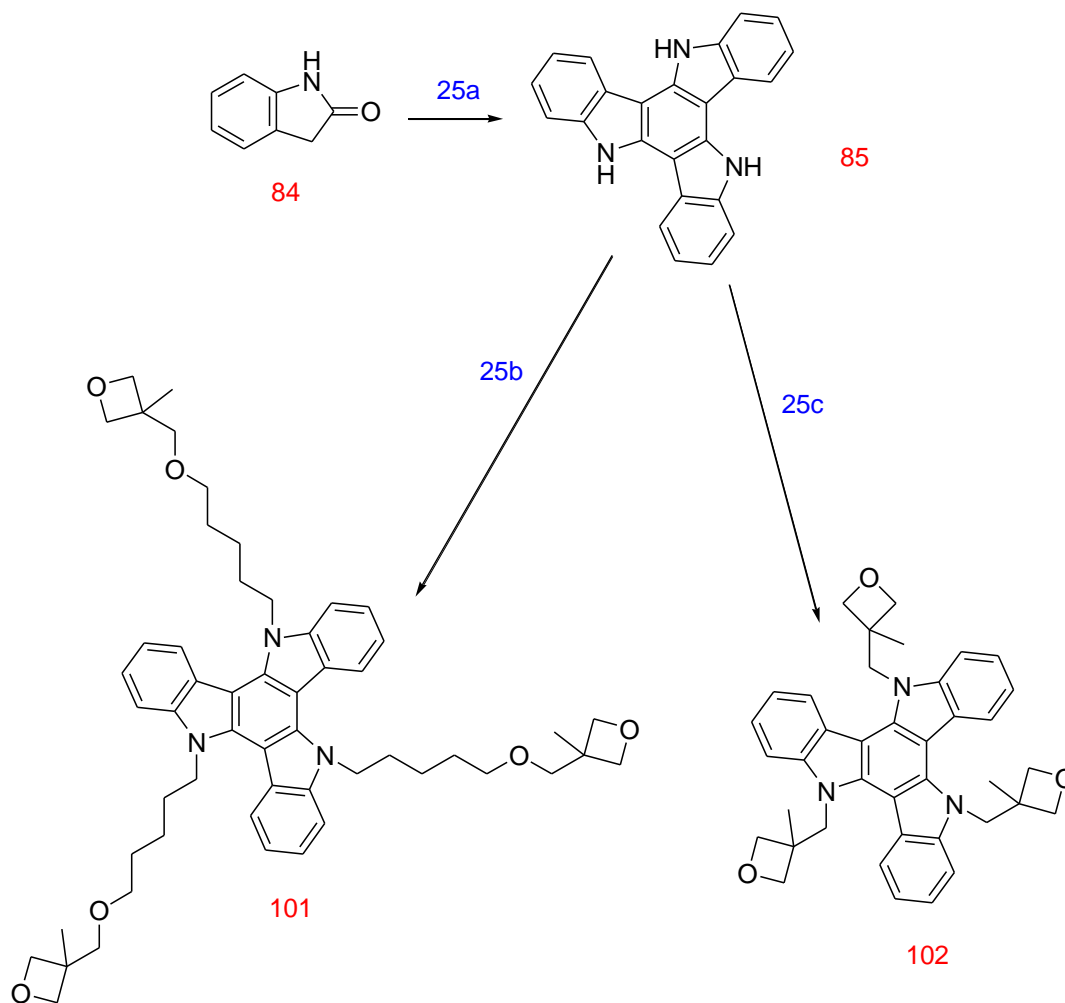23c: NaH (60% dispersion in mineral oil), DMF.

Scheme 24

24a: Phosphorus (V) oxychloride, 100 °C;
24b: Ethyl acetate, triethylamine;
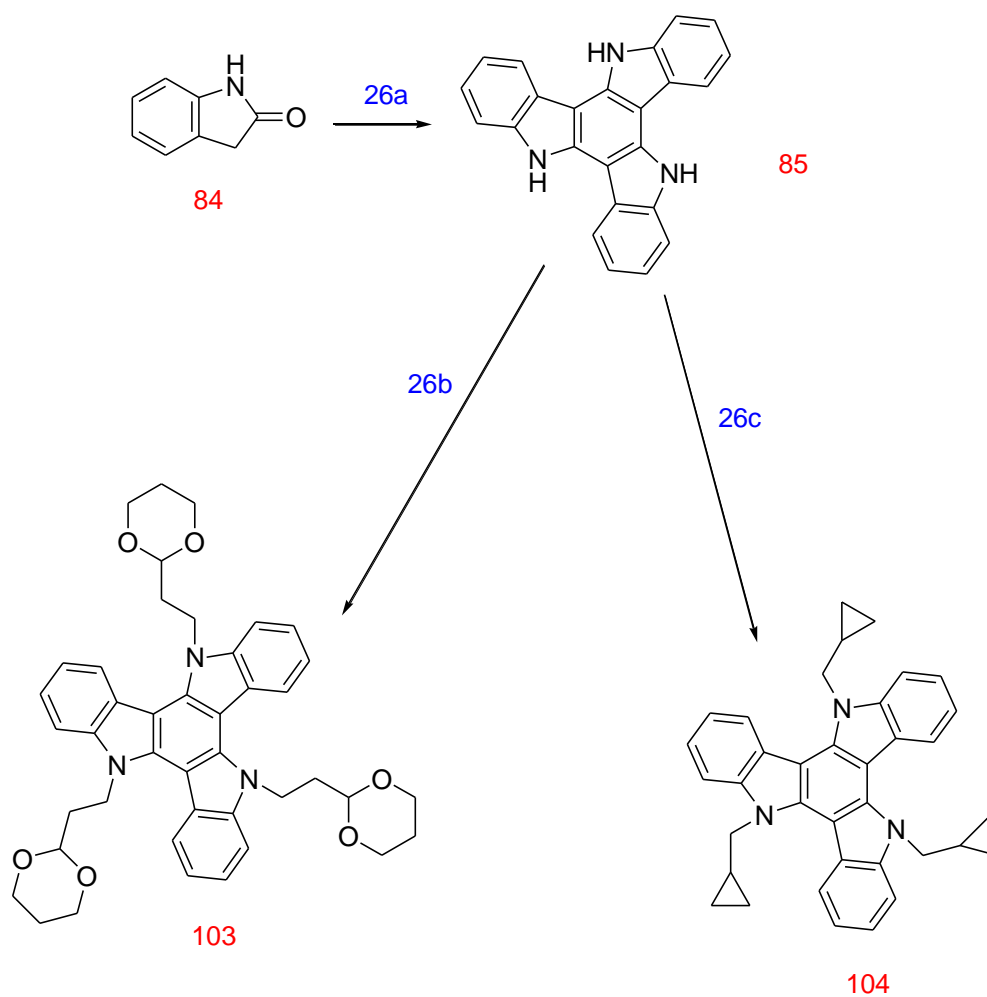24c: NaH (60% dispersion in mineral oil), DMF.

Scheme 25

25a: Phosphorus (V) oxychloride, 100 °C;
25b: 3-[(5-Bromopentyloxy)methyl]-3-methyloxetane, NaH (60% dispersion in mineral oil), DMF;
25c: 3-Bromomethyl-3-methyloxetane, NaH (60% dispersion in mineral oil), DMF.
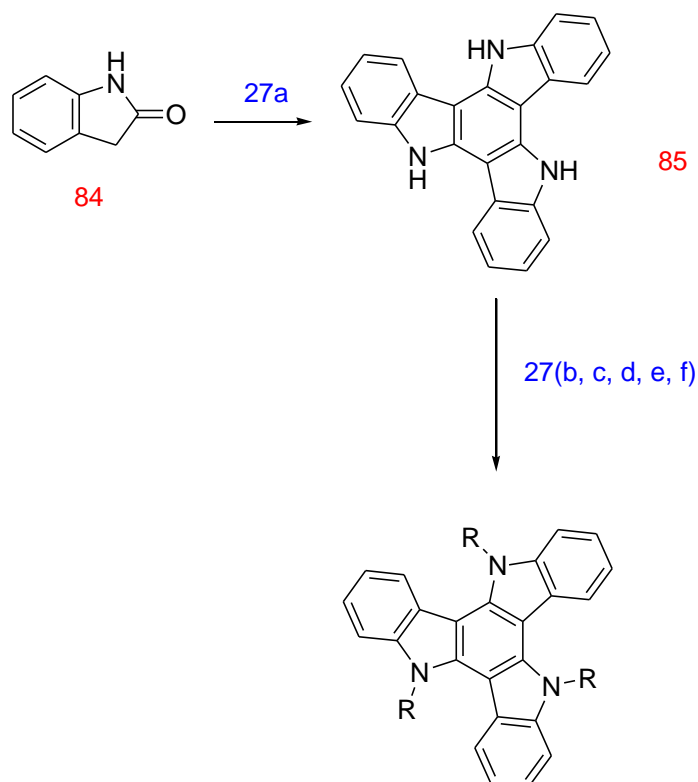
Scheme 26

26a: Phosphorus (V) oxychloride, 100 °C;
26b: (2-(2Bbromoethyl)-1,3-dioxane), NaH (60% dispersion in mineral oil), DMF;
26c: (Bromomethyl)cyclopropane, NaH (60% dispersion in mineral oil), DMF.

Scheme 27

R=   -CH$_2$CH$_2$OCH$_2$CH$_3$ 105

     -CH$_2$CH$_2$OCOCH$_3$ 106

     -CH$_2$COOCH$_2$CH$_3$ 107

     -CH$_2$CH$_2$N=C=O   108

     -(CH$_2$)$_4$CN   109

27a: Phosphorus (V) oxychloride, 100 ^{o}C;
27b: 2-Bromoethyl ethyl ether, NaH (60% dispersion in mineral oil), DMF;
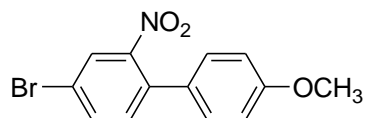27c: 2-Bromoethyl acetate, NaH (60% dispersion in mineral oil), DMF;
27d: Ethyl bromoacetate, NaH (60% dispersion in mineral oil), DMF;
27e: 2-Bromoethyl isocyanate, NaH (60% dispersion in mineral oil), DMF;
27f: 5-Bromovaleronitrile, NaH (60% dispersion in mineral oil), DMF.

3.4 Synthesis of the Materials

4-Bromo-4'-methoxy-2-nitrobiphenyl (3).

Copper powder (19.14 g, 30.1 mmol) was added over 1 h to a stirred molten mixture of 2, 5-dibromonitrobenzene (**1**) (28.10 g, 100.1 mmol) and 4-iodoanisole (**2**) (28.94 g, 123.62 mmol) maintained at 175 °C overnight. The reaction mixture was cooled to operational temperature, extracted with hot toluene (3 × 150 cm^3) and immediately filtered through silica gel. The filtrate was washed with water (2 × 200 cm^3), dried (MgSO$_4$), filtered and the volatiles were removed *in vacuo*. Purification was carried out using recrystallisation from ethanol to give the desired product as yellow needles (17.00 g, 55%).

Melting Point/ °C: 126-127 (Lit. 125-127)[5]. ^{1}H NMR (CDCl$_3$) δ_H: 7.95 (1H, d, J = 2.0 Hz), 7.72 (1H, dd, J = 8.0 & 2.4 Hz), 7.32 (1H, d, J = 8.0 Hz), 7.23 (2H, d, J = 9.6 Hz), 6.96 (2H, d, J = 8.8 Hz), 3.84 (3H, s). MS m/z (EI): 309, 308 (M$^+$), 307, 292.
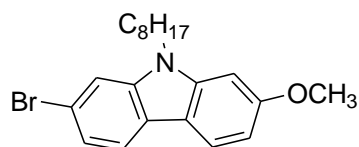
2-Bromo-7-methoxycarbazole (4).
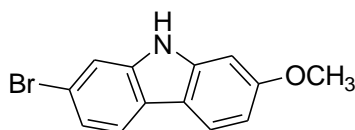
A mixture of 4-bromo-4'-methoxy-2-nitrobiphenyl (**3**) (10.00 g, 32.5 mmol) and triphenyl phosphine (34.05 g, 129.8 mmol) was heated at 175 °C overnight. The reaction mixture was cooled down to room temperature, and then hexane (100 cm^3) was added, stirred for 1 h and then filtered through what under vacuum. Purification was carried out using column chromatography [silica gel, hexane: DCM = 1:1], followed by removal of the volatiles *in vacuo* to afford the desired product as a white solid (6.80 g,

76%).

Melting Point/$^{\circ}$C: 286-287 (Lit. 286)[5]. ^{1}H NMR (CDCl$_3$) δ_H: 11.30 (1H, s), 8.02 (1H, d, J = 6.0 Hz), 7.98 (1H, d, J = 8.0 Hz), 7.64 (1H, d, J = 1.2 Hz), 7.30 (1H, dd, J = 8.0 & 1.0 Hz), 7.04 (1H, d, J = 2.0 Hz), 6.85 (1H, dd, J = 7.6 & 2.2 Hz), 3.89 (3H, s). MS m/z (EI): 277, 276 (M$^+$), 275, 260.
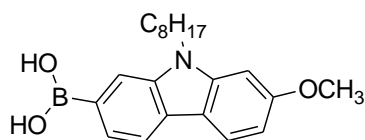
2-Bromo-7-methoxy-*N*-octylcarbazole (5).

Sodium hydride (NaH) (60% in mineral oil) (1.45 g, 36.2 mmol) was added in a small portion into a solution of 2-bromo-7methoxycarbazole (**4**) (5.00 g, 18.11 mmol) in DMF (60 cm^3). The resultant mixture was stirred for 1 h at room temperature, then heated and maintained at 50 $^{\circ}$C for another 1 h. 1-Bromooctane (3.80 g, 19.92 mmol) was added and the resultant mixture was maintained at 50 $^{\circ}$C for 3 h. The mixture was then cooled to room temperature, stirred overnight and then poured into ice-water (100 cm^3). The resultant precipitate was isolated by filtration, washed with ethanol (2 × 100 cm^3) and dried under vacuum to give the desired product as a white powder (5.02 g, 71%).

Melting Point/$^{\circ}$C: 57-58. ^{1}H NMR (CDCl$_3$) δ_H: 7.92 (1H, d, J = 8.0 Hz), 7.82 (1H, d, J = 8.0 Hz), 7.47 (1H, d, J = 1.6 Hz), 7.29 (1H, dd, J = 8.0 & 1.6 Hz), 6.86 (1H, d, J = 2.4 Hz), 6.84 (1H, dd, J = 8.4 & 2.0 Hz), 4.19 (2H, t, J = 7.6 Hz), 3.93 (3H, s), 1.87 (2H, quint, J = 7.6 Hz), 1.24-1.39 (10H, m), 0.88 (3H, t, J = 7.2 Hz). MS m/z (EI): 389, 388 (M$^+$), 387, 372.

(7-Methoxy-9-octyl-carbzole-2-yl)boronic acid (6).

A solution of 2.5 mol/L *n*-BuLi (8.0 cm^3 in hexanes) was added to a solution of 2-bromo-7-methoxy-*N*-octylcarbazole (**5**) (5.00 g, 12.88 mmol) in THF (80 cm^3) at -78 $^{\circ}$C, and the resultant mixture was maintained for 1 h at -78 $^{\circ}$C. 2-triisopropyl borate (6 mL, 25.75 mmol) was added drop-wise to the reaction mixture, which was then stirred for 1 h at -78 $^{\circ}$C, then stirred overnight at room temperature. Hydrochloric acid (21.5 mL, 12 mol/L) was added to the mixture and it was stirred for 1 h. The reaction mixture was quenched with water (50 cm^3) and extracted with diethyl ether (3 × 50 cm^3). The combined organic extracts were washed with water (2 × 100 cm^3), dried (MgSO$_4$), filtered and then concentrated under reduced pressure. The residue was collected by washing with hexane (2 × 100 cm^3) and dried under reduced pressure to give white solid (2.90 g, 63%).

Melting Point/$^{\circ}$C: 189-191. ^{1}H NMR (CDCl$_3$) δ_H: 8.32 (1H, s), 8.18 (1H, dd, *J* = 7.6 & 2.0 Hz), 8.02-8.08 (2H, m), 7.80 (1H, s), 7.52 (1H, d, *J* = 7.2 Hz), 6.90 (2H, d, *J* = 8.0 Hz), 4.42 (2H, t, *J* = 7.2 Hz), 3.98 (3H, s), 2.00 (2H, quint, *J* = 7.2 Hz), 1.26-1.50 (10H, m), 0.84 (3H, t, *J* = 7.2 Hz). MS m/z (EI): 354 (M$^+$), 353, 352, 323, 269, 215, 175, 141, 97.
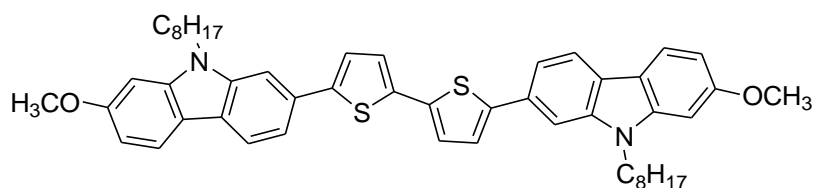
5,5'-Dibromo-2.2'-bithiophene (8).
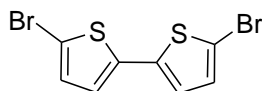
N-bromosuccinimide (NBS) (2.36 g, 13.24 mmol) was added portion-wise to a mixture of 2,2'-bithiophene (**7**) (1.00 g, 6.01 mmol) and silica gel (0.08 g, 1.20 mmol) in DCM (20 cm^3) in the dark. The resultant mixture was stirred overnight at room temperature.

The reaction mixture was filtered to remove the silica gel and the organic filtrate was concentrated under reduced pressure to give crude product, which was recrystallised from EtOH/DCM to afford the desired product as a white solid (1.42 g, 73%).

Melting Point/ ^{o}C: 146-147 (Lit. 144-146)[17] . ^{1}H NMR (CDCl$_3$) δ_H: 6.86 (2H, d, J = 4.0 Hz), 6.96 (2H, d, J = 4.0 Hz). MS m/z (EI): 326, 324 (M^{+}), 322.

**5,5'-*bis*-(7-Methoxy-9-octyl-carbazol-2-yl)-2,2'-bithiophene (9).**

A mixture of Pd(OAc)$_2$ (0.01g, 0.045 mmol), 5,5'-dibromo-2,2'-bithiophene (**8**) (0.20 g, 0.618 mmol), (7-methoxy-9-octyl-carbzole-2-yl)boronic acid (**6**) (0.66 g, 1.854 mmol), K$_2$CO$_3$ (0.52 g, 3.708 mmol), H$_2$O (2 cm^3) and DMF (30 cm^3) was heated at 80 ^{o}C overnight. The cooled reaction mixture was washed with water (100 cm^3) and extracted with DCM (3 × 100 cm^3). The combined organic layers were washed with water (2 × 100 cm^3), dried (MgSO$_4$), filtered and then concentrated under reduced pressure. The residue was purified using column chromatography [silica, DCM/hexane 5:10] to afford the desired product as an orange solid (0.40 g, 83%).

Melting Point/ ^{o}C: 214. ^{1}H NMR (CDCl$_3$) δ_H: 7.98 (2H, d, J = 8.0 Hz), 7.95 (2H, d, J = 8.4 Hz), 7.55 (2H, d, J = 1.0 Hz), 7.48 (2H, dd, J = 7.6 & 1.2 Hz), 7.33 (2H, d, J = 4.0 Hz), 7.24 (2H, d, J = 4.0 Hz), 6.86 (4H, dd, J = 7.2 & 2.0 Hz), 4.28 (4H, t, J = 7.2 Hz), 3.95 (6H, s), 7.33 (2H, d, J = 4.0 Hz), 1.91 (4H, quint, J = 7.2 Hz), 1.26-1.46 (20H, m), 0.86 (6H, t, J = 6.8 Hz). ^{13}C NMR (CDCl$_3$): 159, 145, 143, 141, 136, 130, 124, 123, 121, 120, 117, 107, 105, 93, 56, 43, 32, 29, 28, 27, 22, 14. IR ν_{max}/cm^{-1}: 2920, 2850, 1600, 1500, 1457, 1435, 1389, 1352, 1258, 1198, 1172, 1126, 1056, 936, 889, 823, 801, 785, 768. MS m/z (MALDI): 783, 782, 781 (M^{+}, M100). Combustion analysis: Expected: C, 76.88%; H, 7.23%; N, 3.59%; S, 8.21%; Obtained: C, 76.88%; H, 7.20%; N, 3.64%; S, 8.43%.
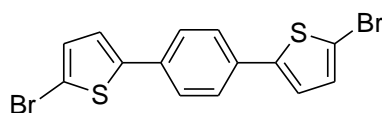
1,4-*bis*-(Thien-2-yl)benzene (12)
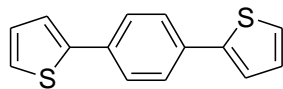
A mixture of Pd(PPh$_3$)$_4$ (0.60 g, 0.52 mmol), 1,4-dibromobenzene (**10**) (6.00 g, 25.43 mmol), 2-thienylboronic acid (**11**) (10.00 g, 76.29 mmol), K$_2$CO$_3$ (14.05 g, 101.72 mmol), H$_2$O (50 cm^3) and DME (100 cm^3) was heated at reflux overnight. The cooled reaction mixture was poured into H$_2$O (150 cm^3) and the crude product isolated by filtration under reduced pressure. The crude product was stirred with methanol for 3 h, and the residual solid isolated by filtration under reduced pressure to afford the desired product as a pale-yellow solid (5.99 g, 97%).

Melting Point/°C: 208 (Lit. 204-206)[18], (Lit. 208)[19]. ^{1}H NMR (CDCl$_3$) δ_H: 7.63 (4H, d, *J* = 1.0 Hz), 7.35 (2H, dd, *J* = 7.2 & 1.0 Hz), 7.31 (2H, dd, *J* = 5.2 & 1.0 Hz), 7.11 (2H, dd, *J* = 4.0 & 1.6 Hz). MS m/z (EI): 244, 243, 242 (M$^+$, M100).
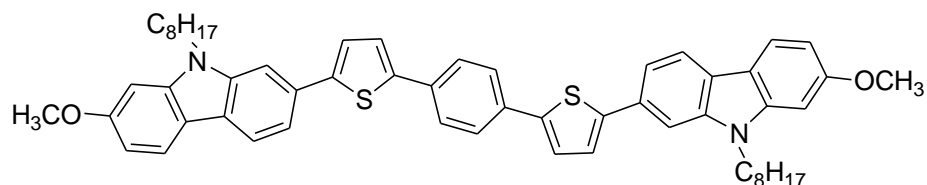
1,4-*bis*-(5-Bromothiophen-2-yl)benzene (13)

N-bromosuccinimide (NBS) (0.84 g, 4.72 mmol) was added in a small portion into a solution of 1,4-*bis*-(thien-2-yl)benzene (**12**) (0.54 g, 2.28 mmol) in DMF (20 cm^3) in the dark. The resultant mixture was stirred overnight at room temperature. The reaction mixture was diluted with ethanol (50 cm^3) and stirred for 1 h. A pale-yellow precipitate was filtered off, washed with ethanol (3 × 50 cm^3) and dried under reduced pressure to give the desired product (0.81 g, 94%).

Melting Point/°C: 255 (Lit. 251-252)[18]. ^{1}H NMR (CDCl$_3$) δ_H: 7.51 (4H, d, *J* = 1.0 Hz), 7.08 (2H, d, *J* = 4.0 Hz), 7.04 (2H, d, *J* = 4.0 Hz). MS m/z (EI): 402, 401, 400(M$^+$).

1,4-*bis*-[5-(7-Methoxy-9-octyl-carbazol-2-yl)thiophen-2-yl]benzene (14)

A mixture of 1,4-*bis*-(5-bromothiophen-2-yl)benzene (**13**) (0.20 g, 0.50 mmol), Pd(OAc)$_2$ (0.01g, 0.045 mmol), P(Ph)$_3$ (0.04 g, 0.12 mmol), K$_2$CO$_3$ (0.42 g, 3.00 mmol), (7-methoxy-9-octyl-carbzole-2-yl)boronic acid (**6**) (0.53 g, 1.50 mmol) and H$_2$O (2 cm^3) in DME (20 cm^3) was heated at reflux overnight. Then the cooled reaction mixture was washed with water (100 cm^3) and extracted with DCM (3 × 100 cm^3). The combined organic layers were washed with water (2 × 100 cm^3), dried (MgSO$_4$), filtered and then concentrated down under reduced pressure. The residue was purified using column chromatography [silica, DCM/hexane 5:10] to afford the desired product as a yellow solid (0.25 g, 60%).

Melting Point/ $^{\circ}$C: Tg 191 Cr 265 N 266 I. ^{1}H NMR (CDCl$_3$) δ_H: 7.99 (2H, d, $J = 8.0$ Hz), 7.96 (2H, d, $J = 8.8$ Hz), 7.69 (4H, d, $J = 0.8$ Hz), 7.57 (2H, d, $J = 0.8$ Hz), 7.52 (2H, dd, $J = 8.0$ & 1.6 Hz), 7.39 (2H, d, $J = 4.0$ Hz), 7.38 (2H, d, $J = 3.6$ Hz), 6.86 (4H, dd, $J = 6.8$ & 2.0 Hz), 4.30 (4H, t, $J = 7.6$ Hz), 3.95 (6H, s), 1.90 (4H, quint, $J = 7.2$ Hz), 1.26-1.46 (20H, m), 0.88 (6H, t, $J = 6.8$ Hz). ^{13}C NMR (CDCl$_3$): 159, 145, 143, 141, 134, 130, 125, 124, 121, 117, 107, 105, 94, 56, 43, 32, 29, 28, 27, 23, 14. IR ν_{max}/cm^{-1}: 2921, 2850, 1600, 1508, 1483, 1458, 1351, 1253, 1166, 1148, 1060, 1033, 951, 834, 790, 769. MS m/z (MALDI): 859, 858, 857 (M$^+$, M100). Combustion analysis: Expected: C, 78.46%; H, 7.05%; N, 3.27%; S, 7.48%; Obtained: C, 78.44%; H, 7.05%; N, 3.36%; S, 7.67%.
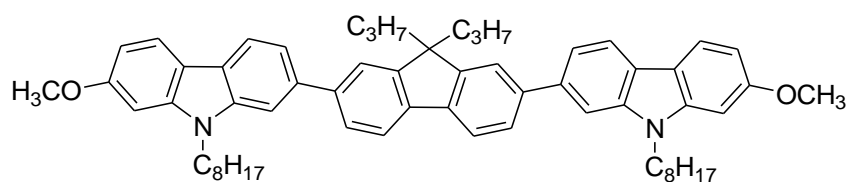
2,7-Dibromo-9,9-dipropyl-fluorene (16)
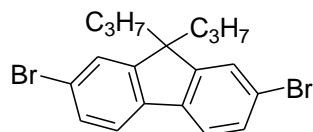
A 50% aqueous solution of sodium hydroxide (NaOH) (70 cm^3) was added to a mixture of *tetra-n*-butylammonium bromide (TBAB) (0.50 g, 1.55 mmol) and 2,7-dibromofluorene (**15**) (10.00 g, 30.86 mmol) in toluene (70 cm^3). 1-Bromopropane (9.49 g, 77.15 mmol) in toluene (10 cm^3) was then added drop-wise at room temperature and the resultant mixture was stirred overnight at reflux. The cooled reaction mixture was washed with water (100 cm^3) and extracted with DCM (3 × 100 cm^3). The combined organic layers were washed with water (2 × 100 cm^3), dried (MgSO$_4$), filtered and then concentrated down under reduced pressure. The crude product was purified using recrystallisation from EtOH/DCM to afford the desired product as a white crystalline solid (10.02 g, 80%).

Melting Point/°C: 138-139 (Lit. 139-140)[20]. ^{1}H NMR (CDCl$_3$) δ$_H$: 7.51 (2H, d, *J* = 1.2 Hz), 7.46 (4H, m), 1.90 (4H, m), 0.62-0.69 (10H, m). MS m/z (EI): 410, 408 (M$^+$), 406.

7,7'-(9,9-Dipropyl-fluorene-2,7-diyl)-*bis*-(2-methoxy-9-octyl-carbazole) (18)
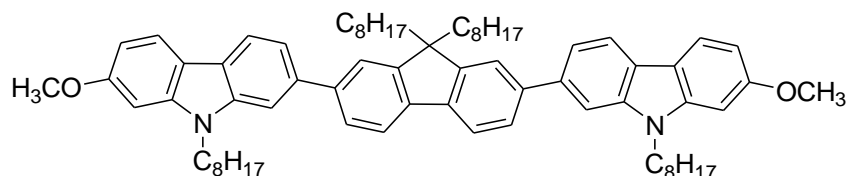

A mixture of Pd(OAc)$_2$ (0.01g, 0.045 mmol), 2,7-dibromo-9,9-dipropyl-fluorene (**16**) (0.20 g, 0.49 mmol), (7-methoxy-9-octyl-carbzole-2-yl)boronic acid (**6**) (0.52 g, 1.47 mmol), K$_2$CO$_3$ (0.41 g, 2.94 mmol) and H$_2$O (1.5 cm^3) in DMF (30 cm^3) was heated at 80 °C overnight. Then, the cooled reaction mixture was washed with water (100 cm^3), and extracted with DCM (3 × 100 cm^3). The combined organic layers were washed with water (2 × 100 cm^3), dried over magnesium sulphate (MgSO$_4$), filtered and then

concentrated down under reduced pressure. The residue was purified using column chromatography [silica, DCM/Hexane 8:10] to afford the desired product as a pale-yellow solid (0.39 g, 93%).

Melting Point/ ^{o}C: 88. ^{1}H NMR (CDCl$_3$) δ_H: 8.08 (2H, d, J = 8.0 Hz), 8.01 (2H, d, J = 8.4 Hz), 7.84 (2H, d, J = 7.6 Hz), 7.72 (4H, dd, J = 7.6 & 1.2 Hz), 7.61 (2H, d, J = 1.0 Hz), 7.55 (2H, dd, J = 8.0 & 1.6 Hz), 6.89 (4H, dd, J = 8.0 & 1.6 Hz), 4.35 (4H, t, J = 7.2 Hz), 3.97 (6H, s), 2.12 (4H, m), 1.95 (4H, m), 1.27-1.46 (20H, m), 0.86 (6H, t, J = 6.4 Hz), 0.74-0.85 (10H, m). ^{13}C NMR (CDCl$_3$): 159, 152, 143, 142, 139, 138, 126, 122, 121, 120, 119, 118, 107, 93, 56, 43, 32, 29, 23, 22, 14. IR ν_{max}/cm^{-1}: 2952, 2845, 1601, 1502, 1457, 1432, 1365, 1244, 1226, 1208, 1165, 1122, 1054, 994, 933, 856, 830, 806, 798. MS m/z (MALDI): 866, 865 (M$^+$, M100). Combustion analysis: Expected: C, 84.68%; H, 8.39%; N, 3.24%; Obtained: C, 84.75%; H, 8.49%; N, 3.19%.

**7,7'-(9,9-Dioctyl-fluorene-2,7-diyl)-*bis*-(2-methoxy-9-octyl-carbazole) (19)**

A mixture of Pd(OAc)$_2$ (0.01g, 0.045 mmol), 2,7-dibromo-9,9-dioctyl-fluorene (**17**) (0.20 g, 0.365 mmol), (7-methoxy-9-octyl-carbzole-2-yl)boronic acid (**6**) (0.40 g, 1.10 mmol), K$_2$CO$_3$ (0.31 g, 2.20 mmol) and H$_2$O (1 cm^3) in DME (30 cm^3) was heated at 80 ^{o}C overnight. The cooled reaction mixture was washed with water (100 cm^3) and extracted with DCM (3 × 100 cm^3). The combined organic layers were washed with water (2 × 100 cm^3), dried over magnesium sulphate (MgSO$_4$), filtered and then concentrated down under reduced pressure. The residue was purified using column chromatography [silica, DCM/Hexane 5:10] to afford the desired product as a pale-yellow solid (0.30 g, 82%).

Melting Point/ ^{o}C: 70. ^{1}H NMR (CDCl$_3$) δ_H: 8.05 (2H, d, J = 8.0 Hz), 7.98 (2H, d, J =

7.6 Hz), 7.81 (2H, d, J = 7.6 Hz), 7.70 (2H, dd, J = 7.6 & 2.0 Hz), 7.66 (2H, d, J = 1.0 Hz), 7.58 (2H, d, J = 1.0 Hz), 7.52 (2H, dd, J = 8.0 & 1.2 Hz), 6.87 (4H, d, J = 8.4 Hz), 4.32 (4H, t, J = 7.2 Hz), 3.94 (6H, s), 2.09 (4H, t, J = 8.0 Hz), 1.92 (4H, m), 1.08-1.48 (40H, m), 0.86 (6H, t, J = 7.2 Hz), 0.77-0.83 (10H, m). ^{13}C NMR (CDCl$_3$): 159, 152, 142, 141, 139, 138, 126, 121, 120, 119, 118, 116, 107, 93, 56, 43, 40, 32, 29, 23, 22, 14. IR ν_{max}/cm^{-1}: 2921, 2849, 1601, 1500, 1457, 1332, 1243, 1208, 1168, 1122, 1054, 994, 860, 798. MS m/z (MALDI): 1006, 1005, 1004 (M$^+$, M100). Combustion analysis: Expected: C, 84.81%; H, 9.22%; N, 2.79%; Obtained: C, 84.78%; H, 9.30%; N, 2.73%.
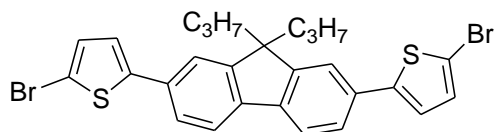
2,7- *bis*(Thien-2-yl)-9,9-dipropyl-fluorene (20)
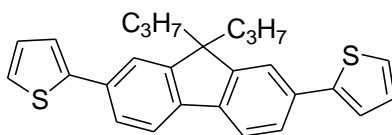
A mixture of Pd(PPh$_3$)$_4$ (0.30 g, 0.26 mmol), 2,7-dibromo-9,9-dipropyl-fluorene (**16**) (5.00 g, 12.20 mmol) and 2-(tributylstannyl)thiophene (11.38 g, 30.50mmol) in DMF (100 cm^3) was stirred and heated to 90 ^{o}C overnight. Then, the cooled reaction mixture was washed with water (100 cm^3) and then extracted with DCM (3 × 100 cm^3). The combined organic layers were washed with water (2 × 100 cm^3), dried over magnesium sulphate (MgSO$_4$), filtered and then concentrated under reduced pressure. The crude product was purified using column chromatography [K$_2$CO$_3$/silica 1:9, DCM/Hexane 5:10] to remove the tin side products and then re-crystallised from EtOH/DCM to afford the desired product as a light yellow solid (3.98 g, 79%).

Melting Point/^{o}C: 168-170 (Lit. 166-168)[21]. ^{1}H NMR (CDCl$_3$) δ_H: 7.66 (2H, d, J = 8.0 Hz), 7.59 (2H, dd, J = 8.0 & 1.6 Hz), 7.55 (2H, d, J = 2.0 Hz), 7.37 (2H, d, J = 3.8 Hz), 7.28 (2H, d, J = 5.2 Hz), 7.10 (2H, dd, J = 7.8 & 1.2 Hz), 2.00 (4H, m), 0.66-0.70 (10H, m). MS m/z (EI): 416, 415, 414 (M$^+$, M100).
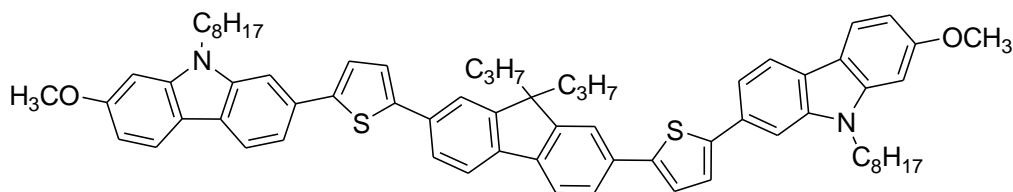
2,7-*bis*-(5-Bromothiophen-2-yl)-9,9-dipropyl-fluorene (21)

N-bromosuccinimide (NBS) (0.95 g, 5.32 mmol) was added in a small portion into a solution of 2,7- *bis*(thien-2-yl)-9,9-dipropyl-fluorene (**20**) (1.00 g, 2.42 mmol) in acetic acid (10 cm^3) and chloroform (10 cm^3) in the dark. The resultant mixture was stirred overnight at room temperature. The reaction mixture was poured into water (100 cm^3) and then extracted with DCM (3 × 100 cm^3). The combined organic layers were washed with water (2 × 100 cm^3), dried over magnesium sulphate (MgSO$_4$), filtered and then concentrated under reduced pressure. The crude product was purified using column chromatography [Hexane] to afford the desired product as a yellow solid (0.95 g, 77%).

Melting Point/ $^{\circ}$C: 165-166 (Lit. 164-166)[21] . ^{1}H NMR (CDCl$_3$) δ_H: 7.65 (2H, d, *J* = 8.0 Hz), 7.48 (2H, dd, *J* = 8.0 & 1.6 Hz), 7.44 (2H, d, *J* = 1.6 Hz), 7.10 (2H, d, *J* = 4.0 Hz), 7.04 (2H, d, *J* = 3.6 Hz), 1.97 (4H, m), 0.66-0.69 (10H, m). MS m/z (EI): 574, 572 (M$^+$), 570.

2,7-[*bis*(Thien-2-yl)-9,9-dipropyl-fluorene-5,5-diyl]-*bis*-(2-methoxy-9-octyl-carbazole) (22)

A mixture of Pd(OAc)$_2$ (0.01g, 0.045 mmol), 2,7-*bis*-(5-bromothiophen-2-yl)-9,9-dipropyl-fluorene (**21**) (0.2 g, 0.35 mmol), (7-methoxy-9-octyl-carbzole-2-yl)boronic acid (**6**) (0.38 g, 1.05 mmol), K$_2$CO$_3$ (0.30 g, 2.10 mmol) and H$_2$O (2 cm^3) in DMF (30 cm^3) was heated at 80 $^{\circ}$C overnight. The cooled reaction mixture was washed with water (100 cm^3) and extracted with DCM (3

$\times$ 100 cm^3). The combined organic layers were washed with water (2 $\times$ 100 cm^3), dried over magnesium sulphate (MgSO$_4$), filtered and then concentrated under reduced pressure. The residue was purified using column chromatography [silica, DCM/Hexane 5:10] to afford the desired product as a yellow solid (0.26 g, 74%).

Melting Point/ ^{o}C: Tg 77 Cr - N 185 I. ^{1}H NMR (CDCl$_3$) δ_H: 7.98 (2H, d, J = 8.0 Hz), 7.95 (2H, d, J = 9.2 Hz), 7.71 (2H, d, J = 8.0 Hz), 7.66 (2H, dd, J = 8.0 & 1.0 Hz), 7.62 (2H, d, J = 1.0 Hz), 7.58 (2H, d, J = 1.0 Hz), 7.53 (2H, dd, J = 6.4 & 1.6 Hz), 7.40 (4H, dd, J = 4.0 & 1.0 Hz), 6.86 (4H, d, J = 7.2 Hz), 4.30 (4H, t, J = 6.8 Hz), 3.95 (6H, s), 2.07 (4H, m), 1.92 (4H, m), 1.23-1.45 (20H, m), 0.87 (6H, t, J = 6.8 Hz), 0.72-0.84 (10H, m). ^{13}C NMR (CDCl$_3$): 159, 152, 145, 144, 142, 141, 133, 131, 124, 121, 120, 117, 107, 105, 93, 55, 43, 32, 29, 27, 23, 17, 14. IR ν_{max}/cm^{-1}: 2922, 2848, 1600, 1500, 1457, 1432, 1344, 1247, 1196, 1165, 1124, 1054, 935, 873, 790, 769. MS m/z (MALDI): 1032, 1031, 1030 (M$^+$), 617 (M100). Combustion analysis: Expected: C, 80.50%; H, 7.44%; N, 2.72%; S, 6.23%; Obtained: C, 80.59%; H, 7.59%; N, 3.00%; S, 6.41%.

3-Ethyl-4-methyl-3,4-dicarboxylate-2-iodothiophene (24)
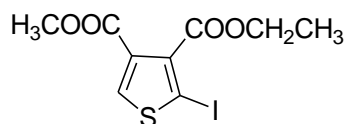
A mixture of 3-ethyl-4-methyl-3,4-dicarboxylate-2-aminothiophene (**23**) (20 g, 87.24 mmol) in concentrated hydrochloric acid (100 cm^3) was stirred at room temperature for 2 h. The resultant mixture was diluted by water (100 cm^3) and ice (400 g). Sodium nitrite (10.66 g, 154.49 mmol) in water (27 cm^3) was then added drop-wise. After 20 minutes, potassium iodide (34.18 g, 205.89 mmol) in small portions was added and the mixture was stirred overnight. The reaction mixture was washed with sodium bisulphate and water (100 cm^3), and extracted with diethyl ether (4 $\times$ 100 cm^3). The combined organic layers were washed with water (2 $\times$ 100 cm^3), dried over magnesium

sulphate (MgSO$_4$), filtered and then concentrated down under reduced pressure. The crude product was purified using column chromatography [silica, DCM/Hexane 5:10] to afford the desired product as dark sticky oil[22-24] (15.13 g, 43%).

^{1}H NMR (CDCl$_3$) δ$_H$: 8.09 (1H, s), 4.42 (2H, quart, J = 7.2 Hz), 3.85 (3H, s), 1.39 (3H, t, J = 7.2 Hz). MS m/z (EI): 342, 341, 340 (M$^+$).

2-Iodothiophene-3,4-dicarboxylic acid (25)

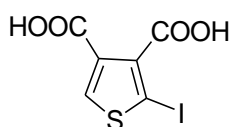
A mixture of 3-ethyl-4-methyl-3,4-dicarboxylate-2-iodothiophene (**24**) (15 g, 44.10 mmol) in concentrated hydrochloric acid (70 cm^3) and water (330 cm^3) was stirred at reflux for 24 h. The cooled reaction mixture was extracted with diethyl ether (4 × 100 cm^3). The combined organic layers were washed with water (2 × 100 cm^3), dried over magnesium sulphate (MgSO$_4$), filtered and then concentrated down under reduced pressure to afford the desired product as a white solid[22-24] (12.67 g, 96%).

Melting Point/ ^{o}C: 185-190. ^{1}H NMR (ACETONE-D$_6$) δ$_H$: 10.90 (2H, s), 8.39 (1H, s). MS m/z (EI): 210, 299, 298 (M$^+$).

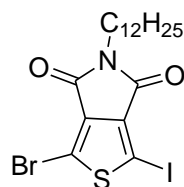**5-Dodecyl-1-iodo-5H-thieno-[3,4-c]pyrrole-4.6-dione (26)**
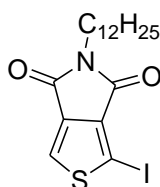
A mixture of 2-iodothiophene-3,4-dicarboxylic acid (**25**) (8.00 g, 26.84 mmol) in acetic anhydride (210 cm^3) was stirred at 75 ^{o}C for 2 h. The solvent was removed and then 1,4-dioxane (200 cm^3), 4-(dimethylamino)pyridine (4.16 g, 34.05 mmol) and

dodecylamine (6.27 g, 33.83 mmol) were added. The mixture was stirred at 90 °C for 20 h. Acetic anhydride (160 cm^3) was then added and the resultant mixture was stirred at 90 °C for 6 h. The cooled reaction mixture was poured into water (600 cm^3) and the solid precipitate was then collected and washed with (3 × 100 cm^3). The crude product was purified using flash column chromatography [DCM] to afford the desired product as a white solid[22-24] (10.72 g, 90%).

Melting Point/°C: 92-93. ^{1}H NMR (CDCl$_3$) δ$_H$: 7.85 (1H, s), 3.62 (2H, t, J = 6.8 Hz), 1.66 (2H, quint, J = 7.2 Hz), 1.26-1.33 (18H, m), 0.89 (3H, t, J = 6.8 Hz). MS m/z (EI): 449, 448, 447 (M$^+$).
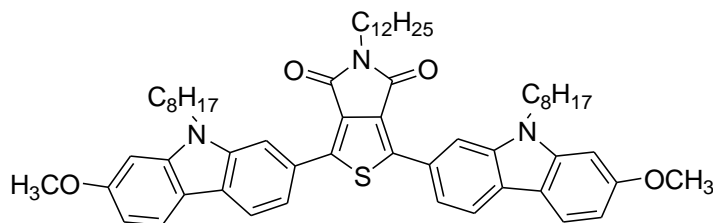
1-Bromo-5-dodecyl-3-iodo-5H-thieno-[3,4-c]pyrrole-4,6-dione (27)

N-bromosuccinimide (NBS) (1.60 g, 8.99 mmol) was added in a small portion into a mixture of 5-dodecyl-1-iodo-5H-thieno-[3,4-c]pyrrole-4.6-dione (**26**) (2.00 g, 4.29 mmol) in trifluoroacetic acid (20 cm^3) and sulfuric acid (8 cm^3) in the dark. The resultant mixture was stirred overnight at room temperature. The reaction mixture was poured onto ice water (200 cm^3) and then extracted with DCM (3 × 100 cm^3). The combined organic layers were dried over magnesium sulphate (MgSO$_4$), filtered and then concentrated down under reduced pressure. The crude product was purified using flash column chromatography [silica, DCM/Hexane 10:10] to afford the desired product as a yellow solid (1.81 g, 77%).

Melting Point/°C: 94-95. ^{1}H NMR (CDCl$_3$) δ$_H$: 3.52 (2H, t, J = 7.6 Hz), 1.56 (2H, quint, J = 7.2 Hz), 1.18-1.24 (18H, m), 0.81 (3H, t, J = 6.8 Hz). MS m/z (EI): 528, 527 (M$^+$), 526.

5-Dodecyl-1,3-*bis*-(7-methoxy-9-octyl-9*H*-carbazol-2-yl)-5*H*-thieno[3,4-*c*]pyrrole-4,6-dione (28)

A mixture of Pd(OAc)$_2$ (0.01g, 0.045 mmol), 1-bromo-5-dodecyl-3-iodo-5*H*-thieno-[3,4-*c*]pyrrole-4,6-dione (**27**) (0.25 g, 0.476 mmol), (7-methoxy-9-octyl-carbzole-2-yl)boronic acid (**6**) (0.51 g, 1.43 mmol), K$_2$CO$_3$ (0.40 g, 2.85 mmol) and H$_2$O (2 cm^3) in DMF (30 cm^3) was heated at 80 ^{o}C overnight. The cooled reaction mixture was washed with water (100 cm^3) and then extracted with DCM (3 × 100 cm^3). The combined organic layers were washed with water (2 × 100 cm^3), dried over magnesium sulphate (MgSO$_4$), filtered and then concentrated down under reduced pressure. The residue was purified using column chromatography [silica, DCM/Hexane 10:10] to afford the desired product as a yellow solid (0.32 g, 72%).

Melting Point/^{o}C: Tg 69 Cr 212 I. ^{1}H NMR (CDCl$_3$) δ_H: 8.63 (2H, d, *J* = 1.0 Hz), 8.02 (2H, d, *J* = 8.4 Hz), 7.99 (2H, d, *J* = 9.2 Hz), 7.81 (2H, dd, *J* = 8.0 & 1.2 Hz), 6.88 (4H, dd, *J* = 6.8 & 2.4 Hz), 4.38 (4H, t, *J* = 7.2 Hz), 3.96 (6H, s), 3.74 (2H, t, *J* = 7.2 Hz), 1.97 (4H, quint, *J* = 6.4 Hz), 1.74 (2H, quint, *J* = 6.4 Hz), 1.22-1.48 (38H, m), 0.86 (9H, t, *J* = 7.2 Hz). ^{13}C NMR (CDCl$_3$): 163, 159, 145, 143, 141, 127, 126, 124, 121, 119, 116, 108, 107, 93, 56, 43, 38, 32, 30, 29, 27, 23, 14. IR ν_{max}/cm^{-1}: 2957, 2919, 2849, 1727, 1601, 1529, 1460, 1434, 1390, 1349, 1243, 1210, 1169, 1077, 1048, 938, 887, 818, 803, 789, 759, 752. MS m/z (MALDI): 938, 937, 936 (M$^+$, M100). Combustion analysis: Expected: C, 76.96%; H, 8.29%; N, 4.49%; S, 3.42%; Obtained: C, 76.90%; H, 8.29%; N, 4.52%; S, 3.31%.
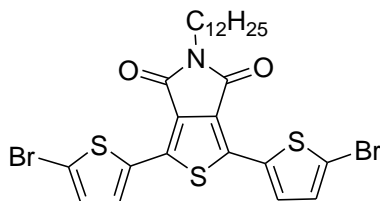
5-Dodecyl-1,3-di(thiophen-2-yl)-5*H*-thieno[3,4-*c*]pyrrole-4,6-dione (29)
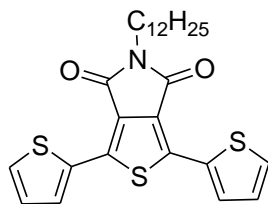
A mixture of Pd(PPh$_3$)$_4$ (0.05 g, 0.043 mmol), 1-bromo-5-dodecyl-3-iodo-5*H*-thieno-[3,4-*c*]pyrrole-4,6-dione (**27**) (2.05 g, 3.90 mmol), 2-thienylboronic acid (**11**) (2.00 g, 15.63 mmol), Na$_2$CO$_3$ (3.32 g, 31.32 mmol) and H$_2$O (16 cm^3) in DME (80 cm^3) was heated at reflux overnight. The cooled reaction mixture was washed with water (100 cm^3) and then extracted with DCM (3 × 100 cm^3). The combined organic layers were washed with water (2 × 100 cm^3), dried over magnesium sulphate (MgSO$_4$), filtered and then concentrated down under reduced pressure. The crude product was purified using column chromatography [silica, DCM/Hexane 5:10] to afford the desired product as a yellow solid (1.16 g, 61%).

Melting Point/ $^{\circ}$C: 64-66. ^{1}H NMR (CDCl$_3$) δ$_H$: 7.99 (2H, d, *J* = 3.6 Hz), 7.42 (2H, d, *J* = 4.0 Hz), 7.12 (2H, dd, *J* = 5.2 & 1.6 Hz), 3.65 (2H, t, *J* = 7.2 Hz), 1.66 (2H, quint, *J* = 6.8 Hz), 1.22-1.30 (18H, m), 0.86 (3H, t, *J* = 7.2 Hz). MS m/z (EI): 487, 486, 485 (M$^+$, M100).

1,3-*bis*-(5-Bromothiophen-2-yl)-5-dodecyl-5*H*-thieno-[3,4-*c*]pyrrole-4,6-dione (30)


Bromine (0.3 cm^3) was added drop-wise to a mixture of 5-dodecyl-1,3-di(thiophen-2-yl)-5*H*-thieno[3,4-*c*]pyrrole-4,6-dione (**29**) (1.16 g, 2.39 mmol) in acetic acid (20 cm^3) and chloroform (100 cm^3). The resultant mixture was stirred overnight at room temperature. After removal of chloroform, methanol was then

added and the precipitate was collected. The crude product was washed with methanol (3 × 100 cm^3), and dried under vacuum to afford the desired product as a yellow solid (1.48 g, 96%)

Melting Point/ ^{o}C: 85. ^{1}H NMR (CDCl$_3$) δ$_H$: 7.65 (2H, d, J = 4.0 Hz), 7.08 (2H, d, J = 4.0 Hz), 3.64 (2H, t, J = 7.2 Hz), 1.65 (2H, quint, J = 6.4 Hz), 1.23-1.31 (18H, m), 0.87 (3H, t, J = 6.4 Hz). MS m/z (EI): 645, 643 (M$^+$), 641.

## 5-Dodecyl-1,3-*bis*-[5-(7-methoxy-9-octyl-9*H*-carbazol-2-yl)thiophen-2-yl]-5*H*-thieno-[3,4-c]pyrrole-4,6-dione (31)
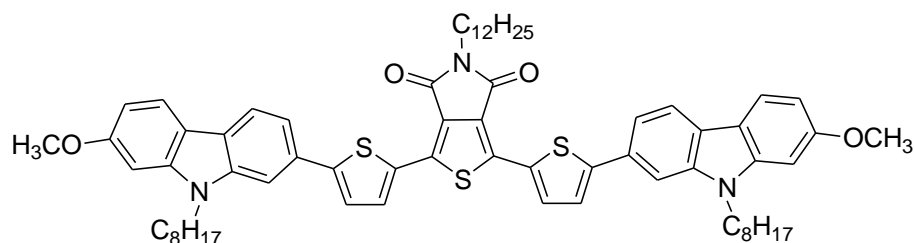
A mixture of Pd(OAc)$_2$ (0.01g, 0.045 mmol), 1,3-*bis*-(5-bromothiophen-2-yl)-5-dodecyl-5*H*-thieno-[3,4-*c*]pyrrole-4,6-dione (**30**) (0.25 g, 0.39 mmol), (7-methoxy-9-octyl-carbzole-2-yl)boronic acid (**6**) (0.42 g, 1.17 mmol), K$_2$CO$_3$ (0.33 g, 2.33 mmol) and H$_2$O (2 cm^3) in DMF (30 cm^3) was heated at 80 ^{o}C overnight. The cooled reaction mixture was washed with water (100 cm^3) and then extracted with DCM (3 × 100 cm^3). The combined organic layers were washed with water (2 × 100 cm^3), dried over magnesium sulphate (MgSO$_4$), filtered and then concentrated down under reduced pressure. The residue was purified using column chromatography [silica, DCM/Hexane 15:10] to afford the desired product as a yellow solid (0.33 g, 76%).

Melting Point/ ^{o}C: 172. ^{1}H NMR (CDCl$_3$) δ$_H$: 8.07 (2H, d, J = 4.0 Hz), 7.97 (4H, t, J = 9.2 Hz), 7.55 (2H, s), 7.51 (2H, d, J = 8.0 Hz), 7.39 (2H, d, J = 4.0 Hz), 6.86 (4H, dd, J = 8.4 & 2.4 Hz), 4.25 (4H, t, J = 6.8 Hz), 3.94 (6H, s), 3.72 (2H, t, J = 6.8 Hz), 1.88 (4H, quint, J = 6.4 Hz), 1.73 (2H, quint, J = 6.4 Hz), 1.22-1.46 (38H, m), 0.88 (9H, t, J = 6.8

Hz). ^{13}C NMR (CDCl$_3$): 163, 159, 149, 143, 141, 136, 131, 129, 124, 121, 120, 117, 116, 107, 105, 93, 56, 43, 39, 32, 29, 27, 23, 14. IR ν_{max}/cm^{-1}: 2957, 2919, 2850, 1736, 1601, 1518, 1498, 1459, 1389, 1356, 1248, 1201, 1165, 1124, 1054, 997, 805, 793, 768. MS m/z (MALDI): 1102, 1101, 1100 (M$^+$, M100). Combustion analysis: Expected: C, 74.21%; H, 7.42%; N, 3.82%; S, 8.74%; Obtained: C, 74.22%; H, 7.39%; N, 3.93%; S, 8.49%

1-Iodo-4-(octyloxy)benzene (33)
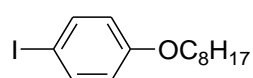
A mixture of 4-iodophenol (32) (20.00 g, 91.0 mmol), 1-bromooctane (16.00 g, 82.8 mmol), K$_2$CO$_3$ (34.40 g, 248.4 mmol) and DMF (200 cm^3) was heated overnight at 120 ^{o}C. The cooled reaction mixture was added to aqueous NaOH (91.0 mmol, 1 mol/L), stirred for 1 h and then extracted with DCM (3 × 100 cm^3). The combined organic layers were washed with water (2 × 100 cm^3), dried (MgSO$_4$), filtered and then concentrated down under reduced pressure. Purification was carried out using column chromatography [silica, DCM/hexane 1:10] to afford the desired product as a colourless liquid[25] (26.20 g, 95%).

^{1}H NMR (CDCl$_3$) δ_H: 7.56 (2H, d, J = 6.8 Hz), 6.68 (2H, d, J = 6.8 Hz), 3.91 (2H, t, J = 6.4 Hz), 1.79 (2H, m), 1.27-1.50 (10H, m), 0.90 (3H, t, J = 6.8 Hz). MS m/z (EI): 333, 332 (M$^+$).

4-Bromo-4'-octyloxy-2-nitrobiphenyl (34)
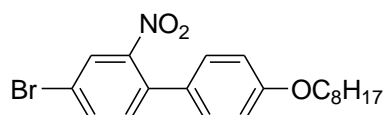
Copper powder (10.20 g, 160.2 mmol) was added over 1 h to a stirred, molten mixture of 2,5-dibromonitrobenzene (1) (15.00 g, 53.4 mmol) and 1-iodo-4-(octyloxy)benzene (33) (21.3 g, 64.08 mmol) maintained at 175 ^{o}C. The resultant reaction mixture was

then heated at 175 °C overnight. The cooled reaction mixture was extracted into hot toluene (3 × 150 cm^3) and the combined organic layers filtered through silica gel. The filtrate was washed with water (2 × 200 cm^3), dried (MgSO$_4$), filtered and then evaporated under reduced pressure. Purification of the crude product was carried out using column chromatography [silica, DCM/hexane 3:10] to afford the desired product as a yellow liquid (15.10 g, 69%)

^{1}H NMR (CDCl$_3$) δ_H: 7.94 (1H, d, J = 2.0 Hz), 7.69 (1H, dd, J = 8.0 & 1.2 Hz), 7.31 (1H, d, J = 8.4 Hz), 7.19 (2H, d, J = 8.4 Hz), 6.94 (2H, d, J = 8.0 Hz), 3.99 (2H, t, J = 6.8 Hz), 1.83 (2H, quint, J = 6.8 Hz), 1.20-1.52 (10H, m), 0.90 (3H, t, J = 6.8 Hz). MS m/z (EI): 407, 405 (M$^+$), 375, 296.

2-Bromo-7-octyloxycarbazole (35)
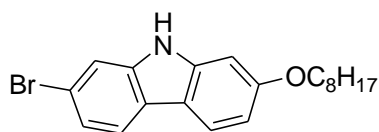
A mixture of 4-bromo-4'-octyloxy-2-nitrobiphenyl (**34**) (10.00 g, 24.61 mmol) and triethyl phophite (20.45 g, 123.06 mmol) was stirred and heated at reflux overnight. The volatiles were removed under reduced pressure. The residue was then poured onto methanol (300 cm^3) and stirred for 3 h. The mixture was then filtered off and the precipitate was collected to afford the desired product as a white solid (7.2 g, 78%).

Melting Point/°C: 265-266 (Lit. 265)[26]. ^{1}H NMR (CDCl$_3$) δ_H: 7.94 (1H, s), 7.89 (1H, d, J = 8.8 Hz), 7.81 (1H, d, J = 8.4 Hz), 7.52 (1H, d, J = 1.6 Hz), 7.31 (1H, dd, J = 8.4 & 1.6 Hz), 6.89 (1H, d, J = 2.2 Hz), 6.87 (1H, dd, J = 8.8 & 2.4 Hz), 4.05 (2H, t, J = 6.8 Hz), 1.85 (2H, quint, J = 6.8 Hz), 1.29-1.52 (10H, m), 0.90 (3H, t, J = 6.8 Hz). MS m/z (EI): 375, 373 (M$^+$).
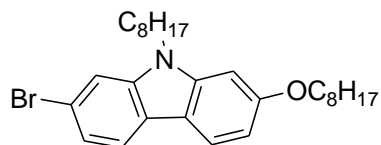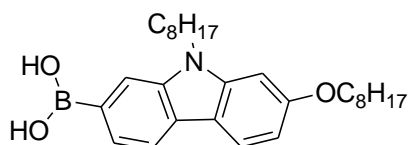
2-Bromo-*N*-octyl-7-(octyloxy)-carbazole (36)

Sodium hydride (NaH) (60% in mineral oil) (2.14 g, 53.43 mmol) was added in a small portion into a solution of 2-bromo-7-octyloxycarbazole (**35**) (10.00 g, 26.72 mmol) in DMF (100 mL). The resultant mixture was stirred for 1 h at room temperature, then heated and maintained at 50 $^{\circ}$C for another 1 h. 1-Bromooctane (5.68 g, 29.39 mmol) was added and the resultant mixture stirred at 50 $^{\circ}$C for 3 h and then at room temperature overnight. The reaction mixture was washed with water (100 cm^3), and extracted with DCM (3 × 100 cm^3). The combined organic layers were washed with water (2 × 100 cm^3), dried over magnesium sulphate (MgSO$_4$), filtered and then concentrated down under reduced pressure. The crude product was purified using column chromatography [DCM/Hexane 1:10] to afford the desired product as a white solid (20.74 g, 99%).

Melting Point/ $^{\circ}$C: 53-54. ^{1}H NMR (CDCl$_3$) δ_H: 7.90 (1H, d, J = 8.8 Hz), 7.82 (1H, d, J = 8.4 Hz), 7.47 (1H, d, J = 1.0 Hz), 7.28 (1H, dd, J = 8.4 & 1.0 Hz), 6.85 (2H, d, J = 7.6 Hz), 4.18 (2H, t, J = 7.6 Hz), 4.08 (2H, t, J = 6.4 Hz), 1.86 (4H, quint, J = 7.2 Hz), 1.25-1.54 (20H, m), 0.89 (3H, t, J = 4.4 Hz), 0.87 (3H, t, J = 5.6 Hz). MS m/z (EI): 487, 486, 485 (M$^+$).

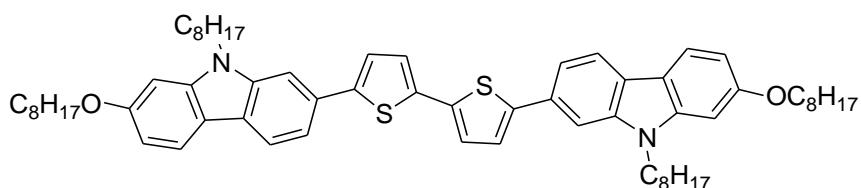## [*N*-octyl-7-(octyloxy)-carbazol-2-yl]boronic acid (37)

A solution of 2.5 mol/L *n*-BuLi in hexanes (12.34 cm^3)x mmol was added drop-wise to a dry THF (150 cm^3) solution of 2-bromo-*N*-octyl-7-(octyloxy)-carbazole (**36**) (10.00 g,

20.56 mmol) at -78 °C, and the resultant mixture was stirred for 1 h at -78 °C. Then 2-triisopropyl borate (9.5 cm^3, 41.12 mmol, 0.815 g cm^{-3}) was added drop-wise to the reaction mixture, which was then stirred for 1 h at -78 °C, allowed to warm to room temperature and then stirred overnight. Hydrochloric acid (34.26 cm^3, 12 mol/L)x mmol was added to the reaction mixture. The resultant mixture stirred for 1 h and then diluted with water (50 cm^3) and extracted with diethyl ether (3 × 100 cm^3). The combined organic extracts were washed with water (2 × 100 cm^3), dried (MgSO$_4$), filtered and concentrated down under reduced pressure. The crude product was purified via washing with hexane (2 × 100 cm^3) and then dried under reduced pressure to give the desired product as a white solid (8.58 g, 92%).

Melting Point/ °C: 127-128 (Lit. 120-122)[26]. ^{1}H NMR (CDCl$_3$) δ_H: 8.33 (1H, s), 8.18 (1H, dd, J = 7.8 & 3.6 Hz), 7.96-8.06 (2H, m), 7.79 (1H, s), 7.50 (1H, d, J = 7.2 Hz), 6.91 (2H, d, J = 8.0 Hz), 4.32 (2H, t, J = 7.2 Hz), 4.08 (2H, t, J = 6.8 Hz), 1.80 (4H, quint, J = 7.2 Hz), 1.24-1.50 (20H, m), 0.86 (3H, t, J = 6.8 Hz), 0.83 (3H, t, J = 6.4 Hz). MS m/z (EI): 452, 451(M$^+$), 450.

5,5'-*bis*-[9-Octyl-7-(0ctyloxy)-carbazol-2-yl]-2,2'-bithiophene (38)

A mixture of Pd(PPh$_3$)$_4$ (0.01g, 0.008 mmol), 5,5'-dibromo-2,2'-bithiophene (**8**) (0.20 g, 0.618 mmol), [*N*-octyl-7-(octyloxy)-carbazol-2-yl]boronic acid (**37**) (0.84 g, 1.85 mmol), K$_2$CO$_3$ (0.52 g, 3.71 mmol) and H$_2$O (2 cm^3) in DMF (30 cm^3) was heated at 80 °C overnight. The cooled reaction mixture was washed with water (100 cm^3) and extracted with DCM (3 × 100 cm^3). The combined organic layers were washed with water (2 × 100 cm^3), dried (MgSO$_4$), filtered and then concentrated down under reduced pressure. The residue was purified using column chromatography [silica, DCM/hexane 5:10] to afford the desired product as an yellow solid (0.49 g, 82%).

Melting Point/ $^{\circ}$C: Cr 136 N 151 I. ^{1}H NMR (CDCl$_3$) δ_H: 7.96 (2H, d, J = 8.0 Hz), 7.93 (2H, d, J = 8.4 Hz), 7.53 (2H, s), 7.48 (2H, d, J = 8.0 Hz), 7.32 (2H, d, J = 4.0 Hz), 7.23 (2H, d, J = 4.0 Hz), 6.85 (4H, dd, J = 7.2 & 2.0 Hz), 4.27 (4H, t, J = 6.8 Hz), 4.10 (4H, t, J = 6.4 Hz), 1.90 (8H, m), 1.26-1.53 (40H, m), 0.91 (6H, t, J = 7.6 Hz), 0.87 (6H, t, J = 7.2 Hz). ^{13}C NMR (CDCl$_3$): 159, 144, 142, 141, 136, 130, 124, 123, 121, 119, 117, 108, 105, 94, 68, 43, 32, 30, 29, 26, 23, 14. IR ν_{max}/cm^{-1}: 2922, 2850, 1599, 1499, 1455, 1439, 1390, 1347, 1248, 1218, 1208, 1167, 1145, 1126, 1056, 935, 880, 839, 801, 786, 768. MS m/z (MALDI): 979, 978, 977 (M$^+$, M100). Combustion analysis: Expected: C, 78.64%; H, 8.66%; N, 2.87%; S, 6.56%; Obtained: C, 78.62%; H, 8.70%; N, 2.83%; S, 6.66%

1,4-*bis*-{5-[9-octyl-7-(octyloxy)-carbazol-2-yl]thiophen-2-yl}benzene (39)
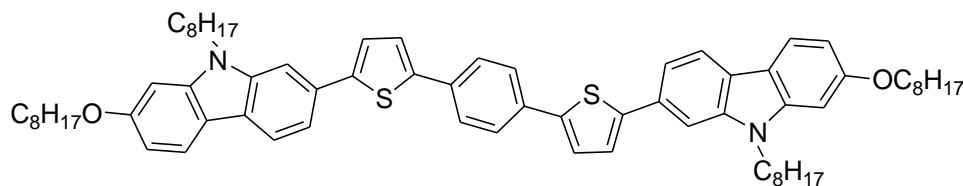
A mixture of Pd(PPh$_3$)$_4$ (0.01g, 0.008 mmol), 1,4-bis-(5-bromothiophen-2-yl)benzene (**13**) (0.20 g, 0.50 mmol), [*N*-octyl-7-(octyloxy)-carbazol-2-yl]boronic acid (**37**) (0.68 g, 1.5 mmol), K$_2$CO$_3$ (0.42 g, 3.00 mmol) and H$_2$O (2 cm^3) in DMF (30 cm^3) was heated at 80 $^{\circ}$C overnight. The cooled reaction mixture was washed with water (100 cm^3) and extracted with DCM (3 × 100 cm^3). The combined organic layers were washed with water (2 × 100 cm^3), dried (MgSO$_4$), filtered and then concentrated under reduced pressure. The residue was purified using column chromatography [silica, DCM/hexane 5:10] to afford the desired product as a yellow solid (0.38 g, 73%).

Melting Point/ $^{\circ}$C: 248. ^{1}H NMR (CDCl$_3$) δ_H: 7.98 (2H, d, J = 8.0 Hz), 7.94 (2H, d, J = 8.4 Hz), 7.69 (4H, s), 7.56 (2H, s), 7.51 (2H, d, J = 8.0 Hz), 7.39 (4H, dd, J = 6.4 & 2.4 Hz), 6.85 (4H, dd, J = 7.2 & 2.0 Hz), 4.28 (4H, t, J = 7.2 Hz), 4.10 (4H, t, J = 6.8 Hz), 1.91 (8H, m), 1.26-1.53 (40H, m), 0.90 (6H, t, J = 7.2 Hz), 0.87 (6H, t, J = 7.2 Hz). ^{13}C NMR (CDCl$_3$): 159, 145, 142, 141, 134, 130, 126, 124, 121, 117, 108, 105, 94, 68, 44,

32, 29, 26, 22, 14. IR ν_{max}/cm^{-1}: 2921, 2850, 1599, 1483, 1460, 1356, 1254, 1166, 1146, 1063, 1029, 949, 834, 823, 791, 769. MS m/z (MALDI): 1055, 1054, 1053 (M^+. M100). Combustion analysis: Expected: C, 79.80%; H, 8.42%; N, 2.66%; S, 6.09%; Obtained: C, 79.77%; H, 8.47%; N, 2.61%; S, 6.15%.

7,7'-(9,9-Dioctyl-fluorene-2,7-diyl)-*bis*-[9-octyl-7-(octyloxy)-carbazole] (41)
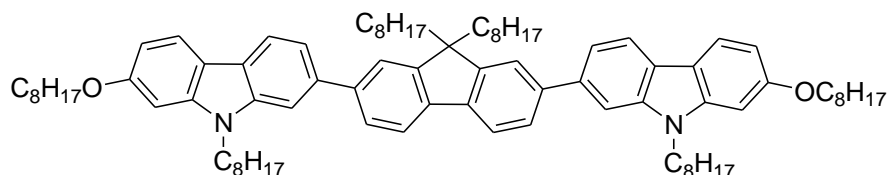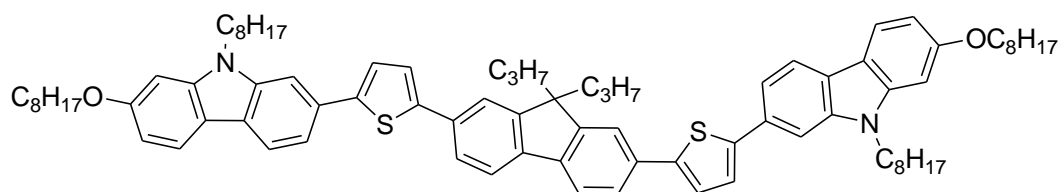

A mixture of Pd(PPh$_3$)$_4$ (0.01g, 0.008 mmol), 2,7-dibromo-9,9-dioctyl-fluorene (**17**) (0.20 g, 0.365 mmol), [*N*-octyl-7-(octyloxy)-carbazol-2-yl]boronic acid (**37**) (0.50 g, 1.10 mmol), K$_2$CO$_3$ (0.31 g, 2.20 mmol) and H$_2$O (2 cm^3) in DMF (30 cm^3) was heated at 80 ^{o}C overnight. The cooled reaction mixture was washed with water (100 cm^3) and then extracted with DCM (3 × 100 cm^3). The combined organic layers were washed with water (2 × 100 cm^3), dried over magnesium sulphate (MgSO$_4$), filtered and then concentrated down under reduced pressure. The residue was purified using column chromatography [silica, DCM/Hexane 3:10] to afford the desired product as a pale-yellow solid (0.32 g, 73%).

Melting Point/^{o}C: 66. ^{1}H NMR (CDCl$_3$) δ_H: 8.06 (2H, d, J = 8.0 Hz), 7.98 (2H, d, J = 8.4 Hz), 7.83 (2H, d, J = 8.0 Hz), 7.71 (2H, d, J = 8.0 Hz), 7.68 (2H, s), 7.59 (2H, s), 7.53 (2H, d, J = 8.0 Hz), 6.88 (4H, dd, J = 8.0 & 2.0 Hz), 4.32 (4H, t, J = 6.8 Hz), 4.12 (4H, t, J = 6.4 Hz), 3.92 (4H, m), 1.94 (8H, m), 1.10-1.48 (60H, m), 0.90 (12H, t, J = 7.2 Hz), 0.75-0.84 (10H, m). ^{13}C NMR (CDCl$_3$): 158, 151, 142, 141, 139, 138, 126, 122, 121, 119, 118, 116, 108, 107, 94, 68, 55, 43, 40, 32, 29, 23, 14. IR ν_{max}/cm^{-1}: 2920, 2850, 1601, 1499, 1460, 1389, 1352, 1245, 1169, 1126, 1060, 1022, 989, 872, 768. MS m/z (MALDI): 1204, 1203, 1202 (M^+, M100). Combustion analysis: Expected: C, 84.94%; H, 10.06%; N, 2.33%; Obtained: C, 84.96%; H, 10.02%; N, 2.36%.

2,7-[*bis*-(Thien-2-yl)-9,9-dipropyl-fluorene-5,5-diyl]-*bis*-[9-octyl-7-(octyloxy)-carbazole] (**42**)

A mixture of Pd(PPh$_3$)$_4$ (0.01g, 0.008 mmol), 2,7-*bis*-(5-bromothiophen-2-yl)-9,9-dipropyl-fluorene (**21**) (0.20 g, 0.35 mmol), [*N*-octyl-7-(octyloxy)-carbazol-2-yl]boronic acid (**37**) (0.48 g, 1.05 mmol), K$_2$CO$_3$ (0.30 g, 2.10 mmol) and H$_2$O (2 cm^3) in DMF (30 cm^3) was heated at 80 ^{o}C overnight. The cooled reaction mixture was washed with water (100 cm^3), and extracted with DCM (3 × 100 cm^3). The combined organic layers were washed with water (2 × 100 cm^3), dried over magnesium sulphate (MgSO$_4$), filtered and then concentrated down under reduced pressure. The residue was purified using column chromatography [silica, DCM/Hexane 4:10] to afford the desired product as a yellow solid (0.36 g, 75%).

Melting Point/ ^{o}C: Tg 32 Cr - N 161 I. ^{1}H NMR (CDCl$_3$) δ_H: 7.99 (2H, d, J = 8.0 Hz), 7.94 (2H, d, J = 8.4 Hz), 7.72 (2H, d, J = 7.6 Hz), 7.68 (2H, d, J = 7.6 Hz), 7.63 (2H, d, J = 1.0 Hz), 7.59 (2H, d, J = 1.0 Hz), 7.54 (2H, dd, J = 8.0 & 1.0 Hz), 7.41 (4H, dd, J = 6.0 & 2.4 Hz), 6.86 (4H, dd, J = 7.6 & 2.0 Hz), 4.28 (4H, t, J = 7.2 Hz), 4.11 (4H, t, J = 6.8 Hz), 2.07 (4H, m), 1.91 (8H, m), 1.26-1.52 (40H, m), 0.90 (12H, t, J = 7.2 Hz), 0.72-0.83 (10H, m). ^{13}C NMR (CDCl$_3$): 158, 151, 145, 143, 142, 140, 133, 131, 124, 123, 121, 120, 117, 108, 106, 94, 68, 56, 43, 32, 29, 27, 26, 23, 14. IR ν_{max}/cm^{-1}: 2921, 2851, 1601, 1501, 1458, 1390, 1347, 1247, 1189, 1170, 1125, 1053, 1021, 993, 872, 769. MS m/z (MALDI): 1228, 1227, 1226 (M$^+$). Combustion analysis: Expected: C, 81.32%; H, 8.55%; N, 2.29%; S, 5.23%; Obtained: C, 81.32%; H, 8.58%; N, 2.40%; S, 5.14%.
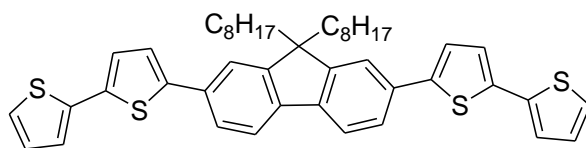
2,2'-(5-Tributylstannanyl)bithiophene (43)
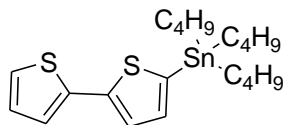
A solution of 2.5 mol/L *n*-BuLi in hexanes (16.0 cm^3) was added drop-wise to a dry THF (150 cm^3) solution of 2,2'-bithiophene (**7**) (6.30 g, 37.89 mmol) at -78 $^{\circ}$C, and the resultant mixture was stirred for 1 h at -78 $^{\circ}$C. Then 2-tributyltin chloride (11.0 cm^3, 38.93 mmol, 1.2 g cm^{-3}) was added drop-wise to the reaction mixture, which was then stirred for 1 h at -78 $^{\circ}$C, allowed to warm to room temperature and then stirred overnight. The reaction mixture was evaporated to remove THF and dried under vacuum to afford the product as a dark liquid (16.43 g, 95%).

^{1}H NMR (CDCl$_3$) δ_H: 7.31 (1H, d, *J* = 3.6 Hz), 7.19 (2H, dd, *J* = 4.0 & 1.2 Hz), 7.07 (1H, d, *J* = 3.2 Hz), 7.01 (1H, dd, *J* = 4.0 & 1.0 Hz), 1.59 (6H, t, *J* = 7.6 Hz), 1.37 (6H, m), 1.13 (6H, m), 0.90 (9H, t, *J* = 7.6 Hz). MS m/z (EI): 456 (M$^+$), 454.

2-{9,9-Dioctyl-7-[5-(thiophen-2-yl)thiophen-2-yl]fluoren-2-yl}-5-(thiophen-2-yl)thiophene (44)

A mixture of Pd(PPh$_3$)$_4$ (0.05 g, 0.043 mmol), 2,7-dibromo-9,9-dioctyl-fluorene (**17**) (2.00 g, 3.66 mmol) and 2,2'-(5-tributylstannanyl)bithiophene (**43**) (5.00 g, 10.98 mmol) in DMF (50 cm^3) was stirred and heated to 100 $^{\circ}$C overnight. The cooled reaction mixture was washed with water (100 cm^3), and extracted with DCM (3 × 100 cm^3). The combined organic layers were washed with water (2 × 100 cm^3), dried over magnesium sulphate (MgSO$_4$), filtered and then concentrated under reduced pressure. The crude product was purified using column chromatography [DCM/Hexane 1:10] to

afford the desired product as a yellow solid (1.66 g, 63%).

Melting Point/$^{\circ}$C: 141-142 (Lit. 144-145)[26]. ^{1}H NMR (CDCl$_3$) δ_H: 7.69 (2H, d, J = 8.0 Hz), 7.60 (2H, dd, J = 7.6 & 1.6 Hz), 7.54 (2H, d, J = 1.2 Hz), 7.30 (2H, d, J = 3.8 Hz), 7.22-7.24 (4H, m), 7.18 (2H, d, J = 4.0 Hz), 7.06 (2H, dd, J = 4.0 & 1.6 Hz), 2.04 (4H, m), 1.06-1.51 (24H, m), 0.79 (6H, t, J = 7.2 Hz). MS m/z (EI): 719, 718 (M$^+$, M100).

2-(5-Bromothiophen-2-yl)-5-{7-[5-(5-bromothiophen-2-yl)thiophen-2-yl]-9.9-dioctyl-fluoren-2-yl}thiophene (45)
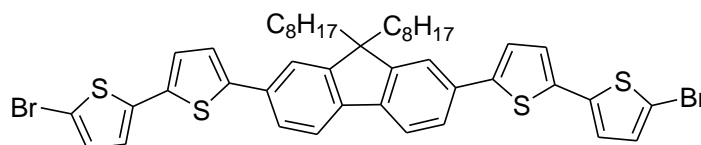
N-Bromosuccinimide (NBS) (0.55 g, 3.06 mmol) was added in a small portion into a mixture of 2-{9,9-dioctyl-7-[5-(thiophen-2-yl)thiophen-2-yl] fluoren-2-yl}-5-(thiophen-2-yl)thiophene (**44**) (1.00 g, 1.40 mmol) and silica gel (0.02 g, 0.30 mmol) in DCM (60 cm^3) in the dark. The resultant mixture was stirred overnight. The reaction mixture was filtered to remove the silica gel and the organic filtrate was concentrated under reduced pressure to give crude product, which was washed with methanol, filtered and dried under vacuum to give the desired product as a yellow solid (1.16 g, 95%).

Melting Point/$^{\circ}$C: 142-144. ^{1}H NMR (CDCl$_3$) δ_H: 7.69 (2H, d, J = 7.6 Hz), 7.59 (2H, dd, J = 7.2 & 1.2 Hz), 7.52 (2H, d, J = 1.2 Hz), 7.29 (2H, d, J = 4.0 Hz), 7.11 (2H, d, J = 3.6 Hz), 7.00 (2H, d, J = 4.0 Hz), 6.96 (2H, d, J = 3.6 Hz), 2.03 (4H, m), 1.06-1.20 (24H, m), 0.79 (6H, t, J = 6.8 Hz). MS m/z (EI): 878, 877, 876 (M$^+$), 874.

3,3'-{5',5'''-(9,9-Dioctyl-fluorene-2,7-diyl)*bis*[(2,2'-bithiophene)-5',5-diyl]}-*bis*-[9-octyl-7-(octyloxy)-carbazole] (46)
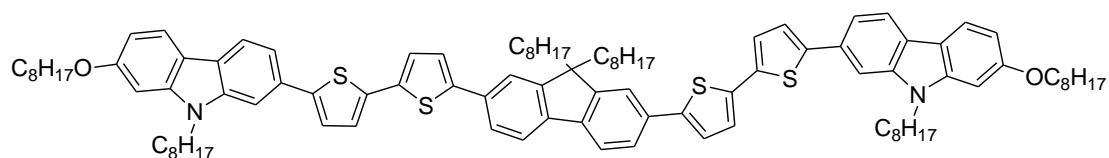

A mixture of Pd(PPh$_3$)$_4$ (0.01g, 0.008 mmol), 2-(5-bromothiophen-2-yl)-5-{7-[5-(5-bromothiophen-2-yl)thiophen-2-yl]-9,9-dioctyl-fluoren-2-yl}thiophene (**45**) (0.20 g, 0.28 mmol), [*N*-octyl-7-(octyloxy)-carbazol-2-yl]boronic acid (**37**) (0.39 g, 0.84 mmol), K$_2$CO$_3$ (0.24 g, 1.68 mmol) and H$_2$O (2 cm^3) in DMF (30 cm^3) was heated at 80 $^{\circ}$C overnight. The cooled reaction mixture was washed with water (100 cm^3), and extracted with DCM (3 × 100 cm^3). The combined organic layers were washed with water (2 × 100 cm^3), dried over magnesium sulphate (MgSO$_4$), filtered and then concentrated down under reduced pressure. The residue was purified using column chromatography [silica, DCM/Hexane 5:10] to afford the desired product as a yellow solid (0.27 g, 72%).

Melting Point/ $^{\circ}$C: Tg 21 Cr - N 137 I. ^{1}H NMR (CDCl$_3$) δ$_H$: 7.98 (2H, d, J = 8.0 Hz), 7.94 (2H, d, J = 8.4 Hz), 7.69 (2H, d, J = 8.0 Hz), 7.61 (2H, d, J = 7.6 Hz), 7.57 (2H, s), 7.53 (2H, s), 7.48 (2H, dd, J = 6.8 & 1.0 Hz), 7.33 (4H, m), 7.23 (4H, m), 6.85 (4H, dd, J = 6.8 & 2.0 Hz), 4.28 (4H, t, J = 7.2 Hz), 4.10 (4H, t, J = 6.8 Hz), 2.06 (4H, m), 1.89 (8H, m), 1.08-1.52 (60H, m), 0.88 (12H, t, J = 6.8 Hz), 0.80 (6H, t, J = 6.8 Hz), 0.66-0.76 (4H, m). ^{13}C NMR (CDCl$_3$): 159, 152, 146, 144, 142, 141, 140, 138, 134, 131, 128, 126, 125, 122, 120, 119, 118, 109, 94, 68, 57, 44, 32, 30, 29, 26, 24, 23, 14. IR ν$_{max}$/cm^{-1}: 2921, 2851, 1602, 1499, 1461, 1326, 1243, 1188, 1168, 1123, 1054, 992, 878, 788. MS m/z (MALDI): 1531, 1530 (M$^+$, M100). Combustion analysis: Expected: C, 79.27%; H, 8.43%; N, 1.83%; S, 8.38%; Obtained: C, 79.32%; H, 8.38%; N, 1.75%; S, 8.47%.

3,7-*bis*-(7-Methoxy-9-octyl-carbazol-2-yl)dibenzo[*b,d*]thiophene (48)
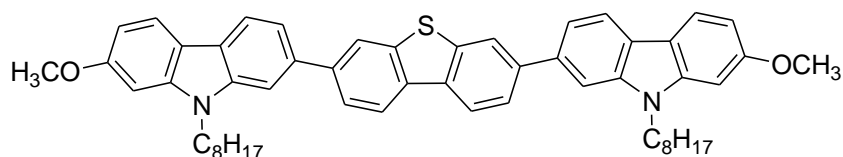
A mixture of Pd(OAc)$_2$ (0.01g, 0.045 mmol), 3,7-dibromodibenzo[*b,d*]thiophene (**47**) (0.20 g, 0.59 mmol), (7-methoxy-9-octyl-carbzole-2-yl)boronic acid (**6**) (0.62 g, 1.76 mmol), K$_2$CO$_3$ (0.50 g, 3.60 mmol) and H$_2$O (2 cm^3) in DMF (30 cm^3) was heated at 80 $^{\circ}$C overnight. The cooled reaction mixture was washed with water (100 cm^3), and extracted with DCM (3 × 100 cm^3). The combined organic layers were washed with water (2 × 100 cm^3), dried over magnesium sulphate (MgSO$_4$), filtered and then concentrated down under reduced pressure. The residue was purified using column chromatography [silica, DCM/Hexane 5:10] to afford the desired product as a pale-yellow solid (0.41 g, 88%)

Melting Point/$^{\circ}$C: Cr 202 N 250 I. ^{1}H NMR (CDCl$_3$) δ_H: 8.25 (2H, d, J = 8.4 Hz), 8.18 (2H, d, J = 1.2 Hz), 8.07 (2H, d, J = 8.0 Hz), 7.98 (2H, dd, J = 8.8 & 0.8 Hz), 7.83 (2H, dd, J = 8.4 & 1.6 Hz), 7.62 (2H, d, J = 0.8 Hz), 7.55 (2H, dd, J = 8.0 & 1.6 Hz), 6.87 (4H, d, J = 8.0 Hz), 4.32 (4H, t, J = 6.8 Hz), 3.94 (6H, s), 1.92 (4H, quint, J = 7.2 Hz), 1.23-1.43 (20H, m), 0.85 (6H, t, J = 6.8 Hz). ^{13}C NMR (CDCl$_3$): 159, 142, 141, 140, 137, 134, 124, 122, 121, 120, 119, 107, 93, 56, 43, 32, 29, 28, 27, 23, 14. IR ν_{max}/cm^{-1}: 2921, 2851, 1600, 1486, 1454, 1431, 1344, 1242, 1210, 1162, 1136, 1120, 1057, 1040, 943, 869, 800, 785. MS m/z (MALDI): 801, 799 (M$^+$, M100). Combustion analysis: Expected: C, 81.16%; H, 7.32%; N, 3.51%; S, 4.01%; Obtained: C, 81.12%; H, 7.30%; N, 3.53%; S, 3.98%.

3,7-*bis*-[9-Octyl-7-(octyloxy)-carbazol-2-yl]dibenzo[*b,d*]thiophene (49)
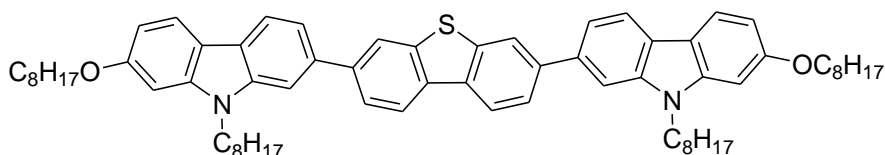
A mixture of Pd(PPh$_3$)$_4$ (0.01g, 0.008 mmol), 3,7-dibromodibenzo[*b,d*]thiophene (**47**) (0.20 g, 0.60 mmol), [*N*-octyl-7-(octyloxy)-carbazol-2-yl]boronic acid (**37**) (0.80 g, 1.76 mmol), K$_2$CO$_3$ (0.50 g, 3.60 mmol) and H$_2$O (2 cm^3) in DMF (30 cm^3) was heated at 80 ^{o}C overnight. The cooled reaction mixture was washed with water (100 cm^3), and extracted with DCM (3 × 100 cm^3). The combined organic layers were washed with water (2 × 100 cm^3), dried over magnesium sulphate, filtered and concentrated under reduced pressure. The residue was purified using column chromatography [silica, DCM/Hexane 4:10] to afford the desired product as a pale-yellow solid (0.49 g, 86%).

Melting Point/^{o}C: Cr 141 N 202 I. ^{1}H NMR (CDCl$_3$) δ_H: 8.26 (2H, d, J = 8.4 Hz), 8.19 (2H, d, J = 1.0 Hz), 8.07 (2H, d, J = 8.0 Hz), 7.98 (2H, d, J = 8.4 Hz), 7.84 (2H, dd, J = 8.0 & 1.0 Hz), 7.62 (2H, s), 7.55 (2H, dd, J = 6.8 & 1.0 Hz), 6.88 (4H, d, J = 8.4 Hz), 4.32 (4H, t, J = 7.2 Hz), 4.11 (4H, t, J = 6.4 Hz), 1.93 (8H, m), 1.24-1.52 (40H, m), 0.90 (12H, t, J = 6.8 Hz). ^{13}C NMR (CDCl$_3$): 158, 142, 141, 140, 137, 135, 124, 122, 121, 120, 119, 118, 108, 107, 94, 68, 43, 32, 29, 23, 14. IR ν_{max}/cm^{-1}: 2919, 2850, 1601, 1499, 1453, 1436, 1392, 1354, 1247, 1190, 1177, 1127, 1045, 992, 872, 797, 768. MS m/z (MALDI): 996, 995 (M$^+$, M100). Combustion analysis: Expected: C, 82.04%; H, 8.71%; N, 2.81%; S, 3.22%; Obtained: C, 82.12%; H, 8.73%; N, 2.72%; S, 3.24%.

4,7-Dibromo-2,1,3-benzothiadiazole (51)
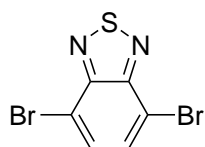
A solution containing bromine (11.3 cm^3, 3.119 g cm^{-3}) in 48% w/w hydrogen bromide solution (100 cm^3) was added dropwise very slowly to a mixture of 2,1,3-benzothiadiazole (**50**) (10.00 g, 73.4 mmol) and 48% w/w hydrogen bromide solution (150 cm^3). After the addition had been completed, the reaction solution was heated at reflux for 6 h. A precipitation of a dark orange solid was noted. The mixture was then cooled to room temperature and a sufficient amount of a saturated aqueous

solution of sodium bisulphite (NaHSO$_3$) was added to completely consume any excess of bromine. The mixture was filtered under vacuum, washed exhaustively with portions of water and then washed with cold diethyl ether (200 cm^3) once. The solid was reiterated with ethanol for 6 h and then dried under vacuum overnight to afford the desired product as a white product. (13.40 g, 62%).

Melting Point/ ^{o}C: 189-190 (Lit. 189-190)[27] . ^{1}H NMR (CDCl$_3$) δ_H: 7.74 (2H, s). MS m/z (EI): 296, 294 (M$^+$), 292.

4,7-*bis*-(7-Methoxy-9-octyl-carbazol-2-yl)benzo[*c*][1,2,5]thiadiazole (52)
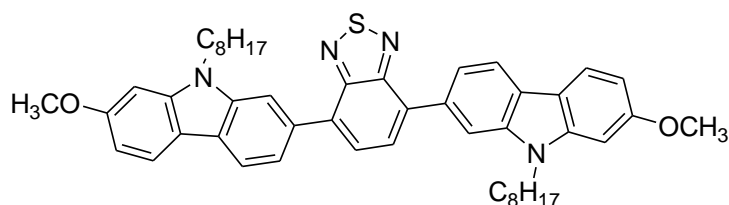
A mixture of Pd(OAc)$_2$ (0.01g, 0.045 mmol), 4,7-dibromo-2,1,3-benzothiadiazole (**51**) (0.20 g, 0.68 mmol), (7-methoxy-9-octyl-carbzole-2-yl)boronic acid (**6**) (0.73 g, 2.04 mmol), K$_2$CO$_3$ (0.57 g, 4.08 mmol) and H$_2$O (2 cm^3) in DMF (30 cm^3) was heated at 80 ^{o}C overnight. The cooled reaction mixture was washed with water (100 cm^3), and extracted with DCM (3 × 100 cm^3). The combined organic layers were washed with water (2 × 100 cm^3), dried over magnesium sulphate (MgSO$_4$), filtered and then concentrated under reduced pressure. The residue was purified using column chromatography [silica, DCM/Hexane 10:10] to afford the desired product as a red solid (0.42 g, 82%).

Melting Point/ ^{o}C: Tg 92 Cr 142 I. ^{1}H NMR (CDCl$_3$) δ_H: 8.16 (2H, d, J = 8.0 Hz), 8.06 (2H, s), 8.03 (2H, d, J = 8.0 Hz), 7.95 (2H, s), 7.81 (2H, d, J = 8.0 Hz), 6.90 (4H, d, J = 8.4 Hz), 4.35 (4H, t, J = 7.2 Hz), 3.97 (6H, s), 1.95 (4H, quint, J = 7.2 Hz), 1.22-1.49 (20H, m), 0.86 (6H, t, J = 6.4 Hz). ^{13}C NMR (CDCl$_3$): 159, 154, 143, 141, 140, 134, 133, 128, 123, 121, 120, 119, 116, 109, 107, 94, 56, 43, 32, 29, 28, 27, 23, 14. IR ν_{max}/cm^{-1}: 2918, 2849, 1599, 1499, 1460, 1434, 1358, 1243, 1210, 1177, 1060, 982, 896,

820, 767. MS m/z (MALDI): 752, 751 (M$^+$, M100). Combustion analysis: Expected: C, 76.76%; H, 7.25%; N, 7.46%; S, 4.27%; Obtained: C, 76.76%; H, 7.26%; N, 7.43%; S, 4.12%.

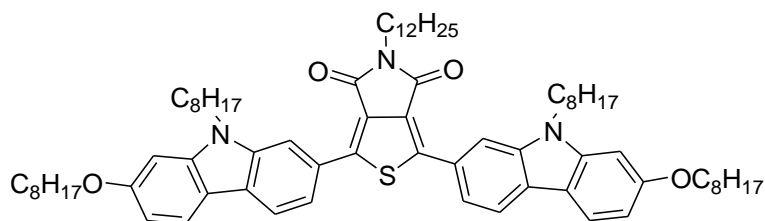## 4,7-*bis*-[9-Octyl-7-(octyloxy)-carbazol-2-yl]benzo[*c*][1,2,5]thiadiazole (53)
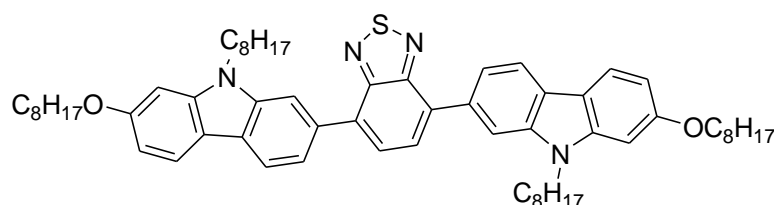
A mixture of Pd(PPh$_3$)$_4$ (0.01g, 0.008 mmol), 4,7-dibromo-2,1,3-benzothiadiazole (**51**) (0.20 g, 0.681 mmol), [*N*-octyl-7-(octyloxy)-carbazol-2-yl]boronic acid (**37**) (0.93 g, 2.04 mmol), K$_2$CO$_3$ (0.57 g, 4.08 mmol) and H$_2$O (2 cm^3) in DMF (30 cm^3) was heated at 80 ^{o}C overnight. The cooled reaction mixture was washed with water (100 cm^3), and extracted with DCM (3 × 100 cm^3). The combined organic layers were washed with water (2 × 100 cm^3), dried over magnesium sulphate (MgSO$_4$), filtered and then concentrated down under reduced pressure. The residue was purified using column chromatography [silica, DCM/Hexane 5:10] to afford the desired product as a red solid (0.60 g, 93%).

Melting Point/ ^{o}C: Tg 85; Cr 105 I (Heating); I 94 N (Cooling). ^{1}H NMR (CDCl$_3$) δ_H: 8.14 (2H, d, *J* = 8.0 Hz), 8.04 (2H, s), 8.01 (2H, d, *J* = 8.4 Hz), 7.93 (2H, s), 7.80 (2H, dd, *J* = 8.0 & 1.0 Hz), 6.89 (4H, d, *J* = 8.4 Hz), 4.34 (4H, t, *J* = 7.2 Hz), 4.12 (4H, t, *J* = 6.8 Hz), 1.96 (8H, m), 1.22-1.52 (40H, m), 0.90 (6H, t, *J* = 6.8 Hz), 0.84 (6H, t, *J* = 7.2 Hz). ^{13}C NMR (CDCl$_3$): 159, 154, 143, 141, 140, 134, 133, 128, 123, 121, 120, 119, 116, 109, 108, 94, 68, 43, 32, 29, 26, 14. IR ν_{max}/cm^{-1}: 2917, 2849, 1600, 1499, 1455, 1439, 1362, 1257, 1211, 1177, 1130, 1056, 982, 895, 819, 801, 766. MS m/z (MALDI): 948, 947 (M$^+$, M100). Combustion analysis: Expected: C, 78.60%; H, 8.72%; N, 5.91%;S, 3.38%; Obtained: C, 78.62%; H, 8.73%; N, 5.91%; S, 3.30%.

5-Dodecyl-1,3-*bis*-[9-Octyl-7-(octyloxy)-carbazol-2-yl]-5*H*-thieno[3,4-*c*]pyrrole-4, 6-dione (54)

A mixture of Pd(PPh$_3$)$_4$ (0.01g, 0.008 mmol), 1-bromo-5-dodecyl-3-iodo-5*H*-thieno-[3,4-*c*]pyrrole-4,6-dione (**27**) (0.20 g, 0.38 mmol), [*N*-octyl-7-(octyloxy)-carbazol-2-yl]boronic acid (**37**) (0.52 g, 1.14 mmol), K$_2$CO$_3$ (0.32 g, 2.28 mmol) and H$_2$O (2 cm^3) in DMF (30 cm^3) was heated at 80 ^{o}C overnight. The cooled reaction mixture was washed with water (100 cm^3) and then extracted with DCM (3 × 100 cm^3). The combined organic layers were washed with water (2 × 100 cm^3), dried over magnesium sulphate (MgSO$_4$), filtered and then concentrated down under reduced pressure. The residue was purified using column chromatography [silica, DCM/Hexane 5:10] to afford the desired product as a yellow solid (0.36 g, 84%).

Melting Point/^{o}C: Tg 87 Cr 164 Sm 184 I. ^{1}H NMR (CDCl$_3$) δ$_H$: 8.61 (2H, s), 8.00 (2H, d, *J* = 8.4 Hz), 7.96 (2H, d, *J* = 9.2 Hz), 7.79 (2H, d, *J* = 8.4 Hz), 6.86 (4H, d, *J* = 6.0 Hz), 4.36 (4H, t, *J* = 6.8 Hz), 4.10 (4H, t, *J* = 6.4 Hz), 3.75 (2H, t, *J* = 7.2 Hz), 1.96 (4H, quint, *J* = 6.8 Hz), 1.88 (4H, quint, *J* = 7.6 Hz), 1.73 (2H, quint, *J* = 7.2 Hz),1.24-1.52 (58H, m), 0.90 (12H, t, *J* = 7.2 Hz), 0.84 (3H, t, *J* = 7.2 Hz). ^{13}C NMR (CDCl$_3$): 163, 159, 146, 143, 140, 127, 126, 124, 121, 119, 116, 109, 108, 94, 68, 43, 38, 32, 30, 29, 27, 23, 14. IR ν$_{max}$/cm^{-1}: 2917, 2849, 1731, 1602, 1524, 1457, 1389, 1352, 1258, 1197, 1174, 1079, 1048, 994, 889, 823, 804, 785, 757, 694. MS m/z (MALDI): 1134, 1133 (M$^+$, M100). Combustion analysis: Expected: C, 78.47%; H, 9.34%; N, 3.71%; S, 2.83%; Obtained: C, 78.51%; H, 9.33%; N, 3.65%; S, 2.76%.
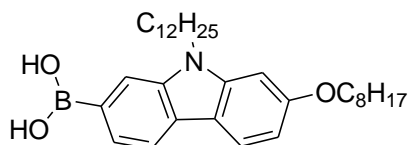
2-Bromo-*N*-dodecyl-7-(octyloxy)-carbazole (55)
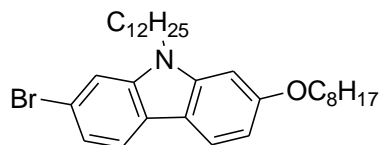
Sodium hydride (NaH) (60% in mineral oil) (0.71 g, 17.64 mmol) was added in a small portion into a solution of 2-bromo-7-octyloxycarbazole (**35**) (3.30 g, 8.82 mmol) in DMF (60 mL). The resultant mixture was stirred for 1 h at room temperature, then heated and maintained at 50 $^{\circ}$C for another 1 h. 1-Bromododecane (2.64 g, 10.59 mmol) was added and the resultant mixture stirred at 50 $^{\circ}$C for 3 h and then at room temperature overnight. The reaction mixture was poured onto ice-water (100 cm^3). The precipitated product was filtered off, washed with ethanol (2 $\times$ 100 cm^3) and dried under vacuum to give the desired product as a white powder (4.10 g, 86%).

Melting Point/$^{\circ}$C: 49-50. ^{1}H NMR (CDCl$_3$) δ_H: 7.91 (1H, d, J = 9.2 Hz), 7.82 (1H, d, J = 8.4 Hz), 7.47 (1H, d, J = 1.4 Hz), 7.28 (1H, dd, J = 6.4 & 1.6 Hz), 6.85 (2H, d, J = 7.6 Hz), 4.18 (2H, t, J = 7.2 Hz), 4.09 (2H, t, J = 6.4 Hz), 1.86 (4H, m), 1.24-1.51 (28H, m), 0.91 (3H, t, J = 6.8 Hz), 0.87 (3H, t, J = 6.8 Hz). MS m/z (EI): 543, 541 (M$^+$).

[*N*-Dodecyl-7-(octyloxy)-carbazol-2-yl]boronic acid (56)

A solution of 2.5 mol/L *n*-BuLi in hexanes (6 cm^3) was added to a THF (80 cm^3) solution of 2-bromo-*N*-dodecyl-7-(octyloxy)-carbazole (**55**) (4.00 g, 7.38 mmol) at -78 $^{\circ}$C, and the resultant mixture was stirred for 1 h at -78 $^{\circ}$C. Then 2-triisopropyl borate (4 cm^3, 14.75 mmol, 0.815 g cm^{-3}) was added drop-wise to the reaction mixture, which was then stirred for 1 h at -78 $^{\circ}$C, allowed to warm to room temperature and then stirred overnight. Hydrochloric acid (12.4 cm^3, 12 mol/L) was added to the reaction mixture.

The resultant mixture stirred for 1 h and then quenched with water (50 cm^3) and extracted with EtOAc (3 × 50 cm^3). The combined organic extracts were washed with water (2 × 100 cm^3), dried (MgSO$_4$), filtered and concentrated down under reduced pressure. The residue was triterated with hexane (2 × 100 cm^3) and then dried under reduced pressure to give the desired product as a white solid (3.20 g, 86%).

Melting Point/^{o}C: 98-99. ^{1}H NMR (CDCl$_3$) δ_H: 8.34 (1H, s), 8.18 (1H, dd, J = 7.2 & 2.0 Hz), 8.02-8.06 (2H, m), 7.79 (1H, s), 7.51 (1H, d, J = 7.2 Hz), 6.91 (2H, d, J = 8.0 Hz), 4.42 (2H, t, J = 7.6 Hz), 4.12 (2H, t, J = 7.2 Hz), 1.94 (4H, m), 1.19-1.34 (28H, m), 0.90 (3H, t, J = 6.8 Hz), 0.82 (3H, t, J = 6.8 Hz). MS m/z (EI): 508, 507 (M$^+$), 506.

5,5'-*bis*-[9-Dodecyl-7-(octyloxy)-carbazol-2-yl]-2,2'-bithiophene (57)
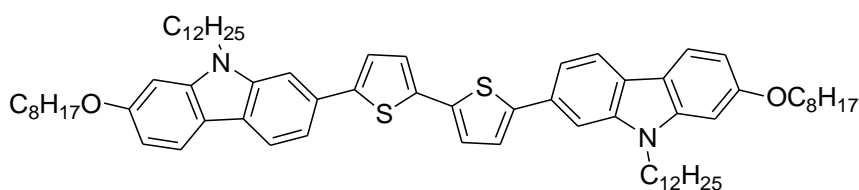
A mixture of Pd(OAc)$_2$ (0.01g, 0.045 mmol) and P(Ph)$_3$ (0.04 g, 0.12 mmol), 5,5'-dibromo-2,2'-bithiophene (**8**) (0.2 g, 0.62 mmol), [*N*-dodecyl-7-(octyloxy)-carbazol-2-yl]boronic acid (**56**) (0.94 g, 1.86 mmol), K$_2$CO$_3$ (0.52 g, 3.71 mmol) and H$_2$O (2 cm^3) in DME (20 cm^3) was heated under reflux overnight. The cooled reaction mixture was washed with water (100 cm^3) and then extracted with DCM (3 × 100 cm^3). The combined organic layers were washed with water (2 × 100 cm^3), dried over magnesium sulphate (MgSO$_4$), filtered and then concentrated down under reduced pressure. The residue was purified using column chromatography [silica, DCM/Hexane 5:10] to afford the desired product as an orange solid (0.43 g, 64%).

Melting Point/^{o}C: 146. ^{1}H NMR (CDCl$_3$) δ_H: 7.97 (2H, d, J = 8.0 Hz), 7.94 (2H, d, J = 9.2 Hz), 7.54 (2H, d, J = 0.8 Hz), 7.49 (2H, dd, J = 7.6 & 1.6 Hz), 7.33 (2H, d, J = 4.0 Hz), 7.23 (2H, d, J = 4.0 Hz), 6.85 (4H, d, J = 7.2 Hz), 4.28 (4H, t, J = 7.6 Hz), 4.10

(4H, t, J = 6.4 Hz), 1.89 (8H, m), 1.24-1.52 (56H, m), 0.91 (6H, t, J = 6.8 Hz), 0.88 (6H, t, J = 7.2 Hz). ^{13}C NMR (CDCl$_3$): 159, 145, 143, 141, 136, 130, 124, 123, 122,121,118, 117, 107, 105, 94, 68, 43, 33, 32, 29, 27, 23, 14. IR ν_{max}/cm^{-1}: 2917, 2847, 1601, 1530, 1500, 1482, 1463, 1362, 1249, 1236, 1203, 1172, 1132, 1051, 1009, 990, 955, 805, 793, 763. MS m/z (MALDI): 1092, 1091, 1090 (M$^+$, M100). Combustion analysis: Expected: C, 79.36%; H, 9.25%; N, 2.57%; S, 5.89%; Obtained: C, 79.12%; H, 9.44%; N, 2.70%; S, 5.61%.

1,4-*bis*-{5-[9-Dodecyl-7-(octyloxy)-carbazol-2-yl]thiophen-2-yl}benzene (58)
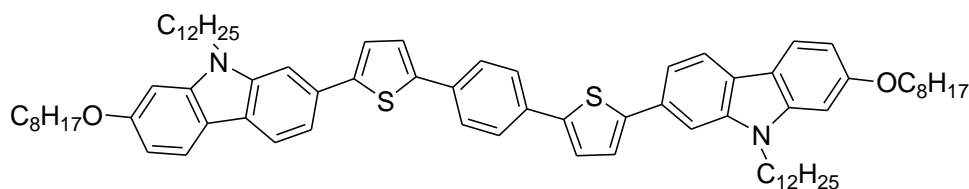
A mixture of Pd(OAc)$_2$ (0.01g, 0.045 mmol), P(Ph)$_3$ (0.04 g, 0.12 mmol), 1,4-*bis*-(5-bromothiophen-2-yl)benzene (**13**) (0.2 g, 0.50 mmol), [9-dodecyl-7-(octyloxy)- carbazol-2-yl]boronic acid (**56**) (0.77 g, 1.5 mmol), K$_2$CO$_3$ (0.42 g, 3.00 mmol) and H$_2$O (2 cm^3) in DME (20 cm^3) at room temperature. The resultant mixture was heated at reflux overnight. The cooled reaction mixture was washed with water (100 cm^3) and extracted with DCM (3 × 100 cm^3). The combined organic layers were washed with water (2 × 100 cm^3), dried (MgSO$_4$), filtered and then concentrated down under reduced pressure. The residue was purified using column chromatography [silica, DCM/hexane 5:10] to afford the desired product as a yellow solid (0.36 g, 62%).

Melting Point/^{o}C: 230. ^{1}H NMR (CDCl$_3$) δ_H: 7.98 (2H, d, J = 8.0 Hz), 7.94 (2H, d, J = 9.2 Hz), 7.69 (4H, s), 7.56 (2H, d, J = 1.2 Hz), 7.51 (2H, dd, J = 8.0 & 1.6 Hz), 7.39 (4H, dd, J = 6.8 & 3.6 Hz), 6.86 (4H, d, J = 6.8 Hz), 4.29 (4H, t, J = 6.8 Hz), 4.11 (4H, t, J = 6.8 Hz), 1.89 (8H, m), 1.24-1.52 (56H, m), 0.91 (6H, t, J = 6.8 Hz), 0.88 (6H, t, J = 7.2 Hz). ^{13}C NMR (CDCl$_3$): 159, 145, 143, 141, 134, 130, 126, 124, 121, 117, 107, 105, 94, 68, 44, 32, 30, 29, 26, 22, 14. IR ν_{max}/cm^{-1}: 2930, 2860, 1598, 1511, 1493,

1432, 1390, 1347, 1303, 1251, 1197, 1142, 1106, 938, 886, 833, 813, 790, 768. MS m/z (MALDI): 1168, 1167, 1166 (M$^+$), 925 (M100). Combustion analysis: Expected: C, 80.36%; H, 8.99%; N, 2.40%; S, 5.50%; Obtained: C, 80.24%; H, 9.16%; N, 2.57%; S, 5.32%.

Heptadecane-9-ol (60)
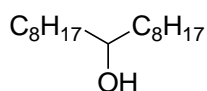
A solution of ethyl formate (**59**) (10.00 g, 135 mmol) in THF (80 mmol) was added dropwise to a fresh solution of octyl magnesium bromide, prepared from 1-bromooctane (58 g, 300 mmol) and magnesium turnings (8.15 g, 340 mmol) in THF (150 cm^3). The reaction mixture was stirred overnight at room temperature, quenched by the addition of methanol (50 cm^3), followed by saturated aqueous NH$_4$Cl. The crude compound was extracted with EtOAc (3 × 100 cm^3). The combined organic layers were washed with brine (2× 100 cm^3), dried (MgSO$_4$), filtered and then evaporated under reduced pressure. The residue was purified by re-crystallisation from acetonitrile to afford the desired product as a white solid (28.50 g, 82%).

Melting Point/ $^{\circ}$C: 60-61 (Lit 58-62)[28]. ^{1}H NMR (CDCl$_3$) δ$_H$: 3.60 (1H, m), 1.26-1.46 (29H, m), 0.89 (6H, t, J = 6.8 Hz). MS m/z (EI): 257, 256 (M$^+$).

Heptadecan-9-yl-4-methylbenzenesulfonate (61)
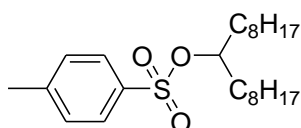
A solution of *p*-toluene-sulfonylchloride (8.92 g, 46.79 mmol) in pyridine (40 cm^3) was added dropwise to a solution of heptadecane-9-ol (**60**) (10.0 g, 38.99 mmol) in pyridine (40 cm^3) at 0 $^{\circ}$C. The resultant reaction mixture was allowed to warm to room

temperature and then stirred overnight. The reaction mixture was poured into ice water (100 cm^3) and extracted with DCM (3 × 100 cm^3). The combined organic layers were washed with brine (2 × 100 cm^3), dried (MgSO$_4$), filtered and then concentrated down under reduced pressure. The residue was purified using column chromatography [silica, DCM/hexane 2:10] to afford the desired product as a colourless liquid, which was transformed into colourless crystalline after vacuum dry. (15.13 g, 95%).

Melting Point/$^\circ$C: 49-50 $^\circ$C (Lit. 50-54 $^\circ$C)[28]. ^{1}H NMR (CDCl$_3$) δ_H: 7.80 (2H, d, J = 6.8 Hz), 7.33 (2H, d, J = 7.6 Hz), 4.56 (1H, m), 2.47 (3H, s), 1.56 (4H, m), 1.16-1.30 (24H, m), 0.89 (6H, t, J = 6.8 Hz).

MS m/z (EI): 410 (M$^+$).

2-Bromo-*N*-(heptadecan-9-yl)-7-methoxy-carbazole (62)
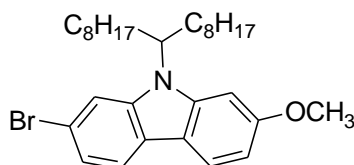
A mixture of 2-bromo-7-methoxycarbazole (**4**) (3.00 g, 10.865 mmol), KOH (6.19 g, 108.65 mmol) and DMSO (30 cm^3) was stirred for 1 h at RT. A solution of 1,4,7,10,13,16-hexaoxacyclooctadecane (18-crown-6) (0.144 g, 0.55 mmol), heptadecan-9-yl-4-methylbenzenesulfonate (**61**) (5.36 g, 13.04 mmol) and DMSO (20 cm^3) was added dropwise to the reaction mixture. The reaction mixture was stirred overnight, poured onto water (100 mL) and extracted with diethyl ether (3 × 100 cm^3). The combined organic layers were washed with water (2 × 100 cm^3), dried (MgSO$_4$), filtered and then concentrated down under reduced pressure. The residue was purified using column chromatography [silica, DCM/hexane 2:10] to afford the desired product as a colourless liquid (4.04 g, 72%)

^{1}H NMR (CDCl$_3$) δ_H: 7.94 (1H, d, J = 8.4 Hz), 7.85 (1H, d, J = 8.8 Hz), 7.47 (1H, d, J

= 1.0 Hz), 7.29 (1H, dd, J = 6.8 & 1.0 Hz), 6.86 (1H, d, J = 2.0 Hz), 6.82 (1H, d, J = 6.4 Hz), 4.41 (1H, m), 3.92 (3H, s), 2.24 (2H, m), 1.92 (2H, m), 1.13-1.30 (24H, m), 0.85 (6H, t, J = 7.2 Hz). MS m/z (EI): 515, 513 (M$^+$).

[*N*-(Heptadecan-9-yl)-7-methoxy-carbazol-2-yl]boronic acid (63)
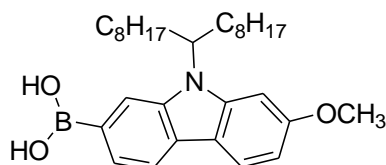
A solution of 2.5 mol/L *n*-BuLi in hexanes (6.0 cm^3) x mmol was added to a solution of 2-bromo-9-(heptadecan-9-yl)-7-methoxy-carbazole (**62**) (3.77 g, 7.33 mmol) in THF (40 cm^3) at -78 ^{o}C. The resultant mixture was maintained for 1 h at -78 ^{o}C, then 2-triisopropyl borate (3.4 cm^3, 14.66 mmol, 0.815 g/ cm^3) was added drop-wise. The reaction mixture was stirred for 1 h at -78 ^{o}C, then allowed to warm to room temperature and stirred overnight. Hydrochloric acid (12.22 cm^3, 12 mol/L) X MMOL was added to the reaction mixture and stirred for 1 h. The reaction mixture was quenched with water (50 cm^3) and extracted with diethyl ether (3 × 50 cm^3). The combined organic extracts were washed with water (2 × 100 cm^3), dried over anhydrous magnesium sulphate (MgSO$_4$), filtered and concentrated down under reduced pressure. The white solid was obtained (3.45 g, 98%).

Melting Point/ ^{o}C: 72-76. ^{1}H NMR (CDCl$_3$) δ_H: 8.40 (1H, m), 8.20 (1H, d, J = 8.8 Hz), 8.00-8.07 (2H, m), 7.84 (1H, s), 7.52 (1H, d, J = 7.2 Hz), 6.93 (2H, d, J = 8.4 Hz), 4.49 (1H, m), 3.97 (3H, s), 2.12 (4H, m), 1.12-1.27 (24H, m), 0.89 (6H, t, J = 7.2 Hz). MS m/z (EI): 480, 479 (M$^+$), 478.

1,4-*bis*-{5-[*N*-(heptadecan-9-yl)-7-methoxy-carbazol-2-yl]thiophen-2-yl}benzene (64)
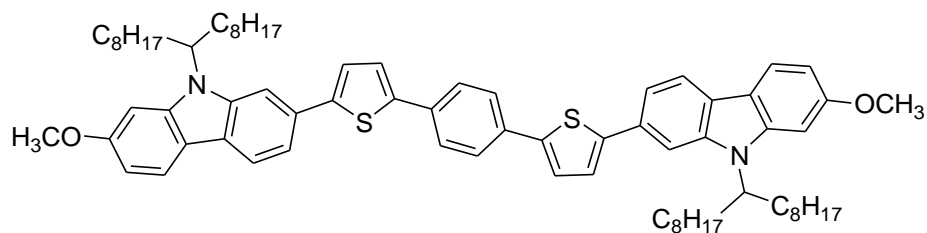
A mixture of Pd(OAc)$_2$ (0.01g, 0.045 mmol), P(Ph)$_3$ (0.04 g, 0.12 mmol), 1,4-*bis*-(5-bromothiophen-2-yl)benzene (**13**) (0.20 g, 0.50 mmol), [*N*-(heptadecan-9-yl)-7-methoxy-carbazol-2-yl]boronic acid (**63**) (0.72 g, 1.50 mmol), K$_2$CO$_3$ (0.42 g, 3 mmol), H$_2$O (2 cm^3) and DME (20 cm^3) was heated at reflux overnight. After being cooled to room temperature, the mixture was washed with water (100 cm^3) and extracted with DCM (3 × 100 cm^3). The combined organic layers were washed with water (2 × 100 cm^3), dried (MgSO$_4$), filtered and then concentrated under reduced pressure. The residue was purified using column chromatography [silica, DCM/hexane 5:10] to afford the desired product as a yellow solid (0.42 g, 76%).

Melting Point/$^{\circ}$C: 141. ^{1}H NMR (CDCl$_3$) δ$_H$: 8.18 (2H, d, *J* = 8.0 Hz), 7.96 (2H, d, *J* = 8.4 Hz), 7.76 (1H, s),7.58 (1H, s), 7.69 (4H, d, *J* = 2.0 Hz), 7.50 (2H, d, *J* = 8.0 Hz), 7.37 (4H, d, *J* = 1.2 Hz), 7.05 (1H, s), 6.85 (3H, d, *J* = 8.4 Hz), 4.59 (1H, m), 4.48 (1H, m), 3.94 (6H, s), 2.32 (4H, m), 1.94 (4H, m), 1.04-1.27 (48H, m), 0.83 (12H, t, *J* = 6.4 Hz). ^{13}C NMR(CDCl$_3$): 159, 144, 143, 141, 134, 131, 128, 125, 122, 119, 118, 109, 94, 56, 55, 34, 32, 30, 29, 27, 23, 14. IR ν$_{max}$/cm^{-1}: 2919, 2850, 1599, 1510, 1462, 1433, 1347, 1250, 1202, 1161, 1143, 1034, 997, 955, 849, 833, 813, 792, 768. MS m/z (MALDI): 1112, 1111, 1110 (M$^+$, M100). Combustion analysis: Expected: C, 80.09%; H, 8.72%; N, 2.52%; S, 5.78%; Obtained: C, 79.84%; H, 8.67%; N, 2.48%; S, 5.87%.

2-Bromo-9-(heptadecan-9-yl)-7-octyloxy-carbazole (65)
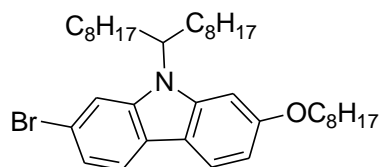
A mixture of 2-bromo-7-octyloxycarbazole (**35**) (4.00 g, 10.69 mmol), KOH (6.00 g, 106.87 mmol) and DMSO (30 cm^3) mixture was stirred for 1 h. A solution of 18-crown-6 (0.16 g, 0.54 mmol) and heptadecan-9-yl-4-methylbenzenesulfonate (**61**) (5.28 g, 12.83 mmol) in DMSO (30 cm^3) were added to this solution drop-wise. Then the reaction mixture was stirred overnight. The reaction mixture was poured into water (100 cm^3), and extracted with ether (3 × 100 cm^3). The combined organic layers were washed with water (2 × 100 cm^3), dried over magnesium sulphate (MgSO$_4$), filtered and then concentrated down under reduced pressure. The residue was purified using column chromatography [silica, hexane] to afford colourless liquid (5.10 g, 78%).

^{1}H NMR (CDCl$_3$) δ_H: 7.91 (1H, d, J = 8.8 Hz), 7.82 (1H, d, J = 8.4 Hz), 7.46 (1H, d, J = 1.0 Hz), 7.28 (1H, dd, J = 6.4 & 1.0 Hz), 6.85 (1H, d, J = 2.4 Hz), 6.82 (1H, d, J = 6.8 Hz), 4.40 (1H, m), 4.07 (2H, t, J = 6.8 Hz), 2.22 (2H, m), 1.90 (2H, m), 1.51 (2H, m), 1.13-1.38 (34H, m), 0.91 (3H, t, J = 7.2 Hz), 0.84 (6H, t, J = 7.2 Hz). MS m/z (EI): 613, 612, 611 (M$^+$).

[9-(Heptadecan-9-yl)-7-octyloxy-carbazol-2-yl]boronic acid (66)
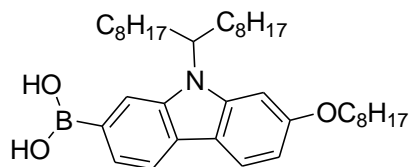
A solution of *n*-BuLi (8.0 cm^3, 2.5 mol/L, 20.0 mmol) in hexane was added to a THF (50 cm^3) solution of 2-bromo-9-(heptadecan-9-yl)-7-octyloxy-carbazole (**65**) (6.00 g, 9.8 mmol) at -78 ^{0}C, and the resultant mixture was stirred for 1 h at -78 ^{0}C. Then

2-triisopropyl borate (5.0 cm^3, 19.6 mmol, 0.815 g/cm^3) was added drop-wise. The reaction mixture was stirred for 1 h at -78 ^{0}C, then warmed to room temperature and stirred overnight. Hydrochloric acid (16.34 mL, 12 mol/L, 196.08 mmol) was added to the mixture and it was stirred for 1 h. The reaction mixture was quenched with water (50 cm^3) and extracted with EtOAc (3 × 50 cm^3). The combined organic extracts were washed with water (2 × 100 cm^3), dried over anhydrous magnesium sulphate (MgSO$_4$), filtered and concentrated down under reduced pressure. The colourless oil liquid was obtained (5.48 g, 97%).

^{1}H NMR (CDCl$_3$) δ$_H$: 8.38 (1H, m), 8.18 (1H, d, J = 8.0 Hz), 7.96-8.04 (2H, m), 7.84 (1H, m), 7.46 (1H, d, J = 6.8 Hz), 6.84 (2H, d, J = 8.0 Hz), 4.40 (1H, m), 4.08 (2H, t, J = 6.8 Hz), 2.22 (2H, m), 1.86 (2H, m), 1.51 (2H, m), 1.10-1.36 (34H, m), 0.89 (3H, t, J = 6.8 Hz), 0.82 (6H, t, J = 6.8 Hz). MS m/z (EI): 578, 577 (M$^+$), 576.

1,4-*bis*-{5-[9-(Heptadecan-9-yl)-7-(octyloxy)-carbazol-2-yl]thiophen-2-yl}benzene (67)
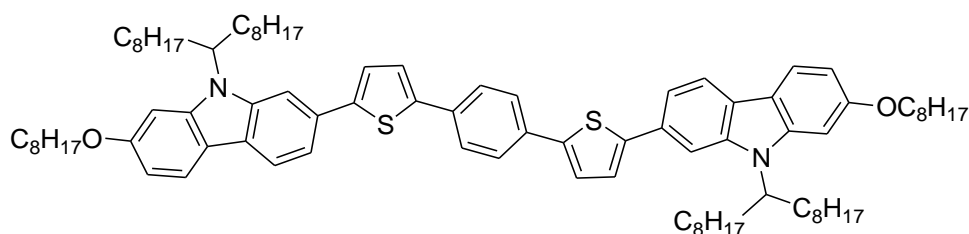
A mixture of Pd(OAc)$_2$ (0.01g, 0.045 mmol) and P(Ph)$_3$ (0.04 g, 0.12 mmol) were added to a mixture of 1,4-*bis*-(5-bromothiophen-2-yl)benzene (**13**) (0.20 g, 0.50 mmol), [9-(Heptadecan-9-yl)-7-octyloxy-carbazol-2-yl]boronic acid (**66**) (0.87 g, 1.50 mmol), K$_2$CO$_3$ (0.42 g, 3 mmol) and H$_2$O (2 cm^3) in DME (20 cm^3) was heated at reflux overnight. The cooled reaction mixture was washed with water (100 cm^3), and extracted with DCM (3 × 100 cm^3). The combined organic layers were washed with water (2 × 100 cm^3), dried over magnesium sulphate (MgSO$_4$), filtered and then concentrated down under reduced pressure. The residue was purified using column chromatography [silica, DCM/Hexane 3:10] to afford the desired product as a yellow

solid (0.30 g, 46%).

Melting Point/ °C: 108. ^{1}H NMR (CDCl$_3$) δ_H: 8.00 (4H, m), 7.76 (1H, s), 7.69 (4H, d, J = 0.8 Hz), 7.58 (1H, s), 7.50 (2H, d, J = 8.0 Hz), 7.37 (4H, d, J = 0.8 Hz), 7.04 (1H, s), 6.86 (3H, d, J = 6.4 Hz), 4.58 (1H, m), 4.46 (1H, m), 4.09 (4H, t, J = 6.4 Hz), 2.32 (4H, m), 1.94 (4H, m), 1.88 (4H, m), 1.06-1.52 (68H, m), 0.91 (6H, t, J = 6.8 Hz), 0.86 (12H, t, J = 6.8 Hz). ^{13}C NMR(CDCl$_3$): 159, 144, 143, 141, 134, 130, 128, 126, 125, 121, 119, 118, 109, 94, 68, 34, 32, 30, 29, 26, 23, 14. IR ν_{max}/cm^{-1}: 2920, 2850, 1599, 1458, 1420, 1386, 1344, 1240, 1170, 1123, 1062, 980, 876, 826, 787, 768. MS m/z (MALDI): 1308, 1307, 1306 (M$^+$, M100). Combustion analysis: Expected: C, 80.93%; H, 9.57%; N, 2.14%; S, 4.91%; Obtained: C, 80.86%; H, 9.62%; N, 2.18%; S, 4.84%.

2,5-Dibromothiophene (69)
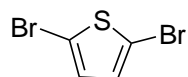
N-Bromosuccinimide (6.00 g, 33.74 mol) was added in a small portion into a mixture of 2-bromothiophene (**68**) (5.00 g, 30.67 mmol) and silica gel (0.4 g, 6.14 mmol) in chloroform (150 cm^3) in the dark. The resultant mixture was stirred overnight at room temperature. The reaction mixture was filtered to remove the silica gel and the organic filtrate was concentrated under reduced pressure to give crude product, which was purified by distillation under vacuum to give the desired product as a dark-red oil[21] (5.53 g, 75%).

^{1}H NMR (CDCl$_3$) δ_H: 6.84 (2H, d, J = 5.6 Hz). MS m/z (EI): 244, 242 (M$^+$), 240.

2,2':5',2''-Terthiophene (70)
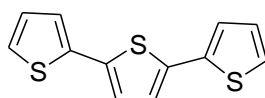
A mixture of Pd(PPh$_3$)$_4$ (0.48 g, 0.42 mmol), 2,5-dibromothiophene (**69**) (5.00 g, 20.67

mmol) and 2-(tributylstannyl)thiophene (23.14 g, 62.00 mmol) in DMF (150 cm^3) was stirred and heated to 90 ^{o}C overnight. The cooled reaction mixture was washed with water (100 cm^3), and extracted with DCM (3 × 100 cm^3). The combined organic layers were washed with water (2 × 100 cm^3), dried over magnesium sulphate (MgSO$_4$), filtered and then concentrated down under reduced pressure. The crude product was purified using column chromatography [K$_2$CO$_3$/silica 1:9, DCM/Hexane 2:1] to remove the tin side products and then re-crystallised from EtOH/DCM to afford the desired product as a yellow solid (4.11 g, 81%).

Melting point/^{o}C: 94-96 (Lit. 89-91)[29]. ^{1}H NMR (CDCl$_3$) δ_H: 7.20 (2H, dd, J = 4.0 & 1.2 Hz), 7.16 (2H, dd, J = 3.8 & 1.0 Hz), 7.10 (2H, d, J =4.0 Hz), 7.02 (2H, dd, J =3.6 & 1.0 Hz). MS m/z (EI): 250,249, 248 (M$^+$).

5,5''-Dibromo-2,2':5',2''-terthiophene (71)
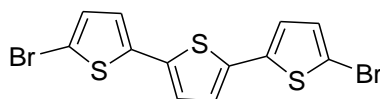
N-bromosuccinimide (NBS) (3.15 g, 17.72 mmol) was added in a small portion into a mixture of 2,2':5',2''-terthiophene (**70**) (2.00 g, 8.05 mmol) and silica gel (0.10 g, 1.61 mmol) in chloroform (50 cm^3) in the dark. The resultant mixture was stirred overnight at room temperature. The reaction mixture was filtered to remove the silica gel and the organic filtrate was concentrated under reduced pressure to give crude product, which was purified via re-crystallisation from EtOH/DCM to give the desired product as a yellow solid (2.69 g, 82%).

Melting point/^{o}C: 159-160 (Lit. 158-158.5)[29]. ^{1}H NMR (CDCl$_3$) δ_H: 6.97 (4H, m), 6.90 (2H, d, J = 4.0 Hz). MS m/z (EI): 408, 406 (M$^+$), 404.

5,5"-*bis*-[9-(Heptadecan-9-yl)-7-methoxy-carbazol-2-yl]-2,2':5',2"-terthiophene (72)

A mixture of Pd(OAc)$_2$ (0.01g, 0.045 mmol) and P(Ph)$_3$ (0.04 g, 0.12 mmol), 5,5"-dibromo-2,2':5',2"-terthiophene (**71**) (0.20 g, 0.50 mmol), [9-(heptadecan-9-yl)-7-methoxy-carbazol-2-yl]boronic acid (**63**) (0.72 g, 1.50 mmol), K$_2$CO$_3$ (0.42 g, 3 mmol) and H$_2$O (2 cm^3) in DME (20 cm^3) was heated at reflux overnight. The cooled reaction mixture was washed with water (100 cm^3) and then extracted with DCM (3 × 100 cm^3). The combined organic layers were washed with water (2 × 100 cm^3), dried over magnesium sulphate (MgSO$_4$), filtered and then concentrated down under reduced pressure. The residue was purified using column chromatography [silica, DCM/Hexane 5:10] to afford the desired product as an orange solid (0.37 g, 67%).

Melting Point/ ^{o}C: 87. ^{1}H NMR (CDCl$_3$) δ_H: 8.01 (4H, m), 7.72 (1H, s),7.54 (1H, s), 7.48 (2H, d, J = 8.0 Hz), 7.30 (2H, d, J = 2.0 Hz), 7.20 (2H, d, J = 4.0 Hz), 7.16 (2H, d, J = 0.8 Hz), 7.04 (1H, s), 6.86 (3H, d, J = 8.8 Hz), 4.58 (1H, m), 4.48 (1H, m), 3.94 (6H, s), 2.31 (4H, m), 1.94 (4H, m), 1.04-1.24 (48H, m), 0.83 (12H, t, J = 6.8 Hz). ^{13}C NMR(CDCl$_3$): 159, 145, 143, 141, 135, 134, 131, 128, 125,122, 121, 120, 119, 108, 107, 94, 56, 55, 34, 32, 30, 29, 27, 22, 14. IR ν_{max}/cm^{-1}: 2919, 2849, 1600, 1510, 1460, 1425, 1390, 1347, 1243, 1205, 1169, 1140, 1060, 987, 938, 887, 813, 789, 759. MS m/z (MALDI): 1118, 1117, 1116 (M$^+$, M100). Combustion analysis: Expected: C, 77.51%; H, 8.49%; N, 2.51%; S, 8.62%; Obtained: C, 77.49%; H, 8.46%; N, 2.60%; S, 8.55%.
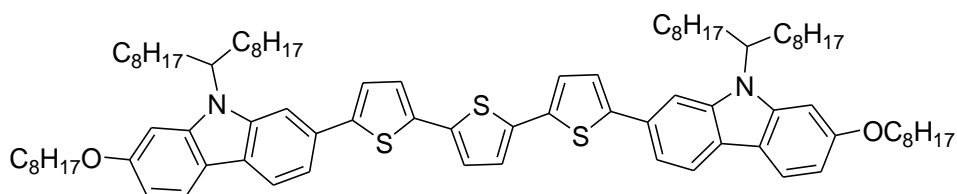
5,5"-*bis*-[9-(Heptadecan-9-yl)-7-(octyloxy)-carbazol-2-yl]-2,2':5',2"-terthiophene (73)

A mixture of Pd(OAc)$_2$ (0.01g, 0.045 mmol) and P(Ph)$_3$ (0.04 g, 0.12 mmol) were added to a mixture of 5,5"-dibromo-2,2':5',2"-terthiophene (**71**) (0.20 g, 0.50 mmol), [9-(Heptadecan-9-yl)-7-octyloxy-carbazol-2-yl]boronic acid (**66**) (0.87 g, 1.50 mmol), K$_2$CO$_3$ (0.42 g, 3 mmol) and H$_2$O (2 cm^3) in DME (20 cm^3) was heated at reflux overnight. The cooled reaction mixture was washed with water (100 cm^3), and extracted with DCM (3 × 100 cm^3). The combined organic layers were washed with water (2 × 100 cm^3), dried over magnesium sulphate (MgSO$_4$), filtered and then concentrated down under reduced pressure. The residue was purified using column chromatography [silica, DCM/Hexane 3:10] to afford the desired product as an orange solid (0.23 g, 36%).

Melting Point/$^{\circ}$C: 84. ^{1}H NMR (CDCl$_3$) δ_H: 7.99 (4H, m), 7.72 (1H, s), 7.54 (1H, s), 7.46 (2H, d, J = 8.0 Hz), 7.31 (2H, d, J = 2.0 Hz), 7.20 (2H, d, J = 3.6 Hz), 7.16 (2H, d, J = 0.8 Hz), 7.04 (1H, s), 6.86 (3H, d, J = 7.2 Hz), 4.56 (1H, m), 4.46 (1H, m), 4.07 (4H, t, J = 6.8 Hz), 2.30 (4H, m), 1.94 (4H, m), 1.86 (4H, m), 1.06-1.52 (68H, m), 0.90 (6H, t, J = 6.8 Hz), 0.83 (12H, t, J = 6.8 Hz). ^{13}C NMR (CDCl$_3$): 159, 145, 143, 141, 135,134,130, 127, 125, 122, 121, 120, 119, 108, 107, 94, 68, 55, 34, 30, 29, 26, 23, 14. IR ν_{max}/cm^{-1}: 2921, 2850, 1600, 1460, 1425, 1358, 1240, 1168, 1118, 1062, 987, 882, 813, 789, 760. MS m/z (MALDI): 1314, 1313, 1312 (M$^+$, M100). Combustion analysis: Expected: C, 78.72%; H, 9.37%; N, 2.14%; S, 7.33%; Obtained: C, 78.83%; H, 9.44%; N, 2.19%; S, 7.25%.

4-Methoxyphenylboronic acid (75)
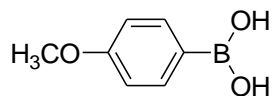
A solution of 2.5 mol/L n-BuLi in hexanes (64.2 cm^3) X MMOL was added to a solution of 1-bromo-4-methoxybenzene (74) (20.00 g, 107.00 mmol) in THF (200 cm^3) at -78 $^{\circ}$C. The resultant mixture was maintained for 1 h at -78 $^{\circ}$C, then 2-triisopropyl borate (52 cm^3, 314.00 mmol, 0.815 g/ cm^3) was added dropwise. The reaction mixture was stirred for 1 h at -78 $^{\circ}$C, then allowed to warm to room temperature and stirred overnight. Hydrochloric acid (180 cm^3, 12 mol/L) was added to the reaction mixture and stirred for 1 h. The reaction mixture was quenched with water (200 cm^3) and extracted with diethyl ether (3 × 150 cm^3). The combined organic extracts were washed with water (2 × 150 cm^3), dried over anhydrous magnesium sulphate (MgSO$_4$), filtered and concentrated down under reduced pressure. The white solid was obtained (14.60 g, 90%).

Melting Point/$^{\circ}$C: 197-201. ^{1}H NMR (CDCl$_3$) δ_H: 8.17 (2H, d, J = 8.4 Hz), 7.68 (1H, d, J = 8.8 Hz), 7.02 (2H, d, J = 8.0 Hz), 6.92 (1H, d, J = 6.8 Hz), 3.88 (3H, s). MS m/z (EI): 152 (M$^+$).

2-(4-Methoxyphenyl)thiophene (76)
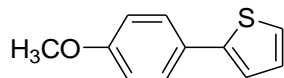
A mixture of Pd(PPh$_3$)$_4$ (1.00g, 0.86 mmol), 2-bromothiophene (68) (7.00 g, 42.94 mmol), 4-methoxyphenylboronic acid (75) (7.84 g, 51.52 mmol), K$_2$CO$_3$ (14.24 g, 103.04 mmol) and H$_2$O (50 cm^3) in DME (200 cm^3) was heated at 80 $^{\circ}$C overnight. The cooled reaction mixture was washed with water (100 cm^3) and extracted with DCM (3 × 100 cm^3). The combined organic layers were washed with water (2 × 100 cm^3), dried (MgSO$_4$), filtered and then concentrated down under reduced pressure. The residue was

purified using flash column chromatography [silica, hexane] to afford the desired product as a white solid (7.46 g, 91%).

Melting Point/ ^{o}C: 107 (Lit. 106-107)[30]. ^{1}H NMR (CDCl$_3$) δ_H: 7.54 (2H, dd, J = 6.8 & 2.4 Hz), 7.20 (2H, m), 7.06 (1H, dd, J = 4.0 & 1.0 Hz), 6.91 (2H, dd, J = 6.8 & 2.4 Hz), 3.85 (3H, s). MS m/z (EI): 190 (M$^+$).

5-(4-Methoxyphenyl)thiophen-2-ylboronic acid (77)
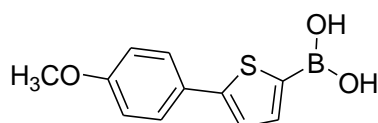
A solution of 2.5 mol/L n-BuLi in hexanes (22.4 cm^3) was added to a solution of 2-(4-methoxyphenyl)thiophene (**76**) (7.00 g, 36.89 mmol) and THF (200 cm^3) at -78 ^{o}C. The resultant mixture was maintained for 1 h at -78 ^{o}C, then 2-triisopropyl borate (17.5 cm^3, 73.78 mmol, 0.815 g/ cm^3) was added drop-wise. The reaction mixture was stirred for 1 h at -78 ^{o}C, then allowed to warm to room temperature and stirred overnight. Hydrochloric acid (60 cm^3, 12 mol/L) was added to the reaction mixture and stirred for 1 h. The reaction mixture was quenched with water (100 cm^3) and extracted with diethyl ether (3 × 100 cm^3). The combined organic extracts were washed with water (2 × 100 cm^3), dried over anhydrous magnesium sulphate (MgSO$_4$), filtered and concentrated down under reduced pressure. The white solid was obtained (8.05 g, 93%)

Melting Point/ ^{o}C: 164-167. ^{1}H NMR (DMSO-D$_6$) δ_H: 8.19 (2H, s), 7.61 (3H, m), 7.39 (1H, d, J = 3.6 Hz), 6.98 (2H, dd, J = 6.4 & 2.0 Hz), 3.77 (3H, s). MS m/z (EI): 234 (M$^+$).

2-Bromo-7-iodofluorene (79)
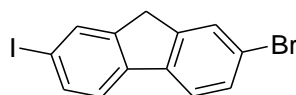
A mixture of 2-bromofluorene (**78**) (10.00 g, 61.50 mmol), acetic acid (200 cm^3), concentrated sulphuric acid (1.8 cm^3) and water (15 cm^3) was stirred and heated at 75 ^{o}C. After the solution became clear and transparent, periodic acid (2.80 g, 12.30 mmol) and pulverized iodine (6.30 g, 24.80 mmol) were then added. The resultant mixture was stirred vigorously for approximately 2 h at 75 ^{o}C until the colour of the mixture changed from deep purple to yellow. The cooled reaction mixture was poured onto water (300 cm^3) and the precipitate was collected. The crude product was purified using recrystallisation from EtOH/DCM to afford a white solid (12.35 g, 68%).

Melting Point/ ^{o}C: 182-183 (Lit. 177-178)[31], (Lit. 184-186)[32]. ^{1}H NMR (CDCl$_3$) δ_H: 7.88 (1H, d, J = 1.2 Hz), 7.71 (1H, dd, J = 7.2 & 1.0 Hz), 7.67 (1H, d, J = 1.2 Hz), 7.61 (1H, d, J = 8.0 Hz), 7.51 (2H, dd, J = 8.0 & 2.0 Hz), 3.86 (2H, s). MS m/z (EI): 372, 371 (M$^+$), 370.

2-Bromo-7-iodo-9,9-dihexylfluorene (80)
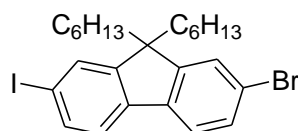
Powered potassium hydroxide (KOH) (7.57 g, 134.8 mmol) was added in a small portion into a mixture of 2-bromo-7-iodofluorene (**79**) (10.00 g, 26.96 mmol), 1-bromohexane (9.80 g, 59.30 mmol), potassium iodide (0.50 g, 2.70 mmol) and DMSO at room temperature. The resultant mixture was stirred for 4 h, washed with water (100 cm^3), and extracted with DCM (3 × 100 cm^3). The combined organic layers were washed with water (2 × 100 cm^3), dried over magnesium sulphate (MgSO$_4$), filtered and then concentrated down under reduced pressure. The residue was purified using flash column chromatography [Hexane] to give the crude product, which was washed with ethanol, and dried under vacuum to afford the desired product as a pale-yellow needles (10.90 g, 75%).

Melting Point/ ^{o}C: 52-53 (Lit. 57-58)[32]. ^{1}H NMR (CDCl$_3$) δ_H: 7.66 (2H, dd, J = 8.0 &

1.6 Hz), 7.53 (1H, d, $J = 8.4$ Hz), 7.46 (1H, d, $J = 1.6$ Hz), 7.43 (1H, d, $J = 2.0$ Hz), 7.40 (1H, d, $J = 8.0$ Hz), 1.91 (4H, m), 1.02-1.13 (12H, m), 0.79 (6H, t, $J = 7.2$ Hz), 0.53-0.60 (4H, m). MS m/z (EI): 540, 539 (M$^+$), 538.

2-(7-Bromo-9,9-dihexyl-fluoren-2-yl)-5-(4-methoxyphenyl)thiophene (81)
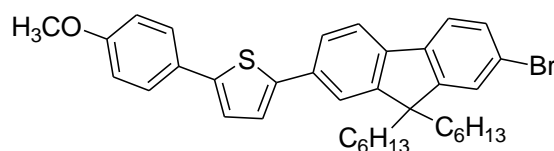
A mixture of Pd(PPh$_3$)$_4$ (0.50g, 0.43 mmol), 2-bromo-7-iodo-9,9-dihexylfluorene (**80**) (12.67 g, 23.50 mmol), 5-(4-methoxyphenyl)thiophen-2-ylboronic acid (**77**) (5.00 g, 21.36 mmol), K$_2$CO$_3$ (5.90 g, 42.72 mmol) and H$_2$O (20 cm^3) in DME (200 cm^3) was heated at 80 ^{o}C overnight. The cooled reaction mixture was washed with water (200 cm^3) and extracted with DCM (3 × 100 cm^3). The combined organic layers were washed with water (2 × 100 cm^3), dried (MgSO$_4$), filtered and then concentrated under reduced pressure. The residue was purified using column chromatography [silica, DCM/hexane 5:10] to give the crude product, which was re-crystallised from ethanol, and dried under vacuum to afford the desired product as a yellow solid (8.28 g, 65%).

Melting Point/ ^{o}C: 98-99. ^{1}H NMR (CDCl$_3$) δ_H: 7.64 (1H, d, $J = 7.2$ Hz), 7.61 (1H, d, $J = 1.6$ Hz), 7.59 (2H, dd, $J = 7.2$ & 2.0 Hz), 7.53 (2H, d, $J = 1.0$ Hz), 7.46 (2H, m), 7.34 (1H, d, $J = 1.0$ Hz), 7.21 (1H, d, $J = 4.0$ Hz), 6.95 (2H, d, $J = 8.8$ Hz), 3.85 (3H, s), 1.97 (4H, m), 1.04-1.11 (12H, m), 0.78 (6H, t, $J = 6.8$ Hz), 0.62-0.68 (4H, m). MS m/z (EI): 602, 601 (M$^+$), 600.

9,9-Dihexyl-7-[5-(4-methoxyphenyl)thiophen-2-yl]-fluoren-2-ylboronic acid (82)
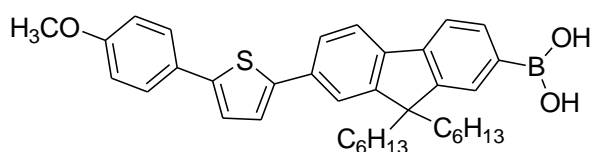
A solution of 2.5 mol/L n-BuLi in hexanes (1.8 cm^3) was added to a solution of

2-(7-bromo-9,9-dihexyl-fluoren-2-yl)-5-(4-methoxyphenyl)thiophene (**81**) (1.80 g, 2.99 mmol) and THF (50 cm^3) at -78 $^{\circ}$C. The resultant mixture was maintained for 1 h at -78 $^{\circ}$C, then 2-triisopropyl borate (1.4 cm^3, 5.99 mmol, 0.815 g/ cm^3) was added drop-wise. The reaction mixture was stirred for 1 h at -78 $^{\circ}$C, then allowed to warm to room temperature and stirred overnight. Hydrochloric acid (2.7 cm^3, 12 mol/L) was added to the reaction mixture and stirred for 1 h. The reaction mixture was quenched with water (100 cm^3) and extracted with diethyl ether (3 × 100 cm^3). The combined organic extracts were washed with water (2 × 100 cm^3), dried over anhydrous magnesium sulphate (MgSO$_4$), filtered and concentrated down under reduced pressure. The yellow solid was obtained (1.20 g, 71%).

Melting Point/$^{\circ}$C: 134-140. ^{1}H NMR (DMSO-D$_6$) δ$_H$: 8.05 (2H, s), 7.82 (2H, d, *J* = 5.6 Hz), 7.76 (1H, d, *J* = 2.8 Hz), 7.72 (1H, d, *J* = 1.0 Hz), 7.64 (3H, m), 7.57 (1H, d, *J* = 3.6 Hz), 7.43 (1H, d, *J* = 3.6 Hz), 7.00 (2H, d, *J* = 8.8 Hz), 6.55 (1H, d, *J* = 1.0 Hz), 3.78 (3H, s). MS m/z (EI): 567, 566 (M$^+$).

3,3'-{5',5'''-(9,9-Dioctyl-9-fluorene-2,7-diyl)*bis*[(2,2'-bithiophene)-5',5-diyl]}-*bis*-{ 9,9-dihexyl-7-[5-(4-methoxyphenyl)thiophen-2-yl]-fluorene} (83)
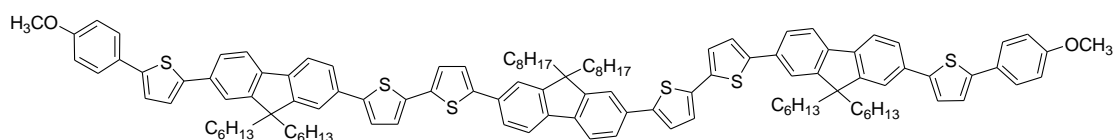
A mixture of Pd(PPh$_3$)$_4$ (0.01g, 0.008 mmol), 2-(5-Bromothiophen-2-yl)-5-{7-[5-(5-bromothiophen-2-yl)thiophen-2-yl]-9.9-dioctyl-fluoren-2-yl}thiophene (**45**) (0.30 g, 0.34 mmol), 9,9-dihexyl-7-[5-(4-methoxyphenyl)thiophen-2-yl]-fluoren-2-ylboronic acid (**82**) (0.60 g, 1.03 mmol), K$_2$CO$_3$ (0.28 g, 2.05 mmol) and H$_2$O (2 cm^3) in DMF (30 cm^3) was heated at 80 $^{\circ}$C overnight. The cooled reaction mixture was washed with water (100 cm^3) and extracted with DCM (3 × 100 cm^3). The combined organic layers were washed with water (2 × 100 cm^3), dried (MgSO$_4$), filtered and then concentrated down

under reduced pressure. The residue was purified using column chromatography [silica, DCM/hexane 5:10] to afford the desired product as a yellow solid (0.55 g, 92%).

Melting Point/ $^{\circ}$C: Tg 68 Cr - N 225 I. ^{1}H NMR (CDCl$_3$) δ_H: 7.68-7.71 (6H, m), 7.62 (6H, dd, J = 8.4 & 1.0 Hz), 7.58 (2H, d, J = 1.2 Hz), 7.57 (6H, d, J = 1.2 Hz), 7.35 (6H, t, J = 7.6 Hz), 7.21-7.24 (8H, m), 6.95 (4H, d, J = 8.8 Hz), 3.86 (6H, s), 2.06 (12H, m), 1.04-1.24 (44H, m), 0.66-0.82 (30H, m). ^{13}C NMR(CDCl$_3$): 159, 152, 144, 143, 141, 140, 136, 133, 132, 127, 126, 124, 120, 119, 114, 55, 40, 31, 29, 24, 23, 14. IR ν_{max}/cm^{-1}: 2922, 2848, 1585, 1508, 1437, 1390, 1347, 1248, 1197, 1175, 1135, 1109, 1036, 948, 879, 826, 790, 769. MS m/z (MALDI): 1763, 1762, 1761 (M$^+$), 1760, 1043, 598 (M100), 522. Combustion analysis: Expected: C, 79.81%; H, 7.44%; S, 10.93%; Expected: C, 79.87%; H, 7.52%; S, 10.85%.

Triazatruxene (85)
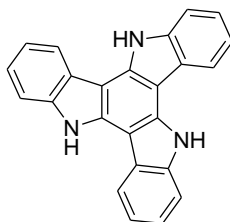
A mixture of 2-indolinone (**84**) (10.00 g, 75.10 mmol) and phosphorous(V)oxychloride (POCl$_3$) (50 cm^3) was heated at 100 $^{\circ}$C overnight. After being cooled to room temperature, the mixture was poured onto solid ice (500 g) slowly and carefully neutralised with KOH until pH = 7-8. After neutralisation, the precipitate was filtered to give the crude product as a brown solid, which was purified using column chromatography [silica, ethyl acetate/hexane 2:10] to afford the desired product as a pale-yellow solid[10] (4.02 g, 45%).

Melting Point/ $^{\circ}$C: > 300. ^{1}H NMR (ACETONE-D$_6$) δ_H: 11.11 (3H, S), 8.47 (3H, d, J = 8.0 Hz), 7.64 (3H, d, J = 7.6 Hz), 7.27 (6H, m). MS m/z (EI): 346, 345 (M$^+$, M100), 344.

Tri-*N*-octyl-triazatruxene (86)
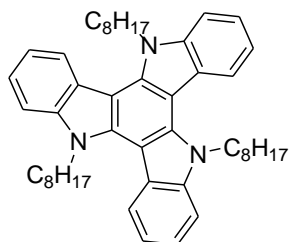
A mixture of triazatruxene (**85**) (0.40 g, 1.13 mmol) and KOH (0.64 g, 11.3 mmol) in THF (20 cm^3) was heated to reflux for 1 h. Then 1-bromooctane (1.10 g, 5.65 mmol) was added and the resultant mixture was heated under reflux overnight. The cooled reaction mixture was washed with water (100 cm^3) and then extracted with DCM (3 × 100 cm^3). The combined organic layers were washed with water (2 × 100 cm^3), dried (MgSO$_4$), filtered and then concentrated down under reduced pressure. The residue was purified using column chromatography [silica, DCM/hexane 4:10] to afford the desired product as a pale-yellow solid[33] (0.56 g, 73%).

Melting Point/$^{\circ}$C: 80-81. ^{1}H NMR (CDCl$_3$) δ_H: 8.29 (3H, d, *J* = 8.0 Hz), 7.64 (3H, d, *J* = 8.0 Hz), 7.46 (3H, t, *J* = 7.2 Hz), 7.35 (3H, t, *J* = 7.6 Hz), 4.93 (6H, t, *J* = 8.0 Hz), 2.00 (6H, m), 1.27 (30H, m), 0.84 (9H, t, *J* = 7.2 Hz). ^{13}C NMR (CDCl$_3$): 140, 138, 123, 122, 121, 119, 110, 103, 47, 31, 29, 26, 22, 14. IR ν_{max}/cm^{-1}: 2952, 2919, 2852, 1605, 1564, 1466, 1408, 1373, 1332, 1282, 1244, 1222, 1183, 1110, 1034, 774, 743, 720. MS m/z (EI): 683, 682 (M$^+$, M100), 494, 392, 306, 157. Combustion analysis: Expected: C, 84.53%; H, 9.31%; N, 6.16%; Obtained: C, 84.70%; H, 9.40%; N, 6.22%.

Tri-*N*-hexyl-triazatruxene (87)
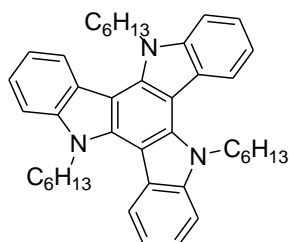
Sodium hydride (NaH) (0.21 g, 5.082 mmol; 60% dispersion in mineral oil) was added

in small portions to a solution of triazatruxene (**85**) (0.30 g, 0.847 mmol) in DMF (40 cm^3). The mixture was then heated to 50 ^{o}C and 1-bromohexane (0.70 g, 4.235 mmol) was added. The resultant mixture was stirred for 3 h at 50 ^{o}C and then was stirred overnight at room temperature. The reaction mixture was washed with water (100 cm^3) and extracted with DCM (3 $\times$ 100 cm^3). The combined organic layers were washed with water (2 $\times$ 100 cm^3), dried (MgSO$_4$), filtered and then concentrated down under reduced pressure. The residue was purified using column chromatography [silica, DCM/hexane 5:10] to afford the desired product as a pale-yellow solid (0.45 g, 88%).

Melting Point/^{o}C: 113-114. ^{1}H NMR (CDCl$_3$) δ_H: 8.30 (3H, d, J = 8.0 Hz), 7.65 (3H, d, J = 8.0 Hz), 7.45 (3H, t, J = 7.6 Hz Hz), 7.34 (3H, t, J = 8.0 Hz), 4.94 (6H, t, J = 8.0 Hz), 1.99 (6H, m), 1.32 (18H, m), 0.82 (9H, t, J = 7.4 Hz). ^{13}C NMR (CDCl$_3$): 141, 138, 123, 122, 121, 119, 110, 103, 47, 31, 30, 26, 22, 14. IR ν_{max}/cm^{-1}: 2954, 2925, 2854, 1606, 1561, 1470, 1408, 1376, 1332, 1286, 1234, 1187, 1171, 1143, 1109, 1025, 983, 742, 720. MS m/z (EI): 600, 599, 598 (M$^+$, M100), 395, 201. Combustion analysis: Expected: C, 84.37%; H, 8.60%; N, 7.03%; Obtained: C, 84.26%; H, 8.76%; N, 7.05%.

Tri-*N*-butyl-triazatruxene (88)

Sodium hydride (NaH) (0.21 g, 5.082 mmol; 60% dispersion in mineral oil) was added in small portions to a solution of triazatruxene (**85**) (0.30 g, 0.847 mmol) in DMF (40 cm^3). The mixture was then heated to 50 ^{o}C and 1-bromobutane (0.58 g, 4.235 mmol) was added. The resultant mixture was kept for 3 h at 50 ^{o}C and then was stirred overnight at room temperature. The reaction mixture was washed with water (100 cm^3) and then extracted with DCM (3 $\times$ 100 cm^3). The combined organic layers were washed with water (2 $\times$ 100 cm^3), dried (MgSO$_4$), filtered and then concentrated down under

reduced pressure. The residue was purified using column chromatography [silica, DCM/hexane 5:10] to afford the desired product as a pale-yellow solid (0.36 g, 81%).

Melting Point/$^{\circ}$C: 116-117. ^{1}H NMR (CDCl$_3$) δ_H: 8.30 (3H, d, J = 8.0 Hz), 7.65 (3H, d, J = 7.6 Hz), 7.45 (3H, t, J = 7.6 Hz), 7.36 (3H, t, J = 8.0 Hz), 4.96 (6H, t, J = 8.0 Hz), 1.98 (6H, m), 1.31 (6H, m), 0.89 (9H, t, J = 7.6 Hz). ^{13}C NMR (CDCl$_3$): 141, 138, 123, 122, 121, 119, 110, 103, 47, 31, 30, 26, 20, 14. IR ν_{max}/cm^{-1}: 2956, 2928, 2870, 1607, 1570, 1461, 1406, 1373, 1331, 1278, 1244, 1105, 1029, 990, 773, 720. MS m/z (EI): 515, 514 (M^{+}, M100), 433, 306, 251, 157, 108. Combustion analysis: Expected: C, 84.17%; H,7.65%; N, 8.18%. Obtained: C, 84.09%; H,7.81%; N, 8.20%.
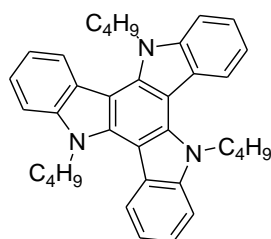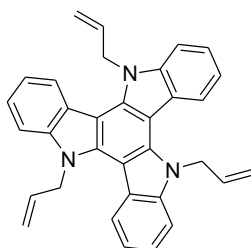
Tri-*N*-allyl triazatruxene (89)

Sodium hydride (NaH) (0.21 g, 5.082 mmol; 60% dispersion in mineral oil) was added in small portions to a solution of triazatruxene (**85**) (0.30 g, 0.847 mmol) in DMF (40 cm^3). The mixture was then heated to 50 $^{\circ}$C and allyl bromide (0.52 g, 4.235 mmol) was added. The resultant mixture was kept for 3 h at 50 $^{\circ}$C and then was stirred overnight at room temperature. The reaction mixture was washed with water (100 cm^3) and extracted with DCM (3 × 100 cm^3). The combined organic layers were washed with water (2 × 100 cm^3), dried (MgSO$_4$), filtered and then concentrated down under reduced pressure. The residue was purified using column chromatography [silica, EtOAc/hexane 1:10] to afford the desired product as a pale-green solid (0.30 g, 75%).

Melting Point/$^{\circ}$C: 222-223. ^{1}H NMR (CDCl$_3$) δ_H: 8.40 (3H, d, J = 8.0 Hz), 7.57 (3H, d, J = 8.0 Hz), 7.43 (3H, t, J = 8.0 Hz), 7.33 (3H, dt, J = 8.0 Hz), 6.51 (3H, m), 5.58 (6H, m), 5.42 (6H, m). ^{13}C NMR(CDCl$_3$): 142, 139, 134, 123, 122, 120, 118, 111, 104, 50.

IR ν_{max}/cm^{-1}: 3049, 2930, 1637, 1607, 1567, 1469, 1446, 1402, 1328, 1296, 1284, 1200, 1171, 1117, 989, 949, 918, 774, 720, 678. MS m/z (EI): 467, 466 (M$^+$, M100), 465, 433, 407, 374, 338, 306, 251, 201, 157, 108. Combustion analysis: Expected: C, 85.13%; H,5.85%; N, 9.03%. Obtained: C, 85.04%; H,5.81%; N, 8.93%.

Tri-*N*-(hex-5-en-1-yl)-triazatruxene (90)

Sodium hydride (NaH) (0.21 g, 5.082 mmol; 60% dispersion in mineral oil) was added in small portions to a solution of triazatruxene (**85**) (0.30 g, 0.847 mmol) in DMF (40 cm^3). The mixture was then heated to 50 ^{o}C and 6-bromo-1-hexene (0.70 g, 4.235 mmol) was added. The resultant mixture was kept for 3 h at 50 ^{o}C and then was stirred overnight at room temperature. The reaction mixture was washed with water (100 cm^3) and extracted with DCM (3 × 100 cm^3). The combined organic layers were washed with water (2 × 100 cm^3), dried (MgSO$_4$), filtered and then concentrated under reduced pressure. The residue was purified using column chromatography [silica, EtOAc/hexane 1:10] to afford the desired product as a pale-green solid (0.38 g, 75%)。

Melting Point/ ^{o}C: 106-107. ^{1}H NMR (CDCl$_3$) δ_H: 8.28 (3H, d, J = 8.0 Hz), 7.64 (3H, d, J = 8.0 Hz), 7.47 (3H, t, J = 8.0 Hz), 7.36 (3H, t, J = 8.0 Hz), 5.72 (3H, m), 4.96 (6H, m), 4.91 (6H, m), 2.03 (12H, m), 1.41 (6H, m). ^{13}C NMR (CDCl$_3$): 141, 138, 123, 122, 121, 119, 115, 110, 104, 47, 33, 29, 26. IR ν_{max}/cm^{-1}: 3048, 2929, 1639, 1606, 1561, 1470, 1408, 1376, 1332, 1284, 1234, 1186, 1144, 1111, 1035, 991, 908, 771, 742, 721. MS m/z (EI): 594, 593, 592 (M$^+$, M100), 419, 338, 251, 157, 108. Combustion analysis: Expected: C, 85.24%; H,7.66%; N, 7.10%; Obtained: C, 85.14%; H,7.80%; N, 7.11%.

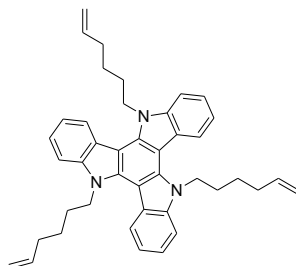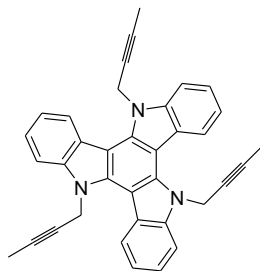**Tri-*N*-(but-2-yn-1-yl)triazatruxene (91)**

Sodium hydride (NaH) (0.21 g, 5.082 mmol; 60% dispersion in mineral oil) was added in small portions to a solution of triazatruxene (**85**) (0.30 g, 0.847 mmol) in DMF (40 cm^3). The mixture was then heated to 50 ^{o}C and 1-bromo-2-butyne (0.57 g, 4.235 mmol) was added. The resultant mixture was kept for 3 h at 50 ^{o}C and then was stirred overnight at room temperature. The reaction mixture was washed with water (100 cm^3) and extracted with DCM (3 × 100 cm^3). The combined organic layers were washed with water (2 × 100 cm^3), dried (MgSO$_4$), filtered and then concentrated down under reduced pressure. The residue was purified using column chromatography [silica, DCM/hexane 5:10] to afford the desired product as a white solid (0.24 g, 62%).

Melting Point/^{o}C: 266. ^{1}H NMR (CDCl$_3$) δ_H: 8.78 (3H, d, *J* = 8.0 Hz), 7.86 (3H, d, *J* = 7.6 Hz), 7.51 (3H, t, *J* = 8.0 Hz), 7.44 (3H, dt, *J* = 8.0 Hz), 5.39 (6H, d, *J* = 2.4 Hz), 2.01 (9H, t, *J* = 2.0 Hz). ^{13}C NMR (CDCl$_3$): 143, 140, 125, 123, 122, 112, 105, 85, 40, 6. IR ν_{max}/cm^{-1}: 3049, 2918, 1610, 1578, 1472, 1443, 1406, 1367, 1328, 1296, 1207, 1173, 1152, 1132, 1017, 942, 916, 829, 759, 742, 716. MS m/z (EI): 503, 502 (M$^+$, M100), 433, 338, 251, 157, 108. Combustion analysis: Expected: C, 86.20%; H,5.43%; N, 8.38%; Obtained: C, 86.24%; H,5.38%; N, 8.16%.
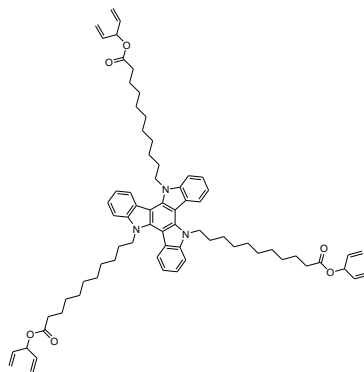
Tri-*N*-[(penta-1,4-dien-3-yl)undecanoat-11-yl]triazatruxene (92)

Sodium hydride (NaH) (0.14 g, 3.39 mmol; 60% dispersion in mineral oil) was added in small portions to a solution of triazatruxene (**85**) (0.2 g, 0.565 mmol) in DMF (40 cm^3). The mixture was then heated to 50 ^{o}C and penta-1,4-dien-3-yl-11-bromoundecanoate (0.94 g, 2.825 mmol) was added. The resultant mixture was kept for 3 h at 50 ^{o}C and then was stirred overnight at room temperature. The reaction mixture was washed with water (100 cm^3) and extracted with DCM (3 × 100 cm^3). The combined organic layers were washed with water (2 × 100 cm^3), dried (MgSO$_4$), filtered and then concentrated down under reduced pressure. The residue was purified using column chromatography [silica, EtOAc/hexane 1:10] to afford the desired product as yellow oil (0.23 g, 36%).

^{1}H NMR (CDCl$_3$) δ_H: 8.29 (3H, d, *J* = 8.0 Hz), 7.64 (3H, d, *J* = 8.0 Hz), 7.44 (3H, t, *J* = 8.0 Hz), 7.33 (3H, t, *J* = 8.0 Hz), 5.86 (6H, m), 5.71 (3H, m), 4.93 (6H, t, *J* = 8.0 Hz), 5.31 (6H, m), 5.22 (6H, m), 2.32 (6H, m) , 1.98 (6H, m) , 1.20-1.47 (36H, m). ^{13}C NMR (CDCl$_3$): 175, 143, 141, 137, 126, 125, 124, 122, 119, 113, 105, 85, 49, 37, 31, 27. IR ν_{max}/cm^{-1}: 2976, 2877, 1736, 1654, 1604, 1567, 1503, 1475, 1380, 1298, 1241, 1171, 983, 936, 876, 798. MS m/z (MALDI): 1099, 1098, 1097 (M$^+$, M100). Combustion analysis: Expected: C, 78.86%; H,8.55%; N, 3.83%; Obtained: C, 78.72%; H,8.63%; N, 3.85%.

N,N-Diallyl-5-bromopentyl-amide (95)
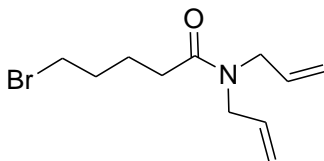
A solution of diallyl amine (**94**) (1.00 g, 10.3 mmol) and pyridine (30 cm^3) was treated with 5-bromovaleryl chloride (**93**) (4.11 g, 20.6 mmol) drop-wise at 0 ^{o}C. Then triethylamine (3.13 g, 30.9 mmol) was added dropwise. The resultant mixture was maintained at 0 ^{o}C for 4 h, then stirred at room temperature overnight, poured into water (100 cm^3), neutralised with hydrochloric acid (pH 6-7) and then extracted with DCM (3 × 100 cm^3). The combined organic layers were washed with water (2 × 100 cm^3), dried (MgSO$_4$), filtered and then concentrated down under reduced pressure. The residue was purified using column chromatography [silica, EtOAc/hexane 5:10] to afford the desired product as pale-yellow oil (1.63 g, 61%).

^{1}H NMR (CDCl$_3$) δ_H: 5.80 (2H, m), 5.14-5.23 (4H, m), 3.99 (2H, d, *J* = 6.0 Hz), 3.88 (2H, m), 3.44 (2H, t, *J* = 6.8 Hz), 2.36 (2H, t, *J* = 7.2 Hz), 1.93 (2H, m), 1.82 (2H, m). MS m/z (EI): 261, 260 (M$^+$), 259.

Tri(*N,N*-diallylpentanamide) triazatruxene (96)
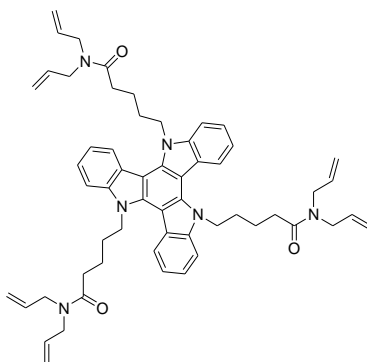
Sodium hydride (NaH) (0.21 g, 5.082 mmol; 60% dispersion in mineral oil) was added in small portions to a solution of triazatruxene (**85**) (0.30 g, 0.847 mmol) in DMF (40 cm^3). The mixture was then heated to 50 ^{o}C and *N,N*-diallyl-5-bromopentanamide (**95**)

(1.11 g, 4.235 mmol) was added. The resultant mixture was kept for 3 h at 50 $^{\circ}$C and then stirred overnight at room temperature. The reaction mixture was washed with water (100 cm^3) and extracted with DCM (3 × 100 cm^3). The combined organic layers were washed with water (2 × 100 cm^3), dried (MgSO$_4$), filtered and then concentrated down under reduced pressure. The residue was purified using column chromatography [silica, EtOAc/hexane 5:10] to afford the desired product as dark-green oil (0.65 g, 86%).

^{1}H NMR (CDCl$_3$) δ_H: 8.27 (3H, d, $J = 8.0$ Hz), 7.65 (3H, d, $J = 8.0$ Hz), 7.46 (3H, t, $J = 7.2$ Hz), 7.36 (3H, t, $J = 7.2$ Hz), 5.70 (6H, m), 4.95-5.08 (18H, m), 3.91 (6H, d, $J = 6.0$ Hz), 3.64 (6H, d, $J = 4.8$ Hz), 2.21 (6H, t, $J = 7.6$ Hz), 2.01 (6H, m), 1.66 (6H, m). ^{13}C NMR (CDCl$_3$): 172, 141, 138, 133, 132, 123, 122, 121, 120, 117, 116, 110, 103, 49, 48, 46, 32, 29, 22. IR ν_{max}/cm^{-1}: 2979, 2877, 1684, 1653, 1582, 1473, 1410, 1335, 1301, 1222, 1185, 1005, 922, 807, 773, 741, 720. MS m/z (MALDI): 885, 884, 883 (M$^+$, M100). Combustion analysis: Expected: C, 77.52%; H, 7.53%; N, 9.52%; Obtained: C, 77.43%; H, 7.63%; N, 9.50%.

N,N-Diallyl-5-bromoacetamide (99)
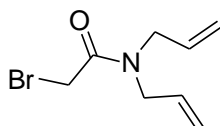
A solution of diallyl amine (**98**) (1.92 g, 19.78 mmol) and ethyl acetate (10 cm^3) was treated with bromoacetyl bromide (**97**) (9.00 g, 43.51 mmol) in ethyl acetate (40 cm^3) and triethylamine (4 cm^3) dropwise at 0 $^{\circ}$C. The resultant mixture was stirred at 0 $^{\circ}$C for 1 h, then warmed to room temperature and kept overnight. The mixture was washed by saturated NaHCO$_3$ solution (3 × 60 cm^3), dried (MgSO$_4$), filtered and then concentrated under reduced pressure. The residue was purified using column chromatography [silica, EtOAc/hexane 1:10] to afford the desired product as pale-yellow oil (2.20 g, 51%).

^{1}H NMR (CDCl$_3$) δ_H: 5.86 (2H, m), 5.20 (4H, m), 4.01 (4H, m), 3.86 (2H, s); MS m/z

(EI): 219, 218 (M$^+$), 217.

**Tri-*N*-(*N,N*-diallylacetamide)-triazatruxene (100)**
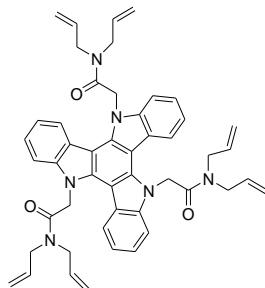
Sodium hydride (NaH) (0.21 g, 5.082 mmol; 60% dispersion in mineral oil) was added in small portions to a solution of triazatruxene (**85**) (0.30 g, 0.847 mmol) in DMF (40 cm^3). The mixture was then heated to 50 ^{o}C and *N,N*-diallyl-2-bromoacetamide (**99**) (0.93 g, 4.235 mmol) was added. The resultant mixture was kept for 3 h at 50 ^{o}C and then was stirred overnight at room temperature. The reaction mixture was washed with water (100 cm^3) and extracted with DCM (3 × 100 cm^3). The combined organic layers were washed with water (2 × 100 cm^3), dried (MgSO$_4$), filtered and then concentrated down under reduced pressure. The residue was purified using column chromatography [silica, EtOAc/hexane 10:10] to afford the desired product as white solid (0.30 g, 46%).

Melting Point/^{o}C: 206. ^{1}H NMR (CDCl$_3$) δ_H: 7.93 (3H, d, *J* = 8.0 Hz), 7.40 (3H, d, *J* = 8.0 Hz), 7.37 (3H, t, *J* = 7.2 Hz), 7.24 (3H, t, *J* = 8.0 Hz), 6.00 (6H, m), 5.49 (6H, s), 5.24-5.34 (12H, m), 4.25 (6H, d, *J* = 6.0 Hz), 4.03 (6H, d, *J* = 4.8 Hz). ^{13}C NMR(CDCl$_3$): 168, 142, 139, 133, 132, 123, 121, 120, 118, 117, 110, 103, 50, 49, 48. IR ν_{max}/cm^{-1}: 3050, 2979, 2876, 1685, 1656, 1581, 1473,1409, 1333, 1300, 1222, 1190, 1124, 1002, 921, 806, 773, 719. MS m/z (EI): 759, 758, 757 (M$^+$, M100), 706, 582, 433, 306. Combustion analysis: Expected: C, 76.16%; H, 6.39%; N, 11.10%; Obtained: C, 76.09%; H, 6.35%; N, 11.11%.

Tri-*N*-{5-[(3-methyloxetan-3-yl)methoxy]pentyl}-triazatruxene (101)

Sodium hydride (NaH) (0.21 g, 5.082 mmol; 60% dispersion in mineral oil) was added in small portions to a solution of triazatruxene (**85**) (0.30 g, 0.847 mmol) in DMF (40 cm^3). The mixture was then heated to 50 ^{o}C and 3-{[(5-brmopentyl)oxy]methyl}-3-methyloxetane (1.07 g, 4.235 mmol) was added. The resultant mixture was kept for 3 h at 50 ^{o}C and then stirred overnight at room temperature. The reaction mixture was washed with water (100 cm^3) and extracted with DCM (3 × 100 cm^3). The combined organic layers were washed with water (2 × 100 cm^3), dried (MgSO$_4$), filtered and then concentrated down under reduced pressure. The residue was purified using column chromatography [silica, EtOAc/hexane 15:10] to afford the desired product as yellow oil (0.31 g, 42%).

^{1}H NMR (CDCl$_3$) δ_H: 8.28 (3H, d, *J* = 8.0 Hz), 7.64 (3H, d, *J* = 8.0 Hz), 7.47 (3H, t, *J* = 7.2 Hz), 7.35 (3H, t, *J* = 7.2 Hz), 4.96 (6H, t, *J* = 8.0 Hz), 4.43 (6H, d, *J* = 6.0 Hz), 4.30 (6H, d, *J* = 5.6 Hz), 3.35 (6H, s), 3.33 (6H, t, *J* = 6.0 Hz), 2.04 (9H, s), 2.00 (6H, m) , 1.39 (6H, m) , 1.33 (6H, m). ^{13}C NMR (CDCl$_3$): 138, 136, 120, 119, 118, 116, 107, 100, 79, 68, 58, 43, 36, 26, 20, 18. IR ν_{max}/cm^{-1}: 2958, 2858, 1603, 1578, 1472, 1380, 1330. 1296, 1237, 1185, 1147, 1023, 972, 925, 830, 748, 728. MS m/z (MALDI): 858, 857, 856 (M$^+$, M100). Combustion analysis: Expected: C, 75.76%; H, 8.12%; N, 4.91%; Obtained: C, 75.69%; H, 8.18%; N, 4.95%.

Tri-*N*-[(3-methyloxetan-3-yl)methyl]-triazatruxene (102)
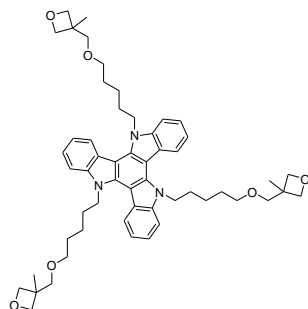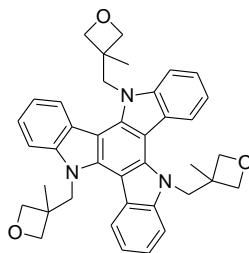

Sodium hydride (NaH) (0.21 g, 5.082 mmol; 60% dispersion in mineral oil) was added in small portions to a solution of triazatruxene (**85**) (0.30 g, 0.847 mmol) in DMF (40 cm^3). The mixture was then heated to 50 ^{o}C and 3-bromomethyl-3-methyloxetane (0.70 g, 4.235 mmol) was added. The resultant mixture was kept for 3 h at 50 ^{o}C and then was stirred overnight at room temperature. The reaction mixture was washed with water (100 cm^3) and extracted with DCM (3 × 100 cm^3). The combined organic layers were washed with water (2 × 100 cm^3), dried (MgSO$_4$), filtered and then concentrated down under reduced pressure. The residue was purified using column chromatography [silica, EtOAc/hexane 15:10] and washed by hexane to afford the desired product as white solid (0.30 g, 58%).

Melting Point/^{o}C: 199-200. ^{1}H NMR (CDCl$_3$) δ_H: 8.03 (3H, d, *J* = 8.0 Hz), 7.53 (3H, d, *J* = 8.0 Hz), 7.45 (3H, t, *J* = 7.2 Hz), 7.36 (3H, t, *J* = 7.6 Hz), 5.15 (6H, s), 4.76 (6H, d, *J* = 6.0 Hz), 4.09 (6H, d, *J* = 6.0 Hz), 1.00 (9H, s). ^{13}C NMR(CDCl$_3$): 141, 139, 123, 121, 120, 111, 103, 80, 52, 43, 22. IR ν_{max}/cm^{-1}: 2961, 2877, 1605, 1578, 1560, 1469, 1398, 1327, 1298, 1238, 1220, 1184, 1111, 1022, 974, 827, 748, 729. MS m/z (EI): 600, 599, 598 (M$^+$, M100), 407, 306, 251, 157. Combustion analysis: Expected: C, 78.36%; H, 6.58%; N, 7.03%; Obtained: C, 78.17%; H, 6.61%; N, 6.95%.

Tri(2-(1,3-dioxan-2-yl)ethyl) triazatruxene (103)

Sodium hydride (NaH) (0.21 g, 5.082 mmol; 60% dispersion in mineral oil) was added in small portions to a solution of triazatruxene (**85**) (0.30 g, 0.847 mmol) in DMF (40 cm^3) under a nitrogen atmosphere. The mixture was then heated to 50 ^{o}C and (2-(2-bromoethyl)-1,3-dioxane) (0.83 g, 4.235 mmol) was added. The resultant mixture was stirred for 3 h at 50 ^{o}C and then was stirred overnight at room temperature. The reaction mixture was washed with water (100 cm^3), and extracted with DCM (3 × 100 cm^3). The combined organic layers were washed with water (2 × 100 cm^3), dried over magnesium sulphate (MgSO$_4$), filtered and then concentrated down under reduced pressure. The residue was purified using column chromatography [silica, EtOAc/Hexane 5:10] and washed by hexane to afford the desired product as brown solid (0.25 g, 43%).

Melting Point/^{o}C: 236. ^{1}H NMR (CDCl$_3$) δ_H: 8.42 (3H, d, J = 8.0 Hz), 7.70 (3H, d, J = 8.0 Hz), 7.46 (3H, t, J = 7.2 Hz), 7.35 (3H, t, J = 7.2 Hz), 5.16 (6H, t, J = 7.2 Hz), 4.24 (3H, t, J = 4.8 Hz), 3.97 (6H, m), 3.50 (6H, m), 2.22 (6H, m), 2.01 (3H, m), 1.24 (3H, m). ^{13}C NMR (CDCl$_3$): 141, 139, 123, 122, 119, 113, 110, 100, 66, 42, 35, 26. IR ν_{max}/cm^{-1}: 2951, 2852, 1607, 1578, 1468, 1405, 1378, 1327, 1278, 1237, 1190, 1169, 1141, 1073, 1036, 1009, 969, 891, 855, 748, 727. MS m/z (EI): 690, 689, 688 (M$^+$, M100), 612, 524, 433, 304, 251, 157. Combustion analysis: Expected: C, 73.34%; H, 6.59%; N, 6.11%; Obtained: C, 73.30%; H, 6.63%; N, 6.04%.

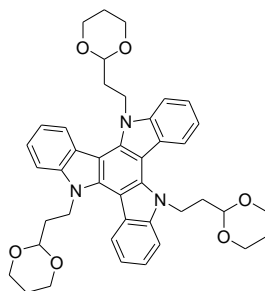**Tri(cyclopropylmethyl) triazatruxene (104)**

Sodium hydride (NaH) (0.21 g, 5.082 mmol; 60% dispersion in mineral oil) was added in small portions to a solution of triazatruxene (**85**) (0.30 g, 0.847 mmol) in DMF (40 cm^3) under nitrogen atmosphere. The mixture was then heated to 50 ^{o}C and (bromomethyl)cyclopropane (0.58 g, 4.235 mmol) was added. The resultant mixture was kept for 3 h at 50 ^{o}C and was then stirred overnight at room temperature. The reaction mixture was washed with water (100 cm^3), and extracted with DCM (3 × 100 cm^3). The combined organic layers were washed with water (2 × 100 cm^3), dried over magnesium sulphate (MgSO$_4$), filtered and then concentrated under reduced pressure. The residue was purified by washing methanol (200 mL) to afford the desired product as a white solid (0.38 g, 87%).

Melting Point/^{o}C: 224. ^{1}H NMR (CDCl$_3$) δ_H: 8.56 (3H, d, J = 8.0 Hz), 7.74 (3H, d, J = 8.0 Hz), 7.47 (3H, t, J = 7.2 Hz), 7.37 (3H, t, J = 7.2 Hz), 4.94 (6H, d, J = 5.2 Hz), 1.41 (3H, m) , 0.53 (6H, m) , 0.35 (6H, m). ^{13}C NMR (CDCl$_3$): 141, 139, 123, 122, 119, 110, 103, 50, 11, 4. IR ν_{max}/cm^{-1}: 2986, 1604, 1561, 1471, 1411, 1385, 1366, 1332, 1294, 1272, 1213, 1174, 1144, 1119, 1025, 982, 934, 873, 830, 807, 752. MS m/z (EI): 509, 508 (M$^+$, M100), 507, 433, 306, 201, 157, 108. Combustion analysis: Expected: C, 85.17%; H, 6.56%; N, 8.28%; Obtained: C, 85.31%; H, 6.45%; N, 8.14%.

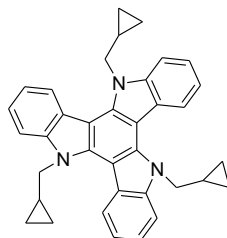**Tri(ethoxyethyl) triazatruxene (105)**

Sodium hydride (NaH) (0.21 g, 5.082 mmol; 60% dispersion in mineral oil) was added in small portions to a solution of triazatruxene (**85**) (0.30 g, 0.847 mmol) in DMF (40 cm^3) under nitrogen atmosphere. The mixture was then heated to 50 $^{\circ}$C and 2-bromoethyl ethyl ether (0.65 g, 4.235 mmol) was added. The resultant mixture was stirred for 3 h at 50 $^{\circ}$C and then was stirred overnight at room temperature. The reaction mixture was washed with water (100 cm^3), and extracted with DCM (3 × 100 cm^3). The combined organic layers were washed with water (2 × 100 cm^3), dried over magnesium sulphate (MgSO$_4$), filtered and then concentrated down under reduced pressure. The residue was purified using column chromatography [silica, EtOAc/Hexane 4:10] to afford the desired product as white solid (0.34 g, 70%).

Melting Point/$^{\circ}$C: 129. ^{1}H NMR (CDCl$_3$) δ_H: 8.37 (3H, d, J = 8.0 Hz), 7.75 (3H, d, J = 8.0 Hz), 7.48 (3H, t, J = 7.2 Hz), 7.37 (3H, t, J = 6.8 Hz), 5.18 (6H, t, J = 7.2 Hz), 3.95 (6H, t, J = 7.2 Hz), 3.46 (6H, q, J = 6.8 Hz), 1.14 (9H, t, J = 7.2 Hz). ^{13}C NMR (CDCl$_3$): 141, 138, 123, 121, 120, 110, 103, 68, 67, 46, 15. IR ν_{max}/cm^{-1}: 2972, 2870, 1606, 1556, 1471, 1407, 1379, 1331, 1294, 1247, 1200, 1176, 1110, 1035, 981, 884, 794, 742, 721. MS m/z (EI): 564, 563, 562 (M$^+$, M100), 338. Combustion analysis: Expected: C, 76.98%; H, 7.00%; N, 7.48%; Obtained: C, 77.13%; H, 7.24%; N, 7.51%.

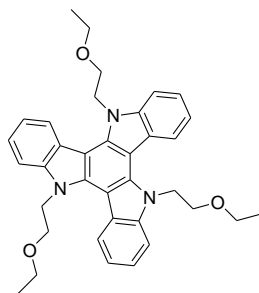**Tri(*N*-ethyl acetyl) triazatruxene (106)**

Sodium hydride (NaH) (0.21 g, 5.082 mmol; 60% dispersion in mineral oil) was added in small portions to a solution of triazatruxene (**85**) (0.30 g, 0.847 mmol) in DMF (40 cm^3) under a nitrogen atmosphere. The mixture was then heated to 50 ^{o}C and 2-bromoethyl acetate (0.71 g, 4.235 mmol) was added. The resultant mixture was stirred for 3 h at 50 ^{o}C and then was stirred overnight at room temperature. The reaction mixture was washed with water (100 cm^3), and extracted with DCM (3 × 100 cm^3). The combined organic layers were washed with water (2 × 100 cm^3), dried over magnesium sulphate (MgSO$_4$), filtered and then concentrated down under reduced pressure. The residue was purified using column chromatography [silica, EtOAc/Hexane 5:10] to afford the desired product as pale-pink solid (0.30 g, 58%).

Melting Point/ ^{o}C: 144. ^{1}H NMR (CDCl$_3$) δ_H: 8.26 (3H, d, *J* = 8.0 Hz), 7.75 (3H, d, *J* = 8.0 Hz), 7.51 (3H, t, *J* = 7.2 Hz), 7.40 (3H, t, *J* = 7.2 Hz), 5.27 (6H, t, *J* = 6.4 Hz), 4.46 (6H, t, *J* = 6.4 Hz), 1.73 (9H, s). ^{13}C NMR (CDCl$_3$): 170, 141, 138, 123, 121, 120, 110, 104, 62, 45, 20. IR ν_{max}/cm^{-1}: 2960, 2856, 1740, 1607, 1584, 1553, 1461, 1403, 1364, 1327, 1288, 1222, 1052, 1036, 955, 929, 866, 815, 793, 752, 728. MS m/z (EI): 605, 604 (M$^+$, M100), 603, 546, 391, 338, 223, 157. Combustion analysis: Expected: C, 71.63%; H, 5.51%; N, 6.96%; Obtained: C, 71.86%; H, 5.59%; N, 6.97%.
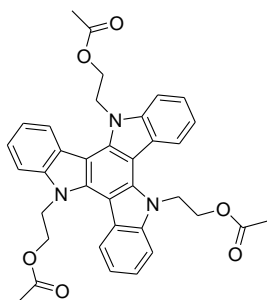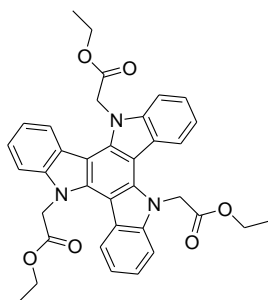
Tri(*N*-acetyl ethyl) triazatruxene (107)

Sodium hydride (NaH) (0.21 g, 5.082 mmol; 60% dispersion in mineral oil) was added in small portions to a solution of triazatruxene (**85**) (0.30 g, 0.847 mmol) in DMF (40 cm^3) under nitrogen atmosphere. The mixture was then heated to 50 ^{o}C and ethyl bromoacetate (0.71 g, 4.235 mmol) was added. The resultant mixture was stirred for 3 h at 50 ^{o}C and then was stirred overnight at room temperature. The reaction mixture was washed with water (100 cm^3), and extracted with DCM (3 × 100 cm^3). The combined organic layers were washed with water (2 × 100 cm^3), dried over magnesium sulphate (MgSO$_4$), filtered and then concentrated down under reduced pressure. The residue was purified using column chromatography [silica, EtOAc/Hexane 4:10] to afford the desired product as pale-pink solid (0.37 g, 71%).

Melting Point/ ^{o}C: 186. ^{1}H NMR (CDCl$_3$) δ_H: 8.08 (3H, d, *J* = 8.0 Hz), 7.44 (6H, m), 7.35 (3H, m), 5.54 (6H, s), 4.37 (6H, q, *J* = 6.8 Hz), 1.30 (9H, t, *J* = 7.2 Hz). ^{13}C NMR (CDCl$_3$): 169, 142, 139, 124, 123, 121, 120, 110, 104, 62, 50, 14. IR ν_{max}/cm^{-1}: 2979, 2876, 1735, 1609, 1580, 1468, 1429, 1404, 1364, 1328, 1298, 1192, 1119, 1039, 1023, 962, 869, 830, 775, 725. MS m/z (EI): 605, 604 (M$^+$, M100), 603, 419. Combustion analysis: Expected: C, 71.63%; H, 5.51%; N, 6.96%; Obtained: C, 71.78%; H, 5.60%; N, 6.94%.

Tri(isocyanatoethyl) triazatruxene (108)

Sodium hydride (NaH) (0.21 g, 5.082 mmol; 60% dispersion in mineral oil) was added in small portions to a solution of triazatruxene (**85**) (0.30 g, 0.847 mmol) in DMF (40 cm^3) under nitrogen atmosphere. The mixture was then heated to 50 ^{o}C and 2-bromoethyl isocyanate (0.64 g, 4.235 mmol) was added. The resultant mixture was stirred for 3 h at 50 ^{o}C and then was stirred overnight at room temperature. The reaction mixture was washed with water (100 cm^3), and extracted with DCM (3 × 100 cm^3). The combined organic layers were washed with water (2 × 100 cm^3), dried over magnesium sulphate (MgSO$_4$), filtered and then concentrated down under reduced pressure. The residue was purified using column chromatography [silica, EtOAc/Hexane 15:10] and washed by hexane to afford the desired product as pale-pink solid (0.19 g, 38%).

Melting Point/ ^{o}C: > 280. ^{1}H NMR (CDCl$_3$) δ_H: 8.34 (3H, d, J = 8.0 Hz), 7.87 (3H, d, J = 7.2 Hz), 7.52 (3H, t, J = 6.8 Hz), 7.46 (3H, t, J = 7.6 Hz), 4.56 (6H, t, J = 9.6 Hz), 4.30 (6H, t, J = 9.6 Hz). ^{13}C NMR (CDCl$_3$): 140, 134, 125, 123, 122, 119, 114, 109, 67. IR ν_{max}/cm^{-1}: 2987, 2876, 1660, 1594, 1460, 1407, 1369, 1325, 1267, 1236, 1196, 1157, 1127, 1098, 1029, 925, 825, 778, 748, 731. MS m/z (EI): 512, 511 (M$^+$, M100), 510, 277. Combustion analysis: Expected: C, 70.58%; H, 3.55%; N, 16.46%; Obtained: C, 70.49%; H, 3.62%; N, 16.44%.
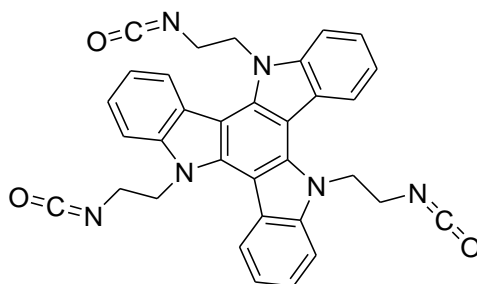
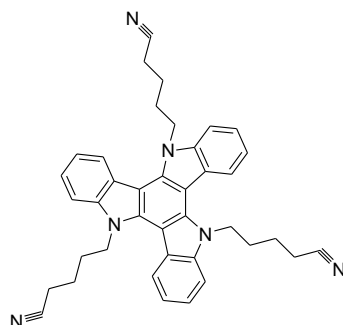**Tri(pentanenitrilyl) triazatruxene (109)**

Sodium hydride (NaH) (0.21 g, 5.082 mmol; 60% dispersion in mineral oil) was added in small portions to a solution of triazatruxene (**85**) (0.30 g, 0.847 mmol) in DMF (40 cm^3) under nitrogen atmosphere. The mixture was then heated to 50 ^{o}C and 5-bromovaleronitrile (0.69 g, 4.235 mmol) was added. The resultant mixture was stirred for 3 h at 50 ^{o}C and then was stirred overnight at room temperature. The reaction mixture was washed with water (100 cm^3), and extracted with DCM (3 × 100 cm^3). The combined organic layers were washed with water (2 × 100 cm^3), dried over magnesium sulphate (MgSO$_4$), filtered and then concentrated under reduced pressure. The residue was purified using column chromatography [silica, EtOAc/hexane 4:10] to afford the desired product as yellow solid (0.34 g, 70%).

Melting Point/^{o}C: 98. ^{1}H NMR (CDCl$_3$) δ_H: 8.24 (3H, d, J = 8.0 Hz), 7.66 (3H, d, J = 8.0 Hz), 7.51 (3H, t, J = 7.2 Hz), 7.41 (3H, t, J = 7.2 Hz), 5.07 (6H, t, J = 7.2 Hz), 2.12 (6H, t, J = 7.2 Hz), 2.01 (6H, m), 1.35 (6H, m). ^{13}C NMR (CDCl$_3$): 143, 140, 137, 135, 131, 128, 122, 121, 120, 116, 110, 103, 58, 56, 29, 23, 17. IR ν_{max}/cm^{-1}: 2952, 2857, 2238, 1606, 1563, 1458, 1422, 1402, 1381, 1325, 1283, 1210, 1174, 1071, 1028, 984, 895, 818, 795, 768, 725. MS m/z (EI): 591, 590, 589 (M$^+$, M100), 358, 157, 108. Combustion analysis: Expected: C, 79.56%; H, 6.16%; N, 14.27%; Obtained: C, 79.62%; H, 6.11%; N, 14.26%.

3.5 OLEDs

3.5.1 OLED Fabrication

The test OLEDs were fabricated by colleagues from Polar OLED as follows. A glass substrate was first coated with transparent indium tin oxide (ITO) as the anode. Then commercially available *poly*(3,4-ethylenedioxythiophene):polystyrenesulfonate (PEDOT:PSS) from Sigma-Aldrich Corp. was deposited from aqueous solution by spin coating (2000 rpm for 30s) using Laurell WS-400-6NPP-Lite Spin Processer as the hole-injection layer (30 nm). The film thickness was measured using Dektak. *N*4,*N*4'-*bis*(4-{6-[(3-Ethyloxetan-3-yl)methoxy]hexyl}phenyl)-*N*4,*N*4'-diphenylbiphenyl-4,4'-diamine (OTPD), purchased from Luminescence Technology Corp., was deposited from a 0.5 wt% in toluene solution by spin-coating (2000 rpm for 30s) to form a hole-transporting layer (15 nm) on top of the PEDOT/PSS hole-injection layer after photochemical crosslinking under 100 J/cm^2 UV with 0.5 wt% (4-octyloxyphenyl) phenyliodonium hexafluoroantimonate (OPPI) as a photoinitiator and being annealed 110 $^\circ$C for 5 min. A thin layer (20 nm) of compounds **38**, **41**, **42**, **49** and **53** was then deposited as the emissive layer by spincoating at 2000 rpm for 30 s from solution (1 wt% in toluene). A layer (20 nm) of 2,7-*bis*(diphenylphosphoryl)-9,9'-spirobifluorene (SPPO13) was used as electron-transporting layer deposited by thermal evaporation using Thermal Evaporator purchased from Glove Box Technology Ltd. at a pressure of 8 x 10^{-6} mbar, followed by a layer (1 nm) of lithium fluoride, used as the electron-injection layer. An aluminum (100 nm) cathode was deposited last under the same vacuum conditions. A general schematic representation of the configuration of the five OLEDs fabricated is shown in **Fig. 3.1**.

Cathode

⊖

| Electrode (100 nm Al) |
| 1 nm LiF
Electron-injection Layer |
| 20 nm SPPO13
Electron-transporting Layer |
| 1wt% Compound
Emissive Layer |
| 0.5wt% OTPD
Cross-linked Hole-transporting Layer |
| PEDOT:PSS, Hole-injection Layer |
| ITO, Substrate, Transparent |

⊕

Anode
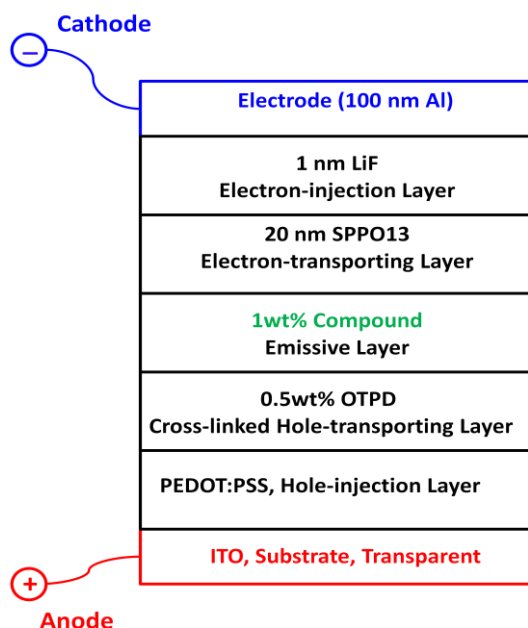
NB: Compounds 38, 41, 42, 49 and 53 as emissive layers
were used in different OLED devices, respectively.

Fig. 3.1 The general schematic representation of OLED devices with 1 wt%
compounds **38, 41, 42, 49** and **53** as different emissive layers, respectively.

3.5.2 OLED Performance Evaluation

The compounds **38**, **41**, **42**, **49** and **53** were investigated as emissive materials in
OLEDs by colleagues in Polar OLED. Five OLEDs were fabricated differeing only in
the nature of the emissive layer, i.e., compounds **38**, **41**, **42**, **49** and **53**, and their
performance, including current density, brightness, efficiency and electroluminescent
(EL) intensity, was measured. LS-100 Luminance Meter from KINICA MINOLTA and
KEITHLEY 2401 Sourcemeter were both controlled by Labview 2012 Program to
give current density, brightness and device efficiency of OLEDs. AvaSpec-2048-SPU
Spectrometer from AVANTES was used to measure Electroluminescent (EL) intensity
of OLED devices.

191

3.6 Charge Carrier Mobility Measurements for Triazatruxenes

3.6.1 Conductivity Measurement

Conductivity traditionally refers to electrical conductivity, which means a material's ability to conduct an electric current. However, in terms of organic electronics, conductivity generally refers to ionic conductivity, which represents ionic charge carrier mobility, especially when the mechanism was found that charge transport was ionic in nature, not electronic[34].

Conductivity measurements were carried out using pre-patterned 50 µm ITO finger electrodes, see **Fig. 3.2**. Current-voltage data was determined using a Keithley SMU and Electrical probe station (2-probe measurement). **Equation 1**[35] was used to measure the conductivity, as follows:

$$\sigma = (d/A) \text{ x } (dI/dV) \qquad \textbf{Eq. 1}$$

where σ is conductivity, d is distance between finger electrodes, A is total area equal to film thickness (T) times length (L) of finger electrodes, (dI/dV) is linear fits to current-voltage curve.
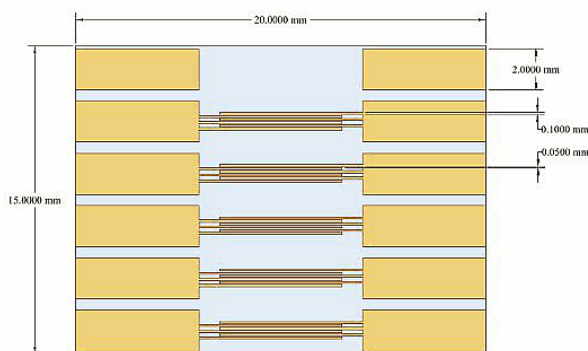
Fig. 3.2 the schematic representation of pre-patterned 50 µm ITO fingers

In order to investigate the effect on the hole-transport properties of the triazatruxene, triazatruxene **100** was chosen as a typical example of this class of materials. 1 wt % of the compound **100** in chlorobenzene was spun coated (2000 rpm for 30s) onto a plasma treated ITO substrate and its current-voltage curves were recorded using both LS-100 Luminance Meter from KINICA MINOLTA and KEITHLEY 2401 Sourcemeter.

3.6.2 Hole-only Test Device Fabrication and Evaluation

In order to further study the effect of cross-linking and doping on conductivity, four hole devices with different hole-transporting layers were fabricated. The schematic representation of these hole-only diode test devices is shown in **Fig. 3.3.** The glass substrate is coated with a thin transparent layer of indium tin oxide (ITO) as the anode. Commercial poly(3,4-ethylenedioxythiophene):polystyrenesulfonate (PEDOT:PSS) purchased from Sigma-Aldrich Corp., is the common hole-injection layer. The hole-transporting material for each individual device includes compound **100**, cross-linked compound **100**, compound **100** doped with 5 wt% 2,3,5,6-tetrafluoro-7,7,8,8-tetracyanoquinodimethane (F4-TCNQ), and cross-linked compound **100** doped with 5 wt% F4-TCNQ. The cathode is made up of a 100 nm aluminum (Al) layer.

NB. Once each of these individual devices has been tested it cannot be tested again due to morphology changes in the hole-transport layers under investigation and charge traps that may have happened during the first scan.
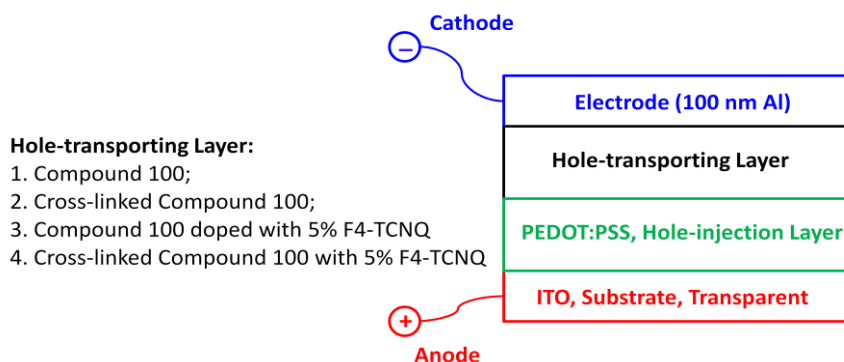
Fig. 3.3 The schematic representation of hole devices

These four hole devices were run under no higher than 10 V of voltage which are consistent with real OLED device. LS-100 Luminance Meter from KINICA MINOLTA and KEITHLEY 2401 Sourcemeter were both controlled by Labview 2012 Program to give the data of current density.

3.7 Cyclic Voltammetry and UV-Visible Absorption

A potentiodynamic electrochemical cyclic voltammetre (CV) with glassy carbon working electrode, silver reference electrode, and platinum counter electrode for potentiodynamic scanning and further equipped with a computer-controlled μ Autolab TypeⅢ scanning potentiostat from METROHM was used to measure the ionisation potential of the organic semiconductors synthesised in this thesis. A sample solution was first coated onto a glassy carbon working electrode using 1 mM of the material dissolved in an initial electrolyte [0.3 M tetrabutylammoniumhexafluorophosphate (TBAHFP) in dichloromethane] and a cyclic voltammetry scan was carried out. This procedure was then repeated using a standard material (1 mM ferrocene in this case)[21]. **Fig. 3.4 (a)** and **(b)** shows cyclic voltammetry scanning curves of the organic semiconductor **14** and the ferrocene, used for calibration, respectively.

(a)   **(b)**
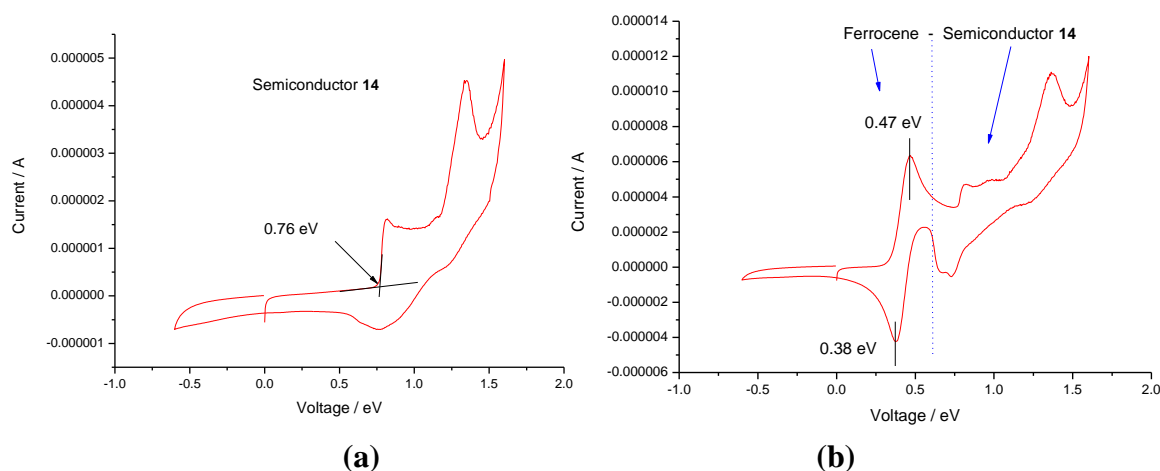
Fig. 3.4 The cyclic voltammetry scanning curves of semiconductor **14** and ferrocene

The **Equation 2**[21] was used to calculate HOMO energy level (IP), as follows:

$$IP\ (eV) = E_{ex} - E^{Fe}_{1/2} + 0.425 + 4.7 \qquad \textbf{Eq. 2}$$

Where E_{ex} is the onset voltage of the semiconductor peak, $E^{Fe}_{1/2}$ is the average voltage from calibration sample ferrocene peaks of oxidation and reduction [(Max+Min)/2], the constant 0.425 eV is that for the ferrocene standard and 4.7 eV is for the oxidation level of electrode silver-silverchloride. Therefore, as shown in the **Fig. 3.4**,

$E_{ex} = 0.76$ eV and $E^{Fe}_{1/2} = [(0.47+0.38)/2] = 0.425$ eV

Thus the ionisation potential (IP) of compound **14** is 5.46 eV.

Evolution 220 UV-Visible spectrophotometer from Thermo Scientific was used to record the absorption of organic semiconductors. **Fig. 3.5** shows the UV-Vis absorption curve of semiconductor **14**.
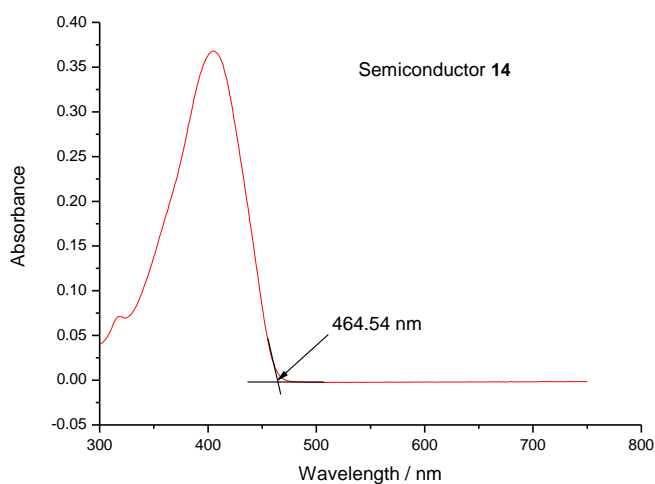
Fig. 3.5 the UV-Vis absorption curve of the organic semiconductor **14**

Equation 3[36] was used to calculate energy gap of HOMO and LUMO (Eg), as follows:

$$Eg \ (eV) = hc/\lambda = 1240/\lambda \ (\lambda: nm) \qquad \textbf{Eq. 3}$$

Where h is the Planck constant (4.135×10^{-15} eV s), c is the speed of light (3.0×10^{17} nm/s), hc = 1240 eV nm and λ is the absorption maximum (nm) extracted from the Uv-vis absorption spectrum of the compound being investigated.

Therefore, as shown in the **Fig. 3.5** for the semiconductor **14**, λ = 464.54 nm, the band gap, Eg, of semiconductor **14** can be calculated as

$Eg = 1240/464.54 = 2.67$ eV

The LUMO energy level (EA) was estimated by the subtraction of the value of the optical band gap (Eg) from the ionisation potential (IP), which does not include any correction for the exciton binding energy.

3.8 References

[1]   A. Baba, K. Onishi, W. Knoll and R. C. Advincula, *J. Phys. Chem. B.,* 2004, **108**, 18949.

[2]   L. Zhang, L. Zou, J. Xiao, P. Zhou, C. Zhong, X. Chen, J. Qin, I. F. A. Mariz and E. Macoas, *J. Mater. Chem.,* 2012, **22**, 16781.

[3]   S. Wakim, J. Bouchard, M. Simard, N. Drolet, Y. Tao and M. Leclerc, *Chem. Mater.,* 2004, **16**, 4386.

[4]   A. V. Dijken, J. J. A. M. Bastiaansen, N. M. M. Kiggen, B. M. W. Langeveld, C. Rothe, A. Monkman, I. Bach, P. Stossel and K. Brunner, *J. Am. Chem. Soc.,* 2004, **126**, 7718.

[5]   D. A. Patrick, D. W. Boykin, W. D. Wilson, F. A. Tanious, J. Spychala, B. C. Bender, J. E. Hall, C. C. Dykstra, K. A. Ohemeng and R. R. Tidwell, *Eur. J. Med. Chem.,* 1997, **32**, 781.

[6]   J. W. Choi, C. Kulshreshtha, G. P. Kennedy, J. H. Kwon, S. H. Jung and M. Chae, Sol. Energ. Mat. Sol. C., *Solar Energy Materials and Solar Cells,* 2011, **95**, 2069.

[7]   D. R. Coulson, L. C. Satek and S. O. Grim, *Inorg. Synth.,* 2007, **13**, 121.

[8]   W. C. Tsoi, M. O'Neill, M. P. Aldred, S. P. Kitney, P. Vlachos and S. M. Kelly, *Chem. Mater.,* 2007, **19**, 5475.

[9]   K. L. Woon, M. P. Aldred, P. Vlachos, G. H. Mehl, T. Stirner, S. M. Kelly and M. O'Neill, *Chem. Mater.,* 2006, **18**, 2311.

[10]   M. Franceschin, L. Ginnari-Satriani, A. Alvino, G. Ortaggi and A. Bianco, *Eur.*

J. Org. Chem., 2010, 134.

[11]   N. Robertson, S. Parsons, E. J. MacLean, R. A. Coxall and A. R. Mount, *J. Mater. Chem.,* 2000, **10**, 2043.

[12]   L. Ginnari-Satriani, V. Casagrande, A. Bianco, G. Ortaggi and M. Franceschin, *Org. Biomol. Chem.,* 2009, **7**, 2513.

[13]   T. Bura, N. Leclerc, S. Fall, P. Leveque, T. Heiser and R. Ziessel, *Org.. Lett.,* 2011, **13**, 6030.

[14]   F. Gallego-Gomez, E. M. Garcia-Frutos, J. M. Villalvilla, J. A. Quintana, E. Gutierrez-Puebla, A. Monge, M. A. Diaz-Garcia and B. Gomez-Lor, *Adv. Funct. Mater.,* 2011, **21**, 738.

[15]   M. S. Yuan, T. B. Li, W. J. Wang, Z. T. Du, J. R. Wang and Q. Fang, *Spectrochim. Acta Part A: Mol. Biomol. Spectrosc.,* 2012, **96**, 1020.

[16]   R. N. Prasad Tulichala and K. C. Kumara Swamy, *Chem. Commun.,* 2015, **51**, 12008.

[17]   R. M. Kellogg, A. P. Schaap and H. Wynberg, *J. Org. Chem.,* 1969, **34**, 343.

[18]   A. Pelter, I. Jenkins and D. E. Jones, *Tetrahedron,* 1997, **53**, 10357.

[19]   P. Riberau and P. Pastour, *Bull. Soc. Chim. Fr.,* 1969, 2076.

[20]   M. P. Aldred, R. Hudson, S. P. Kitney, P. Vlachos, A. Liedtke, K. L. Woon, M. O'Neill and S. M. Kelly, *Liquid Crystals,* 2008, **35**, 413.

[21]   PhD Thesis of W. Bao, "*Liquid Crystalline Organic Semiconductors for Application in Opto-electronic Devices*", University of Hull, 2014.

[22]   P. Berrouard, F. Grenier, J. Pouliot, E. Gagnon, C. Tessier and M. Leclerc, *Org.*

Lett., 2011, **13**, 38.

[23]   P. Berrouard, S. Dufresne, A. Pron, J. Veilleux and M. Leclerc, *J. Org. Chem.,* 2012, **77,** 8167.

[24]   A. Najari, S. Beaupre, P. Berrouard, Y. Zou, J. Pouliot, C. Lepage-Perusse and M. Leclerc, Adv. Funct. Mater., 2011, 21, 718.

[25]   H. Yamanishi, I. Tomita, K. Ohta and T. Endo, *Mol. Cryst. Liq. Cryst.,* 2001, **369**, 47.

[26]   PhD Thesis of M. R. Billa, "*Liquid Crystalline Organic Semiconductors for Application in Opto-electronic Devices*", University of Hull, 2014.

[27]   F. S. Manciha, B. A. DaSilveira Neto, A. S. Lopes, P. F. Moreira Jr., F. H. Quina, R. S. Goncalves and J. Dupont, *Eur. J. Org. Chem.,* 2006, **21**, 4924.

[28]   G. Y. Chen, S. C. Lan, P. Y. Lin, C. W. Chu and K. H. Wei, *J. Polym. Sci. Part A: Polym. Chem.,* 2010, **48**, 4456.

[29]   K. Yui, Y. Aso, T. Otsubo and F. Ogura, *Bull. Chem. Soc. Jpn.,* 1989, **62**, 1539.

[30]   A. Yokooji, T. Satoh, M. Miura and M. Nomura, *Tetrahedron*, 2004, **60**, 6757.

[31]   T. Keumi, T. Umeda, Y. Inoue and H. Kitajima, *Bull. Chem. Soc. Jpn.,* 1989, **62**, 89.

[32]   PhD Thesis of S. P. Kitney, "*Liquid Crystalline Semiconductors for Organic Electronics*", University of Hull, 2008.

[33]   J. Shao, Z. Guan, Y. Yan, C. Jiao, Q. Xu and C. Chi, *J. Org. Chem.,* 2011, **76**, 780.

[34]   Book, *"Flat Panel Display: Advanced Organic Materials",* by S. M. Kelly,

The Royal Society of Chemistry, Cambridge, 2000.

[35]   Y. Wang, G. Han, Z. Tian, M. Wang, J. Li and X. Wang, *RSC Adv.,* 2014, **4,** 47129.

[36]   M. M. Ahmida and S. H. Eichhorn, *ESC Transactions*, 2010, **25**, 1.

4 Results and Discussion

4.1 Discussion of Synthetic Reactions

Plastic electronics are replacing silicon for many consumer electronic applications, such as Organic Light-Emitting Diodes (OLEDs) and Organic Photovoltaics (OPVs), thereby creating new markets and devices. Aromatic compounds are an important source of organic semiconductor materials, due in part to their high degree of conjugation in the aromatic molecular cores. These conjugated systems typically exhibit a high degree of delocalization, which can render organic compounds conductive under certain conditions. Therefore, it is of interest to synthesise novel organic materials containing aromatic cores for the further development of the optoelectronic industry. In this thesis, a wide range of intermediates and final organic compounds were synthesised and different reaction conditions were investigated and optimised when possible. A brief discussion of the syntheses was included in the Experimental Chapter. The following discussion will provide more detailed comparison and analysis for some important reactions used in this thesis, which includes aryl-aryl coupling reactions and *N*-position functionalization of carbazole moieties.

4.1.1 Carbon-carbon bond formation using aryl-aryl cross-coupling reactions

Aryl carbon-carbon (C-C) single bond formation is of vital importance in synthetic organic chemistry. Generally, this process can be achieved with one arene functionalised with a halogen atom, e.g., bromine or iodine, reacting with the other arene containing organometallic moiety, e.g., -B(OH)$_3$, -Sn(Bu)$_3$, -Mg, which are representative of Suzuki Coupling, Stille Coupling and Grignard reaction, respectively. Sometimes direct arylation through C-H bond activation and cleavage is favoured to form aryl C-C bonds, due to a reduction in the number of synthetic steps required to achieve the same conversion. However, the direct arylation method is not always

effective for aryl C-C bond formation. For instance, the direct alylation reactions to create compound **9** by a direct arylation reaction between compounds **5** and **7**, and that to yield compound **14** from compounds **5** and **12** using DMF or NMP as solvent, were unsuccessful as shown in **Fig. 4.1**.
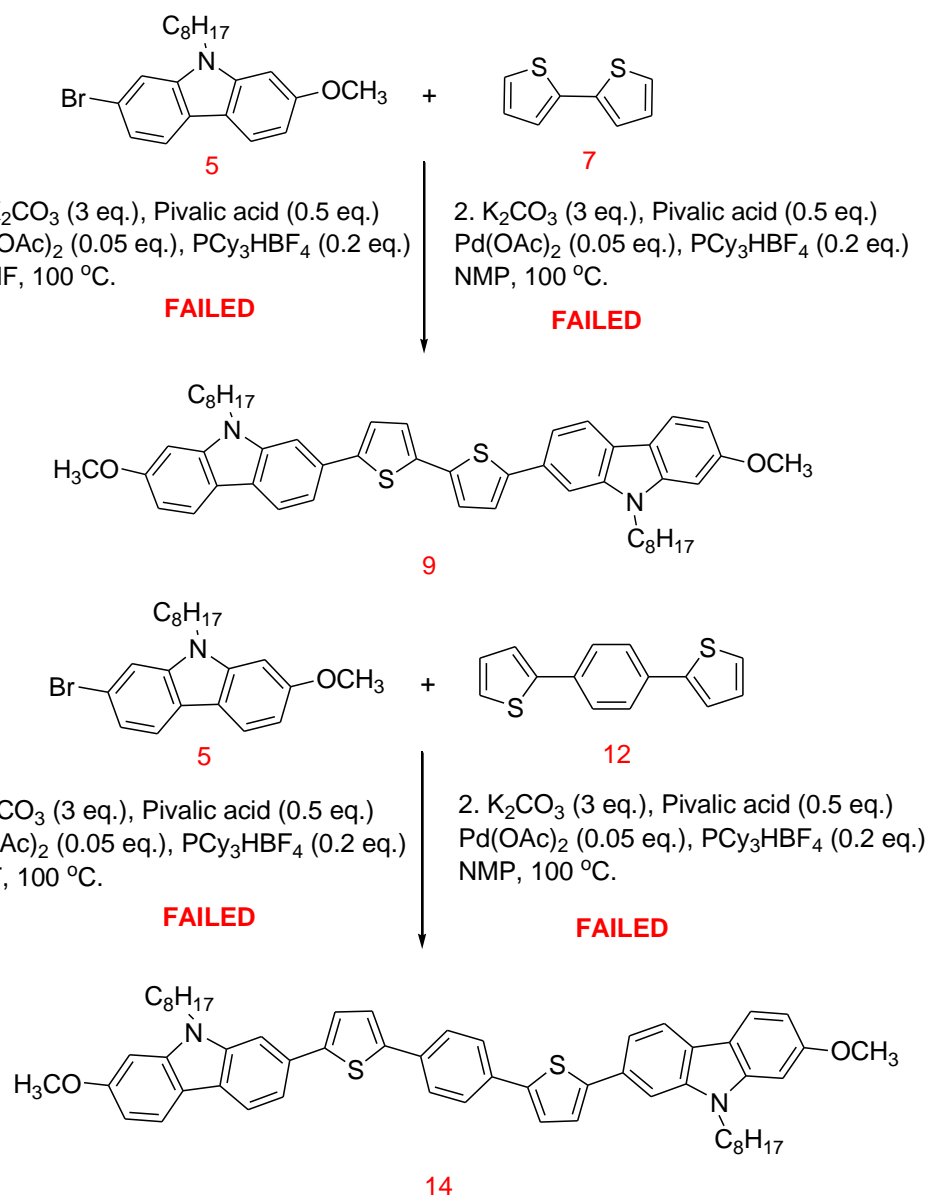
Fig. 4.1 Direct arylation pathway for synthesising compounds **9** and **14** (both with 3 equivalents of starting material **5**)

In theory, thiophene moieties are excellent substrates for direct arylation reactions, due to the typically facile palladation through a concerted metalation-deprotonation (CMD) pathway, which renders the reaction highly selective for the 2- or 5-positions of the thiophene moieties[1]. Therefore, compounds **7** and **12** should be ideal as starting

materials for direct arylation reactions. In this work, this reaction failed. According to the CMD mechanism of direct arylation[2-3], the reaction steps include the oxidative addition of palladium to the C-Br bond of an aryl bromide, the exchange of the halogen ligand, deprotonation of the thiophene substrate with simultaneous formation of a metal-carbon bond, then the formation of an important transition state that determines whether the direct arylation can be achieved or not, and reductive elimination of the transition state. The energy required to form the transition state can be divided into two components including the energy of distorting the C-H bond of thiophene moiety and the interaction energy between distorted fragment and palladium centre, according to density functional theory (DFT) calculations of the CMD mechanism[3-4]. The bromo-substituted carbazole-derivate is sterically bulky and may, therefore, require more energy to form a palladium active centre to react with the distorted C-H bond of thiophene moiety. Furthermore, the bulky structure of the bromo-substituted carbazole-derivate is more likely to trap the palladium centre, preventing the closing of distorted C-H bond. Therefore, as direct arylation was not possible, compound **5** was first lithiated, quenched with a boronate ester and then hydrolysed to obtain the corresponding carbazole-derivate boronic acid. Compounds **7** and **12** were brominated in the required positions. Finally, Suzuki aryl-aryl cross-coupling reactions were carried out to obtain compounds **9** and **14** with good yields, respectively, as shown in the Experimental Chapter.

Compared with specific requirements for C-H bond and C-Br bond of direct arylation, Suzuki aryl-aryl coupling reactions are more tolerant of other functional groups present on the reagents and are also more tolerant of the steric demands of the reactants. In this thesis, a broad range of final compounds and intermediates were synthesised *via* Suzuki aryl-aryl cross-coupling reactions between aryl boronic acids and aryl bromides. Overall, the Suzuki reactions reported in this thesis worked well. A set of Suzuki coupling reactions under different catalyst and solvent were investigated and compared as shown below in **Tab. 4.1**.

Tab. 4.1 The reactants, solvent, catalyst and yield of Suzuki aryl-aryl cross-coupling reactions carried out under consistent temperature and base conditions.
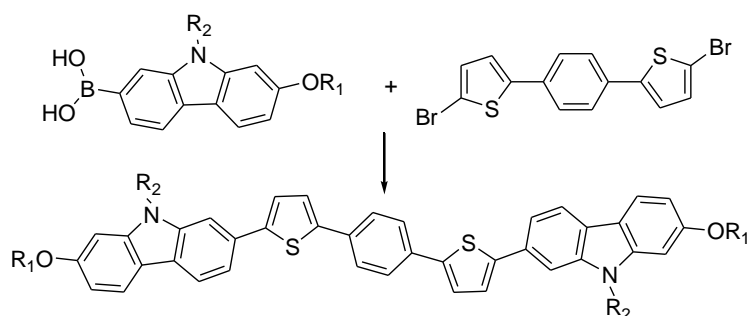
Compound	Boronic Acid		Solvent	Catalyst	Yield
	R_1	R_2			(%)
14	CH_3	C_8H_{17}	DME	$Pd(OAc)_2+P(Ph)_3$	60
14	CH_3	C_8H_{17}	DME	$Pd(PPh_3)_4$	71
14	CH_3	C_8H_{17}	DMF	$Pd(PPh_3)_4$	73
14	CH_3	C_8H_{17}	DMF	$Pd(OAc)_2$	76
39	C_8H_{17}	C_8H_{17}	DMF	$Pd(PPh_3)_4$	73
39	C_8H_{17}	C_8H_{17}	DMF	$Pd(OAc)_2$	72
58	C_8H_{17}	$C_{12}H_{25}$	DME	$Pd(OAc)_2+P(Ph)_3$	62
64	CH_3	$CH(C_8H_{17})_2$	DME	$Pd(OAc)_2+P(Ph)_3$	76
67	C_8H_{17}	$CH(C_8H_{17})_2$	DME	$Pd(OAc)_2+P(Ph)_3$	46

All reactions were carried out using 3.0 equivalent of aryl boronic acid, aqueous K_2CO_3 as base, under N_2 atmosphere at 80 ^{o}C for DMF or reflux for DME.

The efficacy of three different catalyst systems, i.e., $Pd(OAc)_2$, $Pd(PPh_3)_4$ and a combination of $Pd(OAc)_2$ and $P(Ph)_3$, was investigated in the Suzuki aryl-aryl, cross-coupling reactions reported in this thesis. It was found that using a combination of $Pd(OAc)_2$ and $P(Ph)_3$ to generate an active catalyst *in situ* typically led to a lower isolated yield than either using either $Pd(OAc)_2$ or $Pd(PPh_3)_4$. Traditionally, the presence of the triphenyl-phosphine ligand is considered beneficial in palladium-catalysed Suzuki aryl-aryl cross-coupling reactions, helping stabilise the zero valence state of the palladium nanoparticles required for the catalytic reaction and

produce higher yields. However, it was found that the reaction mixture was more difficult to purify, due to the formation of more by-products in the presence of added triphenyl phosphine, which led to the lower isolated yields. In addition, commercially sourced $Pd(PPh_3)_4$ led too poor yields in these Suzuki coupling reactions. Degradation of catalyst was assumed to be the cause of this phenomenon. Hence, fresh *tetrakis*(triphenylphosphine)palladium(0) was synthesised in very good yield using palladium dichloride, triphenyl phosphine, dimethyl sulphoxide and hydrazine hydrate (87%). Therefore, the $Pd(PPh_3)_4$ catalyst used in this thesis was made in the laboratory and stored under a nitrogen atmosphere. Furthermore, it should be pointed out that the $Pd(OAc)_2$-catalysed ligand-free system led to isolation of comparable yields as those obtained with $Pd(PPh_3)_4$ as catalyst. Actually, the 'ligandless' $Pd(OAc)_2$ catalytic systems have been researched and reported for many years and some authors have pointed out that phosphine ligands can act as an inhibitor to reaction progress, limiting catalytic efficiency for certain Suzuki reactions[5-10].

Common polar solvents, such as DMF, DME, or THF, were used in the Suzuki aryl-aryl cross-coupling reactions reported in this thesis. The use of a polar solvent, with a greater basicity and nucleophilicity than non-polar solvents, could facilitate coordination of the polar solvent to the palladium species in the transition state, to form solvent-coordinated transition states that favour oxidative insertion[11]. Water-DMF solvent systems are widely used in Suzuki reactions and show good yield for ligand-free catalyst systems[10]. On the other hand, DME exhibits good solubility for boronic acid reactant and the aqueous base, so that a more homogeneous reaction system is obtained. However, the solubility of starting materials and reaction systems should also be considered when the solvent is chosen for Suzuki reactions.

As shown in **Tab. 4.1**, the yield of compound **64** (76%) with a branched alkyl chain (R_2 = $CH(C_8H_{17})_2$) in the *N*-position, is higher than that of compounds **14** (60%) and **58** (62%) with both straight alkyl chains (R_2 = C_8H_{17} and $C_{12}H_{25}$, respectively) in the *N*-position using a combination of $Pd(OAc)_2$ and $P(Ph)_3$ as catalyst. One possible

reason is that longer and more branched alkyl chains increase the solubility of the reactants in DME. However, compound **67** with long alkyl chains ($R_1 = C_8H_{17}$) and a branched chain ($R_2 = CH(C_8H_{17})_2$) exhibits a lower yield. The reason might be a lower purity of the boronic acid reactant, which is colourless oil in this case and was used directly for next step, due to difficulty in purification.

4.1.2 *N*-position of carbazole moiety substituted reactions

The nature of the alkyl chain in the *N*-position of the carbazole moiety plays an important role in controlling the physical properties of the final materials. In terms of reaction mechanism of *N*-substitution of carbazoles[12], the triazatruxene core is susceptible to electrophilic hydrogen exchange at the nitrogen atoms. Specifically, strong bases, such as KOH or NaH, can deprotonate the N-H bond of the carbazole moiety to give either a N-K or N-Na combination, which can then react with an aliphatic bromide. In the case of the synthesis of symmetrical carbazole-derivatives, all the *N*-positions were alkylated successfully with the desired alkyl groups. These alkylation reactions appeared not to be sensitive to the nature of the base or the solvent.

The yields for the carbazole-derivatives (**5**, **36** and **55**) all exceeded 80%. However, functionalization of all of the *N*-positions of triazatruxene by a wide range of aliphatic bromides or alicyclic bromides proved to be difficult. The nature of the specific functional groups incorporated into the alicyclic or aliphatic bromides, including C-C double bonds, C-C triple bonds, non-conjugated dienes, cyclic ether, ester, nitrile, isocyanate, isothiocyanate, was found to affect the yield of these alkylation reactions. Therefore, the investigation, comparison and analysis of reaction conditions for *N*-substitution of triazatruxene are shown in **Tab. 4.2**.

Tab. 4.2 The reactants, base, solvent and yield of alkylation reactions of triazatruxene carried out under standard conditions.
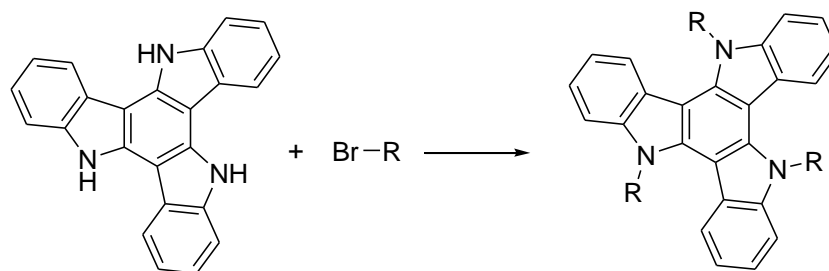
Compound	R	Base	Solvent	Yield/%
86	$-C_8H_{17}$	KOH	THF	73
87	$-C_6H_{13}$	NaH	DMF	88
88	$-C_4H_9$	NaH	DMF	81
92	$-(CH_2)_{10}COOCH(CH=CH_2)_2$	K_2CO_3	DMF	Failed
92	$-(CH_2)_{10}COOCH(CH=CH_2)_2$	KOH	THF	Failed
92	$-(CH_2)_{10}COOCH(CH=CH_2)_2$	NaH	DMF	36
89	$-CH_2CH=CH_2$	NaH	DMF	75
90	$-(CH_2)_4CH=CH_2$	NaH	DMF	75
91	$-CH_2C\equiv CCH_2$	NaH	DMF	62
F01	$-CH_2CH_2CH_2C\equiv CH$	NaH	DMF	Failed
F01	$-CH_2CH_2CH_2C\equiv CH$	K_2CO_3	DMF	Failed
F01	$-CH_2CH_2CH_2C\equiv CH$	K_2CO_3	Butanone	Failed

All reactions were carried out using 5.0 equivalent of BrR under N_2 atmosphere at 50 ^oC for NaH/DMF, 50 ^oC for K_2CO_3/DMF, reflux for KOH/THF or K_2CO_3/Butanone.

Tab. 4.2 (continued) The reactants, base, solvent and yield of alkylation reactions of triazatruxene carried out under standard conditions.
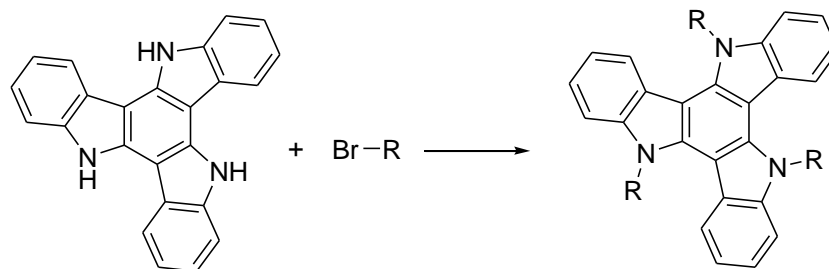
Compound	R	Base	Solvent	Yield/%
96	-(CH$_2$)$_4$CON(CH$_2$CH=CH$_2$)$_2$	NaH	DMF	86
100	-CH$_2$CON(CH$_2$CH=CH$_2$)$_2$	NaH	DMF	46
101		NaH	DMF	42
102		NaH	DMF	58
108	-CH$_2$N=C=O	NaH	DMF	38
F02	-CH$_2$N=C=S	NaH	DMF	Failed
F02	-CH$_2$N=C=S	K$_2$CO$_3$	Butanone	Failed
103		NaH	DMF	43
104		NaH	DMF	87
105	-CH$_2$CH$_2$OCH$_2$CH$_3$	NaH	DMF	70
106	-CH$_2$CH$_2$OCOCH$_3$	NaH	DMF	58
107	-CH$_2$COOCH$_2$CH$_3$	NaH	DMF	71
109	-(CH$_2$)$_4$CN	NaH	DMF	70

All reactions were carried out using 5.0 equivalent of BrR under N$_2$ atmosphere at 50 ^{o}C for NaH/DMF, 50 ^{o}C for K$_2$CO$_3$/DMF, reflux for KOH/THF or K$_2$CO$_3$/Butanone.

The synthesis of compounds **F01** and **F02** with triple bonds at the end of alkyl chain and isothiocyanate failed, although a range of different reaction conditions, including NaH and DMF, K$_2$CO$_3$ and DMF, and K$_2$CO$_3$ and butanone, were tried. ^{1}H NMR analysis carried out on the reaction mixture before purification by column chromatography showed that the triazatruxene core was unaffected, but the

4-bromo-1-butyne and 3-bromopropyl isothiocyanate had been consumed. Therefore, as discussed in the Experimental Chapter, it is possible that the triple bond reacts with the alkyl bromide rather than with than amino-groups (-NH) on the carbazole or triazatruxene core under basic condition. Isothiocyanates are also susceptible to hydrolysis and the triazatruxene core requires a strong base to activate the NH positions.

In addition, the yields of compounds with non-sensitive groups, such as alkyl groups or double bonds, are generally higher than those with relatively labile groups, such as ester bonds, isocyanates and cyclic ethers, especially in the presence of strong base and polar solvent. It is obvious that the positions of the functional groups can affect the reaction efficiency. Specifically, ester bonds are unstable under strong basic conditions, isocyanates could react with themselves and electrophilic isocyanates could be reactive toward a variety of nucleophiles including alcohol, amines, and even water. Thus, these factors probably account for the relatively low yield in these reactions.

The yield (86%) observed for compound **96** with non-conjugated dienes attached to amido bonds in the substituents (R = -$(CH_2)_4CON(CH_2CH=CH_2)_2$) is much higher than that (35%) observed for compound **92** with non-conjugated dienes attached to ester bonds (R = -$(CH_2)_{10}COOCH(CH=CH_2)_2$). However, the reaction to produce compound **100** with a shorter substituent (R = -$CH_2CON(CH_2CH=CH_2)_2$) occurs with a lower yield than compound **96** with a longer, but similar, substituent (R = -$(CH_2)_4CON(CH_2CH=CH_2)_2$). This difference in yield is probably due to the fact that the distance between the two end groups (bromo-substitution and acyl chloride) is too short, which reduces the activity of not only the acyl chloride, but also that of the bromo-leaving group in the compound **99**, as described in the Experimental Section.

4.2 Liquid Crystalline Organic Semiconductors

Both low-molecular-mass materials (LMMMs) and polymeric organic semiconductors have attracted much attention in recent years due to their potential applications as semiconductors in optoelectronic devices, such as OFETs, OPVDs and OLEDs[13-15]. However, the development of conjugated LMMMs with extended π-electron delocalisation is particularly important, because systematic studies of LMMMs can be used to precisely identify the relationships between a variety of photo-physical and electro-chemical properties and molecular structures, so that high device performance can be achieved through rational structural modification. In addition, π-conjugated LMMMs with sophisticated functionality are now key components in molecular electronics[16-17]. Organic semiconductors incorporating carbazole moieties often exhibit useful optical properties, fine delocalisation, low redox potential and high chemical stability. Therefore such carbazole derivatives have been extensively studied as organic semiconductors for use in optoelectronic devices[17]. The presence of electron-donating nitrogen atom can increase the electron density of the entire delocalised π-system and can lead to novel opto-electronic properties. Furthermore, the carbazole moiety can also be easily functionalised at C-2, C-3, or N-positions to create a number of semiconductor materials with the desired values of the appropriate physical properties[18-19].

In this thesis, a library of new organic semiconductor materials incorporating *N*-alkyl-2-substituted-carbazole moieties was synthesised. These highly conjugated compounds with lath-like molecular shapes with a high length-to-breadth (aspect) ratio were designed to yield a range of novel liquid crystalline organic semiconductors possessing a low melting point (Cr-N), a high clearing point (N-I) and a glass transition temperature (Tg) above room temperature (RT).

4.2.1 Thiophene/Phenylene-Based Carbazoles

2,5-Disubstituted thiophene and 1,4-disubstituted phenyl rings are often present in organic semiconductor structures due to their influence on light-emitting characteristics, good charge transport properties, and chemical/environmental stability by influencing the molecular orbital energy levels and extending the degree of π-conjugation[20-21]. A series of thiophene/phenylene-based carbazoles were synthesised with different length of aliphatic chains (R_1 = CH_3 or C_8H_{17} and R_2 = C_8H_{17} and $C_{12}H_{25}$) attached to the phenyl ring and the nitrogen of the carbazole moiety, respectively, in a terminal position of the aromatic core and a different number (n) of 1,4-disubstituted phenyl rings in the centre of the aromatic core. The liquid crystalline transition temperatures ($^{\circ}$C) of these compounds are collated in **Tab. 4.3**.

Tab. 4.3 The crystal-nematic (Cr-N), nematic-isotropic (N-I) and glass transition temperatures (Tg) of the carbazoles **9**, **14**, **38**, **39**, **57** and **58**.
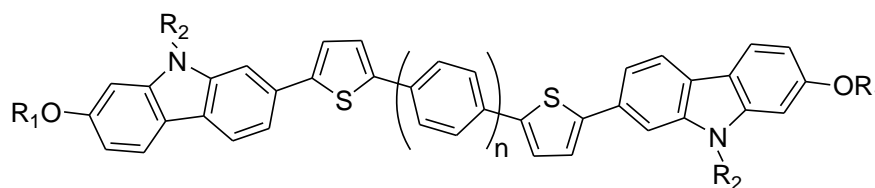

Compound	n	R_1	R_2	Tg		Cr		N		I
9	0	CH_3	C_8H_{17}	•	-	•	214	-	-	•
38	0	C_8H_{17}	C_8H_{17}	•	-	•	136	•	151	•
57	0	C_8H_{17}	$C_{12}H_{25}$	•	-	•	146	•	-	•
14	1	CH_3	C_8H_{17}	•	191	•	265	•	266	•
39	1	C_8H_{17}	C_8H_{17}	•	-	•	248	-	-	•
58	1	C_8H_{17}	$C_{12}H_{25}$	•	-	•	230	-	-	•

The alkoxy substituents in a terminal position (R_1O) were varied in order to study the effect of the alkoxy chains on the mesomorphic behaviour of these compounds and their liquid crystalline transition temperatures. Similarly, the nature of the substituents in lateral positions (R_2) were varied in order to study the effect of long, straight-chain alkylamino-substituent ($-NR_2 = -NC_8H_{17}$ and $-NC_{12}H_{25}$) on the mesomorphism and liquid crystalline transition temperatures of these compounds. The nature and number of 2,5-disubstituted thiophene rings and 1,4-disubstituted-phenyl rings were varied in order to study the effect of the substitution pattern of five-membered aromatic rings, i.e., non-linear and non co-axial, and of six-membered aromatic rings, i.e., linear and co-axial, on the mesomorphic behaviour of these compounds and their liquid crystalline transition temperatures.

Of the bisthiophene carbazoles **9**, **38** and **57**, only compound **38** exhibits nematic liquid crystalline behaviour (Cr-N = 136 ^{o}C and N-I = 151 ^{o}C) without an observable glassy state. Compounds **9** and **57** exhibit crystalline behaviours. Of the (bisthiophen)benzene carbazoles (**14**, **39** and **58**,) only compound **14,** with the shorter alkoxy chains, possesses nematic liquid crystalline behaviour with a glass transition point (Tg-Cr = 191 ^{o}C), melting point (Cr-N = 265 ^{o}C) and clearing point (N-I = 266 ^{o}C). On increasing the length of alkoxy chains or alkylamino chains, the compounds were found to exhibit no observable liquid crystalline phases for either compound **39** or **58**.

The insertion of linear and co-axial six-membered 1,4-disubstituted-phenyl ring into two non-linear and non co-axial five-membered 2,5-disubstituted thiophene rings strengthens the rigid structures of the aromatic main chain. It is a possible reason why compound **14** exhibits liquid crystalline mesomorphic behaviour, while compound **9** does not. However, the addition of phenylene at the central position of the aromatic main-chain leads to a small angle between symmetrical sides of the aromatic backbone. Therefore, when the length of symmetrical terminal alkyl chains was increased, the non-linear and non co-axial structure of the whole molecule caused by the angle was strengthened. Also, the two bonds of an oxygen atom attached to aromatic rings and

alkyl chains have an angle, which means the longer terminal alkyl chains further weaken the linear structure of aromatic main chains and thus decrease the length-to-breadth ratio of a whole molecule. In such case, it can be rationally explained why compound **14** is liquid crystalline while compound **39** is not. On the other hand, non-linear and non co-axial structure of the 5,5'-disubstituted-2,2'-bithiophene can be offset by two longer terminal alkoxy chains, so that a larger length-to-breadth ratio of the whole molecule was achieved. Therefore, compared with compound **9**, compound **38** with longer terminal alkoxy chains exhibits liquid crystalline mesomorphic behaviour. The optimised geometry 3-D molecular models of compounds **9, 14, 38** and **39** shown in **Fig. 4.2** below can clearly reveal their spatial configurations. In addition, the excess length of alkylamino chains in lateral positions decreased the length-to-breadth ratio. Therefore, compounds **57** and **58** are neither liquid crystalline.
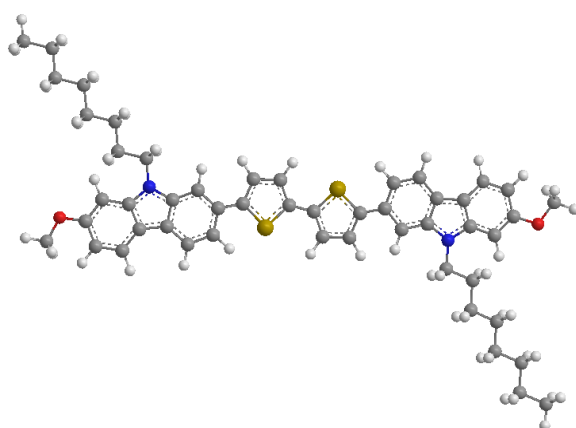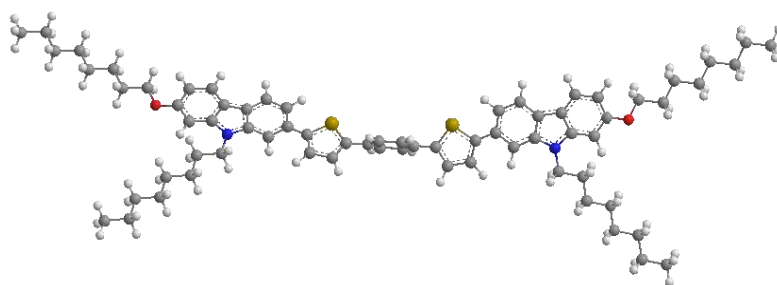

Compound **9**
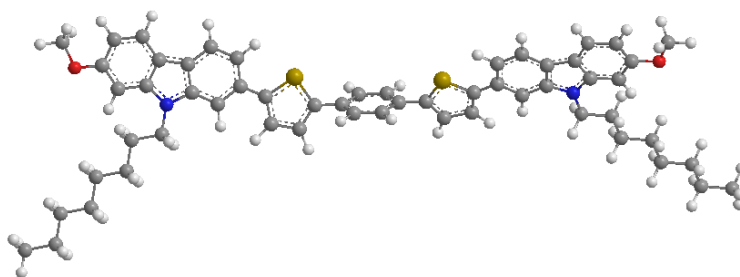
Compound **14**
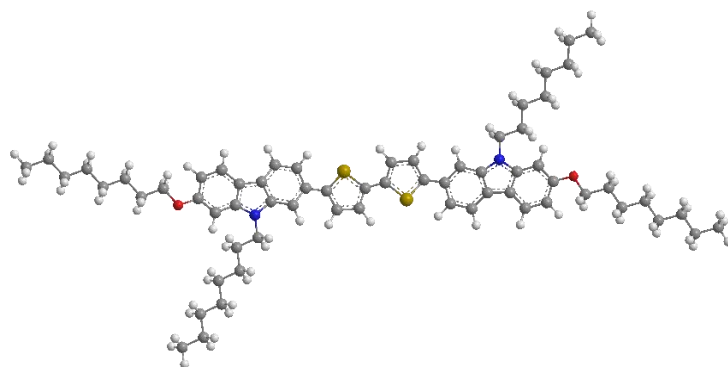
Compound **38**

Compound **39**

Fig. 4.2 Optimised 3-D geometry models of Compounds **9, 14, 38** and **39**

The presence of additional 1,4-disubstituted phenyl rings not only affects the mesomorphic behaviour, but also increases the liquid crystalline transition temperatures. It can be seen from the **Tab. 4.3**, that the melting point and clearing point of the (bisthiophen)benzene carbazole **14** (Tg-Cr = 191 ^{o}C, Cr-N = 265 ^{o}C and N-I = 266 ^{o}C) is significantly higher than those of bisthiophene carbazole **38** (Cr-N = 136 ^{o}C and N-I = 151 ^{o}C) due to a more extended aromatic molecular core and a shorter alkyl chain. The liquid crystalline phase of compounds **14** cannot be observed using OPM when the temperature was increased from room temperature to clearing point. However, on cooling down from the isotropic state, a nematic Schlieren texture shown in **Fig. 4.3** was observed appropriately near the clearing point 266 ^{o}C, although the temperature range exhibiting the liquid crystalline phase is quite short from 266 ^{o}C to 265 ^{o}C.
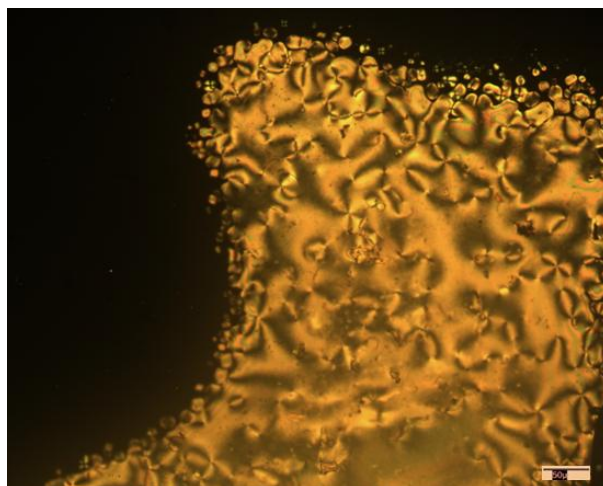
Fig. 4.3 The nematic Schileren texture of compound **14** on cooling at 266 ^{o}C

In addition, the nematic liquid crystalline texture of compound **38**, seen in **Fig. 4.4**, was also only observed on cooling from isotropic state to 136 ^{o}C. DSC analysis was used to confirm further liquid crystalline mesophases and transition temperatures. The DSC curve of compound **38**, shown in **Fig. 4.5** as a typical example, confirms the transition temperatures determined using OPM. Additionally a glassy state could not be detected, clearly seen by the crystalline on cooling. It can be seen that the liquid crystalline phase transition peak of compound **38** is much smaller than the corresponding melting point peak as usual taking into account the fact that the transition between a liquid crystalline phase and an isotropic liquid is a second-order phase transition, sometimes also called weakly first-order transition, with a typically small enthalpy change (0.4 J g^{-1}), while the melting point is a strong first-order transition with a large of enthalpy change (52.9 J g^{-1}).
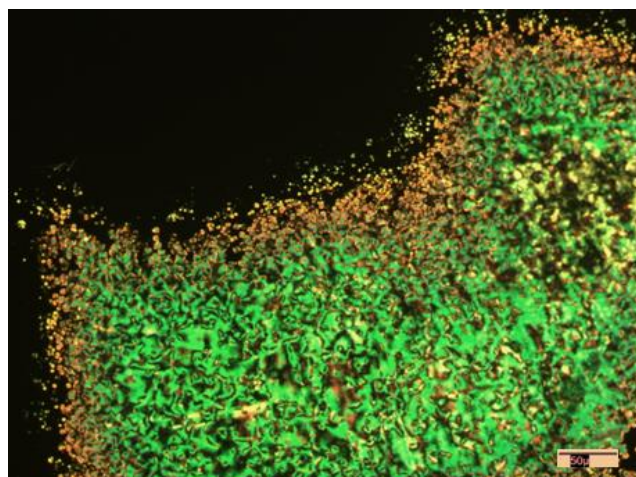
Fig. 4.4 The nematic Schileren texture of compound **38** on cooling at 150 ^{o}C
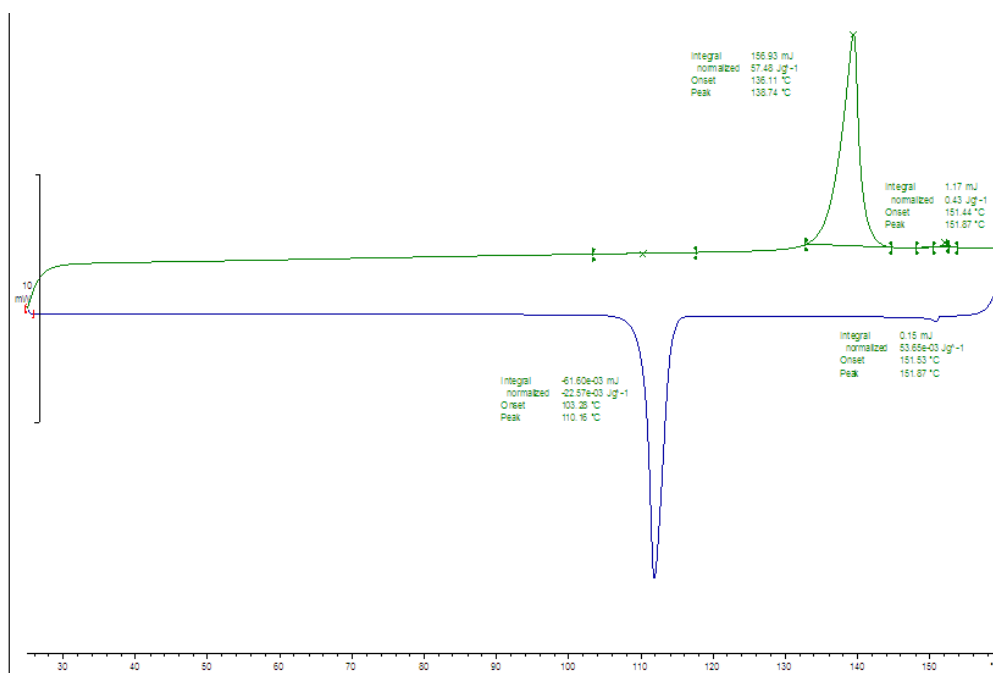
Fig. 4.5 DSC analysis as a function of temperature for compound **38** (scan rate 10 ^{o}C/min)

The high melting points and liquid crystalline transition temperatures of compound **14** and the absence of a glass transition above room temperature for compound **38** mean that both compounds are unsuitable for use in the fabrication of practical OLEDs. Therefore, several approaches were investigated to produce related compounds – hopefully with lower transition temperatures. Unfortunately, the compounds **9, 57, 39**

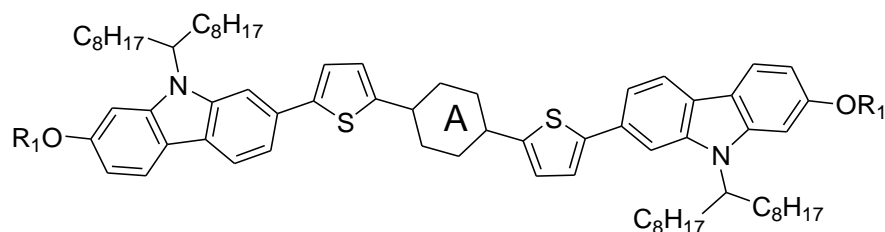and **58** that were synthesised using alternative approaches are not liquid crystalline with high melting points at 214 $^{\circ}$C, 146 $^{\circ}$C, 248 $^{\circ}$C and 230 $^{\circ}$C, respectively, and no observable liquid crystalline transitions. The bisthiophene compounds **57** (R_1O = $C_8H_{17}O$, NR_2 = $NC_{12}H_{25}$) and **58** (R_1O = $C_8H_{17}O$, NR_2 = $NC_{12}H_{25}$), containing longer alkoxy- and alkylamino-chains than those in compounds **9** and **14**, exhibit lower melting points than either the corresponding compounds **9** (R_1O = CH_3O, NR_2 = NC_8H_{17}) and **39** (R_1O = $C_8H_{17}O$, NR_2 = NC_8H_{17}), respectively. The presence of flexible alkyl chains usually serves to lower the intermolecular forces of attraction, e.g., Van der Waals forces, by increasing the intermolecular distance so that lower melting points and other liquid crystalline transition temperatures can be realised. The intrinsic melting points of oligomeric aromatic compounds without terminal and lateral aliphatic substituents are usually very high due to a combination of strong intermolecular forces, such as Van der Waals forces, dipole-induced dipole and dipole-dipole interactions attributable to a short intermolecular distance and often the presence of π-π stacking of adjacent molecules. The inclusion of these long, flexible aliphatic chains serves to increase the core-core distance of these molecules, resulting in less efficient packing and a lessening of intermolecular interactions in aggregate (less π-π-stacking), hence a lowering the melting points.

In a similar strategy, a series of branched alkylamino-chains [R_2 = -$N(C_8H_{17})_2$], rather than straight alkylamino-chains (R_2 = -$NC_{12}H_{25}$), were attached to the aromatic core of this class of compounds in order to produce similar compounds, but with lower values for the transition temperatures of these compounds and, especially the melting point. Unfortunately, as shown in **Tab. 4.4** below, compounds **64**, **67**, **72** and **73** containing the branched alkylamino-chain are all solids well above room temperature (Cr-I = 141 $^{\circ}$C, 108 $^{\circ}$C, 87 $^{\circ}$C and 84 $^{\circ}$C, respectively). They do not exhibit any observable mesomorphic behaviour despite substantial super-cooling below the melting point of each compound. A rationalisation of this behaviour could be that the inclusion of these branched lateral chains results in the decrease in the length-to-breadth ratio, which is usually a crucial parameter for liquid crystalline behaviour to be observed for

compounds with a calamitic, rod- or lathe-like molecular structure. The melting points (Cr-I) of compounds **64** (141 ^{o}C) and **67** (108 ^{o}C), both containing a branched alkylamino-chain (-NCR$_2$ = -NC(C$_8$H$_{17}$)$_2$), are significantly lower than those of compounds **14** (266 ^{o}C) and **39** (248 ^{o}C) that contain a the straight alkylamino-chain (-NR$_2$ = -NC$_8$H$_{17}$). It can also be seen that the substitution of a 1,4-disubstituted phenyl ring in compounds **64** and **67** by a 1,4-disubstituted thiophene ring to produce the corresponding compounds **72** and **73** results in a much lower melting point for the latter compounds compared to those of the former, presumably arising from a non linear molecular structure and consequently a lower aspect ration for compounds **72** and **73**.

Tab. 4.4 The melting points (^{o}C) of the compounds **64**, **67**, **72** and **73**.

Compound	A	R$_1$	Cr		I
64	phenyl	CH$_3$	•	141	•
67	phenyl	C$_8$H$_{17}$	•	108	•
72	thiophene	CH$_3$	•	87	•
73	thiophene	C$_8$H$_{17}$	•	84	•

The values (eV) of the ionisation potential (IP), band gap (Eg) and the electron affinity (EA), measured as described in the Experimental Section, for a range of carbazole compounds are collated in **Tab. 4.5.** All values of energy levels including IP and EA should be negative due to zero of vacuum energy. But it is general to take absolute values for energy levels, and we gave absolute values for discussion in this thesis.

Tab. 4.5 The values (eV) for the energy levels and band gap of the carbazoles **9**, **14**, **38**, **39**, **57**, **58**, **64**, **67**, **72** and **73**.

Compound	IP	Eg	EA
9	5.39	2.60	2.79
38	5.37	2.60	2.77
57	5.38	2.60	2.78
14	5.46	2.67	2.79
39	5.45	2.67	2.78
58	5.45	2.66	2.79
64	5.40	2.66	2.74
67	5.39	2.65	2.74
72	5.22	2.45	2.77
73	5.21	2.45	2.76

Overall, the presence of a combination of the highly electron-rich carbazole and thiophene moieties in the compounds **9**, **14**, **38**, **39**, **57**, **58**, **64**, **67**, **72** and **73** leads to low values for both the ionisation potentials (IP) and energy gaps (Eg) as expected. This suggests that they may be viable materials for use as hole-transporting materials in OLED devices or as electron-donors in OPV devices. It was found that increasing the number of thiophene cores in a molecular structure generally resulted in a lower value of HOMO level and a smaller energy gap, e.g.,

IP and Eg compounds **72** and **73** < **9**, **38** and **57** < **14**, **39**, **58**, **64** and **67**

However, the values for the IP, Eg and EA do not appear to be significantly influenced by the length of alkyl chains and similar IP values and identical Eg values are observed for the compounds **9**, **38** and **57** with the same molecular cores structures but different aliphatic chains. In addition, it seems that the value of the electron affinity is not affected considerably by these small differences in chemical structures, such as the length of alkyl chains or the substitution of a 1,4-disubstituted phenyl ring ring by a

1,4-disubstituted thiophene ring in the aromatic core of the molecule. This has been reported previously[22-23].

NB. Although compounds **72** and **73** do not exhibit any observable liquid crystalline mesophases, they could still be considered as potentially suitable hole-transporting materials due to relatively low values of the HOMO level and the energy gap.

4.2.2 9,9-Dialky-2,7-Disubstituted-Fluorenes

A considerable number of organic semiconductors incorporating one or more 2,7-disubstituted fluorene moieties in the aromatic molecular core are promising light-emitting materials with high photo-luminescence quantum yields and thermal, chemical and environmental stability[24-25]. The fluorene structural unit incorporates a rigidly planar and highly conjugated 4,4'-disubstituted biphenyl moiety, which can provide a high degree of delocalisation, especially when the 2,7-positions of fluorene are designed to attach other symmetrical conjugated aromatic rings, such as a 2,7-disubstituted carbazole or 1,4-disubstituted thiophene rings. In addition, a further advantage of the fluorene moiety is that the bridge carbon atom can be functionalised with two alkyl chains of different length, so that good solubility and low melting points can be achieved for a number of suitably substituted fluorene derivatives. Therefore, as a result of designing compounds with a highly conjugated, planar aromatic cores incorporating such moieties as 2,7-disubstituted fluorene, 2,7-disubstituted carbazole or 2,5-disubstituted thiophene moieties, the length of the alkyl chains in the lateral position of attached to fluorene moiety in the molecular core, the length of alkoxy chains at the terminal positions of symmetrical carbazole moieties, a series of organic semiconductors with good electrical and optical properties were synthesised. Some of these compounds with a large length-to-breadth ratio also exhibit liquid crystalline mesophases. The chemical structures and liquid crystalline transition temperatures of these compounds are collated in **Tab. 4.6**.

Tab. 4.6 The liquid crystalline transition temperatures (^{o}C) for the 9,9-dialkyl-2,7-disubstituted fluorenes **18**, **19**, **22**, **41**, **42**, **46** and **B1**.
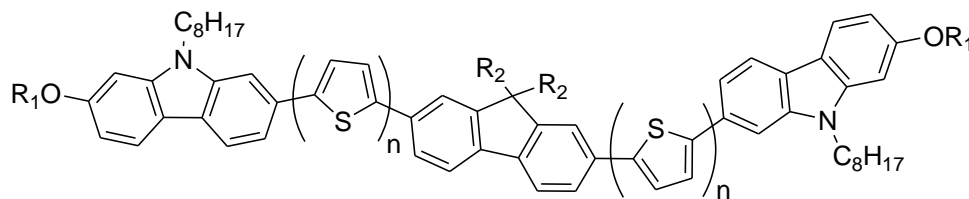

Compound	n	R_1	R_2	Tg		Cr		N		I
18	0	CH_3	CH_3	•	-	•	88	-	-	•
19	0	CH_3	C_8H_{17}	•	-	•	70	-	-	•
B1[a]	0	C_8H_{17}	CH_3	•	-	•	52	•	60	•
41	0	C_8H_{17}	C_8H_{17}	•	-	•	66	-	-	•
22	1	CH_3	CH_3	•	77	•	-	•	185	•
42	1	C_8H_{17}	CH_3	•	32	•	-	•	161	•
46	2	C_8H_{17}	C_8H_{17}	•	21	•	-	•	137	•

Notes: a. Synthesised by Dr M Reddy Billa of the University of Hull[26].
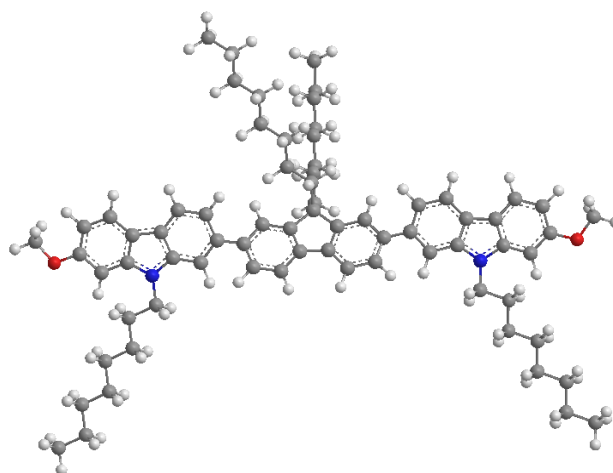
Only compound **B1** of the 9,9-dialkyl-2,7-disubstituted fluorenes **18**, **19**, **B1** and **41** with two *N*-alkyl-2,7-disubstituted carbazole moieties, with no thiophene unit in the aromatic molecular core (n = 0), is liquid crystalline. It does not exhibit an observable glassy state. Compound **B1** possesses either longer chains in a terminal position ($R_1 = C_8H_{17}$) or shorter chains in a lateral position ($R_2 = CH_3$) than those of compounds **18** ($R_1 = R_2 = CH_3$), **19** ($R_1 = CH_3$ and $R_2 = C_8H_{17}$) and **41** ($R_1 = R_2 = C_8H_{17}$). Therefore, compound **B1** exhibits the largest length-to-breadth ratio of this set of four analogues, differing only in the lengths of the aliphatic chains, which is probably responsible for the observation of a nematic phase for this analogue.

Fig. 4.6 indicates the probable structure of compounds **18**, **19**, **B1** and **41** obtained using molecular modelling. The models correspond to the above interpretation of the relative differences in the length-to-breadth ratio. The presence of alkyl chains in lateral positions attached to the 2,7-disubstituted fluorene moiety increase the intermolecular

distances and subsequently weaken Van der Waals interactions between adjacent molecules due to the fact that these alkyl chains lie out of the plane of the conjugated aromatic core. This molecular feature may well be responsible for the fact that the compounds **18** (Cr-I = 88 °C), **19** (Cr-I = 70 °C), **B1** (Cr-N = 52 °C, N-I = 60 °C) and **41** (Cr-I = 66 °C) exhibit relatively low melting and clearing points. The same argument can also be used to explain the fact that the melting point (88 °C) of compound **18** (R_2 = CH_3) is higher than that (70 °C), of compound **19** (R_2 = C_8H_{17}), but not the fact that compound **B1** with short alkyl chains (R_2 = CH_3) in a lateral position, exhibits a lower melting point (52 °C) than that (68 °C) of compound **41** with much longer alkyl chains (R_2 = C_8H_{17}) attached to the fluorene moiety. This phenomenon may be due in part to the presence of liquid crystalline mesophase for compound **B1** while compound **41** is crystalline solid.
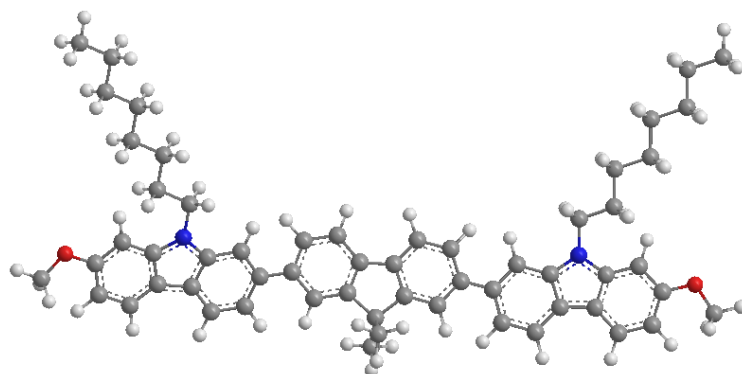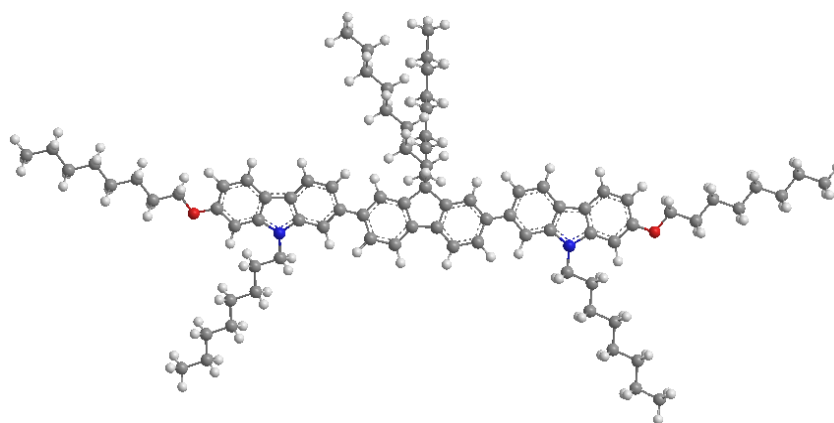

Compounds **18**

Compounds **19**
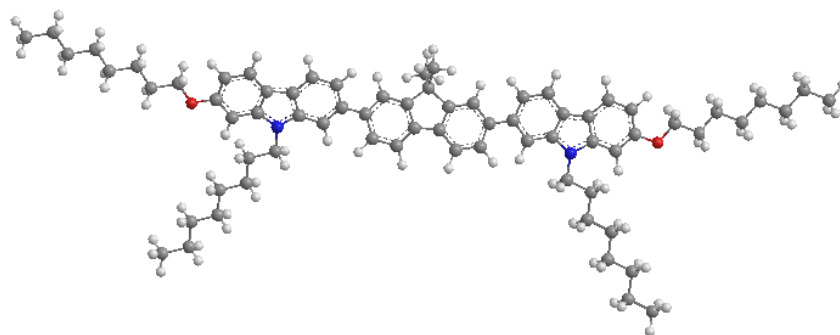
Compounds **B1**

Compounds **41**

Fig. 4.6 Optimised 3-D geometry models of compounds **18**, **19**, **B1** and **41**.

The 9,9-dialkyl-2,7-disubstituted fluorenes **22** ($R_1 = R_2 = CH_3$), **42** ($R_1 = C_8H_{17}$ and $R_2 = CH_3$) and **46** ($R_1 = R_2 = C_8H_{17}$) with two (n = 1) or four (n = 2) 2,5-disubstituted thiophene rings in the aromatic molecular core exhibit a nematic phase with high clearing points (N-I = 185 ^{o}C, 161 ^{o}C and 137 ^{o}C, respectively) and glass transition temperatures above or at room temperature (Tg-Cr = 77 ^{o}C, 32 ^{o}C and 21 ^{o}C, respectively). This fact is probably attributable to the presence of the 2,5-disubstituted thiophene rings in the molecular aromatic core, which gives rise to a large length-to-breadth ratio, in comparison to compounds without 2,5-disubstituted thiophene rings.

Fig. 4.7 shows the Schlieren texture, with point singularities with four and two point brushes, characteristic of the nematic phase, for compound **42**, observed on cooling the OPM sample from the isotropic state into glassy state. DSC analysis was used to

confirm this mesomorphic behaviour. A combination of OPM and DSC reveals that compounds **22**, **42** and **46** possess no observable melting point peak (Cr-N). Instead they soften gradually on increasing the temperature above glass transition temperature until they form an isotropic state above the clearing point. The DSC curve of compound **42** is shown in **Fig. 4.8**.
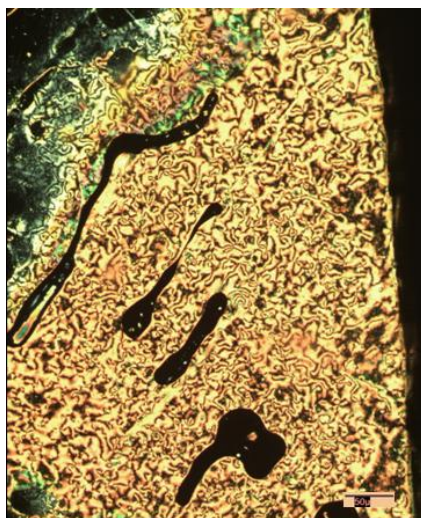

Fig. 4.7 The nematic Schlieren texture observed for compound **42** on cooling from the isotropic state to 147 $^{\circ}$C
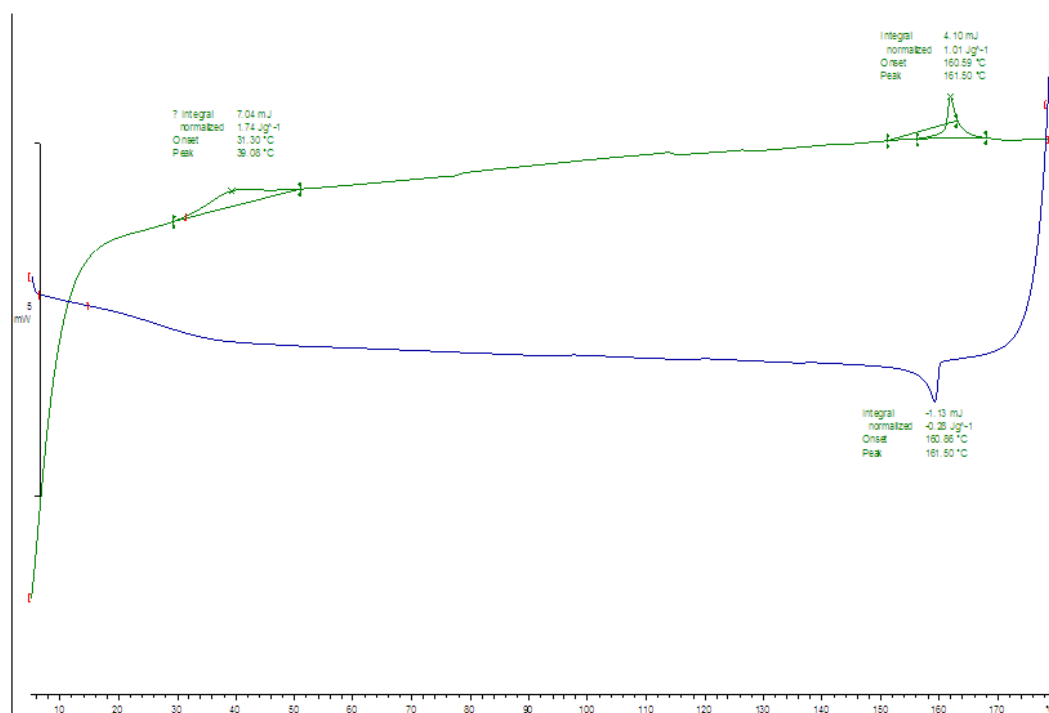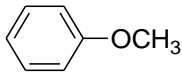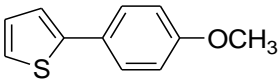

Fig. 4.8 DSC trace as a function of temperature for compound **42** (scan rate 10 $^{\circ}$C/min)

Given the earlier general observation that melting points and phases transitions occur at lower temperatures on increasing the alkyl chain length, it was expected that the same phenomenon would be observed for these 2,7-disubstituted fluorene derivatives. This expectation was confirmed by the observed glass transition temperatures and the clearing points of the compounds, i.e., **22** with the shortest aliphatic substituents (R_1 = R_2 = OCH_3) are higher (Tg-Cr = 77 ^{o}C, N-I = 185 ^{o}C) than those (Tg-Cr = 32 ^{o}C, N-I = 161 ^{o}C) of compound **42** (R_1 = C_8H_{17} and R_2 = CH_3), which are higher, in turn, than those (Tg-Cr = 21 ^{o}C, N-I = 137 ^{o}C) of compound **46** with the longest aliphatic chains (R_1 = R_2 = OC_8H_{17}). It should, however, be noted that compound **46** possesses four 2,5-disubstituted thiophene rings (n = 2) compared to compounds **22** and **42** with two 2,5-disubstituted thiophene rings (n = 1). The presence of the two additional thiophene rings in compound **46** leads to a lower length-to-breadth ratio due to the non co-linear and non-coaxial nature of the substitution pattern of 2,5-disubstituted thiophene rings.

Based on the results above, the 2,7-disubstituted fluorene **83** with a an extended, highly conjugated molecular core with a very high length-to-breadth ratio was synthesised. Compound **83** exhibits a nematic mesophase with the desired mesomorphic behaviour, i.e., a nematic phase, and transition temperatures, i.e., the absence of a melting point, a glass transition temperature above room temperature (Tg-N = 68 ^{o}C) and a very high clearing point (N-I = 225 ^{o}C) as shown in **Tab. 4.7**. NB. In terms of optical-electrical applications, nematic mesophases with orientational order and no positional order, exhibit an enhanced Forster energy transfer, extremely low laser threshold fluence, low loss due to oriented high-quality films, spontaneously homogeneous (in-plane) alignment in mesophase state[27]. In terms of thermal properties, liquid crystalline mesophases exhibit preferred transition temperatures, i.e., glassy state above room temperature and high clearing point, which results in the favourable absence of crystal boundary defects as traps for quenching of electrons or holes injections. Furthermore, nematic mesophases with low viscosity can be easily ordered and macroscopically aligned in thin films at low temperatures[27]. The nematic Schlieren texture of compound **83** shown in **Fig. 4.9** was observed on cooling from the isotropic liquid

using OPM to 225 °C. DSC analysis was used to confirm the transition temperatures (Tg-Cr = 68 °C, N-I = 225 °C) as shown in **Fig. 4.10.**

Tab. 4.7 The chemical structures and transition temperatures (°C) for compounds **83** and **B2**.

Compound	R	Tg	Cr	SmC	N	I
83	⟨benzene⟩—OCH$_3$	• 68	• -	- -	• 225	•
B2[a]	⟨thiophene(S)⟩—⟨benzene⟩—OCH$_3$	• 100	• 210	• 295	- -	•

Notes: a. Synthesised by Dr M Billa Reddy of the University of Hull[26].

Compound **B2**, with two additional 2,5-disubstituted thiophene rings compared to the molecular structure of compound **83**, exhibits a smectic C phase instead of the nematic phase observed for compound **83**. Compounds **83**, **22**, **42** and **46** possess no observable melting point. It should therefore be concluded that the phase change is gradual, with no sharp observable change in phases. These kinds of gradual phase change are often observed with polymers, which are generally observed as a broad peak in DSC measurements. Broad peaks were observed in the DSC measurements of **83**, **22**, **42** and **46**, which are high-molecular-weight oligomers with a high molecular weight.

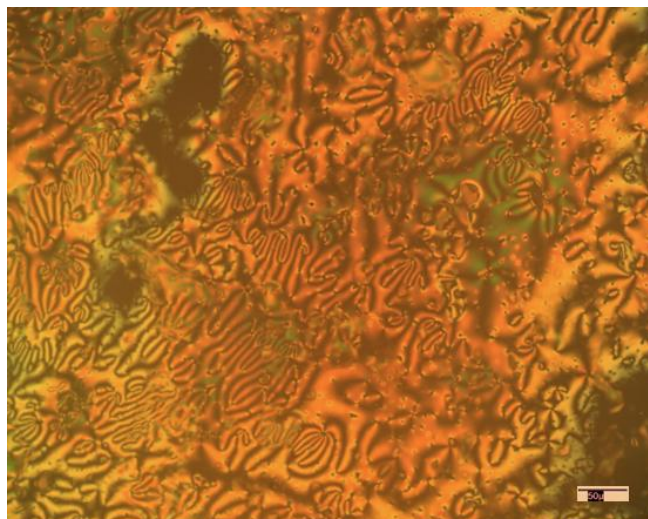**Fig. 4.9** The Schlieren texture characteristic of the nematic phase of compound **83** on cooling at 224 $^{\circ}$C.
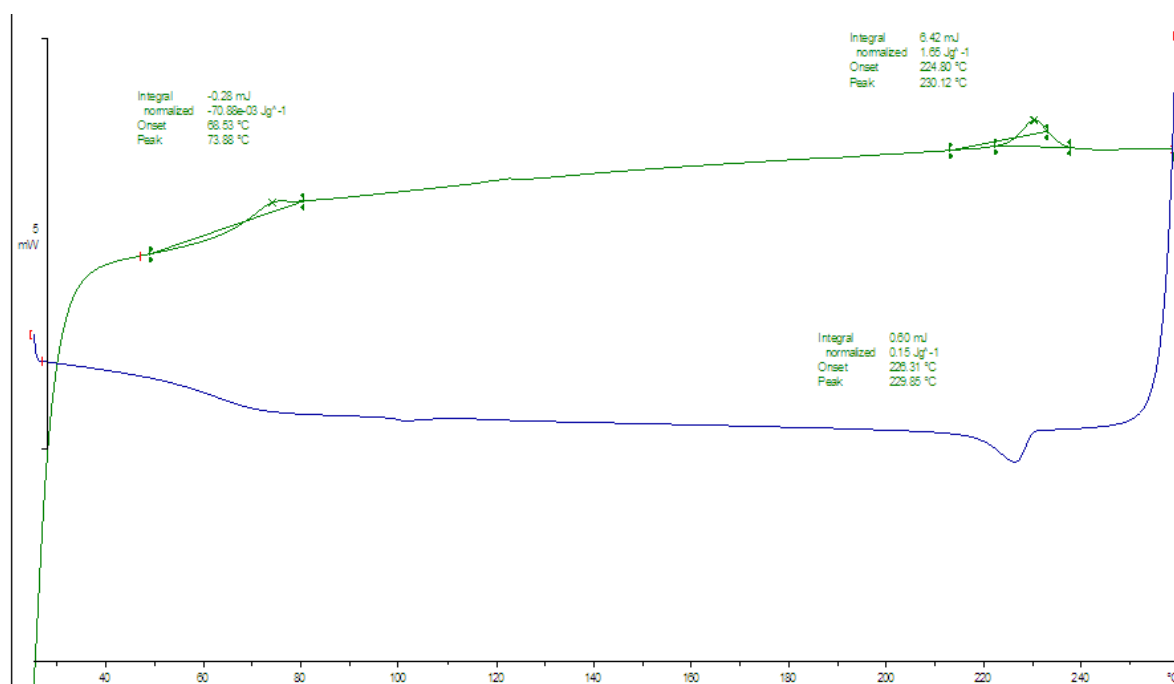

Fig. 4.10 DSC trace for compound **83** (scan rate 10 $^{\circ}$C/min)

The values (eV) of the band gap (Eg), ionisation potential (IP) and electron affinity (EA) for the 2,7-disubstituted fluorenes **18**, **19**, **22**, **41**, **42**, **46** and **83** are listed in **Tab. 4.8**.

Tab. 4.8 The band gap (Eg), ionization potential (IP) and electron affinity (EA) determined for the 2,7-disubstituted fluorenes **18**, **19**, **22**, **41**, **42**, **46** and **83**.

Compound	IP	Eg	EA
18*	5.59	3.09	2.50
19*	5.59	3.09	2.50
41*	5.58	3.08	2.50
22**	5.53	2.63	2.90
42**	5.53	2.64	2.89
46**	5.44	2.50	2.94
83**	5.52	2.49	3.03

Note: * denotes the absence of thiophene moieties in the molecular backbone. ** denotes the presence of thiophene moieties in the molecular backbone.

Compounds **22**, **42**, **46** and **83** incorporating 2,5-disubstituted thiophene units in their chemical structures exhibit slightly to moderately lower values for the ionisation potentials and energy gaps, but significantly higher values for the electron affinity, than those of compounds **18**, **19** and **41** that do not include 2,5-disubstituted thiophene moieties in their molecular structure. Compound **83**, which contains six 2,5-disubstituted thiophene rings, has a similar energy to **46**, which contains four 2,5-disubstituted thiophene rings, exhibits higher IP and EA values than those of **46**. This behaviour suggests that both the HOMO and LUMO are also higher in energy than those of compound **46**. The value of the electron affinity does not appear to be significantly influenced by alkyl chain length.

The 2,7-disubstituted fluorenes **18**, **19**, **22**, **41**, **42**, **46** and **83** exhibit good solubility in common organic solvents used to deposit thin, uniform films of organic compounds from solution, e.g., by spin-coating, drop casting or doctor blade techniques, onto the substrate surfaces of optoelectronic devices, such as OLEDs, OFETs and OPVs. This advantageous property is probably due to the presence of alkyl chains in both terminal

and lateral positions on the molecular structure in spite of a high molecular weight and a calamitic, lathe-like structure with a high length-to-breadth ratio.

4.2.3 Dibenzothiophene carbazoles

The 3,8-disubstituted dibenzothiophene moiety, as a kind of heterocyclic biphenylgroup, with a rigid, planar structure similar to that of a 9-H, 2,7-disubstituted carbazole moiety, has been incorporated into novel opto-electronic materials, that are designed to exhibit high triplet energy and good hole-transporting ability[28-30]. These new compounds incorporating the 3,8-disubstituted dibenzothiophene moiety in the centre of the aromatic molecular core and two *N*-alkyl-2,7-disubstituted carbazole moieties, positioned on either side of the dibenzothiophene moiety, were designed to exhibit a combination of the desired mesomorphic behaviour and very good hole-transporting ability.

Tab. 4.9 gives the chemical structures and transition temperatures for two examples, **48** and **49**, of these dibenzothiophenes differing only in the length of terminal alkoxy chains ($R_1 = CH_3$ and C_8H_{17}, respectively). The dibenzothiophenes **48** and **49** exhibit a thermotropic nematic phase, above relatively high melting points (Cr-N = 202 ^{o}C and 141 ^{o}C, respectively), with high clearing points (N-I = 250 ^{o}C and 202 ^{o}C, respectively). The optimised 3-D geometry modelling of compounds **48** and **49** are shown in **Fig. 4.11**. The presence of longer terminal flexible aliphatic chains results in lower transition temperatures (Cr-N = 141 ^{o}C, N-I = 202 ^{o}C) for compound **49** with long alkoxy chains ($R_1 = C_8H_{17}$) than those (Cr-N = 202 ^{o}C, N-I = 250 ^{o}C) of compound **48** with terminal methyl chains ($R_1 = CH_3$). **Fig. 4.12** and **Fig. 4.13** show the nematic Schlieren texture and DSC thermogram analysis of compound **49**, respectively.
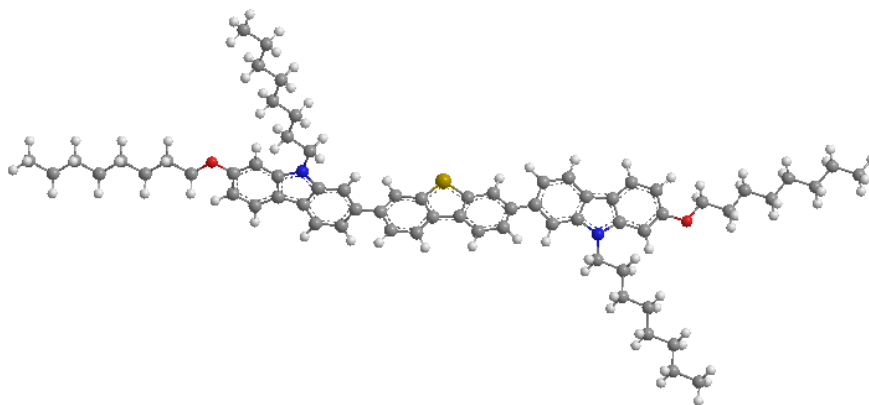
Tab. 4.9 The liquid crystalline transition temperatures (^{o}C) and mesomorphic behaviour of the dibenzothiophenes **48** and **49**.
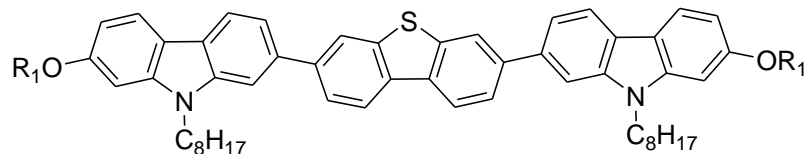
Compound	R_1	Tg		Cr		N		I
48	CH_3	•	-	•	202	•	250	•
49	C_8H_{17}	•	-	•	141	•	202	•
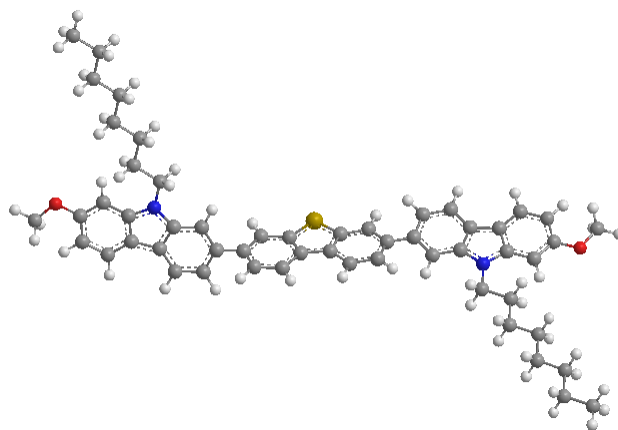
Compound **48**

Compounds **49**

Fig. 4.11 Optimised 3-D geometry models of compounds **48** and **49**

Despite the greatly different chain lengths of the terminal alkoxy groups for compounds **48** (R_1 = CH_3) and **49** (R_1 = OC_8H_{17}) a nematic phase is observed for both compounds. This behaviour is different from that observed for the analogous 2,7-disubstituted fluorenes **18** and **B1** also incorporating two 2,7-disubstituted carbazoles, see **Tab. 4.6**.

Only compound **B1** with a longer terminal alkoxy chain ($R_1 = OC_8H_{17}$) than that of compound **18** ($R_1 = OCH_3$) exhibits a nematic mesophase.

Compared with the bridged sulphur atom (without any aliphatic substituent), the presence of the bridged dialkyl-substituted methylene atom, even with just methyl chains, in the 2,7-disubstituted fluorenes **18** and **B1** leads to a greater intermolecular separation, thereby increasing the intermolecular distance and subsequently decreasing the Van der Waals forces between adjacent molecules in a π-π stacking arrangement of planar molecular cores. Furthermore, the bridged sulphur atom in the molecular structures of the dibenzothiophenes **48** and **49** is electron-rich due to the presence of two lone pairs of electrons, which may well increase the electron density of π-π stacking of conjugated cores and thus help stabilise the molecular backbone. A combination of these elements may well explain why the transition temperatures (Cr-N = 141 $^{\circ}$C, N-I = 202 $^{\circ}$C) of dibenzothiophene **49** are significantly higher than those (Cr-N = 52 $^{\circ}$C, N-I = 60 $^{\circ}$C) of the analogous 2,7-disubstituted fluorene **B1** with an otherwise very similar molecular structure.
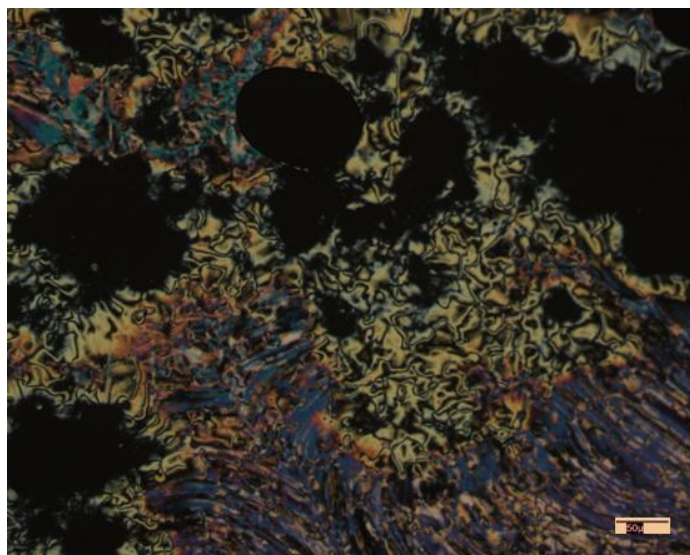

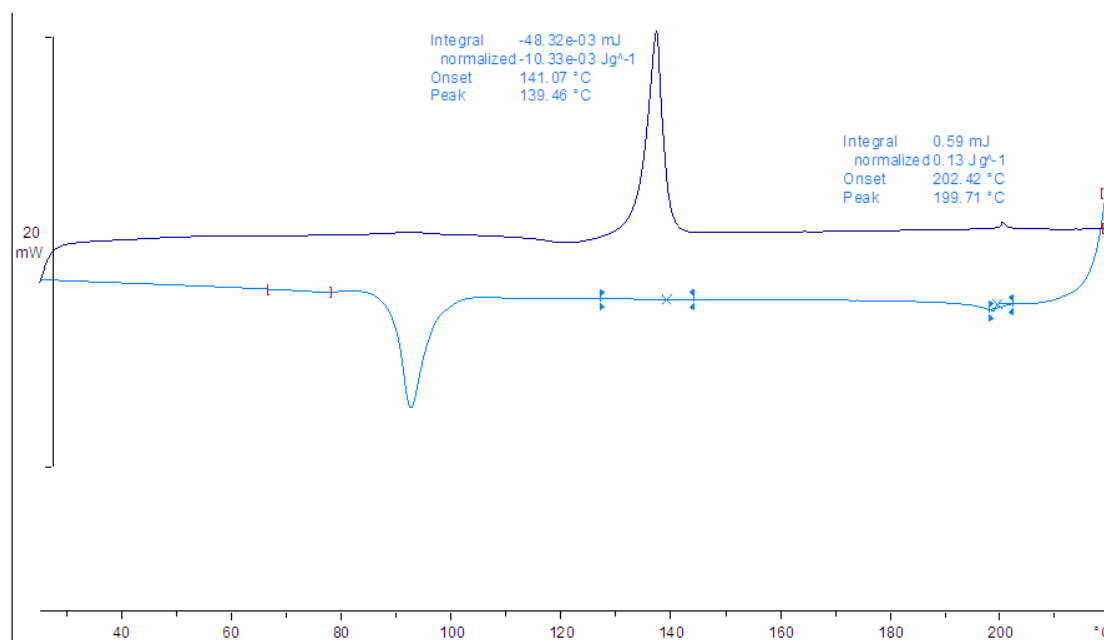**Fig. 4.12** The nematic Schlieren texture for compound **49** observed on cooling from the isotropic state to 198 $^{\circ}$C.

Fig. 4.13 DSC analysis as a function of temperature for compound **46** (scan rate 10 ^{o}C/min).

The magnitude of the HOMO and LUMO energy levels and band gap for dibenzothiophenes **48** and **49**, which appear to have acceptable ionisation potentials and energy gaps for use as hole-transporting materials, are collated in **Tab. 4.10**. However, it should be also noted that the values of the energy gaps of the dibenzothiophene **48** and **49** are relatively high, although the hetero-atoms present in the carbazole units and the central dibenzothiophene unit contribute to low values of HOMO levels and small energy gap. The nature of the aliphatic chains attached to the molecular core does not significantly affect their energy levels and band gap.

Tab. 4.10 The values (eV) for the ionisation potential (IP), band gap (Eg) and the electron affinity (EA) for the dibenzothiophenes **48** and **49**.

Compound	IP	Eg	EA
48	5.57	3.11	2.46
49	5.57	3.10	2.47

It is probable that the presence of additional carbazole or thiophene units with

hetero-atoms would further decrease HOMO energy levels and band gap. However, there is a good chance that the presence of additional biphenyl-like structures within the highly conjugated molecular cores would lead to very high melting points and poor solubility, or indeed complete insolubility, in common organic solvents used to deposit uniform thin films of organic semiconductors from solution, using spin-coating deposition technique for example, on device substrates.

4.2.4 4,7-Disubstituted Benzothiadiazoles

4,7-Disubstituted benzothiadiazole moieties are often important structural components of organic semiconductors used as electron acceptors, whereas 2,7-disubstituted carbazole moieties are often present in organic semiconductors widely used as electron-donating films in organic electronic devices, such as OLEDs and OPVs[31-33]. These and related structural elements have also been combined to form novel organic semiconductors with electron accepting- and donating components in the molecular structure of a particular compound designed to afford promising device performance for many optoelectronic applications[34-35]. Furthermore, such hybrid compounds incorporating both benzothiadiazole and carbazoles moieties exhibit relatively low band gap and a red-shifted absorption spectrum[36-37] The molecules with donor-acceptor-donor (D-A-D) structures have attracted much interests due to feasible achievement for fine tuning of band gap and a red shift extension of the absorption in organic electronic applications[38-41]. The 'Push-Pull' designs and combinations of suitable donors and acceptors allow a possibility of intra-molecular charge transfer from electron-donors with low absolute values of HOMO energy levels to electron-acceptors possessing high absolute values of LUMO energy levels[42-47]. Furthermore, the relatively linear, coplanar and rigid aromatic backbone of such compounds usually have smaller reorganisation energy, which contributes to the achievement of high values for charge-transport in thin layers in organic electronic devices[37].

**Tab. 4.11** The transition temperatures (°C) for **52** and **53**.
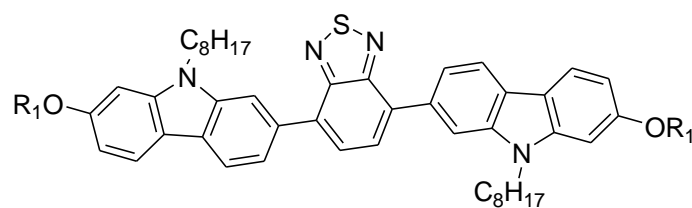
Compound	R_1	Tg		Cr		N		I
52	CH_3	•	92	•	142	•	-	•
53	C_8H_{17}	•	85	•	105	•	(94)	•

( ) represents a monotropic transition

Tab. 4.11 shows the chemical structures, mesomorphic behaviour and transition temperatures for the benzothiadiazoles **52** and **53** differing only in the length of terminal alkoxy chains ($R_1 = CH_3$ and C_8H_{17}, respectively). It can be seen that benzothiadiazole **53** with a long chain ($R_1 = C_8H_{17}$) in a terminal position attached to the aromatic molecular core exhibits a monotropic nematic phase (N-I = 94 °C) on cooling the isotropic liquid formed above the melting point (Cr-I = 105 °C). Further cooling results in the recrystallisation of sample from the nematic state (N-Cr = 85 °C). The analogous compound **52** with much shorter alkoxy chains ($R_1 = CH_3$) does not exhibit any observable liquid crystalline behaviour, despite substantial super-cooling below the melting point (Cr-I = 142 °C, Tg = 92 °C). It is obvious that the presence of longer terminal alkoxy chains in compound **53** contributes to a larger length-to-width ratio, which facilitates the formation of liquid crystalline mesophases. This fact is highlighted by consideration of optimised 3-D geometry modelling of compounds **52** and **53** shown in **Fig. 4.14**.

Furthermore, the presence of lateral octyl chains attached to the nitrogen atoms of the carbazole moieties gives rise to relatively low melting points for calamitic compounds with a highly extended and conjugated, rigid aromatic molecular core. It is reasonable that the melting point (Cr-I = 105 °C) of compound **53** with terminal octyl chains is lower than that (Cr-I = 142 °C) of compound **52** with terminal methyl groups, as expected.

The melting points (Cr-I = 142 $^{\circ}$C and 105 $^{\circ}$C, respectively) of the benzothiadiazoles **52** and **53** are much lower than those (Cr-I = 202 $^{\circ}$C and 141 $^{\circ}$C, respectively) of the analogous dibenzothiophenes **48** and **49** (R$_1$ = CH$_3$ and C$_8$H$_{17}$, respectively) differing only in the presence of these two kinds of heterocyclic aromatic rings. The dibenzothiophenes **48** and **49** also both exhibit a nematic phase with a much higher clearing point (N-I = 250 $^{\circ}$C and 202 $^{\circ}$C, respectively) than that (N-I = 94 $^{\circ}$C) of the benzothiadiazole **53**. NB the benzothiadiazole **52** is non mesomorphic, see **Tab. 4.11**.
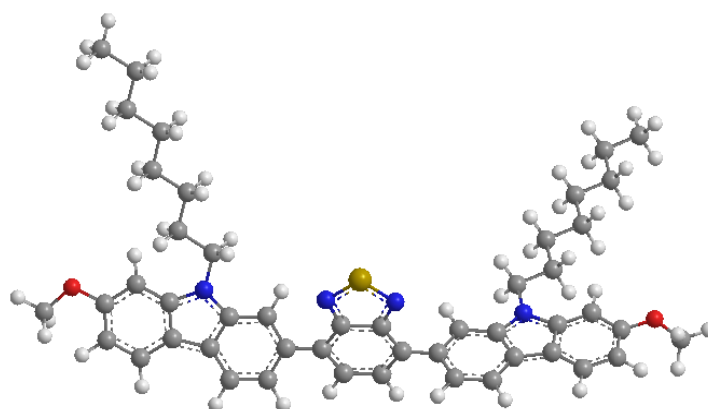
Compound **52**
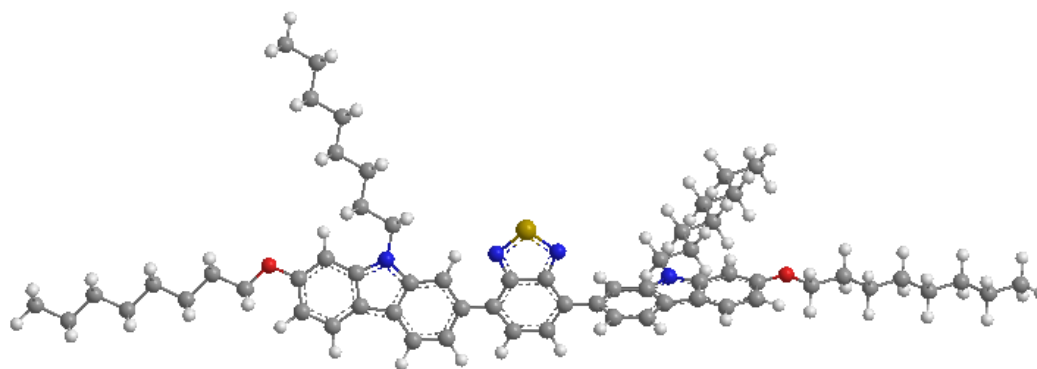
Compound **53**

Fig. 4.14 Optimised 3-D geometry models of compounds **52** and **53**

The nematic Schlieren texture of compound **53** shown in **Fig. 4.15** was observed on cooling to 94 $^{\circ}$C of the isotropic liquid formed above the melting point (Cr-I = 105 $^{\circ}$C). Further cooling results in the formation of a crystalline state with some nematic texture

(Tg = 85 ^{o}C), typically of paramorphism. This mesomorphic behaviour is consistent with the results of DSC analysis, see in **Fig. 4.16**, with the presence of typical mesophase peaks in heating and cooling processes for liquid crystalline samples.
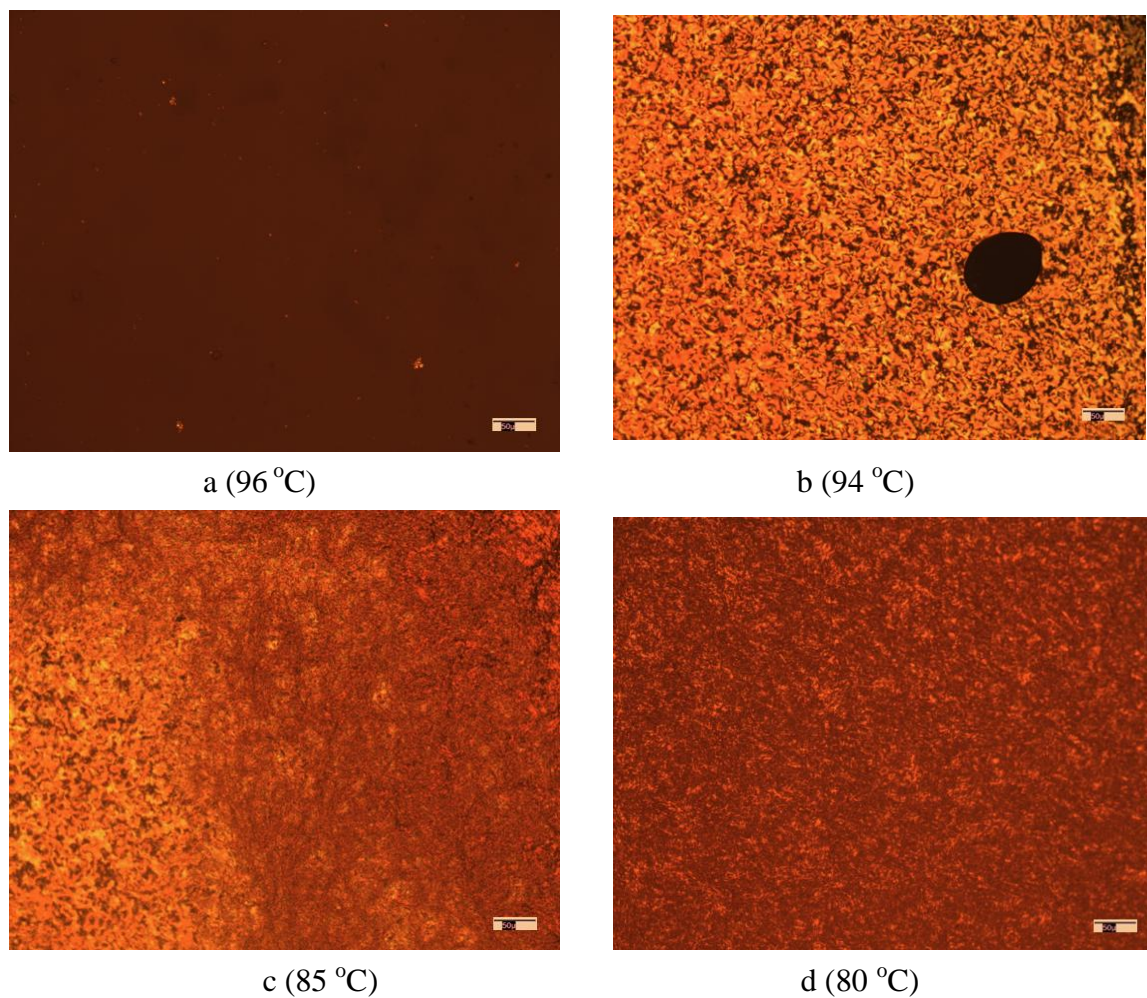

a (96 ^{o}C)

b (94 ^{o}C)

c (85 ^{o}C)

d (80 ^{o}C)

Fig. 4.15 The OPM images for monotropic liquid crystalline compound **53** on cooling at 96 ^{o}C (a), 94 ^{o}C (b), 85 ^{o}C (c) and 80 ^{o}C (d).
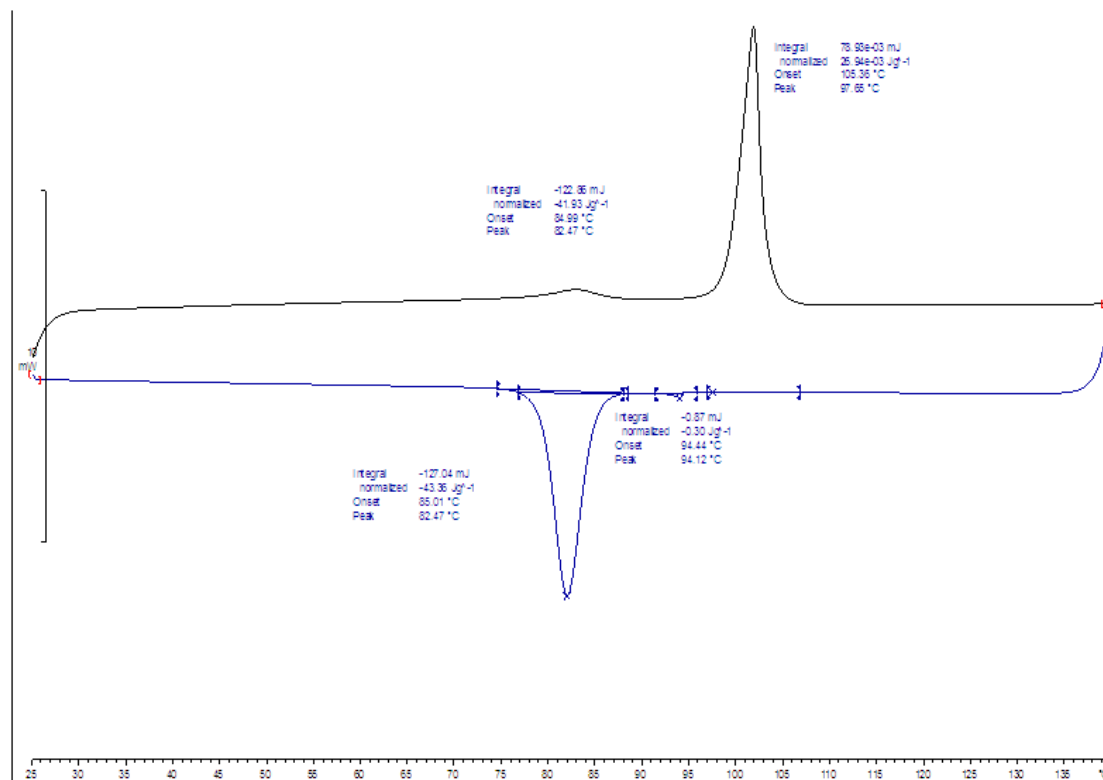
Fig. 4.16 the DSC curve as a function of temperature for compound **53** (scan rate 10 $^{\circ}$C min^{-1}).

The benzothiadiazoles **52** and **53** both exhibit low values of HOMO energy levels and small band gaps as shown in **Tab. 4.12**. Therefore, they can be considered as potential hole-transporting materials and are expected to demonstrate good charge-transporting properties. In addition to the presence of two carbazole units in combination with the central benzothiadiazole unit may well account for the low values of the ionisation potential and the energy gap. These heterocyclic rings, incorporating nitrogen and sulphur atoms with lone pair electrons, lead to highly conjugated, delocalised electron cloud across the aromatic molecular core.

Tab. 4.12 The values (eV) for the band gap and energy levels for the benzothiadiazoles **52** and **53**.

Compound	IP	Eg	EA
52	5.31	2.44	2.87
53	5.30	2.42	2.88

A comparison of the data for compounds **52** and **53** with the same conjugated cores, but differing in the length of alkyl chains ($R_1 = CH_3$ and C_8H_{17}, respectively), also indicates that a negligible difference between the respective values of the HOMO & LUMO energy levels and band gap. This provides further evidence for the reasonable assumption that it is the nature of the aromatic molecular cores, rather than that of the terminal alkyl chains, that influence the energy levels and band gap.

The **52** and **53** exhibit relatively good solubility in common organic solvents due to the presence of flexible aliphatic chains attached in lateral and terminal positions to the carbazole units.

4.2.5 Thieno[3,4-*c*]pyrrole-4,6-diones

Benefiting from the development of optimised physical processing and device fabrication, a wide variety of organic opto-electronic materials have been studied over recent decades[48-49]. In particular, the use of the thieno[3,4-*c*]pyrrole-4,6-dione unit as an electron-deficient molecular building block has been the subject of intense attention in organic semiconductors for use in high-performance plastic electronic devices. The combination of an electron-withdrawing thieno[3,4-*c*]pyrrole-4,6-dione moiety and two electron-donating carbazole units in one molecular structure was designed to achieve the desired photo-physical and electro-chemical properties, such as low energy gap, appropriate HOMO and LUMO energy levels, good charge carrier mobility, stability and lifetime[50].

The compact, rigid and planar structure of the thieno[3,4-*c*]pyrrole-4,6-dione moiety, with a high delocalised electron density, combined with similar highly conjugated molecular building blocks such as carbazole units, should lead to a high degree of electron delocalisation in the aromatic molecular core of compounds incorporating these elements. Such compounds should then exhibit a low energy gap. The facile introduction of a long, flexible aliphatic chain at the nitrogen atom of a thieno[3,4-*c*]pyrrole-4,6-dione unit should facilitate the synthesis of new compounds

incorporating this molecular building block with good solubility in common organic solvents for deposition form solution on device substrates.

In addition, the presence of additional 2,5-disubstituted thiophene moieties in such compounds based on thieno[3,4-c]pyrrole-4,6-dione units will also affect the energy levels and electronic properties and energy gaps in an advantageous manner[51] as well improving the solubility of such compounds in organic solvents.

Tab. 4.13 The molecular structure, mesomorphic behaviour and liquid crystalline transition temperatures (°C) of the thieno[3,4-c]pyrrole-4,6-diones **28**, **54**, **31** and **Y1**.
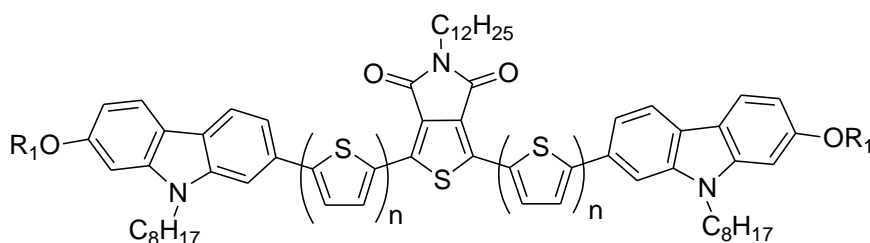
Compound	n	R_1	Tg		Cr		SmA		I
28	0	CH_3	•	69	•	212	-	-	•
54	0	C_8H_{17}	•	87	•	164		184	•
31	1	CH_3	•	-	•	172	-	-	•
Y1[a]	1	$C_{10}H_{21}$	•	-	•	144	-	-	•

Notes: a. Synthesised by Dr S Yang of the University of Hull.

Tab. 4.13 gives the chemical structures and the transition temperatures for the novel thieno[3,4-c]pyrrole-4,6-diones. It was found that the thieno[3,4-c]pyrrole-4,6-dione **54,** that features no thiophene units (n = 0), exhibits an enantiotropic smectic A phase, while compounds **28**, **31** and **Y1** exhibit no observable liquid crystalline behaviour.

A large length-to-breadth ratio is one of the determining factors for the formation of liquid crystalline mesophases for compounds with a calamitic, rod-like molecular structure. This assumption is supported by molecular modelling. **Fig. 4.17** gives the optimised 3-D geometry modelling of compounds **28**, **54**, **31** and **Y1**. As discussed

above, longer terminal straight alkyl chains generally contribute to a larger length-to-breadth ratio, which facilitates the formation of liquid crystalline mesophases. It can explain why compound **54**, with a long alkoxy chain ($R_1 = C_8H_{17}$) in a terminal position attached to the aromatic molecular core is liquid crystalline, while the analogous compound **28**, with a short alkoxy chain ($R_1 = CH_3$) in a similar positions, is not mesomorphic.

The presence of two 2,5-disubstituted thiophene units (n = 1) in the thieno[3,4-*c*]pyrrole-4,6-diones **31** and **Y1** do not exhibit any observable mesomorphic behaviour, although compound **Y1** possesses long terminal alkoxy chains ($R_1 = C_{10}H_{21}$). This may well be due to the non-linear and non co-axial nature of the 2,5-disubstituted thiophene moieties, leading to a less non-linear structure for the compounds as a whole. Compound **31** with much shorter alkoxy chains ($R_1 = CH_3$) has a much higher melting point (Cr-I = 172 $^{\circ}$C) than that (Cr-I = 144 $^{\circ}$C) of compound **Y1** as expected.

Compound **31** with two 2,5-disubstituted thiophene units (n = 1) has a lower melting point (Cr-I = 172 $^{\circ}$C) than that (Cr-I = 212 $^{\circ}$C) of the analogous compound **28**, with no thiophene units (n = 0).

In principle, in simplistic terms, the presence of additional highly conjugated aromatic rings, such as a 1,4-phenyl or 2,5-disubstituted thiophene rings, should lead to a higher melting point due to increased intermolecular forces interactions of attraction, such as Van der Walals forces. However, in contrast to a 1,4-disubstituted phenyl ring, with coaxial and colinear bonds to other substituents, the substitution pattern of the 2,5-disubstituted thiophene ring is both non-linear and non co-axial. Therefore, whereas the presence of additional 1,4-disubstituted phenyl rings usually increases the length-to-breadth ratio, the presence of 2,5-disubstituted thiophene rings reduces the length-to-breadth ratio in most cases. Hence there is often a direct relationship between the length-to-breadth ratio of compounds with a calamitic, rod-like molecular structure and the vaues of the melting point and other liquid crystalline transition temperatures, see above.

In a similar manner, due to the non-linear and non coplanar substitution pattern of the thiophene-{thieno[3,4-c]pyrrole-4,6-dione}-thiophene unit is not always conducive to high transition temperatures in spite of being a highly electron-rich, aromatic moiety. Furthermore, stronger Van der Waals interactions between a sulphur atom and an oxygen atom led to a larger angles between two thiophene units, giving rise to a slightly twisted structure. The sum of sulphur atom and oxygen atom Van der Waals radii is 3.32 A while the distance of sulphur atom (thiophene units) and oxygen atom (carbonyl) of the thiophene-{thieno[3,4-c]pyrrole-4,6-dione}-thiophene molecular structure is shorter with 2.89 A, indicating a significant Van der Waals interactions between a sulphur atom and an oxygen atom[50]. A combination of these parameters could be responsible for the relatively low values for the melting point of the thiophene-{thieno[3,4-c]pyrrole-4,6-dione}-thiophenes **28**, **54**, **31** and **Y1** with a relatively high molecular weight and an extensive, highly delocalised molecular core. These structural factors could also be responsible for the fact that the thiophene-{thieno[3,4-c]pyrrole-4,6-dione}-thiophenes **31** and **Y1** do not exhibit any observable liquid crystalline mesophases.
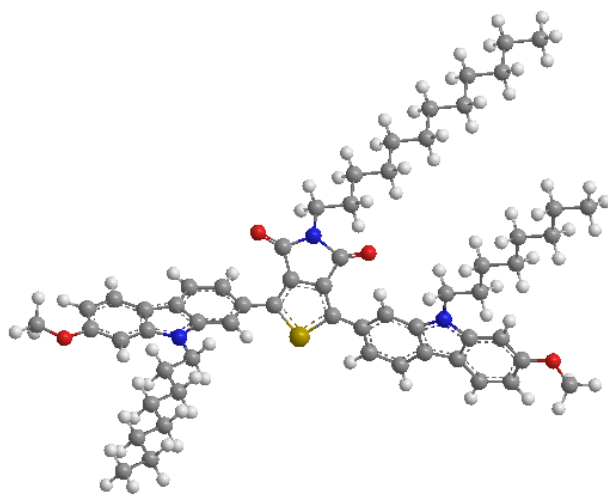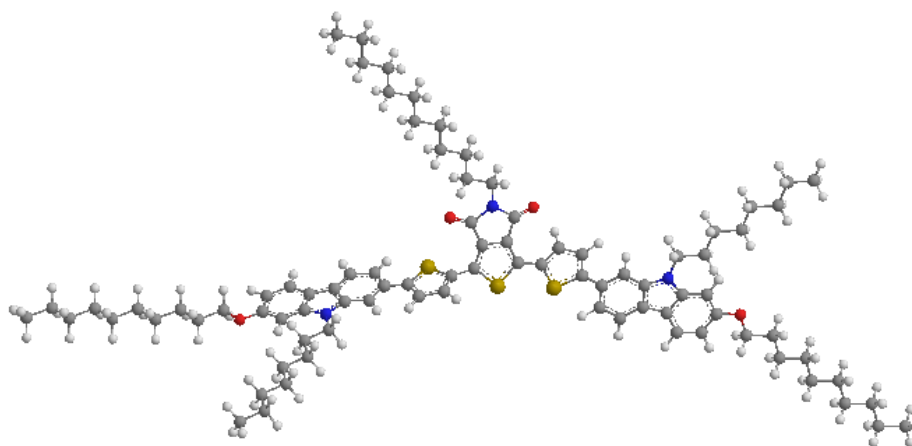

Compounds **28**
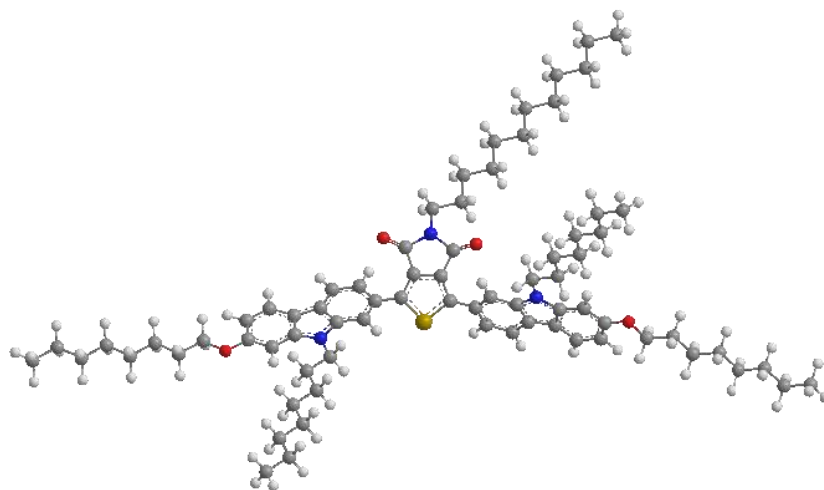
Compounds **54**
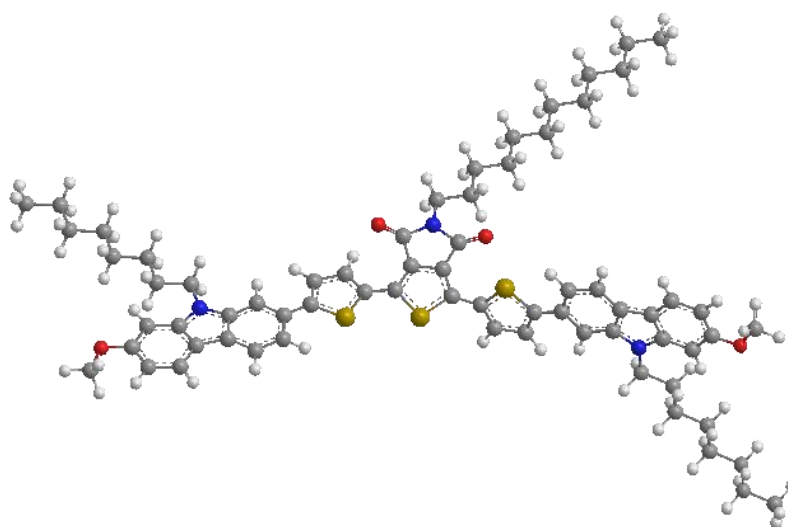
Compounds **31**

Compounds **Y1**

Fig. 4.17 Optimised 3-D geometry models of compounds **28**, **54**, **31** and **Y1**

A smectic A mesophase was observed, instead of a nematic mesophase, for compound

54 on cooling from the clearing point (SmA-I = 184 ^{o}C) to melting point (Cr-SmA =

164 °C). The OPM image of compound **54**, shown in **Fig. 4.18**, reveals the typical fan texture with focal conic unit characteristic of the Smectic A mesophase.

In principle, the smectic liquid crystalline molecules are organized in roughly parallel layers, which results in a formation of H-aggregates with a ladder configuration[27]. This may explain the relatively low efficiency of smectic emitters in OLEDs because some H-aggregation is expected to reduce their photoluminescence quantum efficiency[27]. A strategy to decrease the aggregation is to increase the intermolecular separation. Most efficient light-emitting liquid crystals in thin film, for instance, generally incorporate long flexible lateral chains attached to fluorene or carbazole, since long alkyl chains at bridging positions give rise to a relatively large intermolecular distance and thus decrease the aggregation[52]. The flexible dodecyl lateral chain attached to thieno[3,4-*c*]pyrrole-4,6-dione (Compounds **28, 54** and **31**) was designed as a consideration of decreasing aggregation and thus enhancing quantum efficiency, although long lateral chains are unfavourable for the presence of liquid crystalline mesophases. However, it is obvious that high charge transport generally requires short intermolecular distance and thus may be incompatible with high quantum efficiency caused from aggregation[27]. In addition, compared with a nematic liquid crystalline with the least ordered arrangement, the Schileren texture of a more ordered Smectic phase is more likely to be obscured or even covered by the paramorphosis of the crystalline phase when the material is heated. Therefore, the smectic A phase of compound **54** was only observed on cooling as expected. The liquid crystalline mesomorphic behaviour for compound **54** (Tg-Cr = 87 °C, Cr-SmA = 164 °C, SmA-I = 184 °C) was further confirmed using DSC thermogram analysis shown in **Fig. 4.19**. It was found that the peak of the clearing point at the 184 °C is unexpectedly significantly larger than that of the melting point at the 164 °C. It is probably because the smectic A phase of compound **54** has a very ordered arrangement which may have a bit less ordered than crystalline phase but much more ordered than the isotropic state. Therefore, the enthalpy change for compound **54** between the crystalline phase and the smectic A phase was small, while the enthalpy change between the smectic A phase and

the isotropic state was large.

Fig. 4.18 The Smectic A mesophase of compound **54** using OPM, on cooling, at 171 $^{\circ}$C
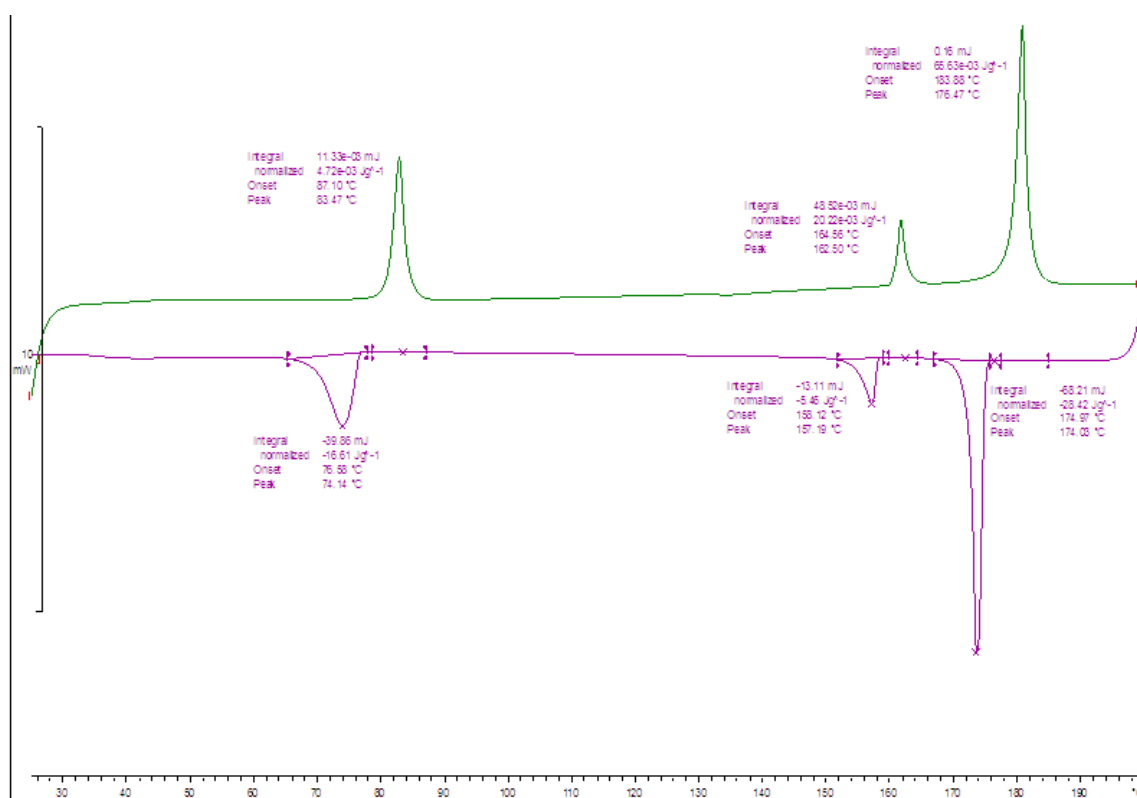

Fig. 4.19 DSC analysis as a function of temperature for compound **54** (scan rate 10 $^{\circ}$C/min)

Tab. 4.14 shows the band gaps and HOMO and LUMO energy levels for thieno[3,4-*c*]pyrrole-4,6-dione **28**, **54**, **31** and **Y1**, which exhibit relatively low values for both the energy gap and the ionisation potential as well as relatively high values for the electron affinity due to the presence of the central thieno[3,4-*c*]pyrrole-4,6-dione unit and thiophene units. Compared with the values for compounds **28** and **54** (n = 1), the presence of two additional 2,5-disubstituted thiophene units (n = 1) in the analogous compounds **31** and **Y1** leads to lower values for the HOMO energy levels and higher LUMO energy levels, hence lowering the band gap. Therefore, compounds **31** and **Y1** are of potential interest as electron-transporting materials for OLEDs.

Furthermore, the long flexible dodecyl chain attached to the central thieno[3,4-*c*]pyrrole-4,6-dione contributes to the favourable solubility of this class of materials.

Tab. 4.14 Band gaps and energy levels for thieno[3,4-*c*]pyrrole-4,6-dione-based carbazoles

Compound	IP / eV	Eg / eV	EA / eV
28	5.60	2.64	2.96
54	5.57	2.63	2.94
31	5.47	2.31	3.16
Y1[a]	5.45	2.30	3.15

Notes: a. Synthesised by Dr. S. Yang of the University of Hull

4.2.6 OLEDs

The compounds **38**, **41**, **42**, **49** and **53** were investigated as emissive materials in OLEDs by colleagues in Polar OLED. Five OLEDs were fabricated differing only in the nature of the emissive layer, i.e., compounds **38**, **41**, **42**, **49** and **53**, and their performance, including current density, brightness, efficiency and electroluminescent (EL) intensity, was measured as described in **Section 3.5.2** of the Experimental Section.

As described in **Section 3.5.1** of the Experimental Section, the device substrate was made of glass coated with a transparent thin layer of indium tin oxide (ITO) acting as the anode. *poly*(3,4-Ethylenedioxythiophene):polystyrenesulfonate (PEDOT:PSS) was used as the hole-injection layer due to its high conductivity (ca 3.0 x 10^{-3} S/cm). *N*4,*N*4'-*bis*(4-{6-[(3-Ethyloxetan-3-yl)methoxy]hexyl}phenyl)-*N*4,*N*4'-diphenylbiphenyl-4,4'-diamine (OTPD) was used as a hole-transporting layer after photochemical crosslinking. A thin layer of one of the compounds **38**, **41**, **42**, **49** and **53** was used as the emissive layer in each of the five test OLEDs. Lithium fluoride was used as the electron-injection layer and 2,7-*bis*(diphenylphosphoryl)-9,9'-spirobifluorene (SPPO13) was used as an electron-transporting layer. Aluminum (100 nm) is used as the cathode.

The chemical structures and the transition temperatures of the compounds **38**, **41**, **42**, **49** and **53** are collated in **Tab. 4.15** to facilitate a comparison of the mesomorphic behavior of these compounds differing only in the nature of the central core of their molecular structure. The data listed in **Tab. 4.15** should also serve as background information in evaluating a potential correlation between the mesomorphic behavior and liquid crystalline transition temepratures of these compounds and their relative performance as emissive materials in test OLEDs.

Tab. 4.15 The transition temperatures (^{o}C) of compounds **38**, **41**, **42**, **49** and **53** differing only in the nature of the central core of their molecular structure.
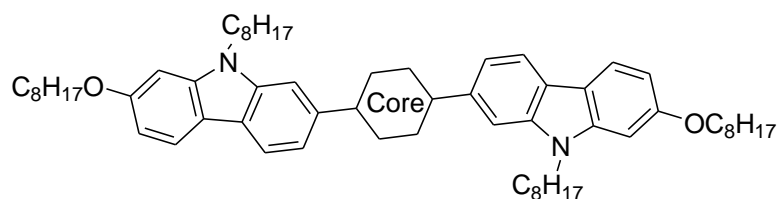
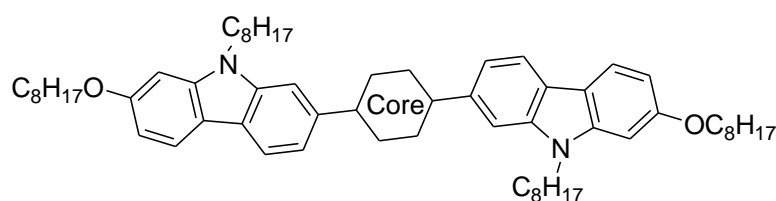| Compound	Core	Tg		Cr		N		I
38		●	-	●	136	●	151	●
41		●	-	●	66	-	-	●
42		●	32	●	-	●	161	●
49		●	-	●	141	●	202	●
53		●	85	●	105	●	(94)	●

( ) represents a monotropic transition

The data collated in **Tab. 4.15** reveals a direct correlation between the length-to-breadth ratio of the molecular core and the value for the nematic clearing point. For example a high clearing point (202 ^{o}C) and a very broad nematic phase are observed for compound **49** incorporating the rigid, planar 3,7-disubstituted dibenzo[*b,d*]thiophene moiety in the molecular core, whereas the analogous 9,9-dioctyl-2,7-disubstituted-fluorene (compound **41**) does not exhibit any observable mesomorphic behaviour. This may well be due to the greater intermolecular distance between adjacent molecules generated by the two long aliphatic chains and a much

lower effective length-to-breadth ratio for the molecular core.

The chemical structures and the energy levels and band gaps of compounds **38**, **41**, **42**, **49** and **53**, differing only in the nature of the central core of their molecular structure, are collated in **Tab. 4.16** to facilitate a comparison of the relative performance of these individual materials as emissive layers in test OLEDs.

Tab. 4.16 The Ionisation Potential (eV), Band Gap (eV) and Electron Affinity of compounds **38**, **41**, **42**, **49** and **53** differing only in the nature of the central core of their molecular structure.

Compound	Core	IP	Eg	EA
38		5.37	2.60	2.77
41		5.58	3.08	2.50
42		5.53	2.64	2.89
49		5.57	3.10	2.47
53		5.30	2.42	2.88

These OLED devices with same hole/electron layers but five different emissive layers

were measured and compared in terms of current density, brightness, efficiency and electroluminescent (EL) intensity. Specifically, the change of device efficiency, current density and brightness with the increase of voltage from zero to 8 V was shown in **Fig. 4.20**.
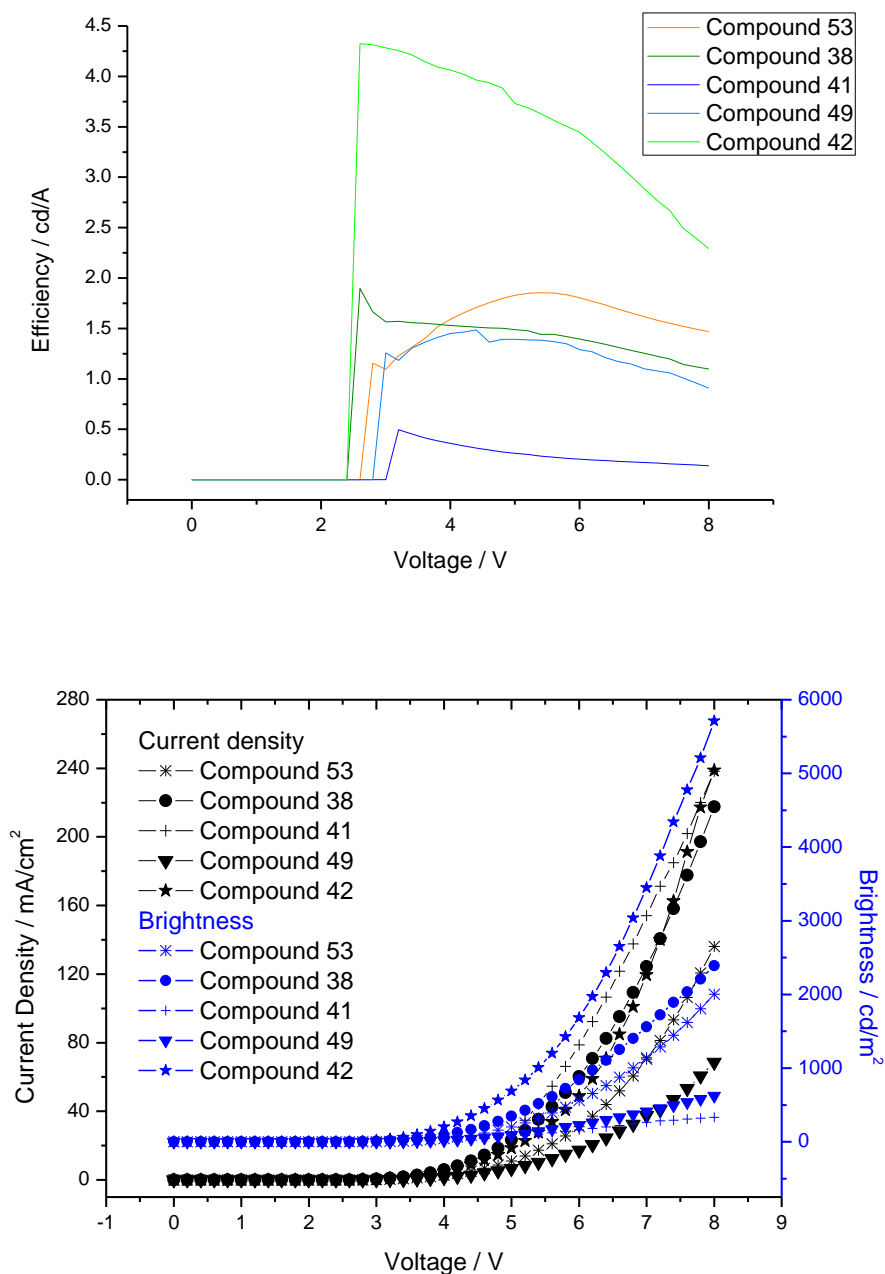

Fig. 4.20 The curves of device efficiency, current density and brightness with the increase of voltage from zero to 8 V

It can be seen from **Fig. 4.20** that each of the test OLEDs exhibits a low switch-on

250

voltage betwee 2.4 V and 3.0 V. The brightness of each of the devices at 8.0 V differs considerably, i.e., from ca 750 cd m^{-2} to ca 6,000 cd m^{-2}. It is also evident from **Fig. 4.20** that a clear correlation exists between the magnitude of the observed brightness and the current density of each of the test OLEDs, as might well be expected.

It was found that the test OLED incorporating compound **42** as the emissive layer exhibits a significantly higher efficiency, current density and brightness than the other test devices using compounds **38**, **53**, **49** and **41** instead of compound **42**. These values may be attributed to the liquid crystalline nature of compound **42** and its advantageous liquid crystalline transition temepratures, i.e., compound **42** possesses a glass transition above room temperature (Tg = 32 ^{o}C), and a nematic phase with a high clearing point (N-I = 161 ^{o}C), see **Tab. 4.15**. The relatively ordered nature of a nematic mesophases without a layer structure might well be assumed to facilitate high charge-carrier mobility as evidenced, perhaps, by the high brightness of the test OLED, i.e., holes and electrons pass readily into this material, where they are confined so that can readily combine in an efficient manner to form excitons, which then relax spontaneously from the excited state to the ground state by the emission of fluorescent light. The nematic phase has been shown to possess less traps than amorpous solids, which should facilitate high charge carrier mobility and the good device performance described above. The combination of a glassy nematic phase above room temperature (Tg = 32 ^{o}C) and a very high clearing point (N-I = 161 ^{o}C), see **Tab. 4.15**, for compound **42** may well result in a highly viscous nematic phase, which maintains a uniform structure during the OLED operation, whereby the temperature of the test device may well increase significantly over time.

There is a good match between the values of the ionization potential (-5.53 eV), see **Tab. 4.16**, of compound **42** and the HOMO energy level of the hole-transport layer OTPD (IP = -5.48 eV[53]). Similarly the electron affinity (EA = -2.89 eV) of compound **42** is similar to the LUMO energy level of electron-transporting layer of SPPO13 (EA = -2.91 eV)[54]. This advantageous combination of energy levels within the test OLED

results in low charge-injection barriers for electrons and holes, respectively, leading to a high current density and a corresponding high density of excitons in the emissive layer where efficient recombination can occur efficiently with emission of light.

The test OLED incorporating compound **41** perform poorly in terms of both efficiency and brightness and exhibit a severe efficiency roll-off. One possible reason for this poor performance may be the absence of liquid crystalline mesophases for compound **41**. However, this test OLED exhibits a high current density probably due to an advantageous value of the ionization potential (IP = -5.58 eV). However, a high-lying LUMO energy level (EA = -2.50 eV), which is unfavourable for electron transport, may well lead to an unbalanced currents of electrons and holes and consequently to poor charge recombination and an associated low device efficiency.

The test OLED incorporating the nematic liquid crystalline compounds **38**, **53** and **49** exhibit similar performance in terms of overall device efficiency. However, the devices incorporating compounds **38** and **53** exhibit higher values for the brightness and a higher current density than those of the test OLED incorporating compound **49**. The presence of less hetero-atoms in the dibenzothiophene central core of compound **49** than that in the bithiophene core of compound **38** and benzothiadiazole core of compound **53** leads to a bigger energy gap (3.10 eV, 2.60 eV and 2.42 eV, respectively) and higher-lying LUMO energy level (-2.47 eV, -2.77 eV and -2.88 eV, respectively), see **Tab. 4.16**. The bigger energy gap and higher-lying LUMO energy level are unfavourable for more efficient electron transport and balanced recombination of holes and electrons, thus causing an adverse effect on brightness and current density.
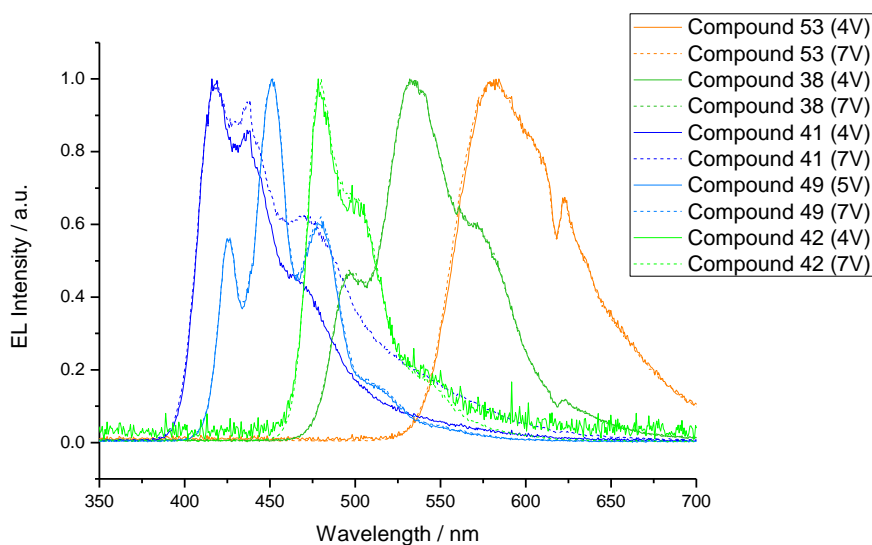
Fig. 4.21 The electroluminescent (EL) intensity of OLED devices

The electroluminescent (EL) intensity of the five OLEDs for each of these compounds as emissive materials is shown in **Fig. 4.21**. It is evident that the electroluminescent emission spectra from these test devices covers most of the visible spectrum, i.e., differences in the core of the molecular structure of these five test compounds gives rise to significant differences in the band gap (Eg) and the corresponding emission spectrum, see in **Fig. 4.22**. The OLEDs incorporating compounds **41** and **49** exhibit blue light, while those incorporating compounds **38** and **42** emit green light and the test device incorporating compound **53** exhibits orange light, see in **Fig. 4.22**. However, the emission bands are broad and overlap to a significant extent, e.g., the emission of compound **42** covers the blue and green wavelengths from 450 nm to 550 nm.
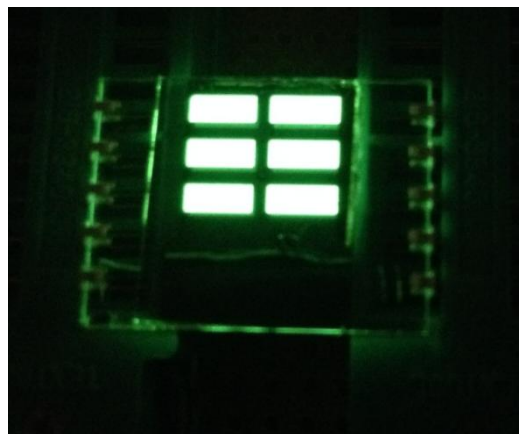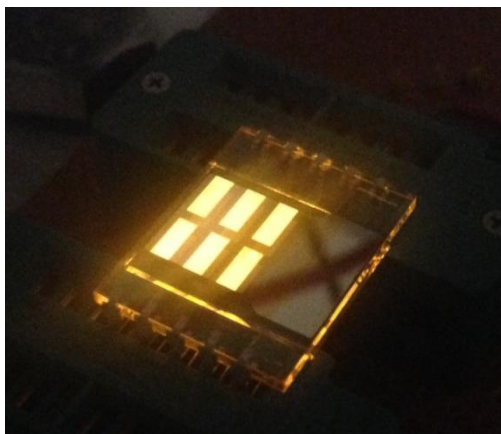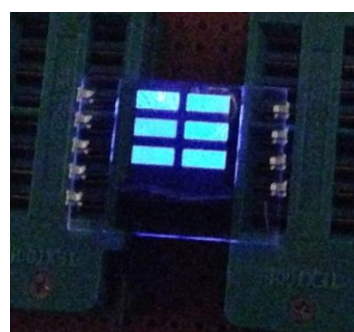
Orange OLED incorporating compound **53**   Green OLED incorporating compound **38**
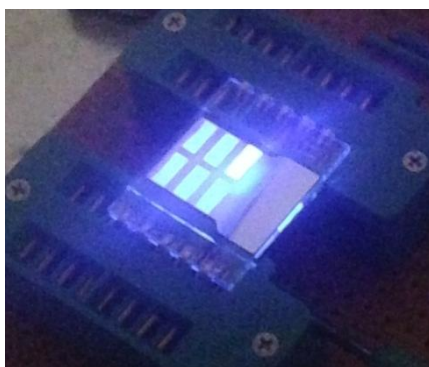
Blue OLED incorporating compound **41**

Green-Blue OLED incorporating   Blue OLED incorporating compound **49**
compound **42**

Fig. 4.22 Test OLEDs emitting different colours using the compounds **38**, **41**, **42**, **49**

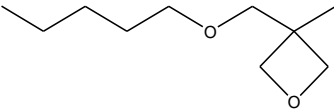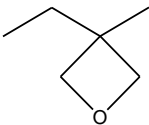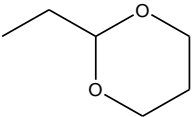and **53** synthesized in this thesis.

4.3 Triazatruxenes

Star-shaped, carbazole-functionalised triazatruxenes with a central aromatic core and flexible aliphatic chains were studied in this work as potential organic semiconductors, especially for organic light-emitting diodes (OLEDs), due to the presence of intense luminescence and suitable hole-transporting ability[55]. The disc-like, C_3-symmetric triazatruxene can be considered as an extended π-system in which three carbazole units are sharing an aromatic ring. The chemical structure resembling the classic hole-transporting carbazole and its planar disc-like nature renders triazatruxene a potentially attractive hole-transporting materials[56]. Moreover, the starburst structure of triazatruxene can be characterized by superior structural uniformity and are capable of preventing close packing and spatial reorientation, thus suppressing self-aggregation and forming high-quality thin films[57]. Although the all carbon counterpart truxene and thiatruxene have been extensively studied for liquid crystals and optical-electrical devices[58], the triazatruxene synthesised from triindole has been rarely researched and reported[59]. Therefore, a series of star-shaped carbazole-functionalised triazatruxene materials were obtained using NH substitution reactions. Some of these triazatruxenes incorporate three or more photopolymerisable endgroups, including C=C double bonds, non-conjugated dienes, C≡C triple bonds, cyclic ethers (oxetanes), and isocyanate units, at the end of aliphatic flexible spacers, so that they can be deposited from solution, by spin casting or coating, for example, as uniform thin layers on a device substrate with the desired thickness and then converted into the corresponding insoluble and intractable polymer networks as thin films for use in multi-layer devices. These photo-polymerisable materials would become insoluble after corss-linking so that multi-layer devices can be easily fabricated without layers dissolved and mixed. It also allows the further possibility of pixellation by photolithography: unexposed and non-crosslinked regions can be easily removed by washing with the original spin-casting solvent. Photopolymerisation or corss-linking can be achieved either by thermal mechanism or photo-initiation of free radicals using ultraviolet light or adding

ionic photo-initiators[60]. The cross-linked mechanism and schematic representation has been described in the introduction part above (Chapter 1.4.1). Furthermore, we also designed and synthesised other triazatruxene derivatives with different functional groups including straight and cyclic alkyl, ester, ether, and nitrile, in order to compare their physical properties for optical-electronic devices.

4.3.1 Cross-linking Properties of Photo-polymerisable Triazatruxenes

Tab. 4.17 The cross-linking properties for potentially polymerisable triazatruxene materials

Compound	R	Cross-link
89	-CH$_2$CH=CH$_2$	NO
90	-(CH$_2$)$_4$CH=CH$_2$	NO
91	CH$_2$C $\equiv$ CCH$_3$	NO
92	-(CH$_2$)$_{10}$COOCH(CH=CH$_2$)$_2$	Oil
K1[a]	-(CH$_2$)$_2$COOCH(CH=CH$_2$)$_2$	72% (800 J/cm^2 UV)
96	-(CH2)$_4$CON(CH$_2$CH=CH$_2$)$_2$	90% (400 J/cm^2 UV)
100	-CH$_2$CON(CH$_2$CH=CH$_2$)$_2$	87% (800 J/cm^2 UV)
101		Oil
102		87% (400 J/cm^2 UV)
103		NO
108	-CH$_2$N=C=O	NO

Notes: a. Synthesised by Dr SP Kitney of the University of Hull.

Overall, it is clear from consideration of the data in **Tab. 4.17** that compounds with

non-conjugated dienes or oxetanes as photopolymerisable endgroups can be photochemically cross-linked to form stable, thin films of highly crosslinked polymer networks. However, triazatruxenes with terminal reactive groups, such as C=C double bond, triple bonds, hexyl cyclic ether, and isocyanate units, at in terminal positions of the aliphatic specer gropus attached to the truxene aromatic core cannot be induced to photoolymerise or only a minimal degree of cross-linking was observed, although different intensities of UV radiation (200J, 400J, 600J and 800J) were trialled. One of the possible reasons for this behaviour is that the number of cross-linkable groups (3) for compounds **89, 90** and **91** is less than that (6) for the non-conjugated dienes **92**, **96** and **100**.

When compound **89** ($-CH_2CH=CH_2$) was synthesised and proved non-crosslinkable under standard conditions, it was thought that this behaviour might be due to the length of aliphatic chains, i.e., the side chains are too short and the alkene bonds are too close to the triazatruxuene core to be able to physically react with adjacent carbon-carbon double bonds. Consequently, compound **90** with a longer spacer group ($-(CH_2)_4CH=CH_2$) was synthesised. Unfortunately, compound **90** [$-(CH_2)_4CH=CH_2$] also proved to be non-crosslinkable under standard conditions.

Compound **103**, with a hexyl cyclic ether as a terminal reactive group, also could not be photochemically cross-linked, probably because the six-membered ring is relatively stable.

Compound **108**, with an isocyanate as a terminal reactive group, also could not be photochemically cross-linked. perhaps because the short straight side chains could be covered by the star-shaped triazatruxene core, so that the polymerisable isocyanate units cannot react with adjacent isocyanate units.

In terms of fabricating films for optical-electrical devices, oils or liquids tend not to assemble spontaneously to form uniform thin films on device substrate surfaces. Compound **92** with a long terminal chain [$-(CH_2)_{10}COOCH(CH=CH_2)_2$] is an oil at

257

room temperature. Therefore, it was decided to synthesise compound **K1** with a much shorter aliphatic chain incorporating a non-conjugated diene [$-(CH_2)_2COOCH(CH=CH_2)_2$] in the hope of preparing a solid at room temperature. This approach was successful in that **K1** was indeed found to be a powder at room temperature.

The UV-Vis absorption spectra for thin films of compound **K1** after exposure to 800 J/cm^2 UV energy are shown in **Fig. 4.23**. In order to prepare these samples of compound **K1** were first dissolved in chlorobenzene and six separate thin films were spun down using the same dilute (1 wt%) solution. Each film was exposed to varying amounts of UV energy (0, 100 J/cm^2, 200 J/cm^2, 400 J/cm^2, 600 J/cm^2, 800 J/cm^2). Unfortunately none of the films shows a high degree of cross-linking even at 800 J/cm^2 (cross-linked yield 72%). One of the possible reasons for imcomplete cross-linking is that the relatively unstable ester bonds attached to non-conjugated dienes could cause degradation to some degree. Furthermore, the shorter side chains [$-(CH_2)_2COOCH(CH=CH_2)_2$] attached to a star-shaped conjugated triazatruxenes for compound **K1** may be too short to allow the physical cross-linking of the adjacent non-conjugated dienes.
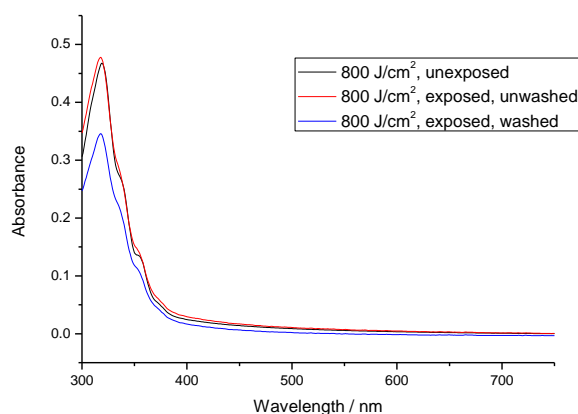

Fig. 4.23 The UV-Vis absorption spectra for compound **K1**.

Compounds **96** and **100** both with tertiary amide attached to non-conjugated dienes were synthesised in order to yield compounds with a greater tendency to

photopolymerise. The tertiary amide function is more chemically and photochemically stable than an ester bond. This change resulted in a higher cross-linked yield (90% @ 400 J/cm^2 UV and 87% @ 800 J/cm^2 UV) for compounds **96** and **100**, respectively, compared with that (72% @ 800 J/cm^2 UV) observed for compound **K1**. Compound **96** was dissolved in chlorobenzene and 2 films were spun coated onto plasma treated glass at 2000 rpm and 2000 acceleration from the same 1wt% solution. Each film for compound **96** was exposed to different UV energy (100 J/cm^2 and 400 J/cm^2), and their UV-Vis absorption spectra were shown in **Fig. 4.24** below. It was found that the first absorption for compound **96** occurs at a wavelength of approximate 370 nm. When the film of compound **96** is exposed to UV energy (100 J/cm^2 or 400 J/cm^2), there is a slight increase in the intensity of the absorbance peak (exposed, unwashed peak). Therefore, it can be assumed that no large-scale degradation occurred during the UV exposure. Then, after the two films (for 100 J/cm^2 or 400 J/cm^2, respectively) of compound **96** were exposed to radiation, they were washed with chlorobenzene to remove any uncrosslinked material. It was found that there is no significant difference in the intensity of the absorbance peak for each for the exposed film before and after washing. Therefore, it can be assumed that polymerisation of the non-conjugated dienes present in compound **96** has occurred to form an insoluble, highly crosslinked polymer network. However, the polymerisation under 100 J/cm^2 UV (cross-linked yield 63%) is not quite complete as evidenced by the relatively significant reduction for the intensity of the absorbance peak after washing. In such case, the UV energy was increased from 100 J/cm^2 to 400 J/cm^2 for more cross-linking. It was found that the intensity of the absorbance peak of the film irradiated at 400 J/cm^2 and then washed with chlorobeneze was only slightly lower (cross-linked yield 90%), which is indicative of an adequate degree of polymerisation to form an insoluble thin film on a substrate.
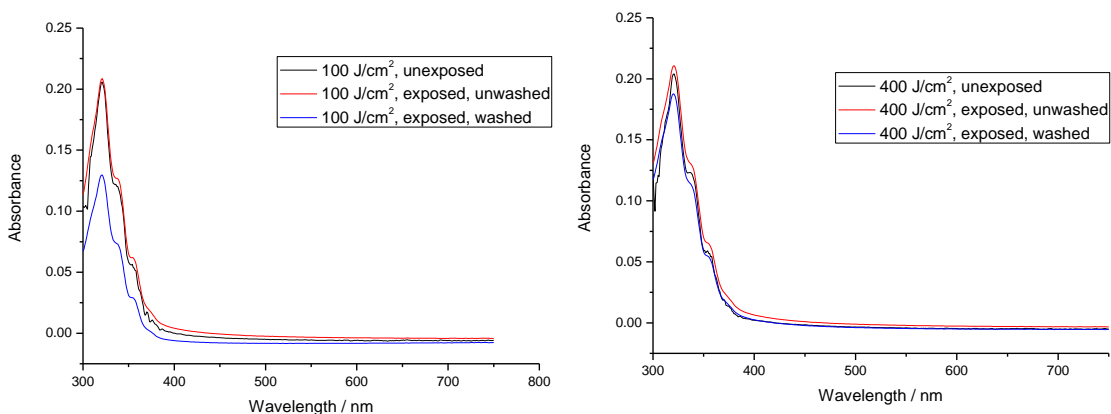
Fig. 4.24 The UV-Vis absorption spectra under 100 J/cm^2 and 400 J/cm^2 for compound

96

The crosslinking properties of an oil, e.g., compound **96** with longer aliphatic side chains [-(CH$_2$)$_4$CON(CH$_2$CH=CH$_2$)$_2$], were compared with that of an analogous solid, e.g., compound **100** with much shorter chains [-CH$_2$CON(CH$_2$CH=CH$_2$)$_2$]. Compound **100** was dissolved in chlorobeneze and six films were spun coated onto plasma-treated glass at 2000 rpm and 2000 acceleration from the same 1 wt% solution. Each film for compound **100** was exposed to different UV energy (0, 100 J/cm^2, 200 J/cm^2, 400 J/cm^2, 600 J/cm^2 and 800 J/cm^2), and their UV-Vis absorption spectra after being washed with chlorobenzene were obtained and compared in **Fig. 4.25 (a)** below. It can be seen that the intensity of the UV absorbance peak of compound **100** has been reduced to almost zero after washing with chlorobenzene when irradiated with low-intensity UV radiation (100 J/cm^2), which suggests that compound **100** was not cross-linked at this level of UV exposure. Their intensity of absorbance increased with increasing intensity of UV radiation to a maximum under an exposure to 800 J/cm^2 UV, see **Fig. 4.25 (b)**. It was found that compound **100** requires higher UV energy (87% @ 800 J/cm^2) to arrive at a similar cross-linked yield compared with compound **96** (90% @ 400 J/cm^2).

The minimum fluence for sufficient photo-polymerisation of non-conjugated dienes depends on the freedom and moving ability of photo-polymerisable end-groups[61]. Therefore, the non-conjugated dienes with shorter side chains attached to the

260

star-shaped triazatruxuene core are more likely to be limited in their ability to react with adjacent photo-polymerisable end-groups. It can well explained why the cross-linked yield under high UV fluence (87% @ 800 J/cm^2) for compound **100** with short side chains [-CH$_2$CON(CH$_2$CH=CH$_2$)$_2$] is still slightly lower than that achieved at lower UV intensity (90% @ 400 J/cm^2) for compound **96** with longer side chains [-(CH$_2$)$_4$CON(CH$_2$CH=CH$_2$)$_2$].

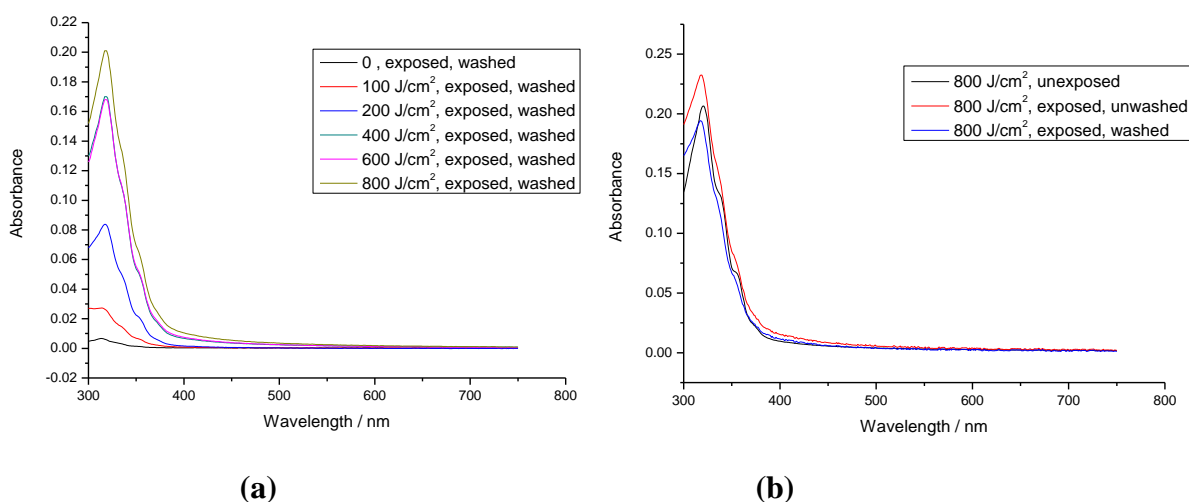**(a)**   **(b)**

Fig. 4.25 The UV-Vis absorption spectra for compound **100**: **(a)** after washed with chlorobenzene under different UV energy (0, 100 J/cm^2, 200 J/cm^2, 400 J/cm^2, 600 J/cm^2 and 800 J/cm^2); **(b)** unexposed, exposed, and washed under 800 J/cm^2 UV.

Oxetanes are one of the most explored cross-linkable functional groups due to high cross-linking conversion, short conversion time, and minor modifications of the optical-electrical properties[62]. Oxetanes are four-membered cyclic ethers that can be polymerised in bulk *via* cationic ring-opening reactions with an adjacent oxetane group. However, the driving force for most ring-opening polymerisation is the ring strain and associated steric considerations[63]. Three-membered or four-membered cyclic ethers have much higher ring strain than six-membered cyclic ether, which explained why compound **103** cannot be photo-polymerised. The UV-induced oxetane ring-opening polymerisation generally requires a photo-initiator, which can induce the initial polymerisation by activating an oxetane ring. The proton photo-initiator is generally

from photo-acid generators, and the typical amount of a photo-initiator is less than 5%[62]. It is because the initial induction does not require much energy for initiation with the subsequent cross-linking continued by the bulk oxetanes. An excessive amount of photo-initiators is also unfavourable, as removing them from thin films after cross-linking in non trivial.

The oxetane **101** with longer side chains incorporating cyclic oxetanes is an oil state whereas compound **102** with shorter side chains incorporating cyclic oxetanes is a solid powder. Compound **102** was spun coated in chlorobenzene from a 1% solution doped 1% with the cationic photo-initiator UVI-6992 (containing a mixture of triarylsulfonium hexafluoroantimonate salts in propylene carbonate). Once mixed together, the solution was spun at 2000 rpm at 2000 acceleration for 30 seconds. The resultant films were exposed to UV light at either 400 J/cm^2 or 800 J/cm^2 and then annealed at 100 ^{o}C for 5 minutes. The result shows the combination of higher UV energy (800 J/cm^2) and the use of photo-initiators gives a moderate cross-linking yield (87%). It suggests that oxetane ring-opening polymerisation requires higher energy than that for analogous non-conjugated dienes. In addition to the nature of oxetane ring-opening polymerisation, the presence of short side chains may also be partly responsible for the high amount of UV energy required to induce polymerisation. The UV-Vis absorption spectra for compound **102** under 800 J/cm^2 UV energy were shown in **Fig. 4.26**.
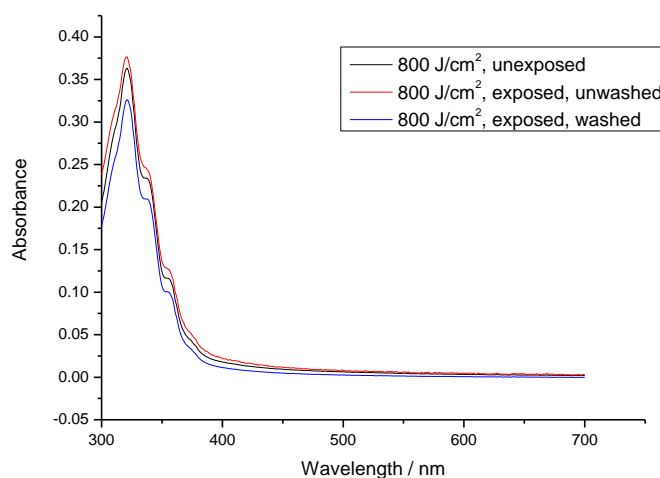

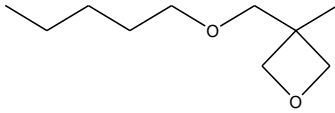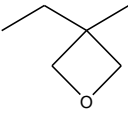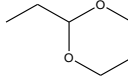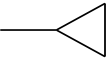**Fig. 4.26** The UV-Vis absorption spectra for compound **102**

4.3.2 Physical properties of the triazatruxenes 86-92, **96** and **100-108**

Tab. 4.18 gives melting points (^{o}C), band gap (eV) and HOMO & LUMO energy levels (eV) for the triazatruxenes **86-92**, **96** and **100-108** incorporating a wide range of side-chains such as alkyl, cyclic alkyl, double bonds, triple bonds, non-conjugated dienes, ether, cyclic ether, ester, nitrile, and isocyanate. It facilitates a comparison of thermal properties and energy levels for these triazatruxene compounds with different functional groups attached to the ends of the flexible side-chains. The triazatruxene compounds possess relatively low HOMO energy levels, which could therefore be of interest as potential hole-transporting materials.

It seems the energy levels and band gap were not influenced significantly by different side-chains with different functional groups, although compounds **106** (ester), **107** (ester) and **108** (isocyanate) exhibit a slightly higher values for both the energy levels and the band gap.

In addition, in terms of melting points of triazatruxene compounds, they all exhibit good thermal stability, due to the star-shaped π-conjugated triazatruxene core. In particular, photo-polymerisable compounds **100** and **102** with non-conjugated dienes and oxetanes exhibit good thermal stability with relatively high melting points of 206 ^{o}C and 200 ^{o}C, respectively, due to short methylene chains linking triazatruxene core and the amido bonds and oxetanes. Furthermore, it is also reasonable that compounds **103** and **104** with stable cyclic structures exhibit high melting points of 236 ^{o}C and 224 ^{o}C, respectively. Compound **108** shows a very high melting point above 280 ^{o}C, due to the presence of short straight side-chains ($-CH_2N=C=O$) and the conjugated double bonds of isocyanate groups.

Tab. 4.18 Melting points (^{o}C), band gap (eV) and energy levels (eV) for triazatruxenes **86-92**, **96** and **100-108**.

Compound	R	Cr-I / ^{o}C	IP / eV	Eg / eV	EA / eV
89	$-CH_2CH=CH_2$	223	5.40	3.38	2.05
90	$-(CH_2)_4CH=CH_2$	107	5.38	3.39	1.99
91	$CH_2C\equiv CCH_3$	266	5.43	3.43	2.03
92	$-(CH_2)_{10}COOCH(CH=CH_2)_2$	Oil	5.36	3.38	1.98
96	$-(CH2)_4CON(CH_2CH=CH_2)_2$	Oil	5.35	3.39	1.96
100	$-CH_2CON(CH_2CH=CH_2)_2$	206	5.37	3.39	2.11
101	(structure)	Oil	5.37	3.39	1.98
102	(structure)	200	5.38	3.37	2.11
103	(structure)	236	5.34	3.38	1.96
105	$-CH_2CH_2OCH_2CH_3$	129	5.36	3.40	1.96
106	$-CH_2CH_2OCOCH_3$	144	5.47	3.40	2.07
107	$-CH_2COOCH_2CH_3$	186	5.51	3.43	2.08
109	$- CH_2CH_2CH_2CH_2CN$	98	5.43	3.38	2.05
108	$-CH_2N=C=O$	> 280	5.61	3.46	2.15
86	$-C_4H_9$	117	5.34	3.38	1.96
87	$-C_6H_{13}$	114	5.34	3.37	1.97
88	$-C_8H_{17}$	81	5.35	3.36	1.99
104	(structure)	224	5.40	3.40	2.00

4.3.3 Charge-Carrier Mobility and Hole-Only Test Devices

In order to investigate the effect on the hole-transport properties of the triazatruxene monomers shown in **Tab. 4.18** and that of the corresponding highly crosslinked polymer networks formed by their photopolymerisation in test optical-electrical devices, triazatruxene **100** was chosen as a typical example of this class of materials. The effect on the hole carrier mobility of doping of compound **100** and its corresponding highly crosslinked polymer network with the highly electronegative *p*-type dopant F4-TCNQ was also studied in order to establish whether this approach would be a viable approach to increase the efficiency of multi-layer OLEDs and PIN devices by increasing the hole charge-carrier mobility.

The conductivity measurements were carried out using hole-only test diode devices fabricated and tested as described in **Section 3.6.1** of the Experimental Section. The data of current-voltage were collected and graphed in **Fig. 4.27**. The average of linear fits to current-voltage data was obtained from **Fig. 4.27** as 2.96×10^{-10} S. The film thickness (T) was measured using Dektak as 10 nm. d = the total distance between finger electrodes = $5 \times (50 \times 10^{-6}$ m), L = the length of finger electrodes = 5×10^{-3} m, thus A = total area = $5 \times (T \times L) = 5 \times (10 \times 10^{-9}$ m $\times 5 \times 10^{-3}$ m) for this ITO finger device. The average conductivity established for compound **100** gives the value of 2.96×10^{-4} S m^{-1} or 2.96×10^{-6} S cm^{-1}.
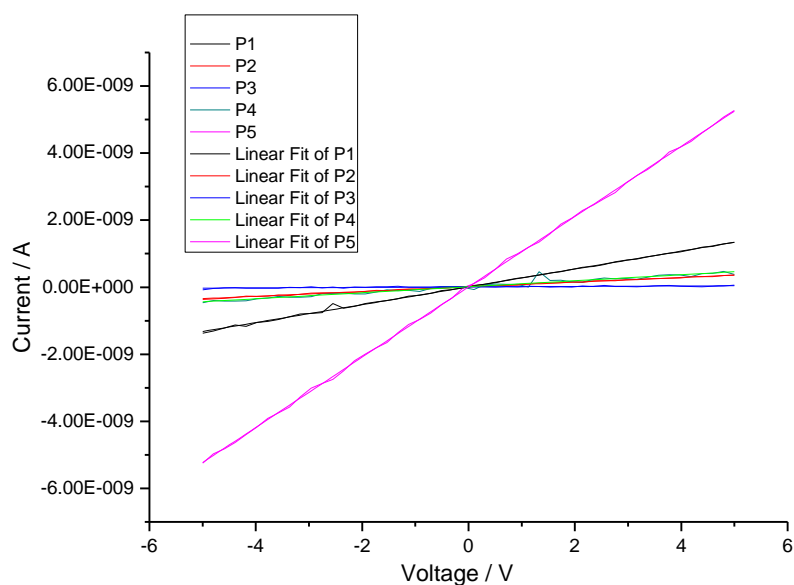
Fig. 4.27 The current-voltage plots of compound **100**.

It can be seen from **Fig. 4.27** that the five different positions of the pre-patterned ITO fingers designed to investigate the uniformity of the conductivity in different locations reveal that the conductivity of compound **100** is generally uniform in different positions. The slightly higher conductivity values exhibited in position P5 might well be attributable to differences in the film thickness and/or in film morphology or inconsistencies introduced in fabrication of the pre-patterned ITO fingers.

In order to study the effect of cross-linking and doping on conductivity of the triazatruxenes designed as hole-transport layers for multi-layer OLEDs and PIN devices, four hole devices with different hole-transport layers were fabricated as described in **Section 3.6.2** of the Experimental Section. The hole-transport layers chosen for study includes compound **100**, cross-linked compound **100**, compound **100** doped (5 wt%) with 2,3,5,6-tetrafluoro-7,7,8,8-tetracyanoquinodimethane (F4-TCNQ), and cross-linked compound **100** doped (5 wt%) with F4-TCNQ. The concentration of the dopant was chosen to be no more than 10 wt% as a concentration above this limit have been found to give rise to self-aggregation of the dopant and thereby create to more charge traps. Once a device has been tested it cannot be tested again due to

morphology changes and charge traps that may have been introduced during the first scan. These four hole-only diode devices were operated under 10 V, which is consistent with the operation of commercial OLEDs. The current density is plotted with common logarithm against voltage in **Fig. 4.28**.
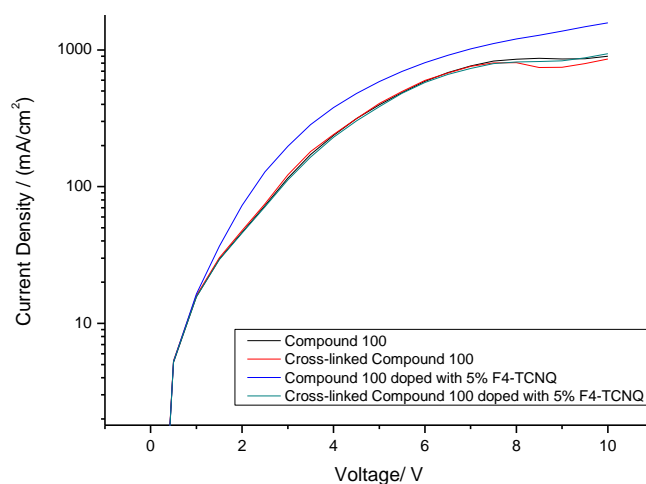
Fig. 4.28 Current Density-Voltage curve for the four test hole devices.

It is evident from consideration of **Fig. 4.28** that there is no reduction in the current density (black curve) when compound **100** is photopolymerised to form a highly cross-linked polymer network (red curve), i.e., there is little difference between the current density vs voltage plots for these two hole-only test devices. It is often observed that polymerization of monomers with more than one polymerizable group to form a highly cross-linked polymer network results in a reduction in the charge-carrier mobility due to the disruption of the molecular order within the thin layer as the polymerisable end-groups form a covalently bonded polymer backbone and/or to the formation of both shallow and deep traps for charge carriers.

The test device incorporating a combination of compound **100** doped with 5 wt% of F4-TCNQ as the hole-transporting layer shows a higher current density (blue curve). than those of the two test devices without dopant (black and the red curves). This result is probably attributable to the fact that the highly electronegative *p*-type dopant F4-TCNQ can produce more free holes in a device by removing electrons from the host

material. Furthermore, the LUMO energy level (EA = -5.24 eV[64]) of F4-TCNQ is closely aligned with the HOMO energy level (IP = -5.37 eV), see **Tab. 4.18**, of the hole-transporting material compound **100**[65].

However, the current density vs voltage plot for the test device incorporating highly cross-linked compound **100** doped with 5 wt% of F4-TCNQ as the hole-transporting layer (green curve) is very similar to that (red curve) observed for the test device incorporating highly cross-linked, but non doped, compound **100**. This fact may be attributable to the formation of a high density of traps and/or to a degree of phase separation whereby the dopant is excluded from the polymer network making up the hole transport layer.

Commercial PEDOT:PSS exhibits excellent hole injection due to its intrinsically high conductivity (3.0×10^{-3} S cm^{-1}). However, a hole-transport layer is required in efficient multi-layer OLEDs to control the current of holes and thereby to avoid unbalanced charge injection and charge mobility in the device. Without a hole-transport layer, charge recombination occurs predominantly near the cathode, which results in quenching of the excitons without light emission. Furthermore, the HOMO energy level of PEDOT:PSS is higher, i.e., -5.2 eV, than that, e.g., -5.5 eV or lower lying, of common emissive materials used in OLEDs, which results in a mismatch of about 0.3 eV or even larger[66]. However, compound **100** exhibits an intermediate HOMO energy level, i.e., -5.37 eV as shown in **Tab. 4.18**, between that of PEDOT:PSS and the emiisive material and its presence in OLEDs reduces hole-injection barrier from the PEDOT:PSS and facilitates the transport of holes to the emissive layer.

Furthermore, the insoluble and intractable nature of highly cross-linked polymer networks facilitates the fabrication of multi-layer OLEDs using wet chemistry techniques without interlayer mixing. Therefore, photopolymerisable triazatruxene monomers, such as those shown in **Tab. 4.18**, and as exemplified by compound **100**, are potentially advantageous as hole-transport layers in plastic electronic devices, such as multi-layer OLEDs and OPVs.

A range of triarylamines has been extensively studied as hole-transport materials in commercial OLEDs due the ready oxidation of the nitrogen centre to form stable radical cation species for the efficient transport of holes[67-71]. Therefore, the performance of the triazatruxene monomers, shown in **Tab. 4.18**, as hole-transport materials is also compared with that of a similarly star-shaped triarylamine monomer with three non-conjugated diene endgroups (**Ref. 1**) see **Fig. 4.29**.

Fig. 4.29 The chemical structure of compound **Ref. 1**

The same procedures and methods as those used to evaluate hole-only test devices incorporating compound **100** and its highly cross-linked polymer network were used to measure the current density of similar devices incorporating compound **Ref. 1** and polymer network formed by the photopolymerisation of compound **Ref. 1** in hole only test devices. A comparison of the current density vs voltage plots of the test devices incorporating the triazatruxene compound **100** and the triarylamine **Ref. 1**, as well as those for the corresponding highly crosslinked polymer networks is shown in **Fig. 4.30**.
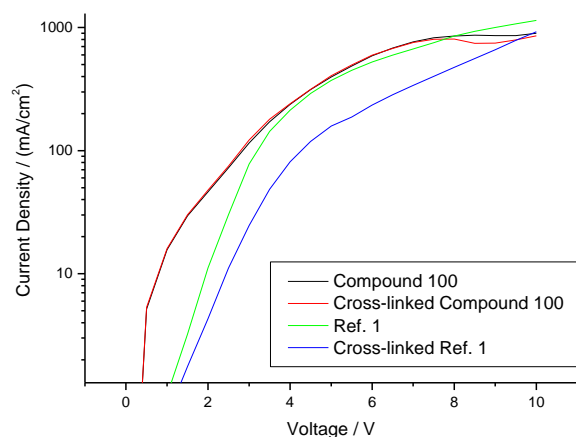
Fig. 4.30 The comparisons of Current Density-Voltage graph for compound **100**, **Ref. 1**, cross-linked compound **100**, and cross-linked **Ref. 1**.

It can be seen clearly that both non cross-linked and cross-linked triarylamine **Ref. 1** (green and blue curve, respectively) exhibit a lower current density and hence hole carrier mobility than that of the corresponding non cross-linked and cross-linked triazatruxene compound **100** (black and red curve, respectively). However, unlike the similar current density vs voltage plots of the non cross-linked and the cross-linked compound **100**, the current density at the same voltage of the cross-linked **Ref. 1** (blue curve) is much lower than that of non cross-linked **Ref. 1** (green curve). This fact may be due to the formation of more charge traps resulting from the more complicated polymer structures. Compared with the triarylamine **Ref. 1** with only a nitrogen atom in the centre of its starburst molecular structure, the triazatruxene derivative **100** also possesses three carbazole units, which may well make a significant contribution to its electron-donating and hole-transporting capability.

4.4 References

[1]   D. J. Schipper and K. Fagnou, *Chem. Mater.,* 2011, **23**, 1594.

[2]   S. I. Gorelsky, Coord. *Chem. Rev.,* 2013, **257**, 153.

[3]   L. G. Mercier and M. Leclerc, *Acc. Chem. Res.,* 2013, **46**, 1597.

[4]   S. I. Gorelsky, D. Lapointe and K. Fagnous, J. Org. Chem., 2012, **77**, 658.

[5]   T. I. Wallow and B. M. Novak, *J. Org. Chem.,* 1994, **59**, 5034.

[6]   W. Han, C. Liu and Z. Jin, *Org. Lett.*, 2007, **20**, 4005.

[7]   G. A. Molander and B. Biolatto, *J. Org. Chem.,* 2003, **68**, 4302.

[8]   G. W. Kabalka, V. Namboodiri and L. Wang, *Chem. Commun.,* 2001, 775.

[9]   H. Sakurai, T. Tsukuda and T. Hirao, *J. Org. Chem.*, 2002, **67**, 2721.

[10]   C. Liu, Q. Ni, F. Bao and J. Qiu, Green Chem., 2011, **13**, 1260.

[11]   F. Proutiere and F. Schoenebeck, *Angew. Chem. Int. Ed.,* 2011, **50**, 8192.

[12]   A. Cipiciani, S. Clementi, P. Linda, G. Marino and G. Savelli, *J. Chem. Soc., Perkin Trans. 2,* 1977, 1284.

[13]   "*Organic electronics: materials, manufacturing and applications*", edited by H. Klauk, Wiley-VCH, Weinheim, 2006.

[14]   T. W. Kelley, P. F. Baude, C. Gerlach, D. E. Ender, D. Muyres, M. A. Haase, D. E. Vogel and S. D. Theiss, *Chem. Mater.,* 2004, **16**, 4413.

[15]   S. R. Forrest and M. E. Thompson, *Chem. Rev.,* 2007, **107**, 923.

[16]   N. J. Tao, *Nat. Nanotechnol.,* 2006, **1**, 173.

[17]   S. Kato, S. Shimizu, A. Kobayashi, T Yoshihara, S Tobita and Y. Nakamura, *J. Org. Chem.,* 2014, **79**, 618.

[18]   P. Data, P. Pander, M. Lapkowski, A. Swist, J. Soloducho, R. R. Reghu and J. V. Grazulevicius, *Electrochim. Acta*, 2014, **128**, 430

[19]   K. H. Park, H. Yun, W. Lu, D. S. Chung, S. Kwon and Y. Kim, *Dyes Pigments,* 2014, **103**, 214.

[20]   M. Mushrush, A. Facchetti, M. Lefenfeld, H. E. Katz and T. J. Marks, *J. Am. Chem. Soc.,* 2003, **125**, 9414.

[21]   A. Pelter, I. Jenkins and D. E. Jones, *Tetrahedron,* 1997, **53**, 10357.

[22]   S. Kumar, P. Singh, R. Srivastava, R. R. Koner, A. Pramanik, J. Mathew, S. Sinha, M. Rawat, R. S. Anand and S. Ghosh, J. Mater. Chem., 2014, 2, 6637.

[23]   J. Shao, J. Chang and C. Chi, Org. Biomol. Chem., 2012, 10, 7045.

[24]   Q. Hou, Y. Xu, W. Yang, M. Yuan, J. Peng and Y. Cao, *J. Mater. Chem.,* 2002, **12**, 2887.

[25]   R. D. J. Vuuren, P. C. Deakin, S. Olsen and P. L. Burn, *Dyes Pigments,* 2014, **101**, 1.

[26]   PhD Thesis of M. R. Billa, "*Liquid Crystalline Organic Semiconductors for Application in Opto-electronic Devices*", University of Hull, 2014.

[27]   Book, *"Liquid Crystalline Semiconductors: Materials, Properties and Applications"*, by R. J. Bushby, S. M. Kelly and M. O'Neill, Springer, The Netherlands, 2013.

[28]   Y. Na, W. Song, J. Y. Lee and S. Hwang, *Dalton Trans.*, 2015, **44**, 8360.

[29]   K. S. Yook and J. Y. Lee, *Adv. Mater.*, 2012, **24**, 3169.

[30]   S. C. Dong, C. H. Gao, X. D. Yuan, L. S. Cui, Z. Q. Jiang, S. T. Lee and L. S. Liao, *Org. Electron.,* 2013, **14**, 902.

[31]   N. Delbosc, W. Z. N. Yahya, N. Lemaitre, S. Berson, F. Fuchs, B. Grevin, J. F. Vincent, J. P. Travers and R. Demadrille, *RSC Adv.*, 2014, **4**, 15236.

[32]   B. N. Yawson, H. S. Lee, D. Seo, Y. Yoon, W. T. Park, K. Kwak, H. J. Son, B. Kim and Y. Y. Noh, *Adv. Mater.,* 2015, **27**, 3045.

[33]   J. Peng, K. Ye, J. Sun, Y. Zhan, J. Jia, P. Xue, G. Zhang, Z. Zhang and R. Lu, *Dyes Pigments*, 2015, **116**, 36.

[34]   A. M. Alsalme, A. A. B. Alghamdi, A. A. G. Q. Alhamdani, A. Iraqi, *Int. J. Electrochem. Sci.*, 2014, **9**, 1920.

[35]   A. Casey, R. S. Ashraf, Z. Fei and M. Heeney, *Macromolecules,* 2014, **47**, 2279.

[36]   Z. Mohsan, A. L. Kanibolotsky, A. J. Stewart, A. R. Inigo, L. Dennany and P. J. Skabara, *J. Mater. Chem. C.,* 2015, **3**, 1166.

[37]   Z. Rong, Y. Deng, Z. Xie, Y. Geng and F. Wang, *Sci. China Chem.*, 2015, **58**, 294-300.

[38]   S. Wang, M. Wang, X. Zhang, X. Yang, Q. Huang, X. Qiao, H. Zhang, Q. Wu, Y. Xiong, J. Gao and H. Li, *Chem. Commun.,* 2014, **50**, 985.

[39]   G. Qian, B. Dai, M. Luo, D. Yu, J. Zhan, Z. Zhang, D. Ma and Z. Y. Wang, *Chem. Mater.,* 2008, **20**, 6208.

[40]   W. Xiao, Z. He, S. R. Buenamanana, R. J. Turner, M. Xu, X. Yang, X. Jing and

A. N. Cammidge, *Org. Lett.,* 2015, **17**, 3286.

[41]   S. Ming, S. Zhen, K. Lin, L. Zhao, J. Xu, B. Lu, L. Wang, J. Xiong and Z. Zhu, *J. Electron. Mater.,* 2015, **44**, 1606.

[42]   R. Matsidik, J. Martin, S. Schmidt, J. Obermayer, F. Lombeck, F. Nubling, H. Komber, D. Fazzi and M. Sommer, *J. Org. Chem.,* 2015, **80**, 980.

[43]   B. Zaifoglu, S. O. Hacioglu, N. A. Unlu, A. Cirpan and L. Toppare, *J. Mater. Sci.,* 2014, **49**, 225.

[44]   P. Sonar, S. P. Singh, P. Leclere, M. Surin, R. Lazzaroni, T. T. Lin, A. Dodabalapur and A. Sellinger, *J. Mater. Chem.,* 2009, **19**, 3228.

[45]   A. Yassin, P. Leriche, M. Allain and J. Roncali, *New J. Chem.,* 2013, **37**, 502.

[46]   J. Pina, J. S. de Melo, D. Breusov and U. Scherf, *Phys. Chem. Chem. Phys.,* 2013, **15**, 15204.

[47]   L. E. Polander, L. Pandey, S. Barlow, S. P. Tiwari, C. Risko, B. Kippelen, J. Bredas and S. R. Marder, *J. Phys. Chem. C,* 2011, **115**, 23149.

[48]   G. Zhang, Y. Fu, Z. Xie and Q. Zhang, *Polymers*, 2011, **52**, 415.

[49]   C. B. Nielsen and T. Bjornholm, *Org. Lett*., 2004, **6**, 3381.

[50]   X. Guo, R. P. Ortiz, Y. Zheng, M. Kim, S. Zhang, Y. Hu, G. Lu, A. Facchetti and T. J. Marks, *J. Am. Chem. Soc.,* 2011, **133**, 13685.

[51]   A. Najari, S. Beaupre, P. Berrouard, Y. Zou, J. Pouliot, C. L. Perusse and M. Leclerc, *Adv. Funct. Mater.,* 2011, **21**, 718.

[52]   S. Droge, M. S. A. Khalifah, M. O'Neill, H. E. Thomas, H. S. Simmonds, J. E. Macdonald, M. P. Aldred, P. Vlachos, S. P. Kitney, A. Lobbert and S. M. Kelly, *J.*

Phys. Chem. B, 2009, **113**, 49.

[53]   P. S. Rudati, D. C. Mueller and K. Meerholz, *J. Appl. Res. Technol.,* 2015, **13,** 253.

[54]   J. Wang, X. Xu, Y. Tian, C. Yao, R. Liu and L. Li, *J. Mater. Chem. C,* 2015, **3,** 2856.

[55]   G. L. Feng, W. Y. Lai, S. J. Ji and W. Huang, *Tetrahedrom Lett*., 2006, **47**, 7089.

[56]   J. Luo, B. Zhao, J. Shao, K. A. Lim, H. S. O. Chan and C. Chi, *J. Mater. Chem.,* 2009, **19**, 8327.

[57]   W. Y. Lai, Q. Q. Chen, Q. Y. He, Q. L. Fan and W. Huang, *Chem. Commun.,* 2006, 1959.

[58]   S. Kumar, *Chem. Soc. Rev.,* 2006, **35**, 83.

[59]   B. Gomez-Lor, B. Alonso, A. Omenat and J. L. Serrano, *Chem. Commun.,* 2006, 5012.

[60]   M. O'Neill and S. M. Kelly, *Adv. Mater.,* 2011, **23**, 566.

[61]   P. Strohriegl, D. Hanft, M. Jandke and T. Pfeuffer, *Mat. Res. Soc. Symp. Proc.*, 2002, **709**, 31.

[62]   A. Charas and J. Morgado, *Curr. Phys. Chem.,* 2012, **2**, 241.

[63]   O. Nuyken and S. D. Pask, *Polymers,* 2013, **5**, 361.

[64]   R. Precht, R. Hausbrand and W. Jaeqermann, *Phys. Chem. Chem. Phys.,* 2015, **17**, 6588.

[65]   A. B. Padmaperuma, *Adv. Mater. Phys. Chem.,* 2012, **2**, 163.

[66]   H. Tang, C. M. Hessel, J. Wang, N. Yang, R. Yu, H. Zhao and D. Wang, *Chem. Soc. Rev.,* 2014, **43,** 4281.

[67]   Z. Ning and H. Tian, *Chem. Commun.,* 2009, 5483,

[68]   Y. Zhang, Z. Wang, Y. Hao, Q. Wu, M. Liang and S. Xue, *Chin. J. Chem. Phys.,* 2015, **28**, 91.

[69]   R. S. Sprick, M. Hoyos, M. S. Wrackmeyer, A. V. S. Parry, I. M. Grace, C. Lambert, O. Navarro and M. L. Turner, *J. Mater. Chem. C,* 2014, **2**, 6520.

[70]   N. Satoh, J. Cho, M. Higuchi and K. Yamamoto, *J. Am. Chem. Soc.,* 2003, **125**, 8104.

[71]   C. Tsai, M. Liao, Y. Chen, S. Cheng, Y. Lai, Y. Cheng and C. Hsu, *J. Mater. Chem. C,* 2015, **3**, 6158.

5 Conclusions

The research for this thesis includes the synthesis, purification and subsequently optical/electro-chemical measurement for a series of organic semiconductors, some of which exhibit the desired nematic mesophase with a low melting point (Cr-N), a high clearing point (N-I) and a glass transition temperature (Tg) above room temperature (RT) as determined by using a combination of optical polarising microscopy (OPM) and differential scanning calorimetry (DSC).

A series of novel thiophene/phenylene-based, fluorene-based, dibenzothiophene-based, benzothiadiazole-based, and thieno[3,4-*c*]pyrrole-4,6-dione-based organic semiconductors incorporating symmetrical carbazole moieties were synthesised and analysed in terms of their relationship of aromatic structures, length of alkyl chains in terminal and lateral positions, and liquid crystalline mesophases. It was proved that in terms of more linear and co-axial aromatic backbones, longer (octyl) straight terminal alkyl chains and shorter (methyl) lateral chains lead to a larger length-to-breadth ratio which contributes to the presence of liquid crystalline mesophases, such as 2,2'-disubstituted bithiophene **38**, Benzothiadiazole **53**, and thieno[3,4-*c*]pyrrole-4,6-diones **54**, all with long terminal octyl chains. However, when the symmetrical sides of aromatic backbones form a small angle, long terminal alkyl chains reversely strengthen the non-linear structure of a molecule and thus decrease its rigidity and length-to-breadth ratio, just as liquid crystalline compound **14** and non liquid crystalline compound **39**. The presence of long and branched flexible alkiphatic chains (-(C_8H_{17})$_2$) (such as compounds **64, 67, 72, 73**) at lateral positions result in a low length-to-breadth ratio, which leads to the absence of liquid crystalline mesophases. In addition, the presence of symmetrically additional 2,5-disubstituted thiophene rings in the aromatic molecular core can effectively increase molecular length and length-to-breadth ratio of these highly conjugated conjugated aromatic cores, such as nematic liquid crystalline compounds **22**, **42** and **46** whereas non liquid crystalline **18**, **19** and **41**. Furthermore, the presence of two paris of symmetrical

2,5-disubstituted thiophene moieties in the fluorenes **46, 83** led to the formation of the desired nematic mesophase, in spite of the presence of long and branched aliphatic chains (-$(C_8H_{17})_2$) attached to the 2,7-disubstituted fluorene moieties in a lateral position.

A combination of UV-Visible spectrometry and potentiodynamic electrochemical cyclic voltammetry (CV) was used to determine the energy gap (Eg) and ionisation potentials (IP, HOMO energy level) of the new organic semiconductors synthesised in this thesis, respectively. The electron affinity (EA, LUMO energy level, eV) is effectively equal to HOMO energy level (eV) minus the band gap (eV) and is calculated in this way from the measured values of the IP and Eg. It was found that the presence of more number of thiophene units contribute to a lower energy gap (i.e., Eg = 2.50 eV for compound **46** with four 2,5-disubstituted thiophene rings while Eg = 3.08 eV for compound **41** with analogous structure to **46**) whereas the values for the IP, Eg and EA do not appear to be significantly influenced by the length of alkyl chains.

The compounds **38**, **41**, **42**, **49** and **53** were investigated as emissive materials in five OLEDs fabricated differing only in the nature of the emissive layer. The result proved that liquid crystalline emissive materials **38**, **42**, **49** and **53**, exhibit lower switch-on voltages and significantly higher device efficiency, current density and brightness, than non liquid crystalline material **41**. Particularly, liquid crystalline **42** proves excellent device performance due to the combined advantages of nematic mesophases with a desired glass transition temperature above room temperature (32 ^{o}C) and high clearing point (161 ^{o}C), high degree of conjugation, the presence of various aromatic heterocyclic moieties, and low charge-injection barriers from appropriate match of energy levels (IP = -5.53 eV and EA = -2.89 eV of compound **42** similar to IP = -5.48 eV of hole-transport material OTPD and and EA = -2.91 eV of electron-transport material SPPO13, respectively) in test OLED devices.

A series of novel star-shaped, carbazole-functionalised triazatruxene materials with different flexible aliphatic chains were also synthesised using simple *N*-position

substitution reactions in the thesis. Some of them were designed with photo-polymerisable sidechains incorporating cross-linkable end-groups such as double carbon-carbon bonds, non-conjugated dienes, triple bonds, cyclic ethers and isocyanate units. The compounds with non-conjugated dienes or oxetane proved to be photo-chemically cross-linkable with excellent cross-linking yield at relatively low UV fluence to form stable polymer networks as uniform, intractable thin films on device subtsrate surfaces. However, triazatruxenes with separate double bonds, triple bonds, hexyl cyclic ether, and isocyanate units at aliphatic chains cannot be photochemically cross-linked at a reasonable fluence or there is a minimal amount of cross-linking, although different intensities of UV (200 J/cm^2, 400 J/cm^2, 600 J/cm^2 and 800 J/cm^2) irradiation were evaluated. Furthermore, it was also found that non-conjugated dienes attached to more chemically and photochemically stable tertiary amides (90.0% @400 J/cm^2 UV for monomer **96**) showed a greater tendency to photopolymerise than that attached to ester bonds (72% @800 J/cm^2 UV for monomer **K1**). Hole test devices using photopolymerisable triazatruxene **100** were fabricated to investigate the effect of cross-linking and doping on charge carrier mobility. The result proves the cross-linking of triazatruxene monomer **100** does not lead to a decrease of current density, and the use of highly electronegative *p*-type doping results in an increase of current density due to the formation of more free holes in a device by removing electrons from the host material.

In addition, a series of related triazatruxenes with a range on non-polymerisble flexible side chains were also designed including straight-chain and cyclic alkyl groups and flexible aliphatic chains incorporating functional groups, such as ester, ether, and nitrile moieties, in order to compare their thermal stability and physical properties with those of the corresponding photopolymerisable anaologues. The results of this research shows that triazatruxene derivatives generally exhibit good thermal stability due to the presence of the large, star-shaped, highly-conjugated, aromatic triazatruxene core.

A number of organic synthetic reactions including palladium-catalysed, aryl-aryl,

cross-coupling reactions, such as Suzuki reactions, Stille reactions, and direct arylations, brominated substitutions with *N*-bromosuccinimide (NBS) or bromine, *N*-alkyl substitutions, ring-closing reactions, etc., were performed and optimised under different reaction conditions. Different palladium-catalysed systems for Suzuki reactions, reaction solvents, base choices of *N*-alkyl substitutions, and the comparison of Suzuki cross-couplings and direct arylations were studied and analysed in this thesis. The Suzuki aryl-aryl, cross-coupling reactions were found to be a more widely applicable and successful reaction method than direct arylations. The reaction conditions were optimised to produce the desired compounds as efficiently as possible. Column chromatography, flash column, recrystallisation, etc., were used to purify final compounds and intermediates. ^{1}H NMR, ^{13}C NMR, Mass Spectrometry (MS), Infrared Spectroscopy (IR) and Elemental Analysis (EA) were used to confirm the molecular structures and purity of these novel compounds.